A novel formulation for skin barrier repair

From ex vivo assessment towards clinical studies

Tineke van Eijk – Berkers

The investigations described in this thesis were performed at the Division of Drug Delivery Technology of the Leiden Academic Center for Drug Research, Leiden University, Leiden, The Netherlands. This research is supported by the Netherlands Organization for Scientific Research (NWO) domain Applied and Engineering Sciences (TTW) (project number 12400), which is partly funded by the Ministry of Economic Affairs and Climate Policy, and the Ministry of Education, Culture and Science. In addition, the following companies provided substantial financial support to the research: Galderma S.A., Evonik Industries AG, and Croda International.

ISBN: 978-94-028-1191-9

Cover: freely transformed lines of the CH_2 rocking vibrations of a FTIR spectrum

Cover and thesis design by Michelle van Boven and Tineke van Eijk-Berkers

Printed by Ipskamp Printing

A novel formulation for skin barrier repair

From ex vivo assessment towards clinical studies

Proefschrift

ter verkrijging van
de graad van Doctor aan de Universiteit Leiden,
op gezag van Rector Magnificus prof. mr. C.J.J.M Stolker,
volgens besluit van het College van Promoties
te verdediging op woensdag 24 oktober 2018
klokke 13.45 uur

door

Martine Arnoldina Johanna van Eijk-Berkers
geboren te Helmond in 1989

Promotor
Prof. Dr. J.A. Bouwstra

Co-promotor
Dr. A.P.M. Lavrijsen

Promotiecommissie
Prof. Dr. H. Irth, Leiden University, LACDR (Chairman)
Prof. Dr. A.P. IJzerman, Leiden University, LACDR (Secretary)
Prof. Dr. Dr.-Ing. J. Lademann, Medical University Berlin, Charité
Prof. Dr. M.H. Vermeer, Leiden University, LUMC
Prof. Dr. W. Jiskoot, Leiden University, LACDR
Prof. Dr. P.I. Spuls, AMC, Amsterdam

Table of contents

List of abbreviations used in this thesis

AD	Atopic dermatitis	FWHM	Full width at half maximum
aSmase	Acid-sphingomyelinase	GBA	β-glucosylcerebrosidase
ATR-FTIR	Attenuated total reflection Fourier transform infrared spectroscopy	HE	Haematoxylin and Eosin
AUC	Area under the curve	HPTLC	High performance thin layer chromatography
BSA	Bovine serum albumin	LB	Lamellar body
C34 CER	Ceramide with 34 carbon atoms	LC/MS	Liquid chromatography/mass spectrometry
CER	Ceramide	LMM	Linear mixed model
CHOL	Cholesterol	LPP	Long periodicity phase
Ctrl	Control	MCL	Mean ceramide carbon chain length
Cul	Cultured	MTT	Mid-point transition temperature
dFA	Perdeuterated fatty acid	MuCER	Mono-unsaturated ceramide
EASI	Eczema area and severity index	MUFA	Mono-unsaturated fatty acid
ELOVL	Elongation of very long chain fatty acids	PC	Principal component
ESRF	European synchrotron radiation facility	PCA	Principal component analysis
FA	Fatty acid	PUFA	Poly-unsaturated fatty acid
FA^{16}	Palmitic acid	Reg	Regenerated
FA^{18}	Stearic acid	SAXD	Small angle X-ray diffraction
FA^{22}	Behenic acid	SB	Stratum basale
FLG	Filaggrin	SC	Stratum corneum
$Form^{(d)FA16}$	FA formulation with (deuterated) palmitic acid	SCD	Steroyl co-enzyme A desaturase
$Form^{(d)FA18}$	FA formulation with (deuterated) stearic acid	SCORAD	Scoring atopic dermatitis
$Form^{(d)FA22}$	FA formulation with (deuterated) behenic acid	SG	Stratum granulosum
$Form^{(d)NS}$	Formulation with (deuterated) CER NS	SPP	Short periodicity phase
$Form^{Basic}$	Basic formulation without CERs	SQ	SquameScan value
$Form^{COMBI}$	Formulation with CER EOS, CER NS, and FA22	SS	Stratum spinosum
$Form^{EOS}$	Formulation with CER EOS	TEWL	Transepidermal water loss
FTIR	Fourier transform infrared spectroscopy	VC	Vernix caseosa

Chapter 1

Introduction, aim,

and outline of this thesis

The skin function and structure

The skin is the largest organ of the human body with a surface area of about 1.5 m^2 in adults.[1] It provides a protective barrier between the body and the external environment by preventing excessive transepidermal water loss (TEWL) (inside-to-outside barrier) and the entry of pathogens, allergens, and irritants (outside-to-inside barrier).[2-4] Besides this function, the skin is a sensory organ and has an important function in thermoregulation and pain.[5,6] Finally the skin is a highly immunogenic organ with a high density of antigen presenting cells.
The skin consists of three main morphological layers, from inside to outside: the subcutaneous fat tissue (hypodermis), the dermis, and the epidermis (Figure 1). The dermis contains blood vessels, nerve endings, hair follicles, and sweat glands. The main cell type is the fibroblast which produces collagen fibers and elastin to give the dermis toughness and elasticity, respectively.[7,8]

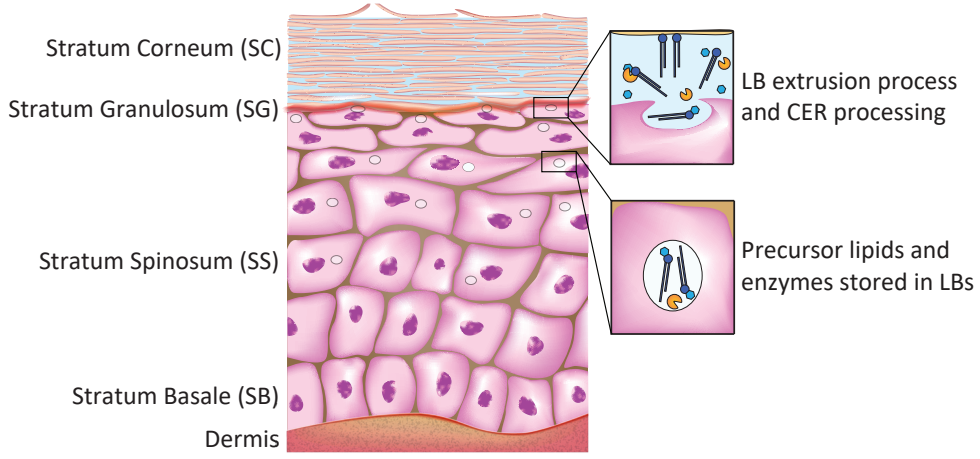

Figure 1. Structure of the skin with dermis and epidermis. The epidermis is subdivided in four strata, the stratum basale, the stratum spinosum, the stratum granulosum, and the stratum corneum. Keratinocytes migrate upwards from the stratum basale towards the stratum corneum where they are shed. The details are showing lamellar bodies containing CERs and enzymes, and the extrusion of the lamellar bodies at the SG-SC interface. Figure adapted from: van Smeden et al. JLR 2017

The most prevalent cell type in the epidermis is the keratinocyte, but the epidermis also contains melanocytes, Langerhans cells, and Merkel cells. The keratinocytes in the epidermis are connected by tight junctions.[3] The epidermis is divided into four strata, depending on the stage of differentiation. These strata are (from inside to outside) the viable stratum basale (SB), stratum spinosum (SS), and stratum granulosum (SG), and the non-viable stratum corneum (SC), with the SC being the outermost layer (Figure 1). Keratinocytes proliferate in the SB and, after escaping from the basal layer, start to differentiate and migrate upwards to the SC. Keratinocytes ultimately become flat enucleated, terminally differentiated cells called corneocytes.[9] At the surface, the corneocytes are shed in the desquamation process. As a consequence, the SC is completely renewed in about 4 weeks.[10,11] During the differentiation process, the keratinocytes start to generate lamellar bodies (LBs) containing lipids and enzymes.

This process starts in the SS and is accelerated in the SG. Most of the lipids stored in the LBs are the precursors of the SC lipids. The LB content is extruded at the SG-SC interface, where the precursor lipids are converted by enzymes to its final form (see below).[12,13]

Structure of the stratum corneum

The SC is 10-15 µm thick and contains about 10-20 corneocyte layers[14-16], in which the corneocytes are connected by corneodesmosomes.[3,13,17,18] Each corneocyte is surrounded by a highly impermeable cornified envelope consisting of a protein layer toward which a monolayer of lipids is chemically attached.[3,4] The corneocytes are embedded in an extracellular lipid matrix which is the only continuous structure in the SC. Therefore, molecules always have to pass the lipid matrix when penetrating the skin.[19-21]

The structure of the SC is often referred to as a "brick-and-mortar" structure with the bricks representing the corneocytes and the mortar representing the lipid matrix, respectively.[22] The lipids in the extracellular matrix are highly ordered in lipid layers (lamellae) stacked on top of each other. The lamellae are oriented approximately parallel to the skin surface (Figure 2). Two lamellar phases have been identified in SC by using small-angle X-ray diffraction (SAXD). The long periodicity phase (LPP) has a repeat distance of about 13 nm, and the short periodicity phase (SPP) has a repeat distance of about 6 nm.[23-27] *In vitro* studies indicated that the LPP is important for a proper skin barrier function.[24,28] Within the lamellae, lipids can adopt a very dense orthorhombic, a less dense hexagonal, or a disordered liquid phase (Figure 2). In healthy human SC, a large fraction of lipids adopt the orthorhombic packing, while a minor lipid fraction forms a hexagonal packing.[27,29-31] A more dense lipid packing is considered beneficial for the skin barrier function.[24,30]

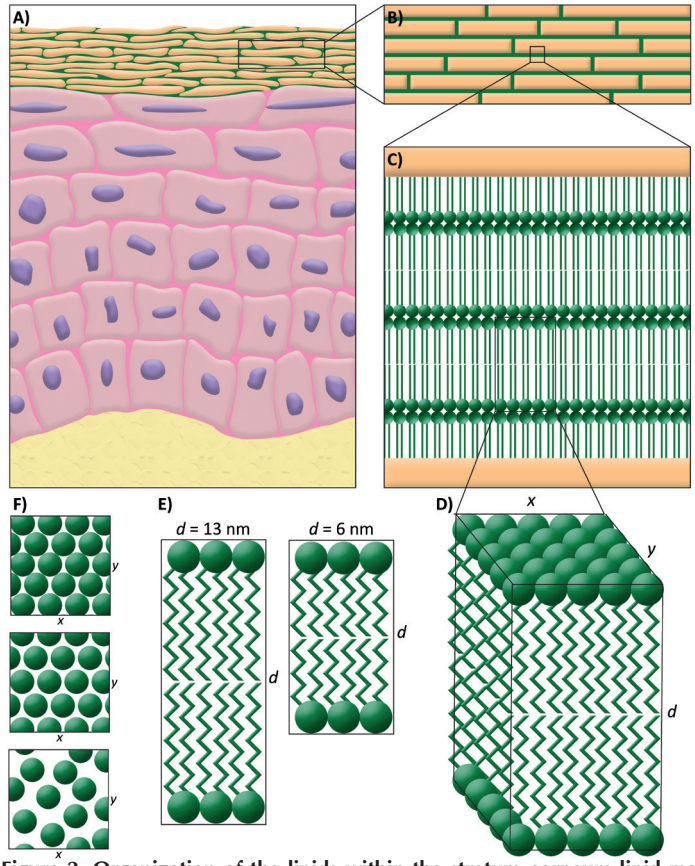

Figure 2. Organization of the lipids within the stratum corneum lipid matrix. A) Schematic overview of the epidermal morphology. **B)** The corneocytes are embedded in the lipid matrix in a brick-and-mortar structure. **C)** The lipids in the matrix are stacked in lamellae in between the corneocytes. **D)** More details of the lipid lamellae. **E)** Two lamellar phases are identified with a repeat distance (d) of either 13 nm (LPP) or 6 nm (SPP). **F)** Within the lamellae, the lipids are organized in either an orthorhombic, hexagonal, or liquid packing (from top to bottom).

Extracellular lipid matrix in the stratum corneum

The main lipid classes in the extracellular lipid matrix are cholesterol, free fatty acids (FAs), and ceramides (CERs) in approximately equimolar ratio.[32-34] FAs in the lipid matrix have a wide chain length distribution. The most abundant FAs in the SC are those with a chain length of 24 and 26 carbon atoms.[35-37] In healthy skin, FAs are primarily saturated, but also mono-unsaturated FAs (MUFAs) are detected.[37] When focusing on the CERs, a wide variety in structural diversity is observed. CERs consist of a sphingoid base linked to a fatty acid chain. To date, at least 18 CER subclasses have been identified in the human SC (Figure 3).[32-34,38-43] These subclasses are named according to their molecular structure. The acyl chain can either be non-hydroxylated (N), α-hydroxylated (A), or ω-hydroxylated (O). The latter can be linked to another fatty acid chain through an ester linkage (esterified ω-hydroxy; EO), or to the polar head group (1-O-ceramides).

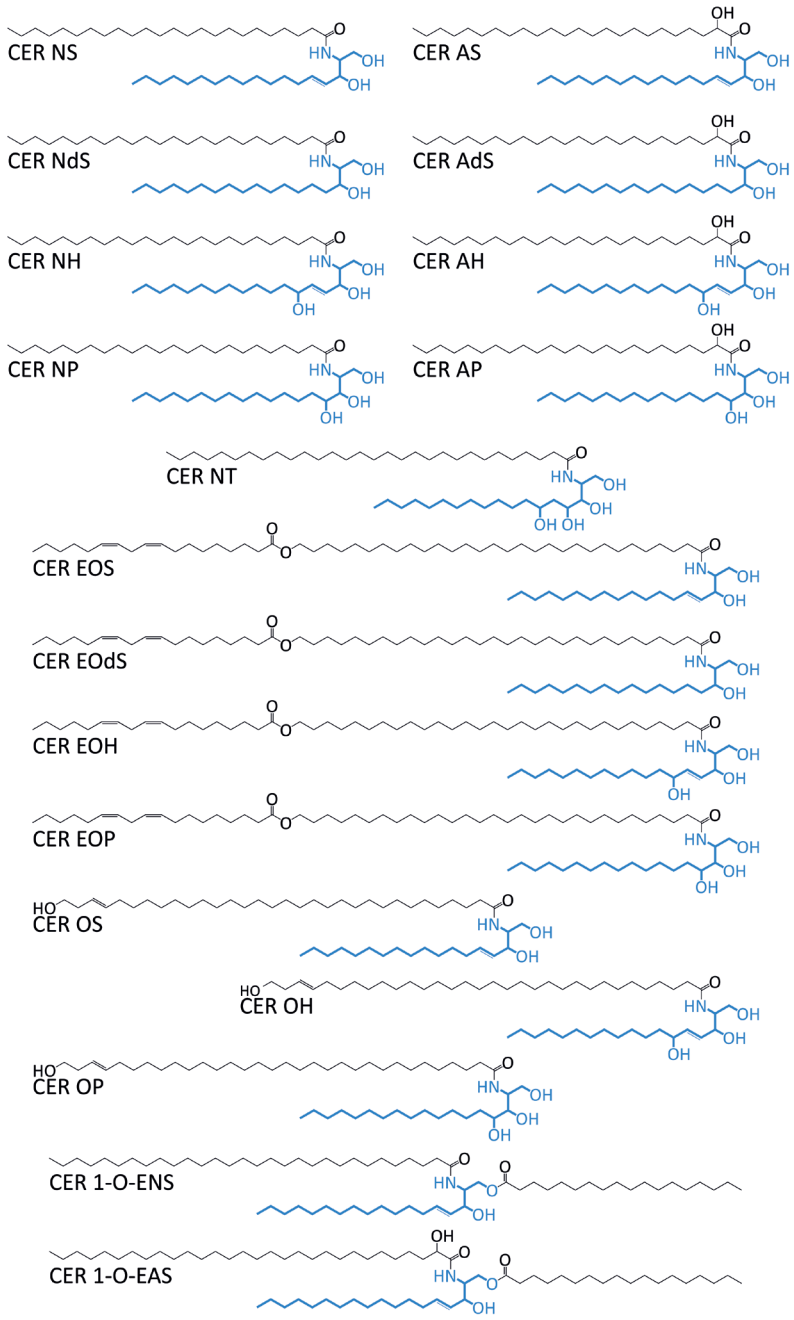

Figure 3. Ceramide subclasses in the stratum corneum lipid matrix. CERs consist of a sphingoid base coupled to a FA, which can both vary in molecular structure. CERs are named according to their molecular structure. The acyl chain can either be non-hydroxylated (N), α-hydroxylated (A), ω-hydroxylated (O), or esterified ω-hydroxylated (EO), whereas the sphingoid base is either a sphingosine (S), dihydrosphingosine (dS), phytosphingosine (P), 6-hydroxysphingosine (H), or dihydroxy dihydrosphingosine (T).

The sphingoid base is either a sphingosine (S), dihydrosphingosine (dS), phytosphingosine (P), 6-hydroxysphingosine (H), or dihydroxy dihydrosphingosine (T). In addition to their variation in molecular structure, a wide variety in total carbon chain length is observed in CERs.
The lipid composition in the SC is important for the barrier function of the SC.[44] For example, the presence of CER EO in the SC is essential for the formation of LPP[25,45-48] and it enhances the assembly of lipids in orthorhombic domains.[45,48]

Lipid synthesis

Several SC lipids can be taken up by the keratinocytes from dietary sources, e.g. essential FAs diffuse into the plasma and are taken up via FA binding protein and FA transport protein.[49] The same occurs for cholesterol. However, most SC lipids are (also) synthesized by the keratinocytes (*de novo* synthesis). Several enzymes are involved in the lipid synthesis from the viable epidermis to the SC layer.
FA with a chain length up to 16 carbon atoms (C16, palmitic acid) are synthesized by fatty acid synthase using acetyl-coenzyme A and malonyl-coenzyme A. FA C16 is elongated in the endoplasmic reticulum by a membrane-associated elongation system using four enzymes, which catalyze a condensation step, a reduction step, a dehydration step, and another reduction step, respectively. Per elongation cycle, two carbon atoms are linked to the FA carbon chain.[50] A series of 7 elongases (ELOVL) is involved in the first condensation step, starting with ELOVL 6 which catalyzes the elongation of FA C16 to FA C18. Subsequently, ELOVL 3, 1, and 4 catalyze the elongation to FAs with chain lengths C20, C26 and >C26, respectively.[50,51] Besides elongation, the FAs can be converted to MUFAs by stearoyl-coenzyme A desaturases. The elongation of MUFAs is catalyzed by ELOVL 3, 7, and 1, whereas ELOVL 5 is involved in the elongation of polyunsaturated FAs (PUFAs).[50,51] ELOVL 2 is not expressed in skin tissue.[50] The synthesized FAs are either transformed to phospholipids and stored in LBs, or used for CER synthesis. The majority of the PUFAs (often essential fatty acids) are taken up by keratinocytes from their environment by FA binding protein and FA transport protein, and are not synthesized de novo.[49]
CERs are synthesized in the endoplasmic reticulum in multiple enzymatic steps. First, the enzyme serine palmitoyl transferase condensates L-serine and palmitoyl-coenzyme A into 3-keto-dihydrosphingosine, which is consecutively reduced to dihydrosphingosine. 6 CER synthases are involved in the next step in which a FA is acylated to form a ceramide with a dS sphingoid base. Each CER synthase is more specific towards a FA chain length or degree of unsaturation. In the final step, the dS-ceramides are converted into the S and P CER subclasses by dihydroceramide desaturase 1 and 2, respectively. The hydroxylation of the H CER subclass occurs by a yet unidentified enzyme. The CERs are transported to the Golgi complex, converted into sphingomyelin or glucosyl-CERs, and stored in LBs.[42]
The LBs contain the lipid precursors (cholesterol, phospholipids, glucosyl-CERs, and sphingomyelins) as well as enzymes that convert the lipid precursors into the barrier lipids.[12,13] The lipids are stacked as lipid layers within the LBs.[4] At the interface of the SG and the SC, the LBs are extruded and the lipids and enzymes are secreted into

the extracellular matrix. During this process, the enzymes start to convert the lipid precursors into their final products. Several phospholipases converts the phospholipids into FAs, and β-glucocerebrosidase and acidic sphingomyelinase convert the glucosyl-CERs and sphingomyelins into CERs, respectively.[2,4]

Skin diseases with an impaired skin barrier function

Some of the inflammatory skin diseases with an impaired skin barrier function are, for example psoriasis, Netherton syndrome and atopic dermatitis (AD).[52-58] Besides barrier proteins, an altered lipid composition compared to healthy skin plays a role in this reduced skin barrier function. Netherton syndrome is a rare genetic skin disorder which is characterized by hair shaft defects, severe atopic manifestations, and erythroderma. In the SC of these patients, a lower fraction of the long chain EO-CERs is observed in addition to an increased level of short chain CERs, an increased level of unsaturated CERs, an increased level of MUFAs and a reduction in mean FA chain length. As a result, a higher degree of disordering of SC lipids was observed besides an altered repeat distance of the lamellar phases.[59] In psoriasis, a chronic inflammatory skin disease with abnormal epidermal proliferation, the level of CER EOS is severely reduced in lesional areas. This is in combination with a reduction of P-subclass CERs and an increase in other S-subclass CERs.[60,61] Furthermore, the X-ray diffraction profiles suggest shorter repeat distances of the lamellar phases in lesional skin.[62]
AD is a chronic, relapsing, noncontagious, inflammatory skin disease characterized by xerosis (dry skin), pruritis (itch), and eczematous skin.[63] It has a prevalence of about 20% in children, but also affects 5-10% of the adult population.[64-66] Since the discovery of mutations in the filaggrin gene (*FLG*) in 2006[67], the development of AD is believed to be an interplay between a defective skin barrier and the innate and adaptive immune response.[68] *FLG* codes for profilaggrin, which is cleaved into 10-12 copies of filaggrin.[69] In healthy skin, filaggrin aligns and aggregates with keratin filaments and is thus involved in the proper formation of the cornified envelope.[70] However, mutations in *FLG* are only present in 20-50% of the AD patients supporting the heterogeneous nature of the disease.[68,71-74] In the past decade, the underlying molecular basis has been increasingly understood, mostly with a focus on barrier dysfunction, cutaneous and systemic immune abnormalities, and the role of the microbiome. It is now clear that all are interconnected, with each abnormality progressively exacerbating another.[75] Numerous studies have demonstrated that skin barrier dysfunction is a critical component of AD.[37,76,77] This skin barrier dysfunction facilitating the interaction of external stimuli (allergens, irritants and pathogens) with skin-resident immune cells and driving the cutaneous inflammation.[77] These inflammatory responses drive the differentiation of naive T-cells, initiate the itch-response, and reduce the expression of filaggrin, causing a vicious cycle.[78]
The SC lipid composition and organization in AD is extensively described. It is characterized by significant reductions in the level of CER EOS[55,58,76,79-81] and NP[76,80,81], an increase in levels of CER NS and AS[55,76], and an increase in short chain CERs and FAs.[37,53,76] Furthermore, a higher fraction of lipids adopting a hexagonal lateral packing was detected at the expense of the fraction forming orthorhombic domains[37,76,82], as

well as a reduction in repeat distance of the lamellar phases.[26,76] These observations were not related to the presence or absence of mutations in the filaggrin-gene (see below)[58,76] and were more pronounced in lesional compared to non-lesional AD skin.[37] Overall, in these inflammatory skin diseases, the levels of CER EOS and CER NP are reduced, and the level of CER NS is increased. Furthermore, these skin diseases are characterized by a reduced average lipid chain length, a higher degree of unsaturated lipids, an altered LPP, and a reduction in lipids assembling in an orthorhombic packing.

Vernix caseosa as treatment for atopic dermatitis

Due to its multifactorial character, AD is difficult to treat properly. Dermatologist reached consensus that appropriate skin care is very important and that moisturization by the use of lipophilic formulations should be the first treatment strategy to treat dry skin of AD patients, but may also be used as an additional protective layer to reduce the entrance of allergens to enter the viable skin.[83-87] If this treatment is insufficient, topical corticosteroids should be used with a step-down approach. This means that treatment starts with a potent corticosteroid and if the desired effect is reached less potent corticosteroids can be used.[83-86] However, topical corticosteroids are associated with side effects such as skin atrophy, striae, and contact dermatitis.[88] On the contrary, it has been suggested that treatment with endogenous skin barrier lipids (e.g. cholesterol, CERs, and FAs) might be beneficial for skin barrier repair in skin diseases.[89]

A possible treatment suggested for AD is application of vernix caseosa (VC). VC is a white, greasy substance covering a fetus during the last trimester of pregnancy, and it is developed at the same time as the development of SC *in utero*.[90] VC protects the fetus from the amniotic fluid, serves as a lubricant during delivery, and protects the newborn from dehydration after being exposed to dry air in the extrauterine environment.[91,92] Furthermore, VC has been suggested to have anti-infective, anti-oxidant, and wound healing properties.[91,92]

VC is known to consist of 80% water, 10% protein, and 10% lipids.[92-95] The lipids in VC are barrier lipids (e.g. cholesterol, FAs, CERs) as well as wax esters, sterols esters, squalene, triglycerides, and phospholipids.[92,94] Of the barrier lipids, the same CER subclasses are present in VC as in SC. However, as opposed to SC, CER subclass AH is most abundant in VC of infants born at term.[94,95] Additionally, FA with chain lengths varying between C14 and C32 are present in VC, with the highest abundance of FA C16.[94,96] Furthermore, the composition of VC varies between boys and girls.[96]

It has been reported that VC is able to enhance skin barrier repair in mice with a severely decreased skin barrier function induced by tape stripping. The recovery time of skin treated with VC was only half of the recovery time of untreated skin.[97] In a subsequent study, it was shown that VC can be replaced by a synthetic mixture (water, polymer-based particles, and synthetic lipids) and reach similar barrier recovery in the same time period.[98] Furthermore, when only the synthetic lipid mixture was applied, the barrier recovery was very similar and better than various formulations on the market.[98] In a wound healing study performed in pigs, a better barrier recovery rate was observed in the initial phase after treating the disrupted area with VC compared to no treatment. However, no treatment and VC treatment did not differ in barrier recovery

rate after 7 days of treatment.[99]
A significantly higher skin hydration, moisture accumulation and water-holding capacity were observed immediately after treating tape-stripped human skin with VC compared to no treatment.[100] However, after a longer treatment period of 5 days, no difference between VC treated and untreated sites were observed regarding barrier recovery, skin hydration or dryness.[99]
Apparently, human skin reacts differently to VC treatment than animal skin. In order to further examine the use of formulations based on VC, studies on human skin are needed. Clinical studies for testing formulations are time consuming and can be burdensome for the subjects. Therefore, human skin models are needed to study skin barrier repair. Frequently used existing human skin models are human skin equivalents, which can be used to study biological skin processes, to generate skin to treat burn wounds, or for irritation screening. However, because of the reduced skin barrier function of these models, their use for penetration studies is limited. Furthermore, many available skin models are time consuming because of the use of cultured of skin cells rather than culturing skin tissue. In this thesis, a skin barrier repair model using excised human skin was generated for the development of a VC based topical lipid formulation to treat AD.

This thesis

Aim of this thesis

The aim of this thesis was to determine whether a novel VC based formulation effectively enhances skin barrier repair in AD patients and normalizes the SC lipid composition and organization. In order to achieve this goal, the following studies were performed:

1. An *ex vivo* human skin barrier repair (SkinBaR) model was developed for studying the interactions between topical applied compounds and the skin barrier. The SC lipid properties during and after skin barrier repair process were examined. The lipid composition and organization in the regenerated SC of this SkinBaR model were compared to the lipid composition and organization in regenerated SC in healthy human skin *in vivo*.
2. The effects of a selected number of barrier FAs and/or CER subclasses applied in a VC based formulation on the SkinBaR model during skin barrier repair were examined. Especially the interactions between the VC components and the SC lipid matrix were studied.
3. The effect of the VC based formulation on skin barrier repair in compromised healthy skin, and in AD skin was assessed.

Outline of this thesis

This thesis is divided in three parts, which address the aforementioned objectives.
Part I (Chapters 2, 3 & 4) covers the development of the SkinBaR model using *ex vivo* human skin which is stripped using cyanoacrylate (superglue). The SC is regenerated during culture in an incubator. In addition, studies are described focusing on whether the barrier properties of the SkinBaR model mimic that of *in vivo* skin after barrier repair.
Part II (Chapters 5 & 6) focusses on the studies performed to investigate the interaction of FAs, CERs, or a combination of CERs and FAs in the VC based formulation with the SC lipid matrix of the *ex vivo* SkinBaR model.
Part III (Chapters 7 & 8) describes two clinical studies in which the effect of topical application of the VC based formulation during skin barrier repair on i) tape-stripped healthy skin and ii) AD skin was examined.

A more detailed outline of this thesis is provided below:
In Chapter 2 studies are described focusing on the development of the *ex vivo* human SkinBaR model. In this model SC was removed by stripping with cyanoacrylate. Subsequently, the SC was regenerated during culturing. The epidermal characteristics of the SkinBaR model are described in this chapter. This model may be an attractive candidate for testing topical formulations which aim to enhance skin barrier repair.
In Chapter 3, studies are described focusing on the extent of barrier disruption of the *ex vivo* SkinBaR model on the lipid organization of the regenerated SC. The changes in the lamellar and lateral lipid organization in the regenerated SC were related to the initial depth of stripping.
In Chapter 4 studies are reported in which the *ex vivo* SkinBaR model was compared

with the regeneration of SC in humans after tape-stripping the skin. The two models for skin barrier repair were compared focusing on lipid composition and organization. Furthermore, the changes in lipid composition and organization were compared with the SC lipid properties of inflammatory skin diseases described in literature.
In Chapter 5 studies are presented in which the *ex vivo* SkinBaR model was used to study the application of FA in a VC based formulation on the SC lipid organization. More specifically FAs with a chain length of 16, 18, or 22 carbon atoms were used. The epidermal morphology, lipid organization, and ordering of the SC lipid matrix were examined and whether or not the applied FA were incorporated in the SC lipid matrix. Liquid chromatography/mass spectrometry (LC/MS) was used to examine whether the applied FAs were elongated.
In Chapter 6 studies are described in which two CER subclasses in the VC based formulations were applied on the SkinBaR model. The effect of the CER subclasses on the lipid organization as well as the mixing properties of the CERs with the SC lipid matrix was investigated. Finally, FAs and CERs were combined in the VC based formulation.
Chapter 7 describes the application of a VC based lipid formulation containing FAs and CERs during skin barrier repair of tape-stripped human skin in a clinical study setting. The repair of the skin barrier function was monitored over time. A VC based formulation was applied on native and regenerated SC and the SC lipid matrix properties were compared.
In Chapter 8, studies are presented in which the same VC based formulation was applied on non-lesional and lesional AD skin for a period of two weeks. The skin barrier function, lipid composition, and lipid organization were examined before and after treatment.
Chapter 9 provides a summary of the obtained results, describes overall conclusions, and provides an overview of the perspectives.

References

1. Burton RF. Estimating body surface area from mass and height: theory and the formula of Du Bois and Du Bois. *Ann Hum Biol* **2008**: 35: 170-184.
2. Feingold KR. The outer frontier: the importance of lipid metabolism in the skin. *J Lipid Res* **2009**: 50 Suppl: S417-S422.
3. Proksch E, Brandner JM, Jensen JM. The skin: an indispensable barrier. *Exp Dermatol* **2008**: 17: 1063-1072.
4. Madison KC. Barrier function of the skin: "la raison d'etre" of the epidermis. *J Invest Dermatol* **2003**: 121: 231-241.
5. Blatteis CM. Age-dependent changes in temperature regulation - a mini review. *Gerontology* **2012**: 58: 289-295.
6. Schmelz M. Neuronal sensitivity of the skin. *Eur J Dermatol* **2011**: 21 Suppl 2: 43-47.
7. Keene DR, Marinkovich MP, Sakai LY. Immunodissection of the connective tissue matrix in human skin. *Microsc Res Tech* **1997**: 38: 394-406.
8. Kielty CM, Shuttleworth CA. Microfibrillar elements of the dermal matrix. *Microsc Res Tech* **1997**: 38: 413-427.
9. Eckert RL. Structure, function, and differentiation of the keratinocyte. *Physiol Rev* **1989**: 69: 1316-1346.
10. Milstone LM. Epidermal desquamation. *J Dermatol Sci* **2004**: 36: 131-140.
11. Egelrud T. Desquamation in the stratum corneum. *Acta Derm Venereol Suppl (Stockh)* **2000**: 208: 44-45.
12. Feingold KR. Lamellar bodies: the key to cutaneous barrier function. *J Invest Dermatol* **2012**: 132: 1951-1953.
13. Wertz PW. Lipids and barrier function of the skin. *Acta Derm Venereol Suppl (Stockh)* **2000**: 208: 7-11.
14. Russell LM, Wiedersberg S, Delgado-Charro MB. The determination of stratum corneum thickness: an alternative approach. *Eur J Pharm Biopharm* **2008**: 69: 861-870.
15. Holbrook KA, Odland GF. Regional differences in the thickness (cell layers) of the human stratum corneum: an ultrastructural analysis. *J Invest Dermatol* **1974**: 62: 415-422.
16. Blair C. Morphology and thickness of the human stratum corneum. *Br J Dermatol* **1968**: 80: 430-436.
17. Ishida-Yamamoto A, Igawa S, Kishibe M. Order and disorder in corneocyte adhesion. *J Dermatol* **2011**: 38: 645-654.
18. Ishida-Yamamoto A, Kishibe M. Involvement of corneodesmosome degradation and lamellar granule transportation in the desquamation process. *Med Mol Morphol* **2011**: 44: 1-6.
19. Johnson ME, Blankschtein D, Langer R. Evaluation of solute permeation through the stratum corneum: lateral bilayer diffusion as the primary transport mechanism. *J Pharm Sci* **1997**: 86: 1162-1172.
20. Michaels AS, Chandrasekaran SK, Shaw JE. Drug permeation through human skin: Theory and invitro experimental measurement.
21. Talreja P, Kleene NK, Pickens WL, et al. Visualization of the lipid barrier and measurement of lipid pathlength in human stratum corneum. *AAPS PharmSci* **2001**: 3: E13.
22. Elias PM. Epidermal lipids, barrier function, and desquamation. *J Invest Dermatol* **1983**: 80: 44s-49s.
23. Bouwstra JA, Gooris GS, van der Spek JA, et al. Structural investigations of human stratum corneum by small-angle X-ray scattering. *J Invest Dermatol* **1991**: 97: 1005-1012.
24. Groen D, Poole DS, Gooris GS, et al. Is an orthorhombic lateral packing and a proper lamellar organization important for the skin barrier function? *Biochim Biophys Acta* **2011**: 1808: 1529-1537.
25. McIntosh TJ, Stewart ME, Downing DT. X-ray diffraction analysis of isolated skin lipids: reconstitution of intercellular lipid domains. *Biochemistry* **1996**: 35: 3649-3653.
26. Janssens M, van Smeden J, Gooris GS, et al. Lamellar lipid organization and ceramide composition in the stratum corneum of patients with atopic eczema. *J Invest Dermatol* **2011**: 131: 2136-2138.
27. Hatta I, Ohta N, Inoue K, et al. Coexistence of two domains in intercellular lipid matrix of stratum corneum. *Biochim Biophys Acta* **2006**: 1758: 1830-1836.
28. de Jager M, Groenink W, Guivernau R, et al. A novel in vitro percutaneous penetration model: evaluation of barrier properties with p-aminobenzoic acid and two of its derivatives. *Pharm Res* **2006**: 23: 951-960.
29. Bommannan D, Potts RO, Guy RH. Examination of stratum corneum barrier function in vivo by infrared spectroscopy. *J Invest Dermatol* **1990**: 95: 403-408.
30. Damien F, Boncheva M. The extent of orthorhombic lipid phases in the stratum corneum determines the barrier efficiency of human skin in vivo. *J Invest Dermatol* **2010**: 130: 611-614.
31. Pilgram GS, Engelsma-van Pelt AM, Bouwstra JA, et al. Electron diffraction provides new information on human stratum corneum lipid organization studied in relation to depth and temperature. *J Invest Dermatol* **1999**: 113: 403-409.
32. Wertz PW, Miethke MC, Long SA, et al. The

composition of the ceramides from human stratum corneum and from comedones. *J Invest Dermatol* **1985**: 84: 410-412.
33. Ponec M, Weerheim A, Lankhorst P, et al. New acylceramide in native and reconstructed epidermis. *J Invest Dermatol* **2003**: 120: 581-588.
34. Masukawa Y, Narita H, Shimizu E, et al. Characterization of overall ceramide species in human stratum corneum. *J Lipid Res* **2008**: 49: 1466-1476.
35. Norlen L, Nicander I, Lundsjo A, et al. A new HPLC-based method for the quantitative analysis of inner stratum corneum lipids with special reference to the free fatty acid fraction. *Arch Dermatol Res* **1998**: 290: 508-516.
36. Ansari MN, Nicolaides N, Fu HC. Fatty acid composition of the living layer and stratum corneum lipids of human sole skin epidermis. *Lipids* **1970**: 5: 838-845.
37. van Smeden J, Janssens M, Kaye EC, et al. The importance of free fatty acid chain length for the skin barrier function in atopic eczema patients. *Exp Dermatol* **2014**: 23: 45-52.
38. Stewart ME, Downing DT. A new 6-hydroxy-4-sphingenine-containing ceramide in human skin. *J Lipid Res* **1999**: 40: 1434-1439.
39. Robson KJ, Stewart ME, Michelsen S, et al. 6-Hydroxy-4-sphingenine in human epidermal ceramides. *J Lipid Res* **1994**: 35: 2060-2068.
40. Farwanah H, Wohlrab J, Neubert RH, et al. Profiling of human stratum corneum ceramides by means of normal phase LC/APCI-MS. *Anal Bioanal Chem* **2005**: 383: 632-637.
41. van Smeden J, Hoppel L, van der Heijden R, et al. LC/MS analysis of stratum corneum lipids: ceramide profiling and discovery. *J Lipid Res* **2011**: 52: 1211-1221.
42. Rabionet M, Gorgas K, Sandhoff R. Ceramide synthesis in the epidermis. *Biochim Biophys Acta* **2014**: 1841: 422-434.
43. t'Kindt R, Jorge L, Dumont E, et al. Profiling and characterizing skin ceramides using reversed-phase liquid chromatography-quadrupole time-of-flight mass spectrometry. *Anal Chem* **2012**: 84: 403-411.
44. Grubauer G, Feingold KR, Harris RM, et al. Lipid content and lipid type as determinants of the epidermal permeability barrier. *J Lipid Res* **1989**: 30: 89-96.
45. Bouwstra JA, Gooris GS, Dubbelaar FE, et al. Role of ceramide 1 in the molecular organization of the stratum corneum lipids. *J Lipid Res* **1998**: 39: 186-196.
46. de Jager MW, Gooris GS, Dolbnya IP, et al. The phase behaviour of skin lipid mixtures based on synthetic ceramides. *Chem Phys Lipids* **2003**: 124: 123-134.
47. Bouwstra JA, Gooris GS, Dubbelaar FE, et al. Phase behavior of lipid mixtures based on human ceramides: coexistence of crystalline and liquid phases. *J Lipid Res* **2001**: 42: 1759-1770.
48. Mojumdar EH, Gooris GS, Bouwstra JA. Phase behavior of skin lipid mixtures: the effect of cholesterol on lipid organization. *Soft Matter* **2015**: 11: 4326-4336.
49. Harris IR, Farrell AM, Memon RA, et al. Expression and regulation of mRNA for putative fatty acid transport related proteins and fatty acyl CoA synthase in murine epidermis and cultured human keratinocytes. *J Invest Dermatol* **1998**: 111: 722-726.
50. Uchida Y. The role of fatty acid elongation in epidermal structure and function. *Dermatoendocrinol* **2011**: 3: 65-69.
51. Ohno Y, Suto S, Yamanaka M, et al. ELOVL1 production of C24 acyl-CoAs is linked to C24 sphingolipid synthesis. *Proc Natl Acad Sci U S A* **2010**: 107: 18439-18444.
52. Bonnart C, Deraison C, Lacroix M, et al. Elastase 2 is expressed in human and mouse epidermis and impairs skin barrier function in Netherton syndrome through filaggrin and lipid misprocessing. *J Clin Invest* **2010**: 120: 871-882.
53. Ishikawa J, Narita H, Kondo N, et al. Changes in the ceramide profile of atopic dermatitis patients. *J Invest Dermatol* **2010**: 130: 2511-2514.
54. Motta S, Monti M, Sesana S, et al. Abnormality of water barrier function in psoriasis. Role of ceramide fractions. *Arch Dermatol* **1994**: 130: 452-456.
55. Imokawa G, Abe A, Jin K, et al. Decreased level of ceramides in stratum corneum of atopic dermatitis: an etiologic factor in atopic dry skin? *J Invest Dermatol* **1991**: 96: 523-526.
56. Shahidullah M, Raffle EJ, Rimmer AR, et al. Transepidermal water loss in patients with dermatitis. *Br J Dermatol* **1969**: 81: 722-730.
57. Rajka G. Transepidermal water loss on the hands in atopic dermatitis. *Arch Dermatol Forsch* **1974**: 251: 111-115.
58. Jungersted JM, Scheer H, Mempel M, et al. Stratum corneum lipids, skin barrier function and filaggrin mutations in patients with atopic eczema. *Allergy* **2010**: 65: 911-918.
59. van Smeden J, Janssens M, Boiten WA, et al. Intercellular skin barrier lipid composition and organization in Netherton syndrome patients. *J Invest Dermatol* **2014**: 134: 1238-1245.
60. Motta S, Monti M, Sesana S, et al. Ceramide composition of the psoriatic scale. *Biochim Biophys Acta* **1993**: 1182: 147-151.
61. Motta S, Sesana S, Ghidoni R, et al. Content of the different lipid classes in psoriatic scale. *Arch Dermatol Res* **1995**: 287: 691-694.
62. van Smeden J, Janssens M, Gooris GS, et al. The important role of stratum corneum lipids for the cutaneous barrier function. *Biochim Biophys Acta* **2014**: 1841: 295-313.

63. Boguniewicz M, Alexis AF, Beck LA, et al. Expert Perspectives on Management of Moderate-to-Severe Atopic Dermatitis: A Multidisciplinary Consensus Addressing Current and Emerging Therapies. *J Allergy Clin Immunol Pract* **2017**: 5: 1519-1531.
64. Alanne S, Nermes M, Soderlund R, et al. Quality of life in infants with atopic dermatitis and healthy infants: a follow-up from birth to 24 months. *Acta Paediatr* **2011**: 100: e65-e70.
65. Slattery MJ, Essex MJ, Paletz EM, et al. Depression, anxiety, and dermatologic quality of life in adolescents with atopic dermatitis. *J Allergy Clin Immunol* **2011**: 128: 668-671.
66. van Valburg RW, Willemsen MG, Dirven-Meijer PC, et al. Quality of life measurement and its relationship to disease severity in children with atopic dermatitis in general practice. *Acta Derm Venereol* **2011**: 91: 147-151.
67. Palmer CN, Irvine AD, Terron-Kwiatkowski A, et al. Common loss-of-function variants of the epidermal barrier protein filaggrin are a major predisposing factor for atopic dermatitis. *Nat Genet* **2006**: 38: 441-446.
68. Bin L, Leung DY. Genetic and epigenetic studies of atopic dermatitis. *Allergy Asthma Clin Immunol* **2016**: 12: 52.
69. Gan SQ, McBride OW, Idler WW, et al. Organization, structure, and polymorphisms of the human profilaggrin gene. *Biochemistry* **1990**: 29: 9432-9440.
70. Manabe M, Sanchez M, Sun TT, et al. Interaction of filaggrin with keratin filaments during advanced stages of normal human epidermal differentiation and in ichthyosis vulgaris. *Differentiation* **1991**: 48: 43-50.
71. Irvine AD. Fleshing out filaggrin phenotypes. *J Invest Dermatol* **2007**: 127: 504-507.
72. Yoon NY, Wang HY, Jun M, et al. Simultaneous detection of barrier- and immune-related gene variations in patients with atopic dermatitis by reverse blot hybridization assay. *Clin Exp Dermatol* **2018**.
73. Noda S, Suarez-Farinas M, Ungar B, et al. The Asian atopic dermatitis phenotype combines features of atopic dermatitis and psoriasis with increased TH17 polarization. *The Journal of allergy and clinical immunology* **2015**: 136: 1254-1264.
74. Weidinger S, Novak N. Atopic dermatitis. *Lancet* **2016**: 387: 1109-1122.
75. Paller AS, Kabashima K, Bieber T. Therapeutic pipeline for atopic dermatitis: End of the drought? *The Journal of allergy and clinical immunology* **2017**: 140: 633-643.
76. Janssens M, van Smeden J, Gooris GS, et al. Increase in short-chain ceramides correlates with an altered lipid organization and decreased barrier function in atopic eczema patients. *J Lipid Res* **2012**: 53: 2755-2766.
77. Egawa G, Kabashima K. Multifactorial skin barrier deficiency and atopic dermatitis: Essential topics to prevent the atopic march. *The Journal of allergy and clinical immunology* **2016**: 138: 350-358.e351.
78. Oyoshi MK, He R, Kumar L, et al. Cellular and molecular mechanisms in atopic dermatitis. *Adv Immunol* **2009**: 102: 135-226.
79. Di Nardo A, Wertz P, Giannetti A, et al. Ceramide and cholesterol composition of the skin of patients with atopic dermatitis. *Acta Derm Venereol* **1998**: 78: 27-30.
80. Yamamoto A, Serizawa S, Ito M, et al. Stratum corneum lipid abnormalities in atopic dermatitis. *Arch Dermatol Res* **1991**: 283: 219-223.
81. Bleck O, Abeck D, Ring J, et al. Two ceramide subfractions detectable in Cer(AS) position by HPTLC in skin surface lipids of non-lesional skin of atopic eczema. *J Invest Dermatol* **1999**: 113: 894-900.
82. Pilgram GS, Vissers DC, van der Meulen H, et al. Aberrant lipid organization in stratum corneum of patients with atopic dermatitis and lamellar ichthyosis. *J Invest Dermatol* **2001**: 117: 710-717.
83. Boukes FS, Wiersma T, Cleveringa JP, et al. [Summary of the practice guideline 'Atopic dermatitis' (first revision) from the Dutch College of General Practitioners]. *Ned Tijdschr Geneeskd* **2007**: 151: 1394-1398.
84. de Vries CJ, de Witt-de Jong AW, Dirven-Meijer PC, et al. [The Dutch College of General Practitioners practice guideline 'Eczema']. *Ned Tijdschr Geneeskd* **2014**: 158: A8009.
85. Saeki H. Management of Atopic Dermatitis in Japan. *J Nippon Med Sch* **2017**: 84: 2-11.
86. Eichenfield LF, Tom WL, Berger TG, et al. Guidelines of care for the management of atopic dermatitis: section 2. Management and treatment of atopic dermatitis with topical therapies. *J Am Acad Dermatol* **2014**: 71: 116-132.
87. van Zuuren EJ, Fedorowicz Z, Christensen R, et al. Emollients and moisturisers for eczema. *Cochrane Database Syst Rev* **2017**: 2: CD012119.
88. Chong M, Fonacier L. Treatment of Eczema: Corticosteroids and Beyond. *Clin Rev Allergy Immunol* **2016**: 51: 249-262.
89. Coderch L, Lopez O, de la Maza A, et al. Ceramides and skin function. *Am J Clin Dermatol* **2003**: 4: 107-129.
90. Chiou YB, Blume-Peytavi U. Stratum corneum maturation. A review of neonatal skin function. *Skin Pharmacol Physiol* **2004**: 17: 57-66.
91. Haubrich KA. Role of Vernix caseosa in the neonate: potential application in the adult population. *AACN Clin Issues* **2003**: 14: 457-464.
92. Hoath SB, Pickens WL, Visscher MO. The

biology of vernix caseosa. *Int J Cosmet Sci* **2006**: 28: 319-333.
93. Pickens WL, Warner RR, Boissy YL, et al. Characterization of vernix caseosa: water content, morphology, and elemental analysis. *J Invest Dermatol* **2000**: 115: 875-881.
94. Rissmann R, Groenink HW, Weerheim AM, et al. New insights into ultrastructure, lipid composition and organization of vernix caseosa. *J Invest Dermatol* **2006**: 126: 1823-1833.
95. Hoeger PH, Schreiner V, Klaassen IA, et al. Epidermal barrier lipids in human vernix caseosa: corresponding ceramide pattern in vernix and fetal skin. *Br J Dermatol* **2002**: 146: 194-201.
96. Mikova R, Vrkoslav V, Hanus R, et al. Newborn boys and girls differ in the lipid composition of vernix caseosa. *PLoS One* **2014**: 9: e99173.
97. Oudshoorn MH, Rissmann R, van der Coelen D, et al. Development of a murine model to evaluate the effect of vernix caseosa on skin barrier recovery. *Exp Dermatol* **2009**: 18: 178-184.
98. Oudshoorn MH, Rissmann R, van der Coelen D, et al. Effect of synthetic vernix biofilms on barrier recovery of damaged mouse skin. *Exp Dermatol* **2009**: 18: 695-703.
99. Visscher MO, Barai N, LaRuffa AA, et al. Epidermal barrier treatments based on vernix caseosa. *Skin Pharmacol Physiol* **2011**: 24: 322-329.
100. Bautista MI, Wickett RR, Visscher MO, et al. Characterization of vernix caseosa as a natural biofilm: comparison to standard oil-based ointments. *Pediatr Dermatol* **2000**: 17: 253-260.

Part 1

Chapter 2

An ex vivo human skin model for studying skin barrier repair

Mogbekeloluwa O. Danso[1], Tineke Berkers[1], Arnout Mieremet[1,2], Farzia Hausil[1], Joke A. Bouwstra[1]

[1] Department of Drug Delivery Technology, Leiden Academic Centre for Drug Research, Leiden University, Leiden, 2333 CC, The Netherlands
[2] Department of Dermatology, Leiden University Medical Centre, Leiden, 2333 ZA, The Netherlands

Exp Dermatol. 2015 Jan;24(1):48-54

Abbreviations

aSmase	Acid-sphingomyelinase
BSA	Bovine serum albumin
CERs	Ceramides
CHOL	Cholesterol
FAs	Free fatty acids
FTIR	Fourier transform infrared spectroscopy
GBA	β-glucosylcerebrosidase
HPTLC	High performance thin layer chromatography
LPP	Long periodicity phase
MTT	Mid-point transition temperature
MUFAs	Mono-unsaturated free fatty acids
SAXD	Small angle X-ray diffraction
SC	Stratum corneum
SCD	Steroyl CoA desaturase
SPP	Short periodicity phase

Keywords

Skin barrier repair, stratum corneum, epidermal differentiation, lipid composition, lipid organization

Abstract

In the studies described in this paper, we introduce a novel *ex vivo* human skin barrier repair model. To develop such a model, we removed the upper layer of the skin, the stratum corneum (SC) by a reproducible cyanoacrylate stripping technique. After stripping the explants, they were cultured *in vitro* to allow the regeneration of the SC. We selected two culture temperatures 32˚C and 37˚C and a period of either 4 or 8 days.

Results show that after 8 days of culture, the explant generated SC at a similar thickness compared to native human SC. At 37˚C, the early and late epidermal differentiation program was executed comparably to native human skin with the exception of the barrier protein involucrin. At 32˚C, early differentiation was delayed, but the terminal differentiation proteins were expressed as in stripped explants cultured at 37˚C. Regarding the barrier properties, the SC lateral lipid organization was mainly hexagonal in the regenerated SC, whereas the lipids in native human SC adopt a more dense orthorhombic organization. In addition, the ceramide levels were higher in the cultured explants at 32˚C and 37˚C than in native human SC. In conclusion, we have selected the stripped *ex vivo* skin model cultured at 37˚C as a candidate model to study skin barrier repair since epidermal characteristics mimic more closely the native human skin than the *ex vivo* skin model cultured at 32˚C. Furthermore, the final product of the differentiation process, the SC, exhibits a very similar lipid composition as in native human skin. Potentially, this model can be used for testing formulations for skin barrier repair.

Introduction

The skin being the largest organ of the body (1.5m^2 in adults) provides protection for the body's interior against the external environment. The barrier function is mainly located in the outermost layer, the stratum corneum (SC).[1] The SC provides an excellent barrier against excessive water loss (inside-outside barrier) and penetration of pathogens and allergens through the skin (outside-inside barrier).[2,3] The SC is 10-15 μm thick with 15-20 corneocyte layers[4,5] and its organization has been described as "brick-and-mortar" structure.[6] The bricks represent the terminally differentiated corneocytes and the mortar the intercellular lipid matrix surrounding the corneocytes.[7,8] The SC lipid composition and organization plays an important role in the barrier function of the skin because the major pathway for penetration of molecules through the SC is via the SC lipid matrix.[9-11] The main lipid classes in native human SC are free fatty acids (FAs), ceramides (CERs) and cholesterol which form two lamellar phases. These include the short periodicity phase (SPP) and the long periodicity phase (LPP) with repeat distances of approximately 6 nm and 13 nm respectively.[12] Within the lipid lamellae, the lipids are mainly organized in a dense orthorhombic packing, although a fraction of lipids adopt a hexagonal packing.[13,14] Within the epidermal strata, tight junction (TJ) proteins are known to contribute to the inside-outside barrier. They form an intercellular barrier between the epidermal cells and function to control the selective movement of water and ions through the epidermis[15] and regulate cell proliferation and differentiation.[16,17] Atopic dermatitis (AD), dry skin conditions, 1st degree burns and sunburned skin are examples of skin conditions associated with an impaired skin barrier function.[18-20] In order to develop novel formulations or active components to enhance skin barrier repair, *in vitro* models are required. Currently, skin barrier repair is mainly studied in animals. This does not provide an optimal situation for translation into humans as the morphology in combination with stratum corneum properties of animal skin varies greatly from human skin.[21-23] Furthermore, removal of SC from animals results in stress and the use of animals in testing cosmetics products and ingredients have been banned in the European union since 2009. Consequently, the use of *in vitro* human skin barrier repair models can play an important role in screening formulations.[24-27]

Currently, no appropriate *in vitro* human skin models are available to study skin barrier repair. The available human skin equivalents may offer a possibility however, applying formulations can only be performed during generation of the human skin equivalents. This is very labor intensive and needs dedicated expertise. In addition, an impaired barrier induced by tape stripping cannot be performed with human skin equivalents, due to the poor epidermal/dermal adhesion.[28]

In the present study, we introduce an *ex vivo* human skin model to study skin barrier repair. Using a reproducible cyanoacrylate stripping technique to remove SC from *ex vivo* human skin, we investigated the regrowth of SC *in vitro* by characterizing the epidermal morphogenesis, differentiation, SC lipid composition and organization. Potentially, this skin barrier repair model can be used for optimizing formulations and active ingredients to study their effect on skin barrier repair. The results show that the stripped skin cultured for 8 days at body temperature (37°C) or skin temperature (32°C) has an actively proliferating and differentiating epidermis resulting in the regeneration of SC *in vitro.* In addition, the regenerated SC lipids are organized in crystalline lamellae

with the presence of the same SC lipid classes and subclasses as seen in native human SC, with some interesting differences.

Materials and methods

Stripping of SC with cyanoacrylate

Human breast skin was obtained from Caucasian skin donors (aged 25-42 years) after written informed consent and handled according to Declaration of Helsinki principles. The skin was dermatomed at 400 µm using a Padgett Electro Dermatome (Model B, Kansas city, KS, USA). 18 mm punch biopsies of the dermatomed skin were used as a control. 26 mm biopsies from the dermatomed skin were fixed into a custom made stripping device (see Supplementary Figure S1). A single droplet of preheated cyanoacrylate (Pattex Gold original, Henkel, Dusseldorf, Germany) at 40˚C was spread on a 20 mm diameter stainless steel cylinder preheated to 40˚C. The cylinder with cyanoacrylate was immediately placed on the skin. Standardized pressure was applied on the cylinder using a 2 kg weight. After 2 minutes the cylinder was removed in one stroke and in alternating directions to ensure even removal of the SC from the skin surface. This stripping procedure was repeated until the skin gave a glossy appearance indicating that most of the SC has been removed (4-5 strips were required to remove the stratum corneum). The unstripped skin at the border of the biopsy was removed using a scalpel, yielding stripped biopsies of 18 mm in diameter. From each donor, at least one stripped skin biopsy was used as control to analyze the number of corneocyte layers remaining on the stripped skin surface by safranin-O-red staining (described below). Stripped and non-stripped biopsies were cultured as described below.

Culture procedure

Non-stripped biopsies (served as controls) and stripped biopsies were washed thrice in sterile phosphate buffered saline (PBS, Braun, Melsungen, Germany) and placed in transwell filter inserts (Corning Life sciences, Amsterdam, Netherlands). The skin biopsies (referred to as explants) were cultured at air-liquid interface for 4 days or 8 days at 37˚C or 32˚C, 90% relative humidity and 7.3% CO_2. The culture medium contained DMEM and Ham's F12 (Invitrogen, The Netherlands) (3:1 v/v) supplemented with 0.5 µM hydrocortisone (Sigma), 1 µM isoproterenol (Sigma), 10 µM L-carnitine (Sigma), 10 mM L-serine (Sigma), 0.053 µM selenious acid (Johnson Matthey, Maastricht, The Netherlands), 0.5 µg/mL insulin (Sigma), 1 µM α-tocopherol acetate (Sigma), 1% penicillin/streptomycin, 25 mM vitamin C (Sigma) and a lipid mixture of 7 µM arachidonic acid (Sigma), 30 µM linoleic acid (Sigma) and 25 µM palmitic acid (Sigma). The medium was refreshed twice a week.

Safranin-O-red staining

The cultured skin explants and the non-cultured (stripped and non-stripped) control biopsies were cryofixed in Tissue-Tek O.C.T.™ (Sakura Finetek Europe B.V., The Netherlands). The sections were stained with Safranin-O as described.[29] Cryofixed skin of 5 µm thickness were stained with 1% (w/v) Safranin-O solution (Sigma) for one minute and thereafter incubated in 2% (w/v) KOH solution for 30 minutes to swell the corneocytes. Five microscopic images (from three donors) per explant or biopsy were taken at 64x magnification.

Morphology and immunohistochemistry

The skin explants and controls were embedded in paraffin, cut at 5 µm thickness and stained with haematoxylin (2 mg/ml) and eosin (4 mg/ml) for morphological analysis. Immunohistochemical analysis of keratin 10, filaggrin, loricrin, involucrin, Ki67, caspase 3, keratin 6, β-glucosylcerebrosidase, steroyl-CoA desaturase and acid-sphingomyelinase expression was also performed on 5 µm paraffin sections. The primary and secondary antibodies are listed in Supplementary Table S1. For further details see supplementary materials and methods.

Lipid extraction and analysis

SC was isolated from the skin explants using trypsin digestion as described by De Jager et al.[30] Briefly, the explants were incubated overnight in 0.1% trypsin solution at 4˚C followed by incubation at 37˚C for 1 hour after which the SC could be peeled off. Lipid extracts from 2 explants per condition, were pooled for lipid analysis. The SC lipids were extracted by a modified Bligh and Dyer procedure.[31,32] Briefly, liquid-liquid extraction from native human SC and cultured stripped and non-stripped explants was performed using 3 different ratios of a chloroform/methanol/water mixture (1/2/0.5;1/1/0;2/1/0). A 0.25 M KCl solution was added to extract the polar lipids. The extracts were dried under a stream of nitrogen gas at 40˚C and reconstituted in chloroform/methanol (2:1). High performance thin layer chromatography (HPTLC): SC lipid composition was quantitatively analyzed by HPTLC[33] described in detail in the supplementary materials and methods.

Fourier transformed infra-red spectroscopy (FTIR) and small angle X-ray diffraction (SAXD)

FTIR and SAXD measurements were performed as described earlier.[34] The SC sheets were hydrated for 24 hours over a 27% NaBr solution prior to measurements. FTIR spectra were collected with a Varian 670-IR FTIR spectrometer (Agilent technologies, CA, USA), containing a broad-band mercury cadmium telluride detector, cooled with liquid nitrogen. SAXD patterns were detected with a Frelon 2000 CCD detector at room temperature for a period of 10 min using a microfocus as described by Bras et al.[35] 3 samples per condition were measured.

Statistical analysis

All statistical outcomes were determined using GraphPad Prism software and a two-tailed student's t-test to analyze the data.

Results

Stripped ex vivo skin generates SC in vitro

The skin was placed in a customized stripping device and using a customized metal cylinder coated with cyanoacrylate, the SC was removed sequentially (see Supplementary Figure S1). The stripping procedure reduced the SC layers in the *ex vivo* skin explant from 13 ± 2 layers to 4 ± 2 layers (Figure 1A,B) as determined by counting the number of corneocyte layers from five different spots of safranin-O stained sections. No difference was observed between the amount of SC removed in the central or boundary areas of the stripped skin. However, less SC at the furrows in the skin was removed compared to the flatter parts of the skin as described previously.[36] After the removal of the SC, these biopsies were cultured to generate SC. After 4 days of culturing at 37˚C, there was no significant increase in SC layers. However, after 8 days of culturing at 37˚C, the SC layers of the stripped skin increased to 10 ± 3 layers (Figure 1B). Decreasing the culture temperature to 32˚C resulted in similar observations. After 4 days of culture no significant increase in the number of corneocyte layers was observed, but after extending to 8 days, the number of corneocyte layers increased to 10 ± 2 layers. Non-stripped controls were also cultured in the incubator for 4 and 8 days at 37˚C and 32˚C. After 8 days these non-stripped controls generated some additional corneocyte layers, but this increase was not as pronounced as with the stripped skin (Figure 1B). Since our goal was to develop a skin barrier repair model, further analysis was performed using skin explants cultured for 8 days as the number of SC layers generated was closer to that in native human skin.

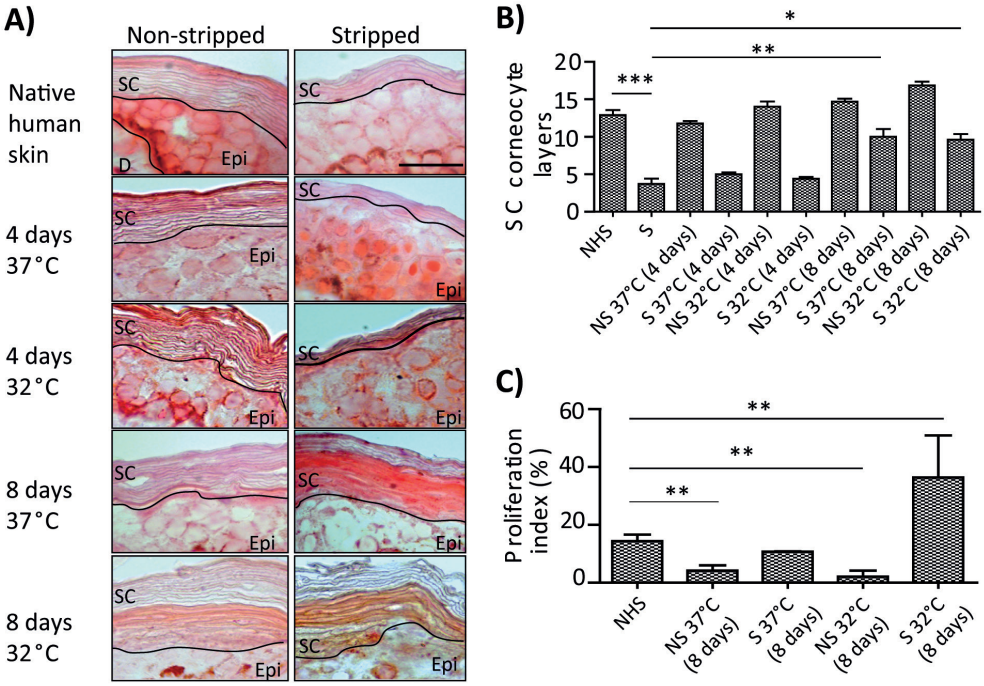

Figure 1. Stratum corneum (SC) layers and proliferation index in cultured *ex vivo* skin. A) Swollen SC cell layers visualized by safranin-O staining. **B)** The number of corneocyte layers was counted from safranin-O stained sections. The cyanoacrylate stripping procedure was efficient to remove the SC which was generated after 8 days of culturing at 37˚C and 32˚C. **C)** Proliferation index of keratinocytes determined by Ki67 staining. The non-stripped skin explants cultured at 37˚C and 32˚C show decreased epidermal proliferation. At 37˚C, the stripped explants show similar proliferation as in native human skin and at 32˚C, a 2x higher proliferation than native human skin. Data represent mean ± SEM of four donors. Five microscopic pictures were taken per explant analysis. Proliferation index was calculated from the number of Ki67 positive basal cells out of 100 counted basal cells from five microscopic images. Scale bar: 30 µm, 64x magnification. NHS: native human skin, S: stripped, NS: non-stripped, Epi: viable epidermis, SC: stratum corneum, D: dermis *p<0.05, **p<0.01, ***p<0.001

Skin explants express epidermal differentiation proteins in vitro

Since SC is generated by cultured stripped skin explants, we examined their epidermal proliferation, morphology and epidermal differentiation. The proliferation index was calculated as the percentage of proliferating cells in the stratum basale by Ki67 staining. The proliferation index was drastically reduced in the non-stripped skin explants after 8 days of culture at 37˚C and 32˚C. In stripped explants cultured at 37˚C, the proliferation was similar to native human skin while at 32˚C proliferation was 2 fold higher compared to the native human skin (Figure 1C).

The stripped and non-stripped skin explants cultured at 37˚C and 32˚C show a normally differentiated epidermis. However in stripped explants cultured at 32˚C, the terminal differentiation is not completely executed demonstrated by nuclei remnants in the SC (indicated by arrows, Figure 2).

The early and terminal epidermal differentiation program was correctly executed

in explants cultured at 37˚C with the exception of involucrin and to a lesser extent filaggrin. Similar to control skin, keratin 10 (K10) was expressed in all suprabasal layers of the epidermis while loricrin and filaggrin were expressed in the stratum granulosum. However, the number of cell layers positive for filaggrin increased to 2-3 layers in both the stripped and non-stripped explants compared to 1 layer in control skin. Conversely, involucrin expression in the skin explants was observed in all epidermal layers in contrast to the stratum granulosum in native human skin.

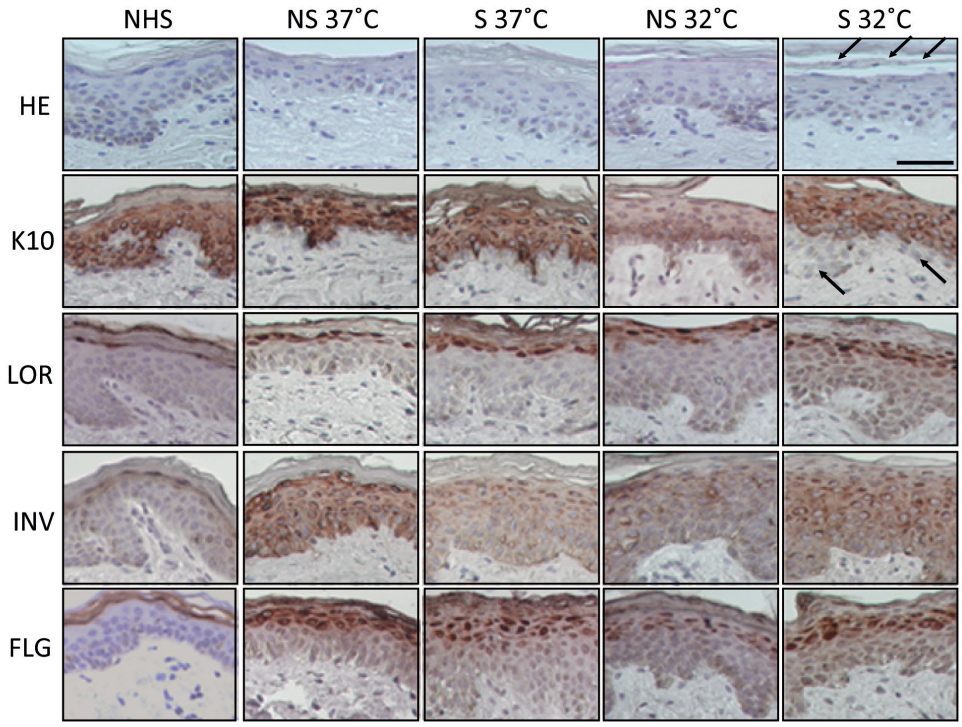

Figure 2. Morphology and epidermal differentiation in native human skin compared to non-stripped and stripped explants cultured for 8 days. Haematoxylin and eosin staining for morphological overview and immunohistochemical staining for keratin 10 (K10), Loricrin (LOR), involucrin (INV) and filaggrin (FLG). The stripped and non-stripped explants still display a differentiated epidermis at 37˚C but at 32˚C parakeratosis is observed mainly in the SC of the stripped explants (indicated by arrows). At 37˚C, the non-stripped and the stripped explants express keratin 10, loricrin and filaggrin with similar localization as in the native human skin. The expression of involucrin in stripped and non-stripped explants was shifted to all epidermal layers rather than in the stratum granulosum. Non-stripped and the stripped explants cultured at 32˚C also express filaggrin and loricrin as in native human skin however, the expression of keratin 10 is delayed and involucrin is expressed in all epidermal layers as with explants cultured at 37˚C. Scale bar: 25 µm. Images are representative of results consistently observed in three different skin donors. NHS: native human skin, S: stripped, NS: non-stripped

When the culture temperature was reduced to 32˚C, K10 expression was delayed in the stripped explants as 2-4 epidermal layers were negative for K10 expression (indicated by an arrow, Figure 2). Loricrin and filaggrin were expressed as in native human skin in both stripped and non-stripped skin explants. However, the number of cell layers positive for filaggrin was also increased in both the stripped and non-stripped explants compared to control skin. In addition, involucrin was expressed in all epidermal layers in stripped and non-stripped explants cultured at 32˚C (Figure 2).
Analysis of keratin 6 (K6) expression in the explants showed that native human skin and non-stripped explants show little or no expression of K6 in the suprabasal layers of the epidermis. Conversely, stripped explants cultured at both temperatures showed a marked increase of K6 expression in the epidermis (Supplementary Figure S5). In addition, the expression of caspase 3 in the stripped and non-stripped explants cultured at 32˚C and 37˚C was very similar to native human skin shown by expression of caspase 3 in the entire epidermis in all conditions (Supplementary Figure S5).

In vitro generated SC from stripped skin shows a similar lamellar lipid organization as native human SC but differences in the lateral packing

The SC lipid properties of the cultured explants were examined in relation to native human SC (the control). The lateral packing was examined using the CH_2 rocking vibrations of the lipid chains in the FTIR spectra from 0˚C-90˚C. A hexagonal lipid organization is portrayed by a single peak at 719 cm^{-1} and an orthorhombic lipid packing by two vibrations at 719 cm^{-1} and 730 cm^{-1} in the spectrum. At 0˚C, the lipids from native human SC adopt an orthorhombic lateral packing demonstrated by two strong contours at 719 cm^{-1} and 730 cm^{-1} (Figure 3A). Around 42.5˚C ± 2.5˚C, the orthorhombic packing is converted into an hexagonal packing. This is characterized by a transition from a doublet to a singlet at 719 cm^{-1}. The non-stripped skin explants cultured at 37˚C show an orthorhombic lateral packing until 40.5˚C ± 5.3˚C (Figure 3B). However, the stripped explants cultured at both temperatures show a strong peak at 719 cm^{-1} and a small peak at 730 cm^{-1} at 0˚C (Figure 3C,E). The orthorhombic packing is only present until 20.7˚C ± 1.2˚C and 29.3 ± 4.2˚C at 37˚C and 32˚C, respectively i.e. the lipids are mainly organized in a hexagonal packing with a small population of lipids still forming an orthorhombic packing.
The conformational order of the lipids was also investigated using the thermotropic behaviour of the CH_2 symmetric stretching frequencies in the spectrum. In a crystalline organization (orthorhombic or hexagonal packing) the conformational order is high with CH_2 symmetric stretching frequencies < 2850 cm^{-1}. In a disordered organization (liquid phase), the CH_2 symmetric stretching frequencies are ≥ 2852 cm^{-1}. Since the order-disorder transition occurs within a temperature range, the mid-point temperature at which the lipid domains change from an ordered state to a disordered liquid state was determined[37] i.e. "Mid-point Transition Temperature" (MTT). The results show that the MTT of the lipids in the regenerated SC of the stripped skin explants (37˚C and 32˚C) is significantly lower than in non-stripped cultured controls and native human SC ($p<0.05$, Figure 3F). The CH_2 stretching frequency at skin temperature (32˚C) was also increased in the stripped skin explants cultured at 37˚C compared to the non-stripped explants ($p<0.05$, Supplementary Figure S2). This indicates an increased

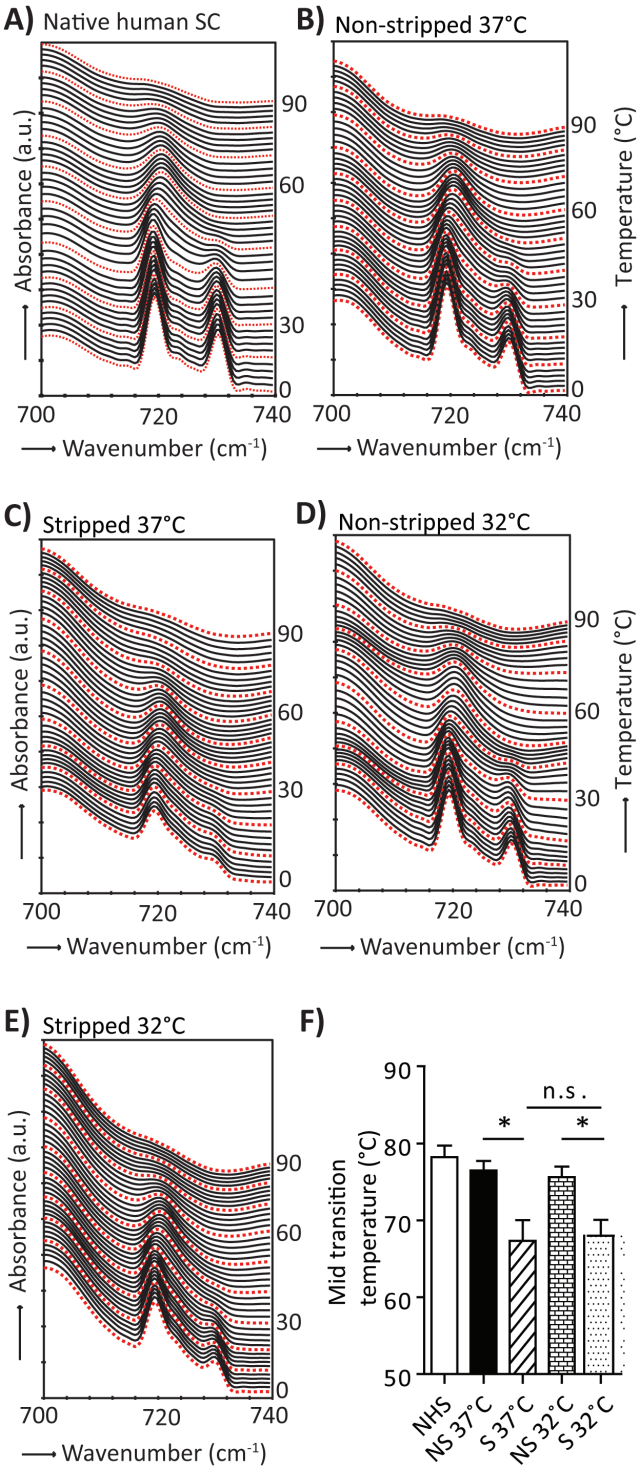

Figure 3. FTIR spectra showing the CH_2 rocking vibrations in the spectra of the stratum corneum (SC) of generated stripped explants as a function of temperature (0°C-90°C). **A)** Native human SC and **B)** non-stripped explants cultured at 37°C and **D)** 32°C, show an orthorhombic lateral organization. The peak intensity of the 730 cm^{-1} band is reduced in stripped explants cultured at **C)** 37°C and **E)** 32°C suggesting a higher population of lipids adopting a hexagonal organization. **F)** Mid-point transition temperature (MTT). Data represents mean ± SEM from three donors, n.s.: not significant, *p<0.05, NHS: native human skin, S: stripped, NS: non-stripped

conformational disorder in the regrown SC of the stripped explants.
The lamellar lipid organization was also examined in the stripped and non-stripped explants in relation to native human skin using SAXD. In native human SC, the diffraction profiles show three diffraction peaks indicating the 1st, 2nd and 3rd order diffraction peak of the LPP (depicted by 1, 2 and 3,) and crystalline cholesterol domains, indicated by an asterisk (*). Peak "2" in native human skin represents both LPP (2nd order) and SPP (1st order). The stripped and non-stripped explants cultured at 37˚C show a very similar profile, and exhibit a 1st - 3rd order diffraction peak of the LPP and crystalline cholesterol (Supplementary Figure S3). As the 1st order peak of the SPP is partly obscured by the 2nd order of the LPP, the presence of the SPP should induce a broadening of this peak. However, we could not obtain evidence for this broadening and thus the presence of this phase. In addition, the explants cultured at 32˚C show similar diffraction profiles as in explants cultured at 37˚C (data not shown).

Generated SC from stripped explants contain the main SC lipid classes

The SC generated by the explants after stripping contains the main SC lipid classes CERs, FAs and cholesterol with some changes in the distribution of these lipid classes as analyzed by HPTLC. The generated SC at 37˚C and 32˚C showed significantly higher CER levels respectively compared to native human skin (Figure 4B, $p=0.03$ and $p=0.06$ respectively, for relative values see Supplementary Figure S4). In addition, the non-stripped controls cultured at both temperatures show a similar trend (Figure 4B, $p=0.04$ and $p=0.07$, for relative values see Supplementary Figure S4).
All the CER subclasses detectable by HPTLC in native human skin were present in the generated SC cultured at both temperatures (Figure 4C, for relative values see Supplementary Figure S4). However, some differences exist in the CER distribution of the cultured explants in relation to native human SC. At 37˚C the levels of CER NS, EOH and AS/NH in regenerated SC were significantly increased compared to native human SC ($p<0.01$, $p<0.05$). Similarly, at 32˚C the regrown SC showed significant increase in CER NS and AS/NH ($p<0.01$, $p<0.05$). The non-stripped explants cultured at 37˚C and 32˚C also have significantly more CER EOH and CER NS respectively than native human skin.
We further examined the expression of β-glucosylcerebrosidase (GBA) and acid-sphingomyelinase (aSmase) involved in the synthesis of CERs from CER precursors. The expression of aSmase in the human epidermis shows a gradient from the basal layer to the granular layer with the highest expression seen in the granular layer. In all cultured explants, the gradient is lost and the expression of aSmase is similar in most epidermal layers (Figure 4D). In native human epidermis, the expression of GBA is localized in the interface between the granular layer and SC. In explants cultured at 32˚C or at 37˚C, the localization of GBA expression is the same as native human epidermis.
Changes in unsaturated FA levels have been shown to be involved in SC lipid organization. Therefore, we also examined the expression of steroyl CoA desaturase (SCD) which mono-unsaturates FAs. SCD expression is seen in the basal layer of the epidermis in native human skin but in non-stripped and stripped explants cultured at 32˚C and 37˚C the expression of SCD is extended to all epidermal layers (Figure 4D).

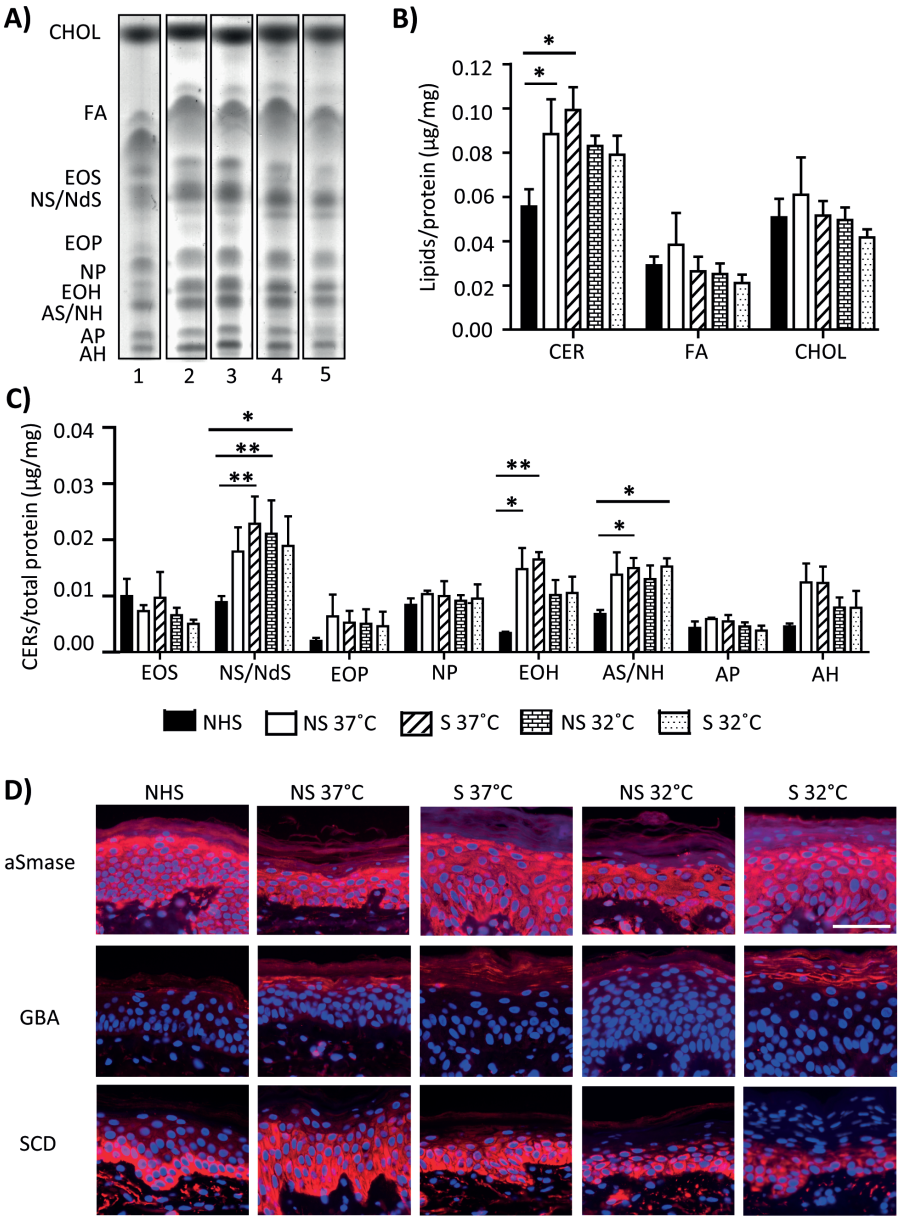

Figure 4. Stratum corneum (SC) lipid composition and epidermal expression of lipid synthesis enzymes in cultured *ex vivo* skin. A) The lipids were separated according to the solvent system provided in Supplementary Table S2. 1-Native human skin, 2-Non-stripped 37˚C, 3-Stripped 37˚C, 4-Non-stripped 32˚C, 5-Stripped 32˚C. **B)** Absolute levels of cholesterol (CHOL), free fatty acids (FA) and ceramides (CERs). **C)** Absolute CER subclasses in cultured *ex vivo* skin. The SC from the non-stripped and stripped explants contains all CER subclasses in native human SC which are visible by high performance thin layer chromatography (HPTLC). **D)** Immunohistochemical analysis of acid-sphingomyelinase (aSmase), β-glucosylcerebrosidase (GBA) and steroyl CoA desaturase (SCD). Data represents mean ± SEM from three donors. Scale bar 25 µm. NHS: native human skin, S: stripped, NS: non-stripped

Discussion

The aim of this study was to establish a human skin model to study skin barrier repair by i) removal of SC from *ex vivo* skin and ii) generation of the SC during *in vitro* culturing of stripped skin. We established a reproducible method of SC removal using a cyanoacrylate stripping technique which served as a starting point. After 8 days of culturing the stripped explants at 32˚C and 37˚C, the number of SC layers regrown was similar to the SC layers before stripping. The recovery of SC to control thickness after stripping *in vivo* ranges from 3-6 days in the arm and leg.[38] In addition, barrier recovery (calculated by recovery of transepidermal water loss values to baseline) after SC removal by tape-stripping in human facial skin reaches ~90% after 1 week and 100% recovery at 4 weeks.[39] Duplan et al. presents an *ex vivo* human skin model for irritation/repair using SDS and vasointestinal peptide. In order to restore native epidermal features, the skin is treated with hydroxydecine in culture. Our present study examines skin barrier repair by removal of stratum corneum and culturing without the addition of a formulation.

Epidermal morphology and SC layers at the end of the 8 days culture period at both temperatures are similar to that of native human skin. However, the stripped explants cultured at skin temperature (32˚C) exhibit parakeratotic epidermis, a feature also observed after repeated tape-stripping *in vivo*.[40] This may occur from increased proliferation induced by stripping as nuclei are observed only in the lower layers of the SC. Parakeratosis is associated with a hyper proliferative epidermis, delayed K10 expression, increased involucrin expression and increased number of epidermal cell layers positive for filaggrin.[40,41] All of these characteristics are observed in stripped skin explants cultured at 32˚C. Stripped explants cultured at 37˚C also display increased filaggrin and involucrin expression, but very importantly no parakeratosis and no delayed expression of K10 is observed.

Proliferation (Ki67 expression) of stripped explants cultured at 37˚C is similar to native human skin but at 32˚C, proliferation is double that of native human skin. However, the number of SC layers generated after 8 days are similar at both temperatures. This may occur from the changes in proliferation index at 4 and 8 days of culture in the explants, as observed in a pilot study. At 4 days of culture, proliferation index in stripped explants cultured at 32˚C is around 1% and 30% at 37˚C (data not shown). However, after 8 days, the proliferation index is ~40% at 32˚C and 12% at 37˚C. This data suggests the increase in proliferation in stripped explants as a response to the SC removal is delayed at 32˚C compared to 37˚C. In addition, the number of corneocytes layers in the SC is an accumulative value and depends on the proliferation rate during the whole culturing period.

The SC lipid properties in the stripped explants show several similarities to native human SC. The SC from the stripped and non-stripped explants cultured at 37˚C contains the main SC lipid classes. However, we observe a significant increase in the absolute level of CERs in the explants cultured at 37˚C and 32˚C. Increase of CER levels also occurs in other full-thickness and epidermal human skin equivalents.[42] Furthermore, when focusing on the CER subclasses, 10 different CER subclasses can be detected, of which CER NdS/NS and CER AS/NH cannot be separated. The composition of these CER subclasses is very similar to that in native human skin, although some important

differences are also noticed. The increase in the level of CERs was accompanied by a stronger staining for aSmase suggesting its role in the increased CER levels. ASmase catalyzes the conversion of sphingomyelin to ceramides. Sphingomyelin is a precursor of CER NS and AS[43,44] and both are increased by approximately 2-3 fold in the cultured explants compared to native human SC. The change in environmental conditions and barrier disruption induces stress in keratinocytes. This may result in increased CERs via sphingomyelinases and up-regulation of the activity of serine palmitoyl-transferase and/or ceramide synthases in *de novo* CER synthesis.[45,46]

Disruption of the SC also results in the loss of the epidermal calcium gradient which is crucial for differentiation.[47,48] The loss of calcium gradient affects the expression of epidermal differentiation proteins including filaggrin and involucrin and may also contribute to the changes in involucrin and filaggrin expression in the cultured skin explants.[49,50] In non-stripped skin, we still observe increased CER levels and altered involucrin expression although there is no barrier disruption. The exact mechanism responsible for these changes in non-stripped explants remains unknown.

SC lipids generated by the stripped explants adopt mainly a hexagonal organization as opposed to an abundant orthorhombic organization in native human SC. The hexagonal lateral organization is also observed in epidermal or full thickness human skin equivalents.[51] In these models an increased relative level of MUFAs was detected, which may be responsible for the abundant hexagonal packing. [42,51] Using lipid model systems we observed indeed that increased levels of MUFA enhances the formation of the hexagonal lateral packing.[52] Therefore, the hexagonal lipid organization in the generated SC in the explants may be attributed to an increased level of MUFAs resulting from increased SCD expression.

Some features of the cultured stripped skin can be observed in barrier related skin diseases such as increase in involucrin expression, CER NS, AS and hexagonal lipid organization.[53-56] However, there are more features which do not resemble diseased skin such e.g. increased CER EOS, similar levels of CER NP and filaggrin, loricrin expression as in native skin etc. This suggests that the cultured stripped skin cannot be used as a diseased skin model.

We suggest that culture of cyanoacrylate stripped skin explants provides a potential model to study i) skin barrier repair *ex vivo* and ii) investigating the effect of culture medium composition and environmental conditions during culture on the restoration of the skin barrier. Firstly, the SC lipid properties in regrown SC bear some aspects observed with altered skin barrier function[56-58] including reduced orthorhombic lipid organization and increased lipid conformational disorder of SC lipids. The presence of these characteristics in the cultured stripped explants can provide a system where formulations can be tested to enhance skin barrier repair.

Secondly, in the development of 3D *in vitro* skin models, no human skin equivalent fully mimics the SC lipid properties of native human skin.[51,59,60] Our model shows some advantages over the available human skin equivalents when applied to optimization of culture conditions to mimic native human SC properties *in vitro*. This is because the culture period is shorter (14-21 days for human skin equivalents) and does not require cell isolation and seeding which saves time and is less labor intensive. It is also possible to examine inter-donor changes in these cultures with human skin.

In conclusion, the removal of SC from *ex vivo* skin and culture for 8 days at 37°C

generates an *ex vivo* human skin model which possesses various similarities in epidermal properties to native human skin than at 32°C. Therefore this model has the potential to be used in studying skin barrier repair.

Acknowledgements

The authors thank the personnel at DUBBLE beam line (BM26), ESRF for assisting with X-ray measurements. This research was financially supported by Dutch Technology Foundation STW (grant no. 12400).

Author contributions

MOD, TB and JAB wrote the manuscript. MOD, TB, AM and FH performed the research. Data was analyzed by MOD, TB, AM and FH.

Author disclosure statement

The authors declare no conflicts of interest

References

1. Burton RF. Estimating body surface area from mass and height: theory and the formula of Du Bois and Du Bois. *Ann Hum Biol* **2008**: 35: 170-184.
2. Proksch E, Brandner JM, Jensen J-M. The skin: an indispensable barrier. *Exp Dermatol* **2008**: 17: 1063-1072.
3. Madison KC. Barrier Function of the Skin: "La Raison d'Etre" of the Epidermis. *J Investig Dermatol* **2003**: 121: 231-241.
4. Holbrook KA, Odland GF. Regional differences in the thickness (cell layers) of the human stratum corneum: an ultrastructural analysis *J Investig Dermatol* **1974**: 62: 415-422.
5. Blair C. Morphology and thickness of the human stratum corneum *Br J Dermatol* **1968**: 80: 430-436.
6. Michaels AS, Chandrasekaran SK, Shaw JE. Drug permeation through human skin: Theory and invitro experimental measurement. *AIChE Journal* **1975**: 21: 985-996.
7. Elias PM. Epidermal Lipids, Barrier Function, and Desquamation. *J Invest Dermatol* **1983**: 80: 44s-49s.
8. Elias P. Epidermal lipids, membranes, and keratinization. *Int J Dermatol* **1981**: 20: 1-19.
9. Bouwstra JA, Ponec M. The skin barrier in healthy and diseased state. *Biochim Biophys Acta - Biomembranes* **2006**: 1758: 2080-2095.
10. Williams ML, Elias PM. The extracellular matrix of stratum corneum: role of lipids in normal and pathological function. *Critical reviews in therapeutic drug carrier systems* **1987**: 3: 95-122.
11. Johnson ME, Blankschtein D, Langer R. Evaluation of solute permeation through the stratum corneum: Lateral bilayer diffusion as the primary transport mechanism. *J Pharm Sci* **1997**: 86: 1162-1172.
12. Bouwstra J, Gooris GS, van der Spek J, et al. Structural investigations of human stratum corneum by small-angle X-ray scattering. *J Invest Dermatol* **1991**: 97: 1005-1012.
13. Bouwstra J, Pilgram G, Gooris G, et al. New Aspects of the Skin Barrier Organization. *Skin Pharmacol Physiol* **2001**: 14(suppl 1): 52-62.
14. Damien F, Boncheva M. The Extent of Orthorhombic Lipid Phases in the Stratum Corneum Determines the Barrier Efficiency of Human Skin In Vivo. *J Invest Dermatol* **2009**: 130: 611-614.
15. Anderson JM, Van Itallie CM. Physiology and function of the tight junction. *Cold Spring Harbor perspectives in biology* **2009**: 1: a002584.
16. Aijaz S, Balda MS, Matter K. Tight junctions: molecular architecture and function. *Int Rev Cytol* **2006**: 248: 261-298.
17. Schneeberger EE, Lynch RD. The tight junction: a multifunctional complex. *Am J Physiol Cell Physiol* **2004**: 286: C1213-1228.
18. Tupker RA, Pinnagoda J, Coenraads PJ, et al. Susceptibility to irritants: role of barrier function, skin dryness and history of atopic dermatitis. *Br J Dermatol* **1990**: 123: 199-205.
19. Elias PM, Hatano Y, Williams ML. Basis for the barrier abnormality in atopic dermatitis: Outside-inside-outside pathogenic mechanisms. *J Allergy Clin Immunol* **2008**: 121: 1337-1343.
20. Church D, Elsayed S, Reid O, et al. Burn Wound Infections. *Clin Microbiol Rev* **2006**: 19: 403-434.
21. Elias. PM, Feingold. KR, eds. Skin barrier. New York: Taylor & francis Group: 2006.
22. Caussin J, Gooris GS, Janssens M, et al. Lipid organization in human and porcine stratum corneum differs widely, while lipid mixtures with porcine ceramides model human stratum corneum lipid organization very closely. *Biochimica et biophysica acta* **2008**: 1778: 1472-1482.
23. Mojumdar EH, Kariman Z, van Kerckhove L, et al. The role of ceramide chain length distribution on the barrier properties of the skin lipid membranes. *Biochimica et biophysica acta* **2014**: 1838: 2473-2483.
24. Ehrlich HP. Understanding experimental biology of skin equivalent: from laboratory to clinical use in patients with burns and chronic wounds. *The American Journal of Surgery* **2004**: 187: S29-S33.
25. Bello Y, Falabella A, Eaglstein W. Tissue-Engineered Skin. *Am J Clin Dermatol* **2001**: 2: 305-313.
26. Garlick JA. Engineering Skin to Study Human Disease – Tissue Models for Cancer Biology and Wound Repair. In: Lee K, Kaplan D, eds. Tissue Engineering II: Springer Berlin Heidelberg, 2007: 207-239.
27. Supp DM, Boyce ST. Engineered skin substitutes: practices and potentials. *Clin Dermatol* **2005**: 23: 403-412.
28. Groeber F, Holeiter M, Hampel M, et al. Skin tissue engineering — In vivo and in vitro applications. *Adv Drug Delivery Rev* **2011**: 63: 352-366.
29. Oudshoorn MHM, Rissmann R, Van Der Coelen D, et al. Development of a murine model to evaluate the effect of vernix caseosa on skin barrier recovery. *Experimental Dermatology* **2009**: 18: 178-184.
30. de Jager M, Groenink W, Bielsa i Guivernau R, et al. A Novel In vitro Percutaneous Penetration Model: Evaluation of Barrier Properties with & P-Aminobenzoic Acid and Two of Its

Derivatives. *Pharm Res* **2006**: 23: 951-960.
31. Bligh EG, Dyer WJ. A rapid method of total lipid extraction and purification. *Can J Biochem Physiol* **1959**: 37: 911-917.
32. Thakoersing VS, Ponec M, Bouwstra JA. Generation of human skin equivalents under submerged conditions-mimicking the in utero environment. *Tissue Eng Part A* **2009**: 16: 1433-1441.
33. Ponec M, Weerheim A, Lankhorst P, et al. New acylceramide in native and reconstructed epidermis. *J Invest dermatol* **2003**: 120: 581-588.
34. Thakoersing V, Gooris G, Mulder A, et al. Unraveling barrier properties of three different in-house human skin equivalents. *Tissue Eng Part C: Methods* **2012** 18: 1-11.
35. Bras W, Dolbnya IP, Detollenaere D, et al. Recent experiments on a small-angle/wide-angle X-ray scattering beam line at the ESRF. *J Appl Crystallogr* **2003**: 36: 791-794.
36. van der Molen RG, Spies F, van 't Noordende JM, et al. Tape stripping of human stratum corneum yields cell layers that originate from various depths because of furrows in the skin. *Arch Dermatol Res* **1997**: 289: 514-518.
37. Thakoersing VS, Danso MO, Mulder A, et al. Nature versus nurture: does human skin maintain its stratum corneum lipid properties in vitro? *Exp Dermatol* **2012**: 21: 865-870.
38. Bargo PR, Walston ST, Chu M, et al. Non-invasive assessment of tryptophan fluorescence and confocal microscopy provide information on skin barrier repair dynamics beyond TEWL. *Exp Dermatol* **2013**: 22: 18-23.
39. Gorcea M, Hadgraft J, Lane ME, et al. In vivo barrier challenge and long-term recovery in human facial skin. *Int J Cosmet Sci* **2013**: 35: 250-256.
40. Gerritsen MJP, Erp PEJ, Vlijmen-Willems IMJJ, et al. Repeated tape stripping of normal skin: a histological assessment and comparison with events seen in psoriasis. *Arch Dermatol Res* **1994**: 286: 455-461.
41. Harrison CA, Layton CM, Hau Z, et al. Transglutaminase inhibitors induce hyperproliferation and parakeratosis in tissue-engineered skin. *Br J Dermatol* **2007**: 156: 247-257.
42. Thakoersing V, van Smeden J, Mulder A, et al. Increased Presence of Monounsaturated Fatty Acids in the Stratum Corneum of Human Skin Equivalents. *J Invest Dermatol* **2013**: 133: 59-67.
43. Gatt S. Enzymic Hydrolysis and Synthesis of Ceramides. *J Biol Chem* **1963**: 238: PC3131-PC3133.
44. Uchida Y, Hara M, Nishio H, et al. Epidermal sphingomyelins are precursors for selected stratum corneum ceramides. *J Lipid Res* **2000**: 41: 2071-2082.
45. Nikolova-Karakashian MN, Rozenova KA. Ceramide in Stress Response. In: Chalfant C, Poeta M, eds. Sphingolipids as Signaling and Regulatory Molecules: Springer New York, 2010: 86-108.
46. Uchida Y. Ceramide signaling in mammalian epidermis. *Biochim Biophys Acta (BBA) - Molecular and Cell Biology of Lipids* **2014**: 1841: 453-462.
47. Menon GK, Elias PM, Feingold KR. Integrity of the permeability barrier is crucial for maintenance of the epidermal calcium gradient. *Br J Dermatol* **1994**: 130: 139-147.
48. Menon GK, Elias PM, Lee SH, et al. Localization of calcium in murine epidermis following disruption and repair of the permeability barrier. *Cell Tissue Res* **1992**: 270: 503-512.
49. Vicanová J, Boelsma E, Mommaas A, et al. Normalization of epidermal calcium distribution profile in reconstructed human epidermis is related to improvement of terminal differentiation and stratum corneum barrier formation. *J Invest Dermatol* **1998**: 111: 97-106.
50. Torma H, Lindberg M, Berne B. Skin Barrier Disruption by Sodium Lauryl Sulfate-Exposure Alters the Expressions of Involucrin, Transglutaminase 1, Profilaggrin, and Kallikreins during the Repair Phase in Human Skin In Vivo. *J Invest Dermatol* **2007**: 128: 1212-1219.
51. Thakoersing. VS, Gooris. GS, Mulder. A, et al. Unraveling Barrier Properties of Three Different In-House Human Skin Equivalents. *Tissue Eng Part C: Methods* **2012**: 18: 1-11.
52. Mojumdar EH, Helder RWJ, Gooris G, et al. Monounsaturated fatty acids reduce the barrier of stratum corneum lipid membranes by enhancing the formation of a hexagonal lateral packing. *Langmuir* **2014**: 30: 6534-6543.
53. Chen J-Q, Man X-Y, Li W, et al. Regulation of Involucrin in Psoriatic Epidermal Keratinocytes: The Roles of ERK1/2 and GSK-3□. *Cell Biochem Biophys* **2013**: 66: 523-528.
54. Jensen J-M, Folster-Holst R, Baranowsky A, et al. Impaired Sphingomyelinase Activity and Epidermal Differentiation in Atopic Dermatitis. *J Investig Dermatol* **2004**: 122: 1423-1431.
55. Imokawa G, Abe A, Jin K, et al. Decreased Level of Ceramides in Stratum Corneum of Atopic Dermatitis: An Etiologic Factor in Atopic Dry Skin? *J Investig Dermatol* **1991**: 96: 523-526.
56. van Smeden J, Janssens M, Gooris GS, et al. The important role of stratum corneum lipids for the cutaneous barrier function. *Biochim Biophys Acta* **2014**: 1841: 295-313.
57. Janssens M, van Smeden J, Gooris GS, et al. Increase in short-chain ceramides correlates with an altered lipid organization and decreased barrier function in atopic eczema

patients. *J Lipid Res* **2012**: 53: 2755-2766.
58. Janssens M, van Smeden J, Gooris GS, et al. Lamellar Lipid Organization and Ceramide Composition in the Stratum Corneum of Patients with Atopic Eczema. *J Invest Dermatol* **2011**: 131: 2136-2138.
59. Tfayli A, Bonnier F, Farhane Z, et al. Comparison of structure and organization of cutaneous lipids in a reconstructed skin model and human skin: spectroscopic imaging and chromatographic profiling. *Exp Dermatol* **2014**: 23: 441-443.
60. Ponec M, Boelsma E, Gibbs S, et al. Characterization of Reconstructed Skin Models. *Skin Pharmacol Physiol* **2002**: 15(suppl 1): 4-17.

Supplementary figures

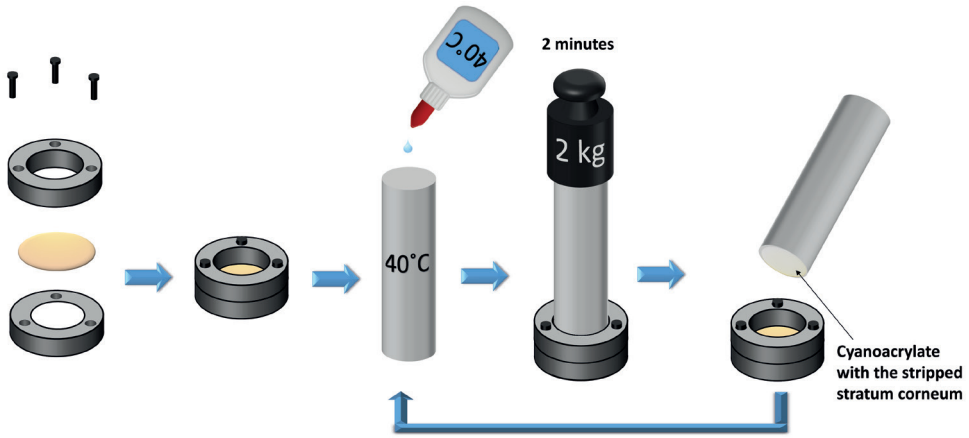

Figure S1. Stripping of stratum corneum (SC) from *ex vivo* skin. 26 mm skin biopsies of 400 µm thickness are fixed into a custom made cyanoacrylate stripping device. A single droplet of preheated cyanoacrylate (40°C) was spread on a 20 mm diameter stainless steel cylinder which was also preheated to 40°C. The cylinder with cyanoacrylate was immediately placed on the skin together with a 2 kg weight to achieve a standardized pressure for 2 minutes. The cylinder was removed in one move, with alternating directions of 180° to ensure even removal of the SC on both sides. This stripping procedure was repeated until the skin gave a glossy appearance indicating that most of the SC has been removed.

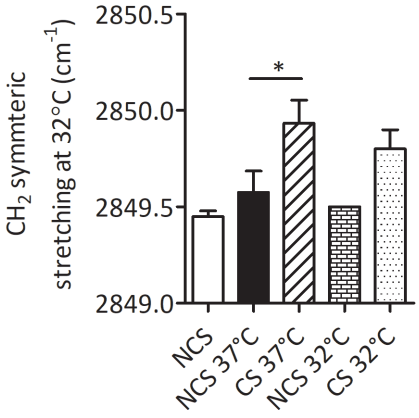

Figure S2. CH_2 symmetric stretching frequency at 32°C in the spectra of the stratum corneum (SC) of cultured explants. Data represents mean ± SEM from three donors, *p<0.05. NHS: native human skin, S: stripped, NS: non-stripped

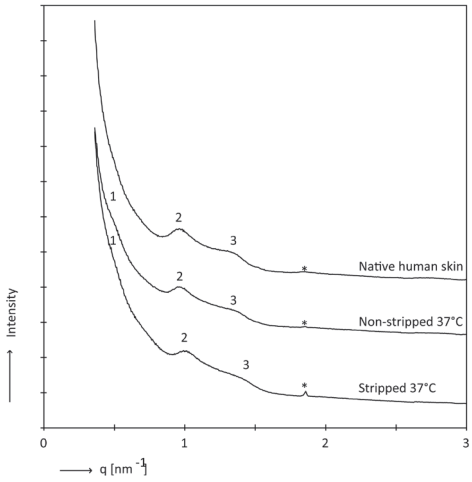

Figure S3. Representative X-ray diffraction pattern of SC from stripped, non-stripped explants and native human skin. 1, 2 and 3 indicate the 1st, 2nd and 3rd order of the long periodicity phase (LPP) respectively. The "2" peak from native human SC and non-stripped SC represent both the 2nd order of the LPP and the 1st order of the short periodicity phase (SPP) Therefore, the repeat distances cannot be calculated directly from this diffraction profile. Crystalline cholesterol is indicated by (*).

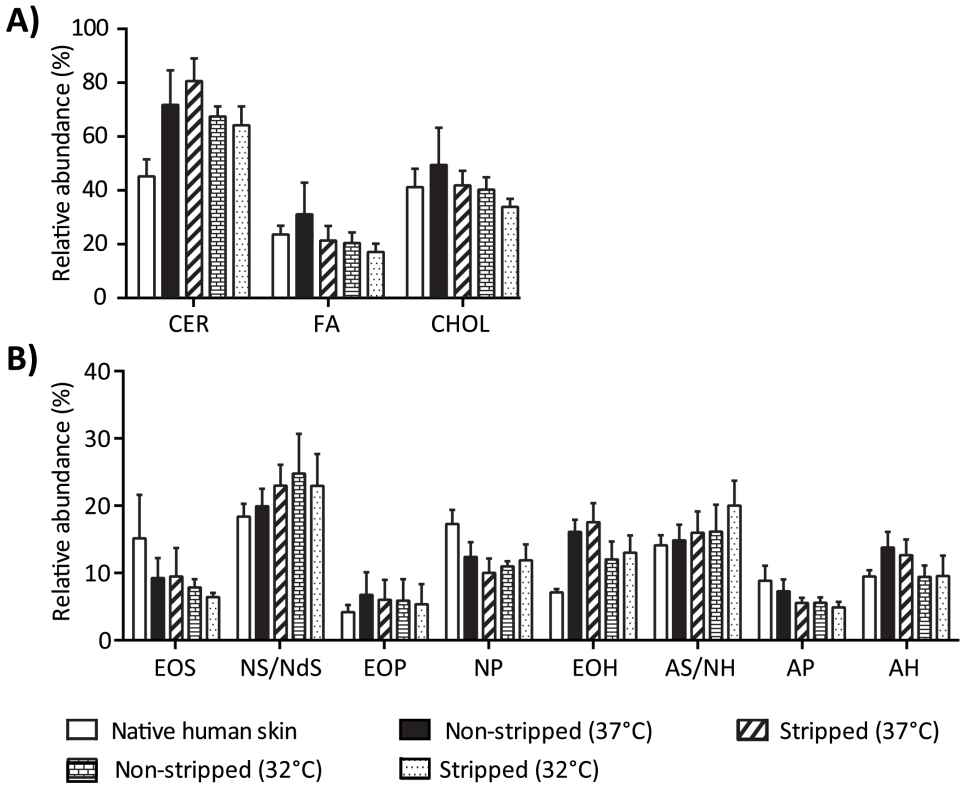

Figure S4. Relative levels of SC lipids in cultured explants. A) Cholesterol (CHOL), free fatty acids (FA) and ceramides (CERs), **B)** various classes of CERs. Data represents mean ± SEM from three donors.

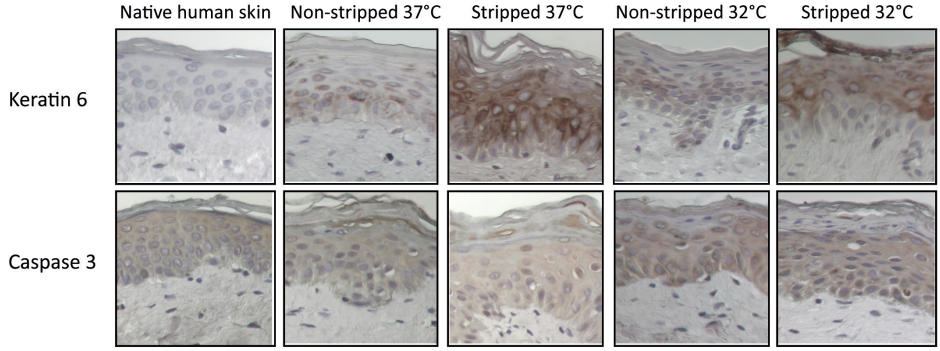

Figure S5. Immunohistochemical staining for Keratin 6 and Caspase 3. Images were taken at 20x magnification. Scale bar: 25 µm

Supplementary tables

Table S1. Primary and secondary antibodies for immunohistochemical staining

Primary antibodies			
Antibody	**Clone**	**Dilution**	**Company**
Mouse Cytokeratin 10 Ab-2	DE-K10	1:800	Neomarkers, USA
Mouse Filaggrin Ab-1	FLG01	1:800	Neomarkers, USA
Rabbit Loricrin	AF62	1:1200	Covance, USA
Mouse Involucrin	SY5	1:1200	Sanbio, The Netherlands
Rabbit SCD	polyclonal	1:100	Sigma-Aldrich
Rabbit Ki67	SP6	1:800	Neomarkers, USA
Rabbit aSmase	plyclonal	1:1000	Abcam, UK
Mouse GBA	IgG2a	1:400	Abcam, UK
Mouse α human keratin 6	LHK6B	1:5	Neomarkers, USA
Rabbit Caspase 3	polyclonal	1:50	BD Biosciences
Secondary antibodies			
Biotinylated universal antibody, anti rabbit/mouse IgG			Vector laboratories, Burlingame, CA, USA
Rhodamine Red-X (goat-anti-rabbit) (IF)		1:300	Jackson immunoresearch laboratory, USA
Cy3 (Goad-anti-mouse) (IF)		1:1000	Jackson immunoresearch laboratory, USA

Table S2. Solvent system used for barrier lipids analysis by thin layer chromatography

Eluent	Composition (v/v)	Distance (mm)
1	Dichloromethane/Ethylacetate/Acetone/Methanol (88:8:4:1)	40
2	Chloroform/Acetone/Methanol (76:8:16)	10
3	Hexane/Chloroform/Acetone/Methanol (6:80:12:2)	70
4	Hexane/Chloroform/Hexylacetate/Acetone/Methanol (6:80:0.1:10:4)	95

Table S3. Ceramide nomenclature

	Non-hydroxy fatty acid (N)	α-hydroxy fatty acid (A)	Esteryfied ω-hydroxy fatty acid (EO)
Dihydrosphingosine (dS)	NdS	Ads	EOdS
Sphingosine (S)	NS	AS	EOS
Phytosphingosine (P)	NP	AP	EOP
6-hydroxy sphingosine (H)	NH	AH	EOH

The human stratum corneum (SC) contains 4 sphingoid bases (dihydrosphingosine (dS), Sphingosine (S), phytosphingosine (P) and 6-hydroxy sphingosine (H)) and three acyl chains (non-hydroxy fatty acid (N), α-hydroxy fatty acid (A) and esterified ω-hydroxy fatty acid (EO)). Together, these result in the 12 ceramide subclasses present in human SC.

Supplementary materials and methods

Morphology and Immunohistochemistry

The skin sections (except the sections stained for aSmase) were incubated in sodium citrate buffer (pH 6) for 30 minutes at 95˚C for antigen retrieval. The sections stained for aSmase were incubated in sodium citrate buffer (pH 6) for 5 minutes at 110˚C in an autoclave (Laboratory autoclave, model A275, Zirbus technology, Germany) for antigen retrieval. Thereafter, all sections were blocked with 2.5% normal horse serum (Vector laboratories Burlingame, CA) for 20 minutes and incubated overnight at 4˚C with the primary antibody diluted in 1% bovine serum albumin (BSA) in PBS.

Staining procedure with amino-ethylcarbazole: Subsequently, the sections were incubated for 30 minutes at room temperature with the secondary antibody (Vector laboratories Burlingame, CA) and the ABC reagent (Vector laboratories Burlingame, CA) for 30 minutes and 10 minutes for Caspase 3. The sections were washed with 0.1M sodium acetate buffer and incubated in amino-ethylcarbazole (Sigma) dissolved in N,N-dimethylformamide (1 g/250 mL) (Sigma) with 0.1% hydrogen peroxide for 30 minutes at room temperature. All sections were counterstained with haematoxylin.

Staining procedure for immunofluorescence: Sections were incubated with the appropriate secondary antibody for 1 hour at room temperature and mounted using DAPI Vectashield (Vector laboratories Burlingame, CA).

Proliferation index: Five microscopic images per explant or biopsy (from three donors) were taken at 20x magnification. For each image, the number of basal cells were counted and the proliferation index was calculated as the percentage of Ki67 positive cells within the basal layer of the epidermis.

High performance thin layer chromatography (HPTLC)

To identify the different classes of lipids, co-chromatography of a standard lipid mixture was performed. This included six subclasses of synthetic CERs (EOS, NS, EOP, NP, AS and AP (Evonik, Germany)), FAs (stearic acid, tricosanoic acid, palmitic acid, behenic acid, arachidonic acid, cerotic acid and lignoceric acid (Sigma)) and cholesterol (Sigma). The ceramide nomenclature is according to the terminology of Motta et al.[1] and Masukawa et al.[2] which is used throughout this article (Supplementary Table S3).

Lipid quantification by HPTLC: The standard lipid mixture and extracted lipids were sprayed on a silica gel plate (Merck, Germany) using a Camag Linomat IV device, (Muttenz, Switzerland) within a concentration range of 4 µg - 30 µg. Variation in the amounts of sprayed standard lipids allowed the calculation of calibration curves for lipid quantification. The lipids were separated using organic solvent mixtures at specific running distances (Supplementary Table S2). The plate was stained with a copper acetate-copper sulfate solution (3:1) and charred at 170˚C for 15 minutes. The images were obtained with a GS800 calibrated densitometer (Bio-Rad, CA, USA) and analyzed with quantity-one software 4.6.5 (Bio-Rad, CA, USA). The amount of each lipid class was determined from a non-linear fit of the calibration curve from its synthetic lipid counterpart. This provided the relative levels of the various lipid classes. The absolute values were provided by weighing the SC before and after extraction.

Fourier transformed infra-red spectroscopy (FTIR) and small angle X-ray diffraction (SAXD)

The SC sheets were hydrated for 24 hours over a 27% NaBr solution and sandwiched between AgBr windows (Pier-optics, Japan). The spectra were collected using a Varian 670-IR FTIR spectrometer (Agilent technologies, CA, USA), equipped with a broad-band mercury cadmium telluride detector, cooled with liquid nitrogen. The spectra were collected in transmission mode, as a co-addition of 256 scans at 1 cm^{-1} resolution during 4 minutes from 0˚C-90˚C at a frequency range of 600-4000 cm^{-1}. The spectra was deconvoluted using enhancement factor of 1.7, half-width of 5 cm^{-1}, and analysed using Bio-Rad Win-IR Pro 3.0 software from Biorad (Biorad laboratories, MA, USA).
The samples were hydrated as described above and SAXD patterns were detected with a Frelon 2000 CCD detector at room temperature for a period of 10 min using a microfocus as described by Bras et al.[3] From the scattering angle, vector q was calculated from the following equation $q= (4\pi\sin\theta)/\lambda$. θ is the scattering angle and λ is the wavelength of the X-ray.

Supplementary references

1. Motta S, Monti M, Sesana S, et al. Ceramide composition of the psoriatic scale. *Biochim Biophys Acta-Molecular basis of disease* **1993**: 1182: 147-151.
2. Masukawa Y, Narita H, Shimizu E, et al. Characterization of overall ceramide species in human stratum corneum. *J Lipid Res* **2008**: 49: 1466-1476.
3. Bras W, Dolbnya IP, Detollenaere D, et al. Recent experiments on a small-angle/wide-angle X-ray scattering beam line at the ESRF. *Journal of Applied Crystallography* **2003**: 36: 791-794.

Chapter 3

Degree of skin barrier disruption affects lipid organization in regenerated stratum corneum

Tineke Berkers[1], Dani Visscher[1], Gert S. Gooris[1], Joke A. Bouwstra[1]

[1] Department of Drug Delivery Technology, Cluster BioTherapeutics, Leiden Academic Centre for Drug Research, Leiden University, Leiden, 2333 CC, The Netherlands

Acta Derm Venereol. 2018 Apr 16;98(4):421-427

Abbreviations

CER	Ceramide
FA	Fatty acid
FTIR	Fourier transform infrared spectroscopy
HE	Haematoxylin and eosin
LPP	Long periodicity phase
MUFA	Mono-unsaturated fatty acid
SAXD	Small angle X-ray diffraction
SC	Stratum corneum
SkinBaR	Skin barrier repair
SPP	Short periodicity phase

Keywords

Skin barrier repair, parakeratosis, lateral lipid organization, lamellar lipid organization, stratum corneum, skin model

Abstract

Previously, a skin barrier repair model was developed to examine the effect of formulations on the lipid properties of compromised skin. In this model, the lipid organization mimics that of several skin diseases with an impaired skin barrier and a less dense lateral lipid organization. Additionally, parakeratosis was occasionally observed. In the present study, we investigated if the extent of initial barrier disruption affects lipid organization and parakeratosis in regenerated SC.

After barrier disruption and SC regeneration the fraction of lipids adopting a less dense lateral organization gradually increased with increasing degree of barrier disruption. Only when 75% of the SC was removed, parakeratosis and a change in lamellar organization were observed. This demonstrates the possibility to use the skin barrier repair model to study the effects of formulations on compromised skin in which the presence of parakeratosis and lipid organization can be modified by the extent of barrier disruption.

Introduction

The skin barrier function is located in the uppermost layer of the epidermis, the stratum corneum (SC). This layer consists of corneocytes embedded in a lipid matrix.[1] The lipids form two crystalline lamellar phases with repeat distances of 13 nm (long periodicity phase, LPP) and 6 nm (short periodicity phase, SPP), see Figure 1.[2-4] Within the lipid lamellae, the lipids mainly adopt a dense orthorhombic lateral packing in healthy skin.[5-8] In several skin diseases, the barrier function is affected, e.g. atopic dermatitis, lamellar ichthyosis, Netherton syndrome, and psoriasis.[9] The reduced barrier function is characterized by e.g. a higher fraction of SC lipids that adopts a hexagonal lateral packing compared to healthy skin.[10] The change in barrier function in several skin diseases depends on the severity of the disease.[9-11]

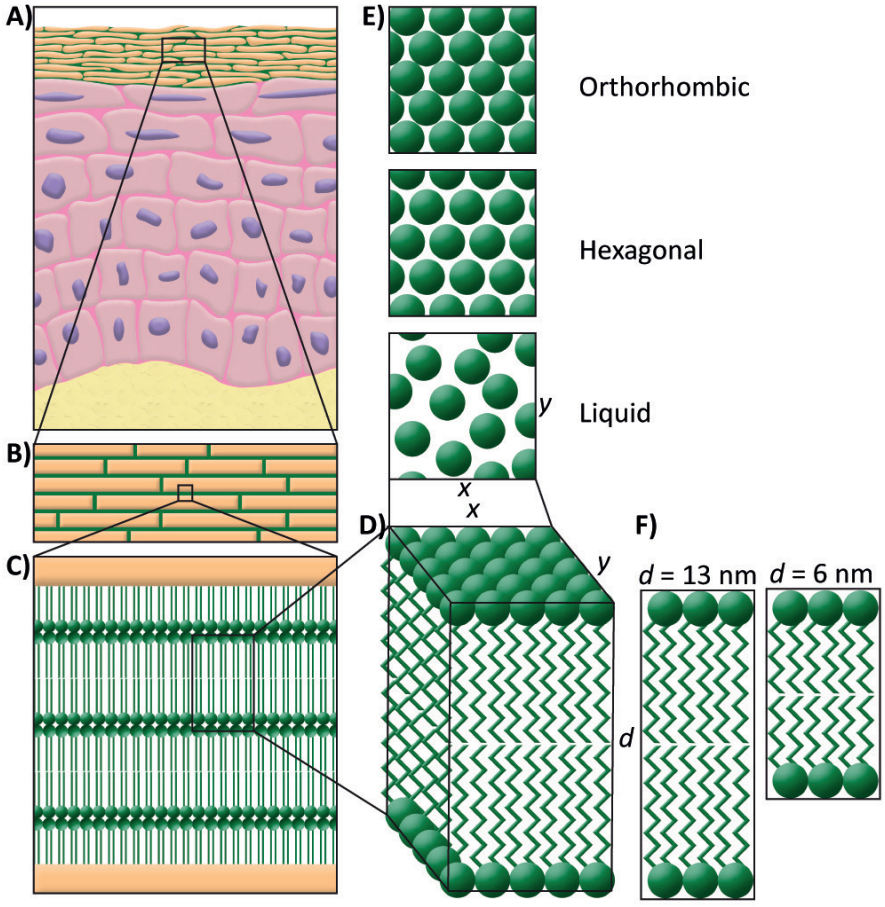

Figure 1. Lipid organization in the SC. A) Schematic overview of the skin, **B)** A brick-and-mortar structure is mimicking the corneocytes embedded in the lipid matrix, **C)** In between the corneocytes, the lipids are stacked in lamellae, **D)** Detail of the lipid lamellae, **E)** Perpendicular to the lamellae, the lipids are organized in a lateral packing. This can be either orthorhombic, hexagonal, or liquid (top view), **F)** The lipid lamellae are stacked on top of each other with a repeat distance (d) of either 13 nm (LPP) or 6 nm (SPP).

Recently, a human skin barrier repair model was developed which can be used to study the interactions of topical formulations with the SC during skin barrier repair.[12] This model is referred to as the SkinBaR model and exhibits several characteristics of the lipid composition and organization in SC of diseased skin, such as Netherton syndrome, lamellar ichthyosis, and atopic dermatitis. In this model, the SC is removed by stripping *ex vivo* human skin and regenerated during a culture period of 8 days. In our previous studies, occasionally nuclei were observed in the regenerated SC after culturing, which is known as parakeratosis. Parakeratosis is also observed in several skin diseases with a disturbed barrier[13], wound healing[14], and after tape stripping *in vivo*.[15] It is caused by abnormal keratinocyte maturation. We hypothesize that the degree of barrier disruption influences the rate at which the barrier is repaired and may therefore be associated with the presence of parakeratosis and the extent the lipid organization in the SC lipid matrix changes, mimicking more closely the lipid organization in SC of diseased skin. If this is the case, the SkinBaR model could be used to study the effects of barrier repair formulations on various levels of altered lipid organization, mimicking several aspects of the lipid organization in diseased skin. The formulations can be applied during or after barrier regeneration.[16]
The aim of this study was to induce several degrees of barrier disruption by stripping *ex vivo* human skin and regenerating the SC during culture. We intended to mimic multiple levels of skin disease severity as analyzed by the morphology and lateral and lamellar lipid organization which are indicative for the skin barrier function.

Methods

Chemicals

Cyanoacrylate (Bison, Goes, the Netherlands) was bought in a local shop. Xylene was purchased from Biosolve (Valkenswaard, the Netherlands), 4% buffered formaldehyde was acquired from Added Pharma (Oss, the Netherlands), paraffin, haematoxylin, and eosin were obtained from Klinipath (Duiven, the Netherlands). DMEM, Ham's F12, and penicillin/streptomycin were purchased from Fisher Scientific (Waltham, Massachusetts, USA). Bovine serum albumin, sodium bromide, ethanol, acetone, trypsin, trypsin inhibitor, selenious acid, hydrocortisone, isoproterenol, L-carnitine, L-serine, insulin, α-tocopherol acetate, vitamin C, arachidonic acid, linoleic acid, and palmitic acid were purchased from Sigma-Aldrich (Zwijndrecht, the Netherlands).

Stripping and culturing of ex vivo skin

Human abdomen or mamma skin from three donors (age 20, 30, and 67) was obtained after abdominoplasty or breast reduction, from a local hospital, after written informed consent, and was used within 12 hours after cosmetic surgery. The subcutaneous fat was removed with a scalpel, and the skin was wiped with 70% ethanol and Millipore water. Subsequently, the skin was dermatomed to a thickness of 600 µm (D80 Dermatome, Humeca, Borne, the Netherlands), punched in circles (ø=26 mm), clamped in a custom made device, and stripped with preheated cyanoacrylate on

a preheated metal cylinder as described before.[12] SC was stripped by removing the cylinder in one stroke. The stripping procedure was repeated to remove either 25%, 50%, or 75% of the SC. After 75% of the SC was removed the skin appeared shiny. Typically, 6-8 strips were needed to reach a shiny appearance of the whole sample, varying between skin donors. Cultured non-stripped (0%) skin and native skin (e.g. non-stripped and not cultured) were used as control. Per donor, the different conditions were cultured in duplo.
The stripped *ex vivo* skin was cultured at the air-liquid interface for 8 days in a deep 6-well culturing plate (Organogenesis, Canton, MA, USA), as previously described.[12] The samples were either cryofixed, paraffin embedded, or SC was isolated.

Isolation of SC

SC was isolated from the (cultured) skin by trypsin digestion. The skin was placed in 0.1% trypsin solution in PBS and kept overnight at 4˚C, followed by one hour at 37˚C. Trypsin is a proteolytic enzyme which is used to separate SC from the epidermis.[17] SC was peeled off, washed in 0.1% trypsin inhibitor, and twice in Millipore water. SC sheets were stored over silica gel under argon until use. SC was used for either infrared spectroscopy measurements or X-ray diffraction measurements.

Safranin-O red and heamatoxylin and eosin staining

To examine the number of corneocyte layers 5 µm cryofixed sections were stained with 1% (w/v) Safranin-O solution for 1 minute followed by 20 minutes incubation in 2% (w/v) KOH solution. Haematoxylin and Eosin (HE) staining was performed on 5 µm paraffin sections to examine the morphology. After Safranin-O and HE staining, at least 3 light microscopy images were taken per culture condition at 20x and 63x magnification.

Fourier transformed infrared spectroscopy

Fourier transformed infrared (FTIR) spectroscopy was used to examine the lateral lipid packing of isolated SC samples as a function of temperature (0-90˚C). The samples were placed over a 27% NaBr solution in D_2O for 24 hours at room temperature, reaching a final hydration level of around 20% in the SC, and sandwiched between two AgBr-windows. Spectra were obtained using a Varian 670-IR FTIR spectrometer (Agilent Technologies, Santa Clara, USA), as described before.[16]
The onset temperature of the ordered-disordered transition was obtained from the peak positions of the CH_2 symmetric stretching vibrations in the FTIR spectra. Peak positions were plotted as a function of temperature. The intercept of two regression lines fitted to the linear parts of the graph was calculated which describes the onset transition temperature, as described before.[16]

Small angle X-ray diffraction

Small angle X-ray diffraction (SAXD) was employed to examine the lamellar organization of the SC lipids. Measurements were performed at the European Synchrotron Radiation Facility (Grenoble, France) using the Dutch-Belgian beamline (station BM26B). 24 hours prior to the measurements, SC samples were hydrated over a 27% NaBr solution at room temperature reaching a hydration level of about 20%. A custom made sample holder was used to orientate the samples parallel to the X-ray beam. Diffraction data was collected at room temperature on a Pilatus 1M detector for a period of 5 or 10 minutes, as described earlier.[18] The scattering vector (q) was calculated using the scattering angle (θ) and the wavelength (λ) by $q=4\pi \sin\theta/\lambda$. The spacing of the lamellar phase can be calculated from the position of the peak maxima (q) using $2\pi/q$.

Statistical analysis

One-way ANOVA with post hoc correction for multiple comparisons or with a post-hoc trend test was used to analyze the data using GraphPad Prism 7 (San Diego, CA, USA). All differences are described relative to native human skin.

Results

Human skin cultured after various degrees of barrier disruption results in complete SC regeneration

After staining with safranin-O, the number of corneocyte layers was determined for at least 3 different spots per image and at least 3 images were taken per culturing condition for each skin donor. Per condition, the results of the three donors were pooled. Native human skin showed 11.0 ± 4.0 (mean ± SD) corneocyte layers, whereas after removing of the SC until the skin surface appeared shiny 3.1 ± 2.8 SC cell layers remained on the viable epidermis, meaning that about 75% of the corneocyte layers was removed. The number of strips needed to remove 75% of the SC was reduced to ¾ and ½ in order to obtain less stripped skin. This resulted in skin with either 5.0 ± 3.4 (=50% stripped) or 7.7 ± 4.4 (=25% stripped) remaining corneocyte layers on the viable epidermis, see Figure 2A. All stripped samples had a significant lower number of corneocyte layers than the native SC ($p<0.001$). A post-hoc test showed that there is a linear trend with decreasing number of corneocyte layers for the samples prior to culture (slope: -2.6, $p<0.0001$). After the 8-day culturing period, the number of corneocyte layers in the regenerated SC is significantly increased to 10.8 ± 3.6, 10.3 ± 2.6, and 11.2 ± 3.1, for 75%, 50%, and 25% stripped SC, respectively, which is comparable to the number of layers in native human skin before stripping.

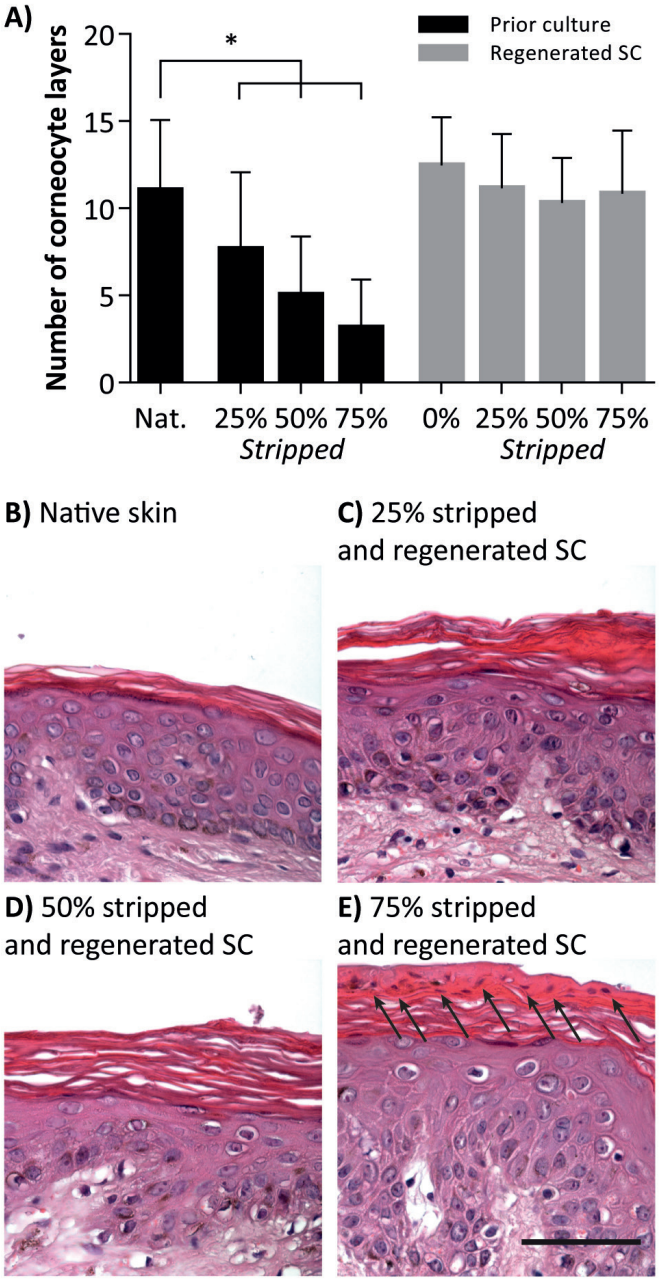

Figure 2. Number of corneocyte layers and morphology. A) The number of layers in native SC (Nat.), stripped SC, and regenerated SC after culturing. Bars represent Mean ± SD. Morphology of **B)** Native skin, and **C-E)** Stripped and cultured skin with regenerated SC. SC was stripped away for 25%, 50%, and 75%, respectively. * $p<0.001$ (ANOVA), arrows: parakeratosis, scale bar: 50 µm.

Parakeratosis is visible when the majority of the SC is removed

The morphology of the cultured skin sections was visualized using HE staining. The staining revealed that after removing 75% of the SC and subsequent culturing, prominent parakeratosis is observed (see arrows in Figure 2E), mainly in the top layers of the regenerated SC. Furthermore, spongiosis with an irregular keratinocyte distribution in the epidermis was observed in skin with SC that was regenerated after 75% of the SC was removed. After 50% or 25% of the SC was removed, the regenerated SC did not exhibit parakeratosis or major differences in morphology.

Lateral lipid organization changes gradually with number of removed corneocyte layers

The lipid organization of the stripped and regenerated SC was examined and compared to native SC. The lateral lipid packing was examined using the CH_2 rocking vibrations in the FTIR spectra in a temperature range between 0°C and 90°C. A hexagonal lateral lipid packing is characterized by a single contour positioned at a wavenumber of 719 cm^{-1}, while an orthorhombic packing is characterized by a doublet positioned at 719 and 730 cm^{-1}. All spectra were scaled at the difference between the absorption at 719 cm^{-1} (peak position) and the absorption at 715 cm^{-1} (base). This difference in absorption was kept constant in all spectra. In this way relative peak heights of the peak at around 730 cm^{-1} could be compared between samples.
Figure 3 shows representative FTIR spectra of one donor. As shown in Figure 3A, in native SC two strong contours were observed at 719 and 730 cm^{-1} at 0°C, indicating that the lipids adopt an orthorhombic lateral lipid packing. The contour positioned at 730 cm^{-1} started to decrease in intensity at around 34°C and disappeared at around 48°C, indicating a phase transition from an orthorhombic to a hexagonal lateral lipid packing. The intensity of the peak at 730 cm^{-1} at 0°C gradually decreased when 25% to 50% and 75% of SC was removed before culturing. When increasing the temperature, the peak at 730 cm^{-1} disappeared between 30°C and 48°C (25% of SC was stripped), and 20°C and 36°C (50% of SC was stripped) in the FTIR spectra of regenerated SC. After removing of 75% of the corneocyte layers and regeneration of the SC, the orthorhombic to hexagonal transition occurred between 8°C and 30°C as monitored by the disappearance of the 730 cm^{-1} in the corresponding FTIR spectrum.

Lipid ordering only affected when significant amount of SC is removed

The conformational ordering of the lipids was examined using the thermotropic behavior of the CH_2 symmetric stretching vibrations in the FTIR spectrum in a temperature range of 0-90°C. Fully extended lipid chains show a high conformational ordering, which is characterized by a CH_2 stretching vibration peak position at wavenumbers below 2850 cm^{-1}. When lipids have a high conformational disordering, e.g. when lipids are in liquid state, the peak position is shifted to wavenumbers higher than 2852 cm^{-1}. The onset transition temperature was determined as described above.
The CH_2 symmetric stretching vibrations obtained from representative data of one donor are plotted as a function of temperature in Figure 3E. The wavenumber at 10°C and the onset transition temperatures are mean values of the spectra of the three donors.

At 10˚C, a wavenumber of 2848.81 ± 0.01 cm^{-1} (mean ± SD) was observed in native SC. The wavenumbers of cultured control skin, and after regeneration of 25% and 50% of the SC were comparable to native SC (p=0.74, p=0.35, and p=0.39, respectively). Only when 75% of the SC was removed, the wavenumber at 10˚C was increased to 2849.38 ± 0.25 cm^{-1} (p=0.04). This indicates that, even at low temperatures, the lipid ordering of the regenerated SC is affected.
Furthermore, the stretching vibrations are used to compare the onset transition temperatures of the ordered-disordered phase transition. For native SC the onset transition temperature was 72.5 ± 3.6˚C (mean ± SD). Furthermore, at around 30-40˚C, a small shift in wavenumber is observed, indicating an orthorhombic to hexagonal transition. Lipids in the SC of cultured control skin (0% of SC was stripped) showed similar temperature dependence as native SC with a transition temperature of 68.9 ± 4.7˚C. After regeneration of the SC after 25% or 50% of the SC was stripped, the onset temperatures of the ordered-disordered phase transition were 68.9 ± 2.9˚C and 67.9 ± 1.3˚C, respectively. These onset transition temperatures were not statistically significant different from that of native SC. However, SC regeneration after 75% of the SC was removed, resulted in a different temperature dependence of the CH_2 stretching vibrations. The onset of the ordered-disordered phase transition took place at a statistically significant lower temperature of 62.9 ± 2.1˚C (p=0.01). This is apparent from the line in Figure 3E which is shifted to the left and increases to higher wavenumbers at lower temperatures. Furthermore, the small shift in wavenumber at around 30-40˚C was not observed in regenerated SC after 50% or 75% of the SC was stripped.

The lamellar repeat distance decreases only after removing most of the SC

The lamellar organization in the lipid matrix was examined using SAXD. Figure 4 shows SAXD patterns of a representative donor of native SC and SC that was regenerated after stripping and culturing. Two weak diffraction peaks (indicated by I and III) and one strong peak (indicated by II) can be observed. The LPP contributes to all three peaks, whereas the SPP only contributes to peak II. The peak corresponding to phase separated cholesterol is marked by an asterisk. The peak position (q) of the main peak (II) was used to examine whether a difference in lamellar spacing was induced by SC disruption. The spacing of the lipids in the stripped and regenerated SC was compared to the spacing of native SC of the same donor. In this way, a mean difference was obtained. The spacing in native SC was 6.3 ± 0.1 nm (mean ± SD). The difference in spacing was 0.05 nm for the SC of the cultured control sample (0% of SC was stripped) and for regenerated SC after 25% or 50% of the SC was stripped this difference was -0.06 nm. None of these changes were statistically different. However, when SC was regenerated after 75% of the SC was removed, the difference in spacing was -0.23 nm, which was statistically significant different from native SC (p=0.001). Furthermore, the intensity of diffraction peaks I and III decreased substantially, indicating a reduction in the presence of the LPP. Additionally, a shoulder appears close to the position of peak II at a q-value of around 1.3 nm^{-1}.

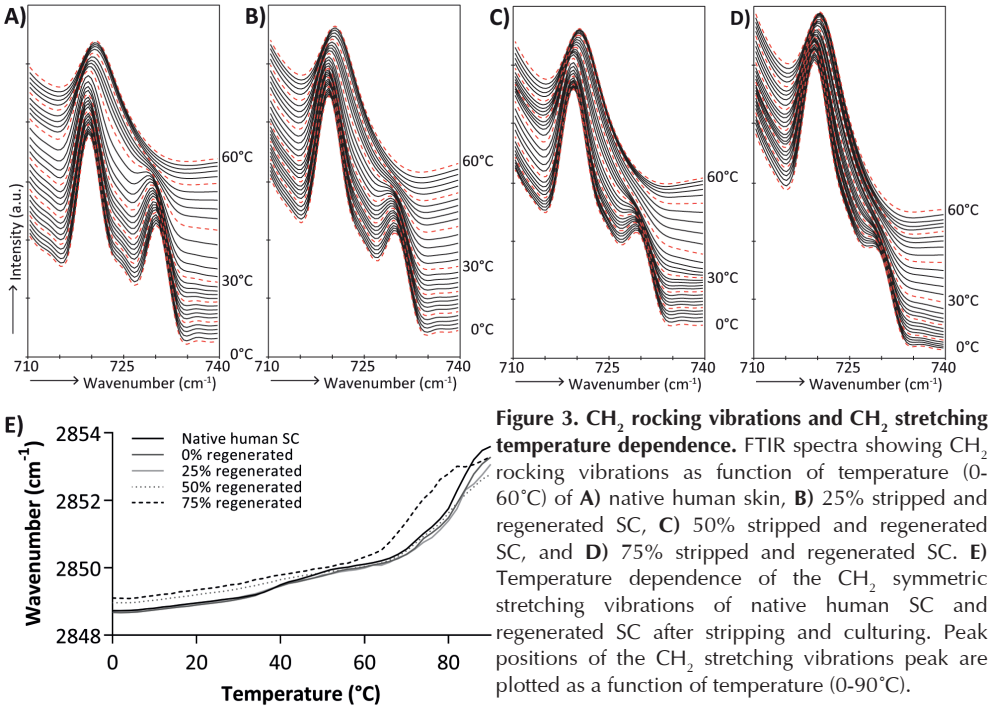

Figure 3. CH_2 rocking vibrations and CH_2 stretching temperature dependence. FTIR spectra showing CH_2 rocking vibrations as function of temperature (0-60˚C) of **A)** native human skin, **B)** 25% stripped and regenerated SC, **C)** 50% stripped and regenerated SC, and **D)** 75% stripped and regenerated SC. **E)** Temperature dependence of the CH_2 symmetric stretching vibrations of native human SC and regenerated SC after stripping and culturing. Peak positions of the CH_2 stretching vibrations peak are plotted as a function of temperature (0-90˚C).

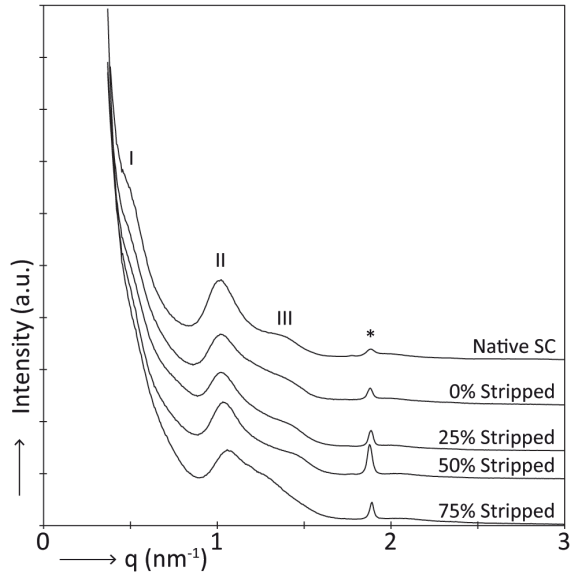

Figure 4. A typical example of SAXD patterns of native SC and regenerated SC after stripping and culturing. The peak positions (q) are indicative for the spacing of the lipid lamellae. The 1st, 2nd, and 3rd order peaks of the LPP are labeled with I, II, and III, respectively. The first order of the SPP also contributes to peak II. Phase separated cholesterol is labeled with *.

Discussion

In this study we showed that in regenerated SC of the SkinBaR model we can on demand gradually decrease the fraction of lipids adopting a dense orthorhombic lateral packing by varying the initial degree of barrier disruption. The obtained changes in lipid lateral packing compared to native SC are very similar to that observed in SC of several inflammatory skin diseases.[9-11] These results indicate that the SkinBaR model can be used to study skin barrier repair formulations that aim to normalize the SC lipid organization in diseased skin. The degree of disruption also influenced the presence of parakeratosis, as we showed that parakeratosis was only present in the examined models when 75% of the SC was removed, resulting in 3 remaining corneocyte layers before the skin started to regenerate the SC. Additionally, parakeratosis was predominantly observed in the upper corneocyte layers. This strongly indicates that only during generation of the initial corneocyte layers parakeratosis is induced, probably as a fast response to repair the skin barrier after disruption. Independent of the degree of barrier disruption, the number of corneocyte layers after 8 days of regeneration was comparable to that in SC of native skin. This indicates that the degree of disruption affects the rate of regeneration, and that the skin is still viable. Previous observations have shown that the proliferation rate, as examined by fraction of Ki-67 positively stained nuclei, immediately after SC removal was higher than the proliferation rate after a longer recovery period.[12,15] It is known that cultured skin does not desquamate and that the corneocyte layers accumulate during culture.[19] However, this is believed to be of little influence on the SkinBaR model since the non-stripped cultured SC showed a non-significant increase of only 1.4 corneocyte layers during culturing indicating that the formation of the SC is inhibited.

When focusing on the lateral lipid organization, the lipid density, which is the fraction of lipids forming an orthorhombic lateral packing, of the regenerated SC decreased when the degree of barrier disruption was increased. At skin temperature (32˚C), in the FTIR spectrum no contour at 730 cm^{-1} was observed when 75% of the SC was regenerated, demonstrating that at this temperature the lipids had adopted a hexagonal packing. However, when removing less corneocyte layers, the contour at 730 cm^{-1} was visible as a shoulder (after 50% of SC was stripped) or as a peak (native or after 25% of SC was stripped) at 32˚C. An indication of the lipid ordering is provided by the CH_2 stretching vibrations. When comparing these stretching vibrations of regenerated SC after 75% of SC was stripped to that of regenerated SC after less intensive disruption of SC, the onset temperature of the ordered-disordered phase transition was significantly lower and the position of the CH_2 vibrations at 32˚C were at higher frequency. These observations suggest a less ordered organization of the lipids in the regenerated SC after 75% SC removal, even at low temperatures. Also the lamellar organization was only affected in regenerated SC after 75% of the SC was removed. These results indicate that the lateral lipid packing is more responsive to barrier disruption than the conformational ordering and the lamellar organization.

Previously, a more abundant presence of lipids adopting a hexagonal packing has been related to a higher level of mono-unsaturated fatty acids (MUFAs)[20], and shorter fatty acid (FA) and ceramide (CER) chain length.[21] In the SkinBaR model, both an increased level of short chain CER and unsaturated CER were observed.[22] Mono-unsaturated

CERs are derived from a chemical linkage of a MUFA to a sphingoid base.[23] The enzyme stearoyl-CoA desaturase catalyzes the conversion of saturated FAs to MUFAs. In the SkinBaR model, we have demonstrated an extended stearoyl-CoA desaturase expression compared to native human skin, suggesting also an increased level of MUFAs.[12]

Similar changes in lipid organization and composition have been observed in atopic dermatitis skin. In lesional and non-lesional skin of atopic dermatitis patients a higher fraction of lipids adopts a hexagonal lipid organization, which coincides with a higher fraction of MUFAs and a reduced chain length of FAs and CERs.[10,24,25] These changes are more pronounced in lesional skin than in non-lesional skin.[10] Besides atopic dermatitis, several other skin diseases are characterized by a disrupted skin barrier.[9,11] Again, the extent of barrier disruption may vary depending on the severity of the disease. This may be of influence on the effect of topically applied barrier repair formulations.

The results in this study show that the degree of barrier disruption of the SkinBaR model can be controlled and that the changes in lipid organization and the level of parakeratosis depend on the initial extent of barrier disruption. This means that if less corneocyte layers remain before regeneration is initiated, the deviations in lateral and lamellar lipid organization compared to native SC are more substantial. This variation in the degree of deviation of the lipid organization in the SkinBaR model can be used in studying the effect of barrier repair formulations on the lipid organization. In this way the SkinBaR model can serve as a model for the lipid organization in several skin diseases of which the lipid organization deviates in a similar manner from that in native human skin. Previously, other skin models (the human skin equivalents) have been used to test topical formulations.[26] However, the 8-day culturing period of the SkinBaR model is less time-consuming than a culturing period of 2-3 weeks often used to generate human skin equivalents.[27-29] Furthermore, it is a challenge to influence the lateral packing of the skin equivalents by modifying the culture conditions[27,30,31], while the lateral packing of the SkinBaR model can be adjusted on demand. Unlike these human skin equivalents, the SkinBaR model offers the possibility to apply topical barrier repair formulations directly after several degrees of barrier disruption and study the lamellar and lateral lipid organization of regenerated SC.

Acknowledgements

The authors thank the personnel at DUBBLE beam line (BM26) at European Synchrotron Radiation Facility in Grenoble, France for assistance during X-ray measurements. This research was financially supported by Dutch Technology Foundation TTW (grant no. 12400).

References

1. Michaels AS, Chandrasekaran SK, Shaw JE. Drug permeation through human skin: Theory and invitro experimental measurement. *AIChE journal* **1975**: 21: 985-996.
2. Groen D, Gooris GS, Bouwstra JA. New insights into the stratum corneum lipid organization by X-ray diffraction analysis. *Biophys J* **2009**: 97: 2242-2249.
3. Bouwstra J, Pilgram G, Gooris G, et al. New aspects of the skin barrier organization. *Skin Pharmacol Appl Skin Physiol* **2001**: 14 Suppl 1: 52-62.
4. McIntosh TJ, Stewart ME, Downing DT. X-ray diffraction analysis of isolated skin lipids: reconstitution of intercellular lipid domains. *Biochemistry* **1996**: 35: 3649-3653.
5. Pilgram GS, Engelsma-van Pelt AM, Bouwstra JA, et al. Electron diffraction provides new information on human stratum corneum lipid organization studied in relation to depth and temperature. *J Invest Dermatol* **1999**: 113: 403-409.
6. Damien F, Boncheva M. The extent of orthorhombic lipid phases in the stratum corneum determines the barrier efficiency of human skin in vivo. *J Invest Dermatol* **2010**: 130: 611-614.
7. Goldsmith LA, Baden HP. Uniquely oriented epidermal lipid. *Nature* **1970**: 225: 1052-1053.
8. de Jager MW, Gooris GS, Dolbnya IP, et al. The phase behaviour of skin lipid mixtures based on synthetic ceramides. *Chem Phys Lipids* **2003**: 124: 123-134.
9. van Smeden J, Janssens M, Gooris GS, et al. The important role of stratum corneum lipids for the cutaneous barrier function. *Biochim Biophys Acta* **2014**: 1841: 295-313.
10. van Smeden J, Janssens M, Kaye EC, et al. The importance of free fatty acid chain length for the skin barrier function in atopic eczema patients. *Exp Dermatol* **2014**: 23: 45-52.
11. Sahle FF, Gebre-Mariam T, Dobner B, et al. Skin diseases associated with the depletion of stratum corneum lipids and stratum corneum lipid substitution therapy. *Skin Pharmacol Physiol* **2015**: 28: 42-55.
12. Danso MO, Berkers T, Mieremet A, et al. An ex vivo human skin model for studying skin barrier repair. *Exp Dermatol* **2015**: 24: 48-54.
13. Brady SP. Parakeratosis. *J Am Acad Dermatol* **2004**: 50: 77-84.
14. Usui ML, Underwood RA, Fleckman P, et al. Parakeratotic corneocytes play a unique role in human skin wound healing. *J Invest Dermatol* **2013**: 133: 856-858.
15. Gerritsen MJ, van Erp PE, van Vlijmen-Willems IM, et al. Repeated tape stripping of normal skin: a histological assessment and comparison with events seen in psoriasis. *Arch Dermatol Res* **1994**: 286: 455-461.
16. Berkers T, van Dijk L, Absalah S, et al. Topically applied fatty acids are elongated before incorporation in the stratum corneum lipid matrix in compromised skin. *Exp Dermatol* **2017**: 26: 36-43.
17. Kligman AM, Christophers E. PREPARATION OF ISOLATED SHEETS OF HUMAN STRATUM CORNEUM. *Archives of dermatology* **1963**: 88: 702-705.
18. Bras W, Dolbnya IP, Detollenaere D, et al. Recent experiments on a small-angle/wide-angle X-ray scattering beam line at the ESRF. *J Appl Cryst* **2003**: 36: 791-794.
19. Ponec M, Kempenaar J, Weerheim A. Lack of desquamation - the Achilles heel of the reconstructed epidermis. *Int J Cosmet Sci* **2002**: 24: 263-272.
20. Mojumdar EH, Helder RW, Gooris GS, et al. Monounsaturated fatty acids reduce the barrier of stratum corneum lipid membranes by enhancing the formation of a hexagonal lateral packing. *Langmuir* **2014**: 30: 6534-6543.
21. Mojumdar EH, Kariman Z, van KL, et al. The role of ceramide chain length distribution on the barrier properties of the skin lipid membranes. *Biochim Biophys Acta* **2014**: 1838: 2473-2483.
22. Boiten W, Absalah S, Vreeken R, et al. Quantitative analysis of ceramides using a novel lipidomics approach with three dimensional response modelling. *Biochim Biophys Acta* **2016**: 1861: 1652-1661.
23. Kihara A. Synthesis and degradation pathways, functions, and pathology of ceramides and epidermal acylceramides. *Prog Lipid Res* **2016**: 63: 50-69.
24. Janssens M, van Smeden J, Gooris GS, et al. Increase in short-chain ceramides correlates with an altered lipid organization and decreased barrier function in atopic eczema patients. *J Lipid Res* **2012**: 53: 2755-2766.
25. Janssens M, Mulder AA, van Smeden J, et al. Electron diffraction study of lipids in non-lesional stratum corneum of atopic eczema patients. *Biochim Biophys Acta* **2013**: 1828: 1814-1821.
26. Bouwstra JA, Nahmoed N, Groenink HW, et al. Human skin equivalents are an excellent tool to study the effect of moisturizers on the water distribution in the stratum corneum. *Int J Cosmet Sci* **2012**: 34: 560-566.
27. Thakoersing VS, Gooris GS, Mulder A, et al. Unraveling barrier properties of three different in-house human skin equivalents. *Tissue Eng Part C Methods* **2012**: 18: 1-11.
28. el-Ghalbzouri A, Gibbs S, Lamme E, et al. Effect of fibroblasts on epidermal regeneration. *Br J*

Dermatol **2002**: 147: 230-243.
29. Stark HJ, Boehnke K, Mirancea N, et al. Epidermal homeostasis in long-term scaffold-enforced skin equivalents. *J Investig Dermatol Symp Proc* **2006**: 11: 93-105.
30. van Drongelen V, Danso MO, Mulder A, et al. Barrier properties of an N/TERT-based human skin equivalent. *Tissue Eng Part A* **2014**: 20: 3041-3049.
31. van Drongelen V, Alloul-Ramdhani M, Danso MO, et al. Knock-down of filaggrin does not affect lipid organization and composition in stratum corneum of reconstructed human skin equivalents. *Exp Dermatol* **2013**: 22: 807-812.

Chapter 4

Compromising human skin in vivo and ex vivo to study skin barrier repair

T. Berkers[1]*, W.A. Boiten[1]*, S. Absalah[1], J. van Smeden[1,2], A.P.M. Lavrijsen[3], J.A. Bouwstra[1]

[1] Department of Drug Delivery Technology, Cluster BioTherapeutics, Leiden Academic Centre for Drug Research, Leiden University, Leiden, the Netherlands
[2] Centre for Human Drug Research, Leiden, The Netherlands.
[3] Department of Dermatology, Leiden University Medical Centre, Leiden, the Netherlands
* Both authors contributed equally to this work

Prepared for submission

Abbreviations

AD	Atopic dermatitis
C34 CER	Ceramide with 34 carbon atoms
CER	Ceramide
Ctrl	Control
Cul	Cultured
FTIR	Fourier transform infrared spectroscopy
LC/MS	Liquid chromatography/mass spectrometry
LMM	Linear mixed model
MCL	Mean ceramide carbon chain length
MuCER	Mono-unsaturated ceramide
Reg	Regenerated
SC	Stratum corneum
SkinBaR model	Skin barrier repair model
TEWL	Transepidermal water loss

Abstract

Ex vivo regenerated stratum corneum (SC) can be used as a model to study the barrier function of compromised skin. Yet, details about how close the regenerated SC model mimics the lipid properties (e.g. lipid composition and lipid ordering) of the *in vivo* situation are not known. Here, we examined whether human *ex vivo* regenerated SC showed similar lipid properties as human *in vivo* regenerated SC, since lipid properties in SC affect the barrier function. Both *in vivo* and *ex vivo* regenerated SC had an altered ceramide subclass composition, with increased levels of S subclass and decreased levels of P subclass ceramides, a reduced mean ceramide chain length, and a higher level of unsaturated ceramides. Overall, regenerating SC *ex vivo* showed more pronounced changes compared to the *in vivo* response. One of the purposes of these models is to use them to mimic compromised skin of inflammatory skin diseases. The altered lipid properties in compromised skin were comparable to those observed in several inflammatory skin diseases. The *ex vivo* model simulates the barrier properties of the *in vivo* model and both models showed many similarities with altered lipid barrier properties in inflammatory skin.

Introduction

The main skin barrier function is located in the uppermost epidermal layer, the stratum corneum (SC), consisting of terminally differentiated corneocytes embedded in a lipid matrix.[1] A proper lipid organization and lipid composition in this matrix are important for a well-functioning skin barrier.[2-4] The SC barrier lipids (e.g. ceramides (CERs), fatty acids, and cholesterol) are mainly assembled in a dense orthorhombic lateral packing while a smaller lipid fraction adopts a less dense hexagonal packing.[5,6] The SC CER fraction consists of a specific set of CER subclasses defined by their sphingoid base and acyl chain. Both chains can vary in carbon chain length and polar head group, resulting in a wide array of differently structured CER species, see Figure S1.

Tape-stripped healthy human skin *in vivo* is used as a model to study skin with a compromised barrier. This model has been employed to study several aspects of inflammatory skin diseases[7], to examine the penetration of compounds through the skin[8,9], to increase the bioavailability of topical products in the deeper epidermal layers[10], and to generate a compromised skin barrier to examine the biological processes of skin barrier repair.[11,12] One of these processes is restoring the lipid composition and lipid ordering (lipid properties) in the SC. However, little is known about the effect of barrier disruption by tape-stripping on the lipid properties of the regenerated SC, and if the regenerated SC lipid properties mimic healthy or diseased skin.

An alternative model to study skin barrier repair is by using stripped *ex vivo* skin which regenerates SC over time in the incubator (skin barrier repair (SkinBaR) model).[13] Several aspects of the lipid properties of this model have been studied and are known to mimic to some extent the lipid properties of inflammatory skin diseases.[13,14] However, it is unknown to what extent the CER composition of the SkinBaR model reflects that of tape-stripped and regenerated human skin *in vivo*. In the present study we examine the regenerated SC lipid properties of the *ex vivo* SkinBaR model and of *in vivo* tape-stripped and regenerated skin, in order to determine if the SkinBaR model can potentially replace skin barrier repair studies in clinical settings.

The SC of five skin conditions were examined: SC from $Ctrl^{In\text{-}vivo}$ and $Reg^{In\text{-}vivo}$ were obtained from healthy *in vivo* control skin and regenerated tape-stripped skin, respectively. SC from $Ctrl^{SkinBaR}$, $Cul^{SkinBaR}$, and $Reg^{SkinBaR}$ were obtained from *ex vivo* control skin, cultured skin, and regenerated cyanoacrylate-stripped skin, see Figure 1. The results show that the CER subclass composition and CER chain length of $Reg^{SkinBaR}$ SC reflect those observed in $Reg^{In\text{-}vivo}$ SC. Both models show that regeneration alters the CER composition and mimics important aspects encountered in inflammatory skin diseases, such as atopic dermatitis (AD).

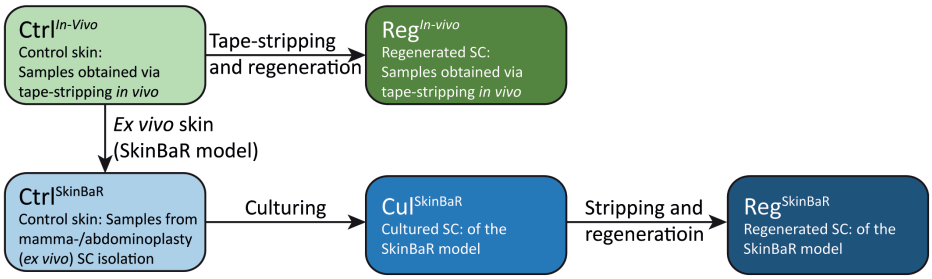

Figure 1. Explanation of the skin samples. The SC of five different skin conditions were examined. The first two conditions were obtained from *in vivo* skin. The first condition is healthy *in vivo* control skin (hereafter called Ctrl$^{In\text{-}vivo}$). The second condition is tape-stripped and regenereted *in vivo* skin (named Reg$^{In\text{-}vivo}$). The other three conditions are obtained from *ex vivo* skin. These are a control condition for the *ex vivo* skin (called Ctrl^{SkinBaR}), non-stripped cultured *ex vivo* skin (Cul^{SkinBaR}), and *ex vivo* skin that was stripped and cultured for regeneration (Reg^{SkinBaR}).

Results

To examine if SC regeneration induced changes in CER profile, and whether *ex vivo* is differently affected compared to *in vivo*, the SC CER composition of the tape-strips obtained in the *in vivo* study and the isolated SC of the SkinBaR model were quantified using liquid chromatography/mass spectrometry (LC/MS). In the present study we quantified the ceramide subclasses, (see Figure S1) as well as the mean total chain length (MCL, total number of carbon atoms sphingoid base and acyl chain). We present those parameters that correlated with skin barrier function in previous studies.[3,15-17] These parameters were CER subclass, the CER MCL, and the level of CERs with a total chain length of 34 carbon atoms (C34 CERs).

Ceramide subclass profile and MCL change due to SC regeneration

The CER subclass profiles of the 5 different skin conditions were examined. Figure 2 shows an altered CER profile due to regeneration (differences of Reg$^{In\text{-}vivo}$ vs. Ctrl$^{In\text{-}vivo}$ and Reg^{SkinBaR} vs. Cul^{SkinBaR}, respectively). Both regenerated models showed increased levels of S subclass CERs, whereas all three P subclasses and NH subclass CERs were decreased. The levels of AH subclass CERs were only affected in the Reg^{SkinBaR} samples and not in the Reg$^{In\text{-}vivo}$ samples. No variation in the dS CER subclasses was observed. All CER O subclasses increased in both Reg$^{In\text{-}vivo}$ and Reg^{SkinBaR} samples. Table S1 shows the results of the linear mixed model (LMM) analysis which indicated that the increased S subclasses and decreased P and NH subclasses in the regenerated SC (both *in vivo* and SkinBaR) compared to their respective controls were statistically significant.
CER subclasses showed similar trends in both Reg$^{In\text{-}vivo}$ and Reg^{SkinBaR}, but in the Reg^{SkinBaR} samples the changes were more pronounced. An exception were changes in the acyl-CERs (EO subclasses) which showed inverse effects in the SkinBaR model (decrease

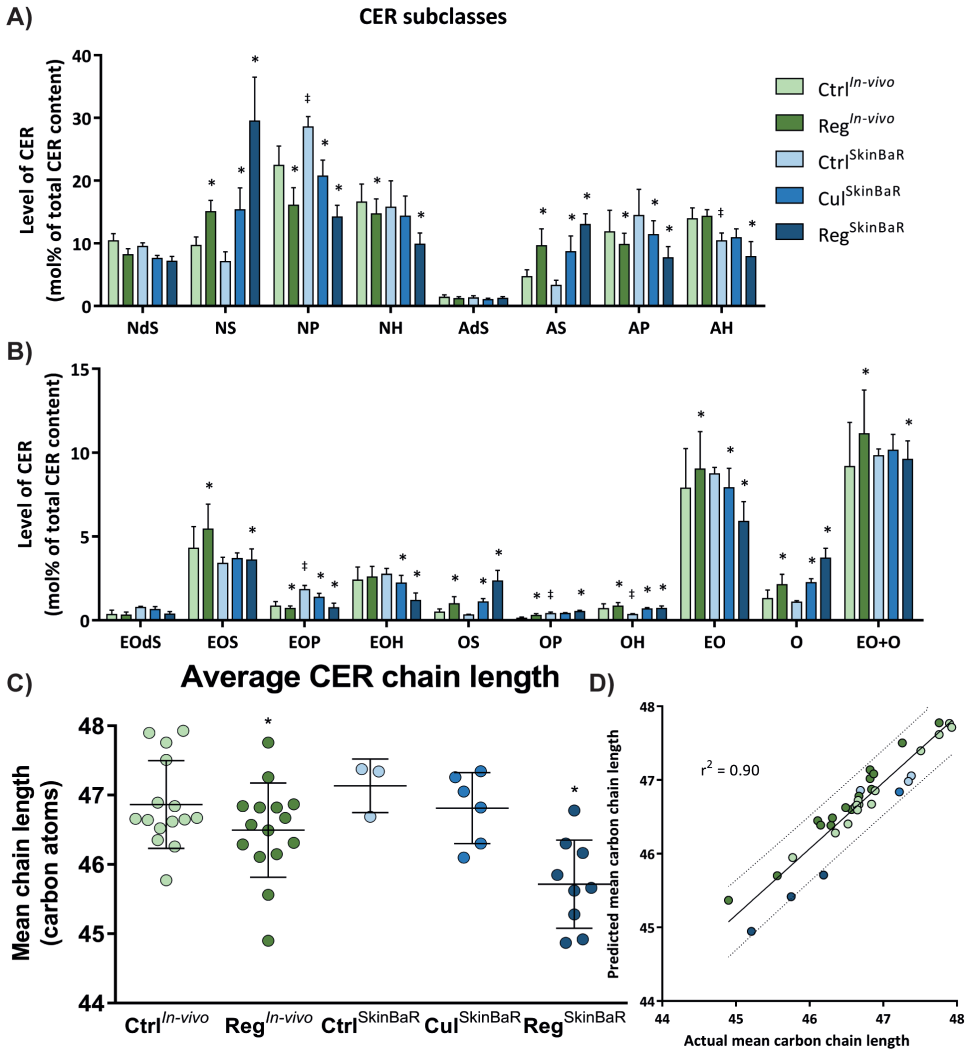

Figure 2. ***In vivo*** **and SkinBaR model ceramide profiles and mean ceramide chain length. A-B)** The total molar amount of all CERs was set at 100%. Bar show the relative molar abundance of the CER subclasses in mol%. N=15 for *in vivo* samples, N=3, 6, and 9 for $Ctrl^{SkinBaR}$, $Cul^{SkinBaR}$ and $Reg^{SkinBaR}$, respectively. **C)** The mean carbon atom chain length of all CERs. **D)** Correlation of the mean CER chain length with the predicted mean carbon chain length (for residuals: see Figure S3). Dotted lines: 95% confidence interval. Bars: mean ± SD, * $p<0.05$ compared to its respective control, ‡ $Ctrl^{SkinBaR}$ is different from $Ctrl^{In\text{-}vivo}$ ($p<0.05$).

in regenerated SC) compared to *in vivo* skin (increase in regenerated SC). When the EO and O CERs within each sample type were combined, there was only a minor difference in total (EO and O) CERs induced by regeneration (see Figure 2B and Table S2).
Because the total CER chain length is important, the MCL of all CERs was calculated (Figure 2C and Table S2). Ctrl$^{In\text{-}vivo}$ skin had a MCL of 46.9 carbon atoms, and Ctrl^{SkinBaR} and Cul^{SkinBaR} skin did not show a significant difference. Significant reductions in MCL with approximately 0.4 and 1 carbon atom were observed due to regeneration in *in vivo* and SkinBaR skin, respectively (Table S3).

Increased level of C34 ceramides and unsaturated ceramides in regenerated SC

Another parameter of interest is the level of C34 CERs. Ctrl$^{In\text{-}vivo}$ and Ctrl^{SkinBaR} had similar levels of C34 CERs. Compared to these controls, the mol% C34 CERs was significantly increased due to culturing and regeneration. The effect of regeneration was significantly larger in SkinBaR samples than in *in vivo* samples (Figure S2, Table S4). To determine if the increase in C34 CERs was subclass independent, the relative amount of C34 within each subclass was determined. This showed that for each subclass, the mol% C34 CERs for Ctrl$^{In\text{-}vivo}$ and Ctrl^{SkinBaR} did not significantly differ. Within the subclasses, the levels of C34 CERs were increased in Cul^{SkinBaR} samples compared to the control. Furthermore, in both Reg$^{In\text{-}vivo}$ and Reg^{SkinBaR}, a further increase in the level of C34 within the subclasses NS, AS, NH, and AH was observed (Figure 3, Table S4). For the CER subclasses NP, NdS, AP, and AdS a similar increase was observed (Figure S2). Due to the limited amount of SC acquired by tape-stripping (*in vivo*), C34 levels of these CER subclasses fall below the detection limit.

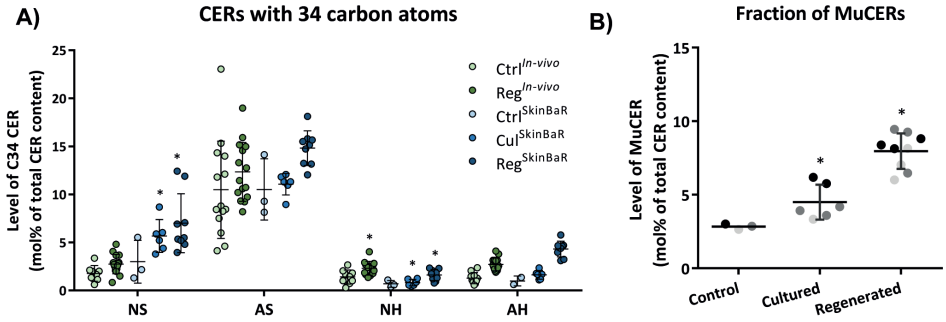

Figure 3. Level of C34 ceramides and unsaturated ceramides in the SC of the *in vivo* study and SkinBaR models. The total amount of all CERs was set at 100%. **A)** The level of C34 per CER subclass. **B)** The level of the mono-unsaturated CERs in mol%. Data of 3 donors was analyzed, indicated by different shades of gray. Bars: mean ± SD, * $p<0.05$ compared to its respective control.

As C34 CERs together with EO CERs with exceptional long chain lengths have been shown to influence the MCL, we investigated whether a LMM with the parameters EO CERs and C34 CERs could be used to predict the MCL (Table S5). A high correlation between the predicted and measured MCL was observed (Figure 2D), indicating 90% of the variation in MCL could be explained by the percentage EO CERs and C34 CERs. Another important parameter of the CER composition is the relative amount of mono-unsaturated CERs (MuCERs). Although MuCERs were detected in *in vivo* tape-strip samples, these were mostly below the limit of quantification. The MuCER percentages of the three SkinBaR sample groups were compared using an LMM (Table S6). In $Ctrl^{SkinBaR}$ SC 2.8 mol% MuCERs were present. This fraction significantly increased to 4.4 mol% in $Cul^{SkinBaR}$ samples ($p=0.04$) and to 8.0 mol% in $Reg^{SkinBaR}$ SC ($p<0.01$), see Figure 3B.

Regeneration does not affect lipid ordering

The lipid ordering was analyzed using Fourier-transform infrared spectroscopy (FTIR). For the SkinBaR samples, CH_2 stretching vibrations in the FTIR spectra could be obtained over a temperature range from 0 to 90°C. In order to compare the results obtained from the *in vivo* study and the SkinBaR model, the lipid ordering was examined using the center of gravity of the CH_2 stretching vibration peak in the FTIR spectra at skin temperature (32°C), see Figure 4A. A peak position below 2850 cm^{-1} indicates a conformational ordering of the lipids. If the peak position is increased to wavenumbers above 2852 cm^{-1}, the lipids in the stratum corneum are mainly in a conformational disordered state. In spectra from both $Ctrl^{In\text{-}vivo}$ and $Reg^{In\text{-}vivo}$ samples, the CH_2 peak was positioned at 2848.7 cm^{-1}. For the $Ctrl^{SkinBaR}$ and $Cul^{SkinBaR}$ samples the peak position was located at wavenumbers of 2849.2 cm^{-1} and 2849.3 cm^{-1}, respectively, which was significantly higher than in the *in vivo* samples. Although the peak position of $Reg^{SkinBaR}$ is substantially higher than that of $Ctrl^{SkinBaR}$, this difference was not statistically significant in the LMM (Table S7).

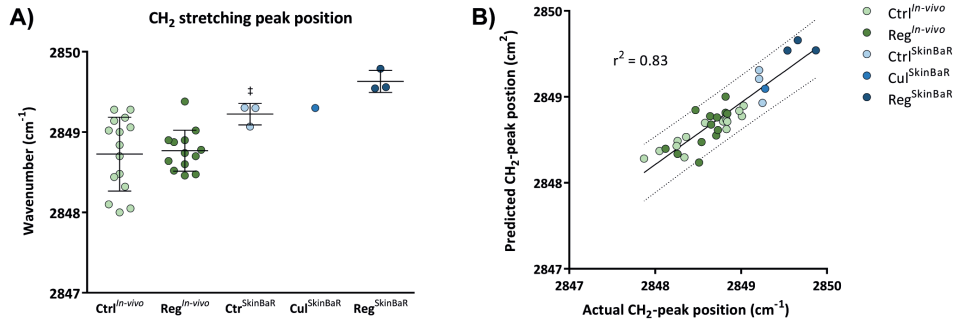

Figure 4. Center of gravity of the CH_2 stretching vibrations of *in vivo* study and SkinBaR skin models and correlation of predicted values for the CH_2 stretching peak with observed values. A) The center of gravity of the CH_2 stretching peak positions of the FTIR spectra at skin temperature of 32°C. Bars: mean ± SD, ‡ $Ctrl^{SkinBaR}$ is different from $Ctrl^{In\text{-}vivo}$ (LMM: $p<0.05$). **B)** The linear mixed model used to predict the CH_2 stretching peak includes C34 CERs, EO CERs, and two CER subclass ratios (for residuals: see Figure S4). Dotted lines: 95% confidence interval.

Using ceramide composition data to predict the lipid ordering

As the lipid disordering in SC of the SkinBaR model was higher compared to the conformational ordering in SC in the clinical setting, the relation between ceramide composition and lipid conformational ordering in (regenerated) SC was examined. This will provide insight in how the CER composition contributes to the lipid ordering. To obtain insight in the contribution of parameters related to ceramide composition, these were used to make a predictive model for the lipid ordering (i.e. CH_2 stretching peak position). We included the following ceramide related parameters in a LMM (Table S8): C34 and EO percentage (together being an MCL predictor) and the following subclass molar ratios: (dS+P+H)/S (excluding EO ceramides) and N/A, the former ratio correlated with barrier function in a previous study.[18] For more details about the subclass ratios, see Supplementary Methods. Figure 4B depicts the actual CH_2-peak position compared to the predicted position. The r^2 indicates that 83% of the variation was explained, with normally distributed residuals. This model showed that the combination of these CER-related parameters could, to a large extend, predict the lipid conformational ordering in SkinBaR and *in vivo* samples.

Discussion

In general, skin models have been used to i) model either healthy or diseased skin,[7,19,20] ii) examine treatment by formulations or active compounds,[8,9] iii) to study the dynamic process of SC regeneration,[11,12] iv) to study biological processes in the skin, and v) for screening of toxicity and irritation of compounds. Previously, we developed the SkinBaR model that has the potential to be used for multiple of these purposes.[13] However, the regenerated SC CER composition and lipid organization of this model have not been evaluated in detail and the correlation to an *in vivo* tape-stripping method is unknown. Therefore, the aim of this study was to examine to what extent the lipid matrix properties of the *ex vivo* and *in vivo* compromised skin models are comparable, and to determine if *ex vivo* models can (partly) replace clinical studies with regards to skin barrier repair.
In general, the changes in CER levels and lipid properties in the $Reg^{SkinBaR}$ samples were very similar, but more pronounced than in the $Reg^{In\text{-}vivo}$ samples as discussed below.

i) Both regenerated SC models showed a decrease in CER P subclasses and increase in S subclasses compared to control SC samples. This might be caused by an imbalance in activity of the enzymes acid sphingomyelinase and β-glucocerebrosidase, both involved in post-synthetic modification of CERs.[21] Although the expression of these enzymes was not affected in the SkinBaR model,[13] the activity can be altered.[22] With regard to properties of the CER chains, both the $Reg^{SkinBaR}$ and $Reg^{In\text{-}vivo}$ samples showed a decreased CER MCL, and an increase in levels of C34 CERs, while the level of unsaturated CERs was predominantly increased in $Reg^{SkinBaR}$ SC. In agreement with the elevated level of unsaturated CERs, the expression of Stearoyl-CoA desaturase was increased in the SkinBaR model.[13]
ii) The only substantial difference between the *in vivo* model and the SkinBaR

model was the change in level of EO CERs, which was increased in the $Reg^{In\text{-}vivo}$ samples and decreased in the $Reg^{SkinBaR}$ samples.

iii) The lipid ordering was not significantly affected by regeneration in both *in vivo* and *ex vivo* conditions. This might be due to less deep stripping in the present study compared to previous studies. Previously, lipids in the regenerated SC of the SkinBaR model were less ordered when almost all SC was removed.[14] Although the difference in CH_2 stretching peak position between $Ctrl^{In\text{-}vivo}$ and $Ctrl^{SkinBaR}$ was significant, different spectrum collection methods could have played a role. However, as the lipid composition could be used to accurately predict the lipid ordering, the difference mainly originated from a difference in lipid composition. These variances in lipid composition might have originated from the different method of SC sample collection, i.e. only tape 5-8 for *in vivo* conditions vs whole SC for *ex vivo* conditions, a similar difference as performed in collection of the FTIR data.

The tape-stripping method has been developed and used for several purposes, such as to specifically study the dynamic process of SC production,[23] to determine the penetration of topically applied products,[24] and to increase the bioavailability of these products in the deeper epidermal cell layers. As barrier function recovery of stripped healthy skin takes at least 14 days,[25] tape-stripped skin is also a suitable model to study skin barrier repair. Previously, it has been shown that in both *in vivo* and SkinBaR skin the proliferation rate immediately after barrier disruption is higher than after a recovery period of several days.[7,13] However, in the SkinBaR model, the proliferation rate was at its normal level after 8 days of culturing,[13] whereas in *in vivo* skin, the proliferation rate remained elevated for at least 10 days.[7]

It has been shown that tape-stripping healthy skin induced parakeratosis,[7] and induced an inflammatory response by secretion of cytokines.[26,27] Furthermore, in both AD and psoriasis pro-inflammatory cytokines are secreted.[28,29] Therefore, tape-stripped healthy skin has been used as an alternative for several inflammatory skin diseases.[7] During skin barrier repair of healthy *in vivo* skin, this inflammatory response slows down the repair process.[30] The lack of this systemic response in the SkinBaR model therefore substantiates the rapid barrier repair process. This also indicates that, during skin barrier repair, the *in vivo* skin is closer to skin homeostasis.

In contrast to the differences in proliferation rate and cytokine excretion, the expression pattern of proliferation proteins is very similar during *in vivo* and *ex vivo* skin barrier repair.[7,13]

When comparing the lipid properties of regenerated SC to that in SC of inflammatory diseased skin, many similarities can be observed. When compared to AD skin, these are i) similar changes in CER subclasses,[15] ii) a decreased MCL,[31] iii) an increase in levels of C34 CERs,[15,31] and iv) an increased level of unsaturated lipids.[32] Most of these changes correlated with an impaired skin barrier function.[3,15,17] Although the degree of changes vary, many of these alterations in CER composition have also been observed in other inflammatory skin diseases like psoriasis, and Netherton syndrome.[33,34] Additionally, a less dense lipid packing observed in $Reg^{SkinBaR}$ SC[14] also corresponds to findings in SC of these inflammatory skin diseases: a higher fraction of lipids adopting a less dense hexagonal lateral packing has been reported.[35]

A few limitations apply to this study. Skin of three donors was used for the SkinBaR

samples, and multiple samples of the same donor were used to generate the cultured and regenerated samples. Ideally, skin of the same participants is used for both the *in vivo* and SkinBaR experiments. However, the SkinBaR samples are difficult to culture with small biopsies. Furthermore, multiple biopsies of one donor would be required. This is difficult to achieve. Lastly, the lipid properties of both models were compared to skin of inflammatory skin diseases based on data found in literature. In future experiments, the SkinBaR model should be directly compared to non-lesional and lesional diseased skin in the same experiment to minimize difference between measurements.

In conclusion, this study shows that the changes in lipid properties in both the $Reg^{SkinBaR}$ and $Reg^{In\text{-}vivo}$ models are very similar and mimic the lipid properties in inflammatory skin diseases. This concerns changes in CER subclass profiles, MCL, level of CER unsaturation, and conformational ordering. Therefore, the SkinBaR model can be used to predict the *in vivo* response with regards to the lipid composition after application of topical barrier repair treatments aiming to restore the normal CER composition. By doing so, the need for clinical studies is reduced.

Materials and methods

Compromised in vivo skin barrier

15 healthy Caucasian volunteers (7 male, 18-29 years) participated in the study. The study was approved by the ethical committee of Leiden University Medical Center and performed according to the Declaration of Helsinki. Volunteers signed written informed consent. To exclude interference with topical products, the volunteers were asked not to use soaps or cosmetics on their ventral forearms during the whole study period. After a 1-week washout period, the SC barrier was disrupted by tape-stripping an area of 3.5 x 2.5 cm on the ventral forearm using D-Squame tape (CuDerm, Dallas, TX). Consecutive tape-strips were used until transepidermal water loss (TEWL) values over 60 $g/m^2/h$ were reached and the skin had a shiny appearance.[23] An AquaFlux AF200 (Biox, London, UK) was used to monitor the TEWL. To obtain SC after the 16-day recovery period, 21 tape-strips were harvested at the regenerated site and a control site using polyphenylene sulfide tape (Nichiban, Tokyo, Japan). The first tape-strip (tape 0) was discarded. An infrared spectrum was recorded after each second tape-strip in order to examine the lipid organization (see below).

Ex vivo human skin (SkinBaR) model

Ex vivo human skin was obtained from a local hospital, used within 12 hours after surgery, and handled according to the Declaration of Helsinki principles. The skin was cleaned, processed, stripped, and cultured as described before.[13] SC was isolated and SC sheets were stored over silica gel under argon atmosphere until use for CER extraction or infrared spectroscopy (see below).

Ceramide analysis by LC/MS

Lipid extraction, LC/MS measurements, and quantification of the tape-strips and SC sheets was performed as described elsewhere.[18] The obtained tape-strips were punched to Ø 16 mm, and extracted using a modified 4 step Bligh and Dyer at 40°C. Extracts of tapes 5-8 were combined in one sample. After extraction and evaporation of the extraction solvents, samples were dissolved in heptane:chloroform:methanol (95:2.5:2.5)(v:v:v). CERs were analyzed using an Acquity UPLC H-class (Waters, Milford, MA) connected to an XEVO TQ-S mass spectrometer (Waters, Milford, MA). Processing and post-processing were performed as described before.[18] The total molar amount of all CERs was determined quantitatively and used to calculate the molar percentage of each individual CER. The analyzed CER subclasses are depicted in Figure S1, synthetic CERs that were used for calibration are listed in Table S9.

SC lipid lateral organization and conformational ordering

FTIR was used to examine the SC lateral lipid organization and the conformational ordering of the SC lipids of *in vivo* and *ex vivo* skin samples.[36] All FTIR spectra were recorded using a Varian 670-IR spectrometer (Agilent Technologies, Santa Clara, CA). For more details, see the Supplementary Methods.

Statistical analyses

SPSS (v23, IBM, New York, NY) was used for group-wise comparisons using LMMs with nested terms. LMMs were used because of the advantages of i) analysis of multiple variables and their interactions in one model, ii) advanced data pairing (e.g. multiple conditions within one subject) can be examined, iii) the ability to handle missing data, and iv) the use of nested variables. LMMs were used to examine differences between the $Ctrl^{In\text{-}vivo}$ and $Ctrl^{SkinBaR}$ samples, and the change in the parameter (effect size) of culturing and regeneration of SC. For more details, see Supplementary Methods.

Conflict of interest

The authors state no conflict of interest.

Acknowledgements

The authors express their gratitude to Evonik for supplying the synthetic CERs. This research was financially supported by Dutch Technology Foundation TTW (grant no. 12400).

References

1. Michaels ASC, S.K.; Shaw J.E. Drug permeation through human skin – theory and in vitro experimental measurement. *American Institute of Chemical Engineers Journal* **1975**: 21: 12.
2. Mojumdar EH, Kariman Z, van Kerckhove L, et al. The role of ceramide chain length distribution on the barrier properties of the skin lipid membranes. *Biochim Biophys Acta* **2014**: 1838: 2473-2483.
3. Janssens M, van Smeden J, Gooris GS, et al. Increase in short-chain ceramides correlates with an altered lipid organization and decreased barrier function in atopic eczema patients. *J Lipid Res* **2012**: 53: 2755-2766.
4. Stahlberg S, Lange S, Dobner B, et al. Probing the Role of Ceramide Headgroup Polarity in Short-Chain Model Skin Barrier Lipid Mixtures by (2)H Solid-State NMR Spectroscopy. *Langmuir* **2016**: 32: 2023-2031.
5. Pilgram GS, Engelsma-van Pelt AM, Bouwstra JA, et al. Electron diffraction provides new information on human stratum corneum lipid organization studied in relation to depth and temperature. *J Invest Dermatol* **1999**: 113: 403-409.
6. Damien F, Boncheva M. The extent of orthorhombic lipid phases in the stratum corneum determines the barrier efficiency of human skin in vivo. *J Invest Dermatol* **2010**: 130: 611-614.
7. Gerritsen MJ, van Erp PE, van Vlijmen-Willems IM, et al. Repeated tape stripping of normal skin: a histological assessment and comparison with events seen in psoriasis. *Arch Dermatol Res* **1994**: 286: 455-461.
8. Wu X, Biatry B, Cazeneuve C, et al. Drug delivery to the skin from sub-micron polymeric particle formulations: influence of particle size and polymer hydrophobicity. *Pharmaceutical research* **2009**: 26: 1995-2001.
9. Gao Y, Wang X, Chen S, et al. Acute skin barrier disruption with repeated tape stripping: an in vivo model for damage skin barrier. *Skin research and technology : official journal of International Society for Bioengineering and the Skin (ISBS) [and] International Society for Digital Imaging of Skin (ISDIS) [and] International Society for Skin Imaging (ISSI)* **2013**: 19: 162-168.
10. Dickel H, Goulioumis A, Gambichler T, et al. Standardized tape stripping: a practical and reproducible protocol to uniformly reduce the stratum corneum. *Skin Pharmacol Physiol* **2010**: 23: 259-265.
11. Ghadially R, Brown BE, Sequeira-Martin SM, et al. The aged epidermal permeability barrier. Structural, functional, and lipid biochemical abnormalities in humans and a senescent murine model. *The Journal of clinical investigation* **1995**: 95: 2281-2290.
12. Williams MG, Hunter R. Studies on epidermal regeneration by means of the strip method. *The Journal of investigative dermatology* **1957**: 29: 407-413.
13. Danso MO, Berkers T, Mieremet A, et al. An ex vivo human skin model for studying skin barrier repair. *Exp Dermatol* **2015**: 24: 48-54.
14. Berkers T, Visscher D, Gooris GS, et al. Degree of Skin Barrier Disruption Affects Lipid Organization in Regenerated Stratum Corneum. *Acta Derm Venereol* **2018**: 98: 421-427.
15. Ishikawa J, Narita H, Kondo N, et al. Changes in the ceramide profile of atopic dermatitis patients. *J Invest Dermatol* **2010**: 130: 2511-2514.
16. Grubauer G, Feingold KR, Harris RM, et al. Lipid content and lipid type as determinants of the epidermal permeability barrier. *Journal of lipid research* **1989**: 30: 89-96.
17. Boiten WA, Berkers T, Absalah S, et al. Applying a vernix caseosa based formulation accelerates skin barrier repair by modulating lipid biosynthesis. *Journal of lipid research* **2018**: 59: 250-260.
18. Boiten W, Absalah S, Vreeken R, et al. Quantitative analysis of ceramides using a novel lipidomics approach with three dimensional response modelling. *Biochim Biophys Acta* **2016**: 1861: 1652-1661.
19. Sextius P, Marionnet C, Bon FX, et al. Large scale study of epidermal recovery after stratum corneum removal: dynamics of genomic response. *Exp Dermatol* **2010**: 19: 259-268.
20. Breternitz M, Flach M, Prassler J, et al. Acute barrier disruption by adhesive tapes is influenced by pressure, time and anatomical location: integrity and cohesion assessed by sequential tape stripping. A randomized, controlled study. *Br J Dermatol* **2007**: 156: 231-240.
21. Uchida Y, Hara M, Nishio H, et al. Epidermal sphingomyelins are precursors for selected stratum corneum ceramides. *Journal of lipid research* **2000**: 41: 2071-2082.
22. van Smeden J, Dijkhoff IM, Helder RWJ, et al. In situ visualization of glucocerebrosidase in human skin tissue: zymography versus activity-based probe labeling. *Journal of lipid research* **2017**: 58: 2299-2309.
23. Pinkus H. Examination of the epidermis by the strip method of removing horny layers. I. Observations on thickness of the horny layer, and on mitotic activity after stripping. *The Journal of investigative dermatology* **1951**: 16: 383-386.
24. Lademann J, Jacobi U, Surber C, et al. The tape

stripping procedure--evaluation of some critical parameters. *European journal of pharmaceutics and biopharmaceutics : official journal of Arbeitsgemeinschaft fur Pharmazeutische Verfahrenstechnik eV* **2009**: 72: 317-323.
25. Tanaka M, Zhen YX, Tagami H. Normal recovery of the stratum corneum barrier function following damage induced by tape stripping in patients with atopic dermatitis. *Br J Dermatol* **1997**: 136: 966-967.
26. Dickel H, Gambichler T, Kamphowe J, et al. Standardized tape stripping prior to patch testing induces upregulation of Hsp90, Hsp70, IL-33, TNF-alpha and IL-8/CXCL8 mRNA: new insights into the involvement of 'alarmins'. *Contact dermatitis* **2010**: 63: 215-222.
27. Nickoloff BJ, Naidu Y. Perturbation of epidermal barrier function correlates with initiation of cytokine cascade in human skin. *J Am Acad Dermatol* **1994**: 30: 535-546.
28. Ogawa E, Sato Y, Minagawa A, et al. Pathogenesis of psoriasis and development of treatment. *The Journal of dermatology* **2017**.
29. Kouris A, Pistiki A, Katoulis A, et al. Proinflammatory cytokine responses in patients with psoriasis. *European cytokine network* **2014**: 25: 63-68.
30. Lin TK, Zhong L, Santiago JL. Anti-Inflammatory and Skin Barrier Repair Effects of Topical Application of Some Plant Oils. *International journal of molecular sciences* **2017**: 19.
31. van Smeden J, Bouwstra JA. Stratum Corneum Lipids: Their Role for the Skin Barrier Function in Healthy Subjects and Atopic Dermatitis Patients. *Current problems in dermatology* **2016**: 49: 8-26.
32. van Smeden J, Janssens M, Kaye EC, et al. The importance of free fatty acid chain length for the skin barrier function in atopic eczema patients. *Exp Dermatol* **2014**: 23: 45-52.
33. Tawada C, Kanoh H, Nakamura M, et al. Interferon-gamma decreases ceramides with long-chain fatty acids: possible involvement in atopic dermatitis and psoriasis. *The Journal of investigative dermatology* **2014**: 134: 712-718.
34. van Smeden J, Janssens M, Boiten WA, et al. Intercellular skin barrier lipid composition and organization in Netherton syndrome patients. *The Journal of investigative dermatology* **2014**: 134: 1238-1245.
35. van Smeden J, Janssens M, Gooris GS, et al. The important role of stratum corneum lipids for the cutaneous barrier function. *Biochim Biophys Acta* **2014**: 1841: 295-313.
36. Boncheva M, Damien F, Normand V. Molecular organization of the lipid matrix in intact Stratum corneum using ATR-FTIR spectroscopy. *Biochimica et biophysica acta* **2008**: 1778: 1344-1355.

Supplementary Results

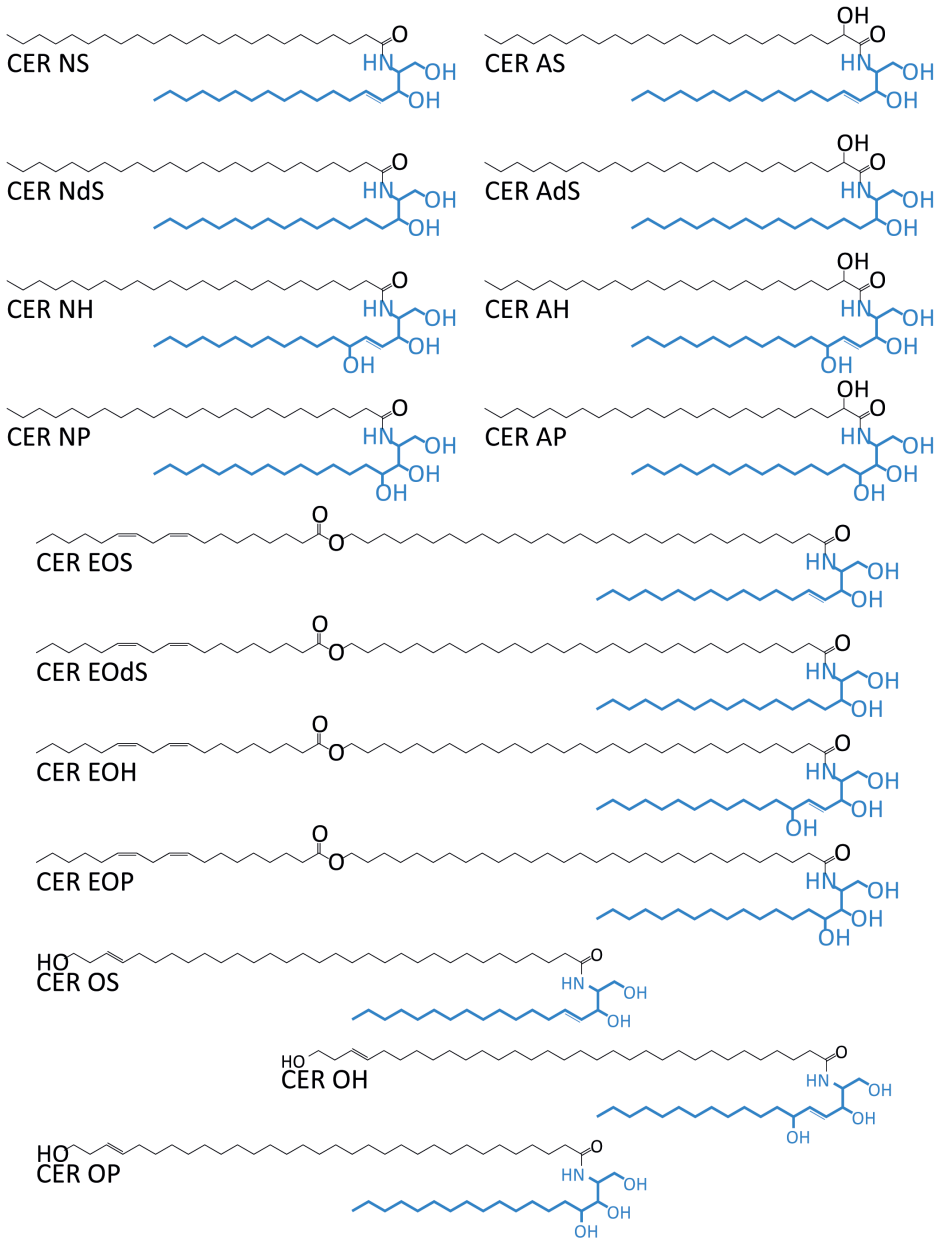

Figure S1. Ceramides subclasses in the stratum corneum lipid matrix. CERs consist of a sphingoid base coupled to a FA, which can both vary in molecular structure. CERs are named according to their molecular structure. The sphingoid base can either be a sphingosine (S), dihydrosphingosine (dS), phytosphingosine (P), 6-hydroxysphingosine (H), whereas the acyl chain is either non-hydroxylated (N), α-hydroxylated (A), ω-hydroxylated (O), or esterified ω-hydroxylated (EO). Both the sphingoid base (blue) and the fatty acid chain (black) can vary in the number of carbon atoms.

Table S1. Outcome of the linear mixed models for several CER subclasses. The intercept indicates the mol% of selected CER subclass in the Ctrl$^{In\text{-}vivo}$ situation. The effect size indicates the amount in mol% with which the variable changes the intercept. Multiple effect sizes can be added to obtain an estimate (see Supplementary Figure 5). * p<0.05.

Parameter	NS	NP	NH	AS	AP	AH	EOS	EOP	EOH	OS	OP	OH
Intercept (Ctrl$^{In\text{-}vivo}$)	9.6	22.4	16.6	4.7	11.8	13.9	4.3	0.8	2.4	0.5	0.1	0.7
Regenerated	5.4*	-6.3*	-1.9*	4.9*	-2.0*	0.4	1.1*	-0.1*	0.2	0.5*	0.2*	0.1*
SkinBaR	-2.6	6.1*	-0.8	-1.4	2.6	-3.5*	-0.9	1.0*	0.4	-0.2	0.3*	-0.3*
Cultured	8.8*	-8.0*	-1.9	5.6*	-3.0*	0.2	0.2	-0.5*	-0.6*	-0.8*	0.0	0.3*
SkinBaR(Cul.(Reg))	8.2*	-0.0	-2.1	-0.8*	-1.8	-3.0	-1.1*	-0.4*	-1.1*	0.7*	-0.1	-0.1

Table S2. Outcome of the linear mixed models for CER subclasses EO and O. The intercept indicates the mol% of the CER subclasses in the Ctrl$^{In\text{-}vivo}$ situation. The effect size indicates the amount in mol% with which the variable changes the intercept. * p<0.05.

Parameter	EO	O	EO and O
Intercept (Ctrl$^{In\text{-}vivo}$)	7.9	1.3	9.2
Regenerated	1.1*	-0.8*	2.0*
SkinBaR	0.9	-0.2	0.6
Cultured	-1.1*	1.2*	0.1
SkinBaR(Cul.(Reg))	-2.8*	0.6*	-2.2*

Table S3. Outcome of the linear mixed models for ceramide chain length. The intercept indicates the average number of carbon atoms of the CERs in Ctrl$^{In\text{-}vivo}$ situation. The effect size indicates the number of carbon atoms with which the variable changes the intercept. * p<0.05.

Parameter	Chain length
Intercept (Ctrl$^{In\text{-}vivo}$)	46.9
Regenerated	-0.4*
SkinBaR	0.3
Cultured	-0.4
SkinBaR(Cul.(Reg))	-0.6

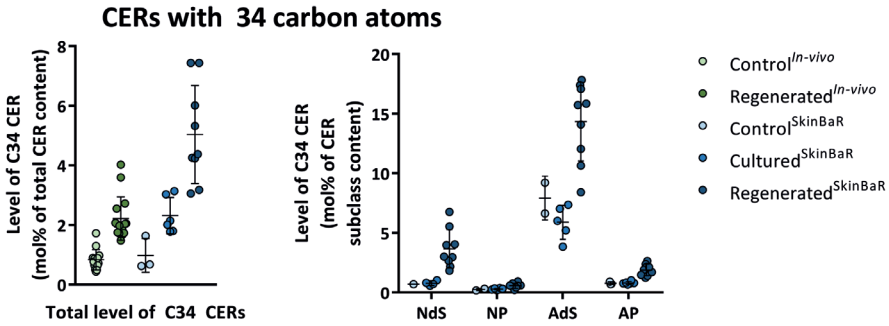

Figure S2. Amount of C34 ceramides in the SC of the clinical study and SkinBaR models. The total amount of all CERs was set at 100%. **Left:** The level of C34 CERs as percentage of the total CER content. **Right:** The level of C34 CERs as mol% within each subclass. C34s in these subclasses could only be detected in SkinBaR samples and not in *in vivo* samples. Bars: mean ± SD.

Table S4. Outcome of the linear mixed models for C34 ceramides. The intercept indicates the average number of carbon atoms of the CERs in Ctrl$^{In\text{-}vivo}$ situation. The effect size indicates the mol% with which the variable changes the intercept, corrected for variance in other subclasses. * p<0.05.

Parameter	C34 Total mol% of total CERs	C34 NS mol% within subclass	C34 NH mol% within subclass	C34 AS mol% within subclass	C34 AH mol% within subclass
Intercept (Ctrl$^{In\text{-}vivo}$)	-0.8	1.6	10.6	1.4	1.3
Regenerated	1.4*	1.2	1.8*	0.9	1.4
SkinBaR	0.1	1.4	-0.1	-0.7	-0.3
Cultured	1.4*	3.1*	0.5	0.2	0.7
SkinBaR(Cul.(Reg))	1.3*	-0.2	2.0	-0.2	1.3

Table S5. Outcome of the linear mixed models predicting the mean carbon chain length. The effect size indicates the change of the MCL relative to the intercept for a single variable. For example, add the effect size of EO CERs to the intercept for each mol% EO CERs in the sample (e.g. EO CER percentage for the sample is 9: add 9*0.2 to the intercept). * p<0.05.

Parameter	Predicted MCL
Intercept	45.3
EO CER mol%	0.2*
C34 CER mol%	-0.3*

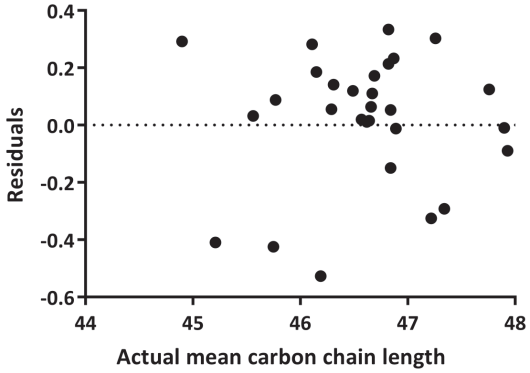

Figure S3. Residuals of the linear mixed model predicting MCL

Table S6. Outcome of the linear mixed models for mono-unsaturated ceramides in the SkinBaR SC conditions. The intercept indicates the level of MuCERs in the Ctrl^{SkinBaR} situation. The effect size indicates the change of the MuCER level relative to the intercept. * p<0.05.

Parameter	MuCERs mol% of total CERs
Intercept (Ctrl^{SkinBaR})	2.8
Regenerated	3.6*
Cultured	1.6*

Table S7. Outcome of the linear mixed models for lipid ordering in the SC matrix. The intercept indicates the average peak position of the stretching vibrations at 32°C in the Ctrl$^{In\text{-}vivo}$ situation. The effect size indicates the change of the peak position relative to the intercept. * p<0.05.

Parameter	Stretching peak position at 32°C
Intercept (Ctrl$^{In\text{-}vivo}$)	2848.7
Regenerated	0.0
SkinBaR	0.5*
Cultured	0.1
SkinBaR(Cul.(Reg.))	0.3

Table S8. Outcome of the linear mixed models predicting the peak position of the CH_2 stretching peak of the FTIR spectrum. The effect size indicates the change of the MCL relative to the intercept for a single variable. For example, add the effect size of EO CERs to the intercept for each mol% EO CERs in the sample (e.g. C34 CER percentage for the sample is 3: add 3*0.2 to the intercept). * p<0.05.

Parameter	Stretching peak position at 32°C
Intercept	2848.3
mol% C34 CERs (C34)	0.2*
mol% EO CERs (EO)	0.0
Ratio between CER subclasses ((dS+P+H)/S)	0.1
Ratio between CER subclasses (N/A)	0.0

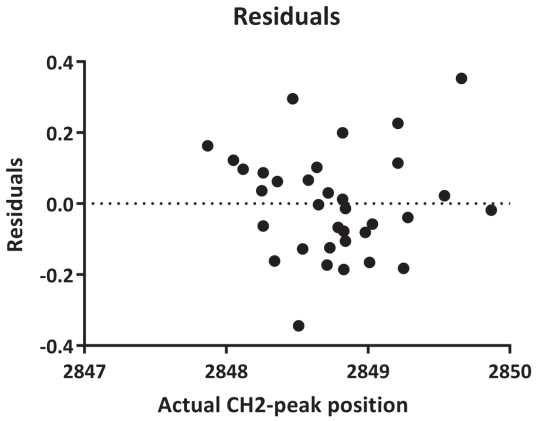

Figure S4. Residuals of the linear mixed model predicting the CH_2 stretching peak position

Supplementary methods

Chemicals

For culturing the SkinBaR skin model the following chemicals and materials were used: Cyanoacrylate (Bison, Goes, the Netherlands) was locally purchased, DMEM, Ham's F12, and penicillin/streptomycin were obtained from Fisher Scientific (Waltham, Massachusetts, USA), bovine serum albumin, sodium bromide, ethanol, acetone, trypsin, trypsin inhibitor, selenious acid, hydrocortisone, isoproterenol, L-carnitine, L-serine, insulin, α-tocopherol acetate, vitamin C, arachidonic acid, linoleic acid, and palmitic acid were purchased from Sigma-Aldrich (Zwijndrecht, the Netherlands).
For SC lipid extraction and LC/MS analysis the following solvents were purchased: methanol and chloroform were obtained from Lab-Scan (HPLC grade, Gliwice, Poland), isopropanol and ethanol were bought from Biosolve (UPLC grade, Valkenswaard, the Netherlands), and heptane was acquired from Actu-All (HPLC grade, Oss, the Netherlands). The synthetic CERs listed in Table S9 were used as calibrators for LC/MS analysis.

Table S9. Synthetic ceramides that were used as calibrators for LC/MS analysis. Numbers in brackets indicate the number of carbon atoms in the fatty acid chain and sphingosine chain, respectively.

Ceramides	
N(24)dS(18) [1]	A(24)S(18) [1]
N(18)dS(18) [1]	A(R)(22)S(18) [1]
N(24)dS(18) [1]	A(R)(16)S(18) [1]
N(24)S(18) [2]	N(24)P(18) [2]
N(22)S(18) [1]	N(22)P(18) [2]
N(20)S(18) [1]	N(16)P(18) [2]
N(18)S(18) [1]	E(18:2)O(30)S(18) [2]
N(16)S(18) [1]	E(18:2)O(27)S(18) [2]
N(24deu)S(18) [2]	E(18:2)O(30)P(S18) [2]
A(R)(24)P(18) [1]	E(18:2)O(27)P(18) [2]

[1] Avanti polar lipids (Alabaster, USA)
[2] Evonik Industries (Essen, Germany)

Inclusion and exclusion criteria for in vivo study

Prior inclusion, a dermatologist checked whether the volunteer was eligible for participation. Exclusion criteria were: (history of) dermatological disorders, chronic inflammatory disease, use of systemic drug therapies, abundant hair or unnatural abnormalities on the ventral forearm, (history of) drug abuse, and pregnancy.

Stratum corneum isolation from ex vivo skin

SC was isolated from the *ex vivo* skin samples by placing the skin overnight in a 0.1% trypsin solution in PBS (pH 7.4) and 1 hour at 37°C. Subsequently, the SC was peeled off, washed in 0.1% trypsin inhibitor solution, and twice in Millipore water.

FTIR analysis

All measurements were performed on a spectrometer equipped with a broadband mercury-cadmium-telluride detector and cooled with liquid N_2. Dry air constantly purged the sample compartments. Due to practical reasons, spectra for the *in vivo* SC and the SkinBaR SC were collected in reflection and transmission mode, respectively.
In vivo samples: In order to measure the lipid organization in the SC on the arms of the volunteers, attenuated total reflection FTIR (ATR-FTIR) was used. The spectrometer was connected to an external ATR accessory with a single reflection diamond (GladiATR, PIKE technologies, Maddison USA). Each spectrum was an average of 150 scans with a spectral resolution of 2 cm^{-1} measured at skin temperature. The instrument software Resolutions Pro 4.1 (Agilent Technologies) was used for data treatment. The center of gravity of the CH_2 symmetric stretching peak was determined at 90% of the peak height to determine the lateral ordering of the lipids. The centers of gravity 5 spectra were combined (e.g. after tape 2-10, and after tape 12-20) for analysis. The lateral lipid packing was analyzed by using the CH_2 scissoring vibrations. The full width at half maximum (FWHM) was determined in the second derivative of the spectra. Again, 5 spectra were combined for analysis.
SkinBaR samples: 24 hours prior to data collection, the isolated SC sheets were hydrated over a 27% NaBr solution in D_2O at room temperature. After hydration, the SC sheet was sandwiched between two AgBr-windows and measured in transmission mode. During the measurement, the sample temperature increased from 0 to 90°C. Spectra were recorded during 2 minutes at a 1°C interval, and as a co-addition of 128 scans using 1 cm^{-1} resolution. The center of gravity of the CH_2 symmetric stretching peak at skin temperature (32°C) was determined as described above. The lateral lipid packing was determined from the CH_2 rocking vibrations.

Statistical analysis

Linear mixed models were used in order to compare the means of several variables regarding CER composition and lipid organization between the five sample groups. The linear mixed models in this paper are used to calculate the effect sizes of the conditions 'Cultured' and 'Regenerated' compared to the controls. The formula $y=a_1x_1+a_2x_2+\ldots a_nx_n+b$ is used, in which 'a_1', 'a_2' and 'a_n' are effect sizes, 'b' is the intercept (= calculated mean of control situation), each 'x' depicts a specific condition, and 'y' is the calculated mean of the variable in the sample group.
The conditions 'SkinBaR', 'cultured', and 'regenerated' are included in the model to calculate the mean of each sample group. Each condition can either be 1 (yes) or 0 (no), e.g. $Ctrl^{in\text{-}vivo}$ samples are not cultured (0), not regenerated (0), and not SkinBaR model (0), and are therefore described by the intercept. In order to obtain the value for

the regenerated samples of the *in vivo* study ($Reg^{In\text{-}vivo}$), add the value for 'Regenerated' to the intercept. Similarly, add the value of 'SkinBaR' to the intercept to obtain the estimate for the $Ctrl^{SkinBaR}$ samples. Since $Cul^{SkinBaR}$ samples are described by both cultured and SkinBaR, both values of 'SkinBaR´ and 'Cultured' need to be added to the intercept.
The $Reg^{SkinBaR}$ samples are per definition also cultured (no non-cultured regenerated *ex vivo* samples exist). Therefore, a nested term was created in which this connection is described. So, $Reg^{SkinBaR}$ samples are cultured (1), regenerated (1), SkinBaR model (1), and cultured(regenerated) (=nested term; 1), and thus all effect sizes need to be added to the intercept in order to obtain the correct calculated mean value. The nested term is also used to describe the difference between the effect sizes of $Reg^{In\text{-}vivo}$ samples and $Reg^{SkinBaR}$ samples, since the effect size does not need to be similar. For an example calculation, see Figure S5.
To obtain a predictive model for the CH_2 stretching peak position, a simple linear mixed model was build using summarizing lipid parameters as covariant. We chose variables that have previously been used or are expected to affect the lipid ordering. C34 and EO percentage were chosen, as both have been related to lipid organization[1] and they are predictors of the average chain length[1] therefore omitting the mean chain length in the model. Ratios between the subclasses have been shown to affect the lipid organization.[2-4] Here, two ratios were chosen that are expressions of sphingoid bases, as EO ceramides are included as a separate factor these were left out of these ratios. The model uses these 4 parameters as covariant and has intercept set as a random variable of sample donor.

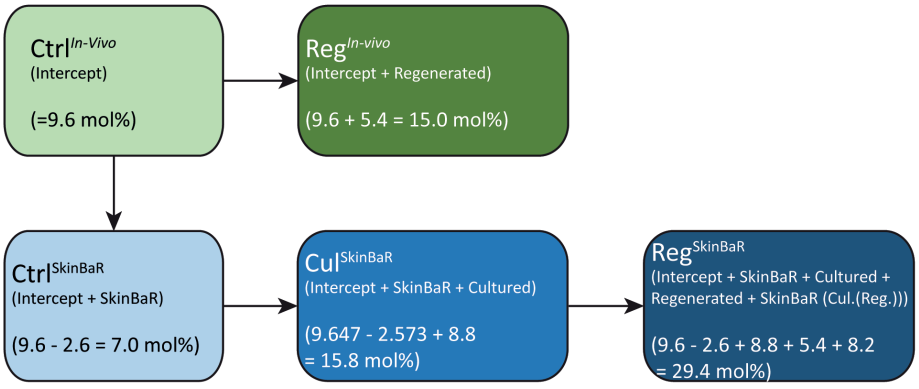

Figure S5. Sample overview and explanation of linear mixed models with example calculation. Linear mixed models were used to interpret the data described throughout this paper and to compare outcomes between the different sample types. In all cases, the values obtained from the control site in the *in vivo* study ($Ctrl^{In\text{-}vivo}$) are indicated by the intercept. All other values are changes relative to the intercept. Example calculations show the level of CER NS in each sample group with values obtained from the linear mixed model described in Table S1. P-values below 0.05, depicted by * in tables S1-S8, indicate a significant change compared to the $Ctrl^{In\text{-}vivo}$ (=intercept). All intercepts were statistically different from 0, and therefore not further indicated as statistically significant.

Supplementary references

1. Janssens M, van Smeden J, Gooris GS, et al. Increase in short-chain ceramides correlates with an altered lipid organization and decreased barrier function in atopic eczema patients. *J Lipid Res* **2012**: 53: 2755-2766.
2. Boiten WA, Berkers T, Absalah S, et al. Applying a vernix caseosa based formulation accelerates skin barrier repair by modulating lipid biosynthesis. *Journal of lipid research* **2018**: 59: 250-260.
3. Groen D, Poole DS, Gooris GS, et al. Investigating the barrier function of skin lipid models with varying compositions. *European journal of pharmaceutics and biopharmaceutics : official journal of Arbeitsgemeinschaft fur Pharmazeutische Verfahrenstechnik eV* **2011**: 79: 334-342.
4. Skolova B, Kovacik A, Tesar O, et al. Phytosphingosine, sphingosine and dihydrosphingosine ceramides in model skin lipid membranes: permeability and biophysics. *Biochimica et biophysica acta* **2017**: 1859: 824-834.

Part 2

Chapter 5

Topically applied fatty acids are elongated before incorporation in the stratum corneum lipid matrix in compromised skin

Tineke Berkers[1], Lauri van Dijk[1], Samira Absalah[1], Jeroen van Smeden[1], Joke A. Bouwstra[1]

[1] Department of Drug Delivery Technology, Leiden Academic Centre for Drug Research, Leiden University, Leiden, 2333 CC, The Netherlands

Exp Dermatol. 2017 Jan;26(1):36-43

Abbreviations

AD	Atopic dermatitis
CER	Ceramide
Chol	Cholesterol
dFA	Perdeuterated fatty acid
ELOVL	Elongation of very long chain fatty acids
ESRF	European synchrotron radiation facility
FA	Fatty acid
FA^{16}	Palmitic acid
FA^{18}	Stearic acid
FA^{22}	Behenic acid
$Form^{(d)FA16}$	FA formulation with (deuterated) palmitic acid
$Form^{(d)FA18}$	FA formulation with (deuterated) stearic acid
$Form^{(d)FA22}$	FA formulation with (deuterated) behenic acid
FTIR	Fourier transform infrared spectroscopy
LC/MS	Liquid chromatography/mass spectrometry
SC	sStratum corneum
SkinBaR model	Skin barrier repair model
TEWL	Transepidermal water loss
VC	Vernix caseosa

Keywords

Skin barrier repair, topical formulation, lipid organization, lipid synthesis

Abstract

In several skin diseases both the lipid composition and organization in the stratum corneum (SC) are altered which contributes to the impaired skin barrier function in patients. One of the approaches for skin barrier repair is treatment with topical formulations to normalize SC lipid composition and organization. Vernix caseosa, a white cheesy cream on the skin during gestational delivery, has shown to enhance skin barrier repair. In the present study, we examined how a fatty acid containing formulation mimicking the lipid composition of vernix caseosa interacts with the lipid matrix in the SC. The formulation was applied on *ex vivo* human skin after SC removal. Subsequently, the *ex vivo* human skin generated SC during culture. The effect of fatty acid (FA) containing formulations on the lipid organization and composition in the regenerated SC was analyzed by Fourier transformed infrared (FTIR) spectroscopy and liquid chromatography/mass spectroscopy (LC/MS), respectively. FTIR results demonstrate that the FAs are intercalated in the lipid matrix of the regenerated SC and partition in the same lattice with the endogenous SC lipids, thereby enhancing the fraction of lipids forming an orthorhombic (very dense) packing in the SC. LC/MS data show that the topically applied FAs are elongated before intercalation in the lipid matrix and are thus involved in the lipid biosynthesis in the skin.

Introduction

Stratum corneum (SC) forms the main barrier for diffusion of compounds through the skin. This upper skin layer consists of corneocytes, embedded in a lipid matrix.[1] The main lipid classes in SC are free fatty acids (FAs), ceramides (CERs), and cholesterol (CHOL).[2-4] In between the corneocytes, lipids are organized in lamellae forming either a long periodicity phase or short periodicity phase.[5-7] In these lipid lamellae, lipids are assembled in either a dense orthorhombic packing, a less dense hexagonal packing or a loosely packed liquid phase, also referred to as the lateral packing[8-12], see Supplementary Figure 1. In healthy subjects, the majority of the lipids adopts the dense orthorhombic packing.[9]

The skin barrier function is decreased in multiple skin diseases, e.g. lamellar ichthyosis, psoriasis, Netherton syndrome, and atopic dermatitis (AD).[13] For instance, AD is a very common disease characterized by clinical features such as red, dry and itchy skin, in which the correlation between SC lipid organization and skin barrier function is extensively described.[14] Evidence has been reported that the reduction in lipid chain length in SC of lesional and non-lesional skin of AD patients correlated with this reduced skin barrier function.[15-18] Related to these changes in composition, lipids in SC of AD patients adopt a more hexagonal lateral lipid packing compared to healthy skin.[19] Changes in lipid organization and barrier function are also observed in other skin diseases.[13] It might be possible to restore skin barrier defects and optimize lipid composition and organization with topical application of lipid formulations.

To develop topical formulations to treat impaired skin barrier, often animal skin or clinical studies are used as no proper *ex vivo* skin models are available. However, this is far from optimal because animal skin is different from human skin[20] and in a formulation development phase only a limited number of formulations can be tested in clinical settings. Therefore, recently an *ex vivo* human skin barrier repair (SkinBaR) model has been developed that can be used to study the effect of formulations on skin barrier repair.[21] In this model, the SC is removed by stripping. Subsequently, stripped skin is cultured during which the skin generates SC. The regenerated SC of this model has several characteristics in SC lipid composition and organization mimicking AD, e.g. an increased level of lipids forming a hexagonal packing and an altered CER profile that in several aspects mimics the CER subclass composition observed in lesional and non-lesional AD skin.[21] Furthermore, recently it has been observed that the level of shorter chain length CERs is increased in this *ex vivo* model mimicking that in SC of AD patients.[22]

In previous studies, topical formulations were developed based on vernix caseosa (VC), a white cheesy film which is formed during the last trimester of pregnancy. VC contains the barrier lipids FAs, CERs, and CHOL in addition to sterol esters, wax esters, triglycerides, and squalene and has been shown to enhance barrier repair in mice.[23-25] Because of the barrier repair properties of VC, we question whether VC components form an extra layer on the skin surface or will be incorporated in the SC lipid matrix during barrier repair. To study this, synthetic perdeuterated and protiated fatty acids (dFAs and FAs, respectively) in a formulation mimicking many aspects of the VC, referred to in this paper as FA formulation, were applied on the SkinBaR model and the regenerated SC lipid matrix was examined in detail. Our results show that the applied

FAs are incorporated in the SC lipid matrix and that FAs with a shorter chain length are elongated.

Materials and methods

Composition of FA formulations

Formulations consist of super sterol esters, Miglyol 812 (triglycerides), squalene, CHOL, and FAs in a weight ratio of 50.5, 37.6, 6.7, 3.7, and 1.5%, respectively. With regard to FAs, formulations contained either palmitic acid (FA^{16}), stearic acid (FA^{18}) or behenic acid (FA^{22}). FAs were either protiated or perdeuterated. The control formulation contains all lipids except FAs. For preparation and application of formulations see supplementary material.

Preparation and culturing of ex vivo skin

Human abdomen or mamma skin was obtained after surgery from a local hospital and handled according to principles of the Declaration of Helsinki. *Ex vivo* skin was used within 12 hours after surgery. Subcutaneous fat was removed, the skin was wiped with 70% EtOH and Millipore water, and dermatomed to a thickness of 600 µm (Deca Dermatome, DePuy Healthcare, Leeds, UK). SC was removed by sequential stripping. By using 6-8 strips, the skin became shiny indicating most of the SC was removed. After stripping of SC, the skin was cultured as described in the supplement.
Studies were performed with 5 different conditions at least in triplicate:

i) Native skin (non-cultured)
ii) Cultured skin
iii) Stripped and cultured skin
iv) Stripped and cultured skin + control formulation
v) Stripped and cultured skin + FA formulations containing either protiated or deuterated a) FA^{16}, b) FA^{18}, or c) FA^{22} ($Form^{(d)FA16}$, $Form^{(d)FA18}$, and $Form^{(d)FA22}$, respectively)

After 8 days of culturing, skin was harvested and processed for embedding in paraffin, cryofixation in Tissue-Tek O.C.T.™ (Sakura Finetek Europe B.V., Alphen aan den Rijn, The Netherlands), and SC isolation (see supplement).

Fourier transform infrared spectroscopy

Fourier transform infrared spectroscopy (FTIR) was used to examine the conformational ordering and lateral packing of the lipid matrix in native and regenerated SC with and without FA formulation. SC samples were hydrated at room temperature for 24 hours over a 27% NaBr solution in D_2O, resulting in a final hydration level of around 20% in the SC. All FTIR spectra were recorded using a Varian 670-IR FTIR spectrometer (Agilent Technologies, Santa Clara, USA), equipped with a broadband mercury-cadmium-telluride detector. For further details see supplement.

Liquid chromatography mass spectrometry

The lipid composition of SC was examined using liquid chromatography/mass spectrometry (LC/MS). Only saturated FAs with even carbon chain length were applied and analyzed.
Lipid extraction was performed on isolated SC samples using a modified Bligh and Dyer method (Boiten et al., unpublished observations). The lipids were stored in chloroform/methanol (1:2) at 4°C until use. The samples were analyzed using a LC/MS method optimized for detection of FAs. The detailed analysis method is described in the supplement.
All LC/MS data was analyzed and processed using MassLynx and TargetLynx software (V4.1 SCN951, Waters, USA).

Statistical analysis

One-way ANOVA with Tukey multiple comparisons post-hoc test was used to analyze the data using GraphPad Prism 6 software (Graphpad software Inc., San Diego, CA, USA).

Results

FAs from formulations are incorporated in newly formed SC

To determine conformational ordering of the lipids, thermotropic behavior was examined of CH_2 symmetric and CD_2 asymmetric stretching vibrations in the FTIR spectrum. When the chains are fully extended and show a high conformational ordering, peak positions of the CH_2 and CD_2 stretching vibrations in the FTIR spectrum are below a wavenumber of 2850 and 2195 cm^{-1}, respectively. When the lipids show conformational disordering (e.g. if lipids are assembled in a liquid state), peak positions are shifted to wavenumbers higher than 2852 and 2196 cm^{-1} for CH_2 symmetric and CD_2 asymmetric stretching vibrations, respectively. The onset transition temperature at which the ordered-disordered shift starts can be determined from the thermotropic response. Peak positions of stretching vibrations are plotted against temperature. Two linear regression lines were fitted to the linear parts before and after the onset of the ordered-disorder transition, and the intercept of the two lines was determined. This procedure was used for both SC samples and formulations alone.
Figure 1A depicts CD_2 asymmetric stretching vibrations of $Form^{dFA16}$, $Form^{dFA18}$, and $Form^{dFA22}$ as a function of temperature. All three formulations are disordered already at 20°C, but some ordering is observed in $Form^{dFA22}$ at low temperatures.
CD_2 and CH_2 stretching vibrations of control SC and after topical application of $Form^{dFA16}$, $Form^{dFA18}$, or $Form^{dFA22}$ on stripped skin are plotted in Figure 1B-E.
We first focus on CH_2 stretching vibrations of native and regenerated SC. These show a small shift at around 40°C attributed to the orthorhombic to hexagonal phase transition.[26] A further increase in temperature results in a shift in the spectrum due to ordered-disordered phase transition between approximately 60°C and 70°C. These

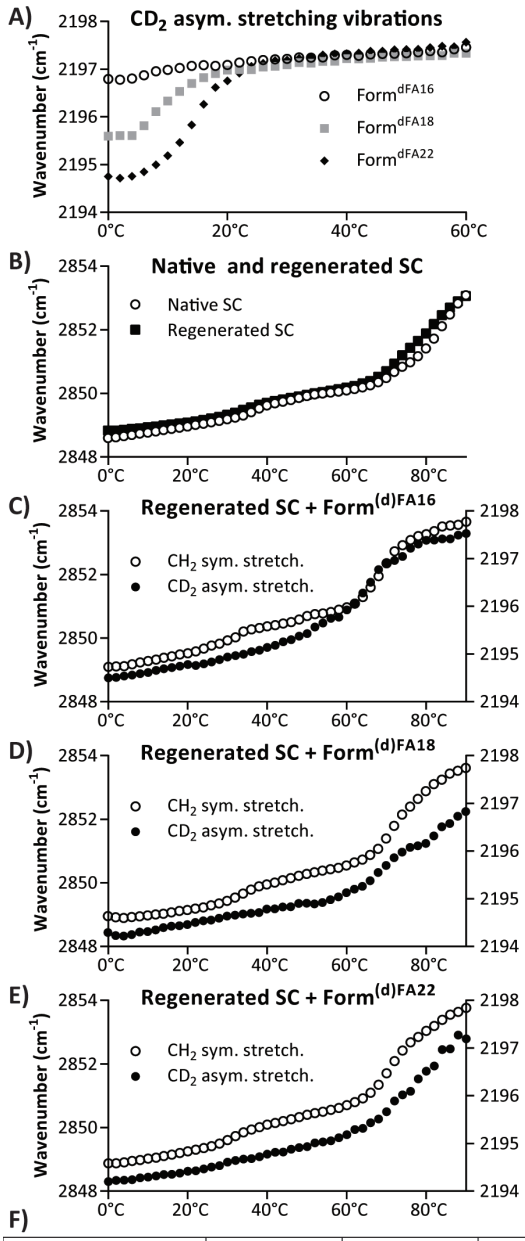

Figure 1. Peak positions of CH_2 symmetric stretching and CD_2 asymmetric stretching vibrations of FTIR spectra plotted as a function of temperature. A) Asymmetric stretching vibrations of CD_2 groups in $Form^{dFA16}$, $Form^{dFA18}$, and $Form^{dFA22}$ start at 0°C with a frequency of 2196.8, 2195.6 and 2194.7 cm^{-1}, respectively. This indicates that dFA^{16} in the formulation adopts a liquid packing already at low temperatures. For $Form^{dFA18}$ and $Form^{dFA22}$, the dFAs show some ordering at low temperatures. The CD_2 stretching vibrations show a shift in wavenumber reaching a wavenumber of 2197 cm^{-1} indicating a transition to a more disordered state. **B)** The CH_2 symmetric stretching vibrations of native SC and regenerated SC show a small shift at around 40°C (orthorhombic to hexagonal phase transition). Another phase transition from ordered to disordered is observed at around 60-70°C. **C-E)** SC on which $Form^{dFA16}$, $Form^{dFA18}$, or $Form^{dFA22}$ was applied, respectively. CH_2 stretching vibrations show a similar profile as native SC and regenerated SC. CD_2 stretching vibrations of the formulations show a wavenumber of around 2194 cm^{-1} at 0°C, increase gradually to around 2195 cm^{-1} at approximately 60°C, followed by a steep increase to circa 2197 cm^{-1} at 90°C. **F)** Onset temperature of ordered-disordered phase transition of SC lipids of regenerated SC determined by thermotropic response of CH_2 or CD_2 stretching vibrations with and without topical application of formulations. n.a.: not applicable

Topical formulations on SC	CH_2 sym. stretching Average ± SD	CD_2 asym. stretching Average ± SD	ANOVA p-value
Native SC	69.1 ± 4.9 °C	n.a.	
Regenerated SC	60.5 ± 5.3 °C	n.a.	
Reg. SC + Form$^{(d)FA16}$	61.2 ± 2.6 °C	59.4 ± 4.5 °C	0.999
Reg. SC + Form$^{(d)FA18}$	59.5 ± 3.0 °C	53.7 ± 2.8 °C	0.466
Reg. SC + Form$^{(d)FA22}$	60.7 ± 2.2 °C	61.2 ± 0.8 °C	1

transitions are also observed in the same temperature ranges in regenerated SC on which FA formulations were applied (Figure 1C-E, open circles).
When focusing on the CD_2 asymmetric stretching vibrations in the FTIR spectrum, the ordered-disordered phase transition is located at around 60˚C.
Figure 1F shows temperatures at which the ordered-disordered transitions start. Onset transition temperatures are obtained from CH_2 symmetric and CD_2 asymmetric stretching vibrations. As indicated in the table, the temperature at which the transition starts is highest in native SC. After stripping and regeneration, with or without a formulation, the onset temperature of the ordered-disordered transition are comparable, but significantly lower than in native SC. Onset transition temperatures of regenerated SC and SC with various formulations were not statistically significant different from each other (see Supplementary Figure 3).
Onset transition temperatures of the ordered-disordered phase transitions obtained from CD_2 stretching vibrations of dFA in the topically applied formulations were compared to those obtained from CH_2 stretching vibration of the corresponding SC. There was no significant difference between CH_2 and CD_2 onset transition temperatures indicating that the thermotropic response of the protonated and deuterated stretching vibrations are very similar.

Topically applied deuterated FAs and protiated SC lipids participate in one lattice

The lateral organization of the lipids in the SC was analyzed using CH_2 rocking vibrations of FTIR spectra in a range from 0 to 90˚C. Lipids adopting a hexagonal packing display only one vibration in the rocking mode in the FTIR spectrum at a position of around 719 cm^{-1}. When lipid chains assemble in an orthorhombic packing, adjacent chains in rocking modes interact via short-range coupling, resulting in splitting of contours. This results in two peaks at wavenumbers 719 and 730 cm^{-1}. When deuterated chains participate in the same lattice as the protiated chains, deuterated chains interfere resulting in a reduction of short-range coupling and thus a reduction in intensity or even a disappearance of the 730 cm^{-1} peak. All spectra of SC samples are displayed with a similar ratio between the lowest point at around 715 cm^{-1} and the top at around 719 cm^{-1}.
The FTIR spectrum of regenerated SC (Figure 2A) shows a reduction in intensity of the 730 cm^{-1} band at 0˚C compared to native SC (Supplementary Figure 5), indicating a reduced level of lipids adopting an orthorhombic lipid packing. The 730 cm^{-1} band starts to decrease in intensity at 20˚C and disappears at around 42˚C demonstrating a shift in phase transition to a lower temperature range than in native SC.
In order to investigate whether formulations with only protiated lipids increased the lateral packing density, these formulations were applied on the SkinBaR model. As can be observed in Figure 2C, CH_2 rocking vibrations in the FTIR spectrum of SC after application of $Form^{FA16}$ shows a strong peak at 719 cm^{-1} and a less strong peak at 730 cm^{-1}, even relatively lower than in regenerated SC. However, after topically applying $Form^{FA18}$ and $Form^{FA22}$ (Figure 2E/G) the relative intensity of the band at 730 cm^{-1} compared to that of the 719 cm^{-1} band is higher, indicating that these FAs increase the level of lipids forming an orthorhombic packing. $Form^{FA22}$ has the strongest increase in relative peak intensity of the 730 cm^{-1} band. This effect can be attributed to the

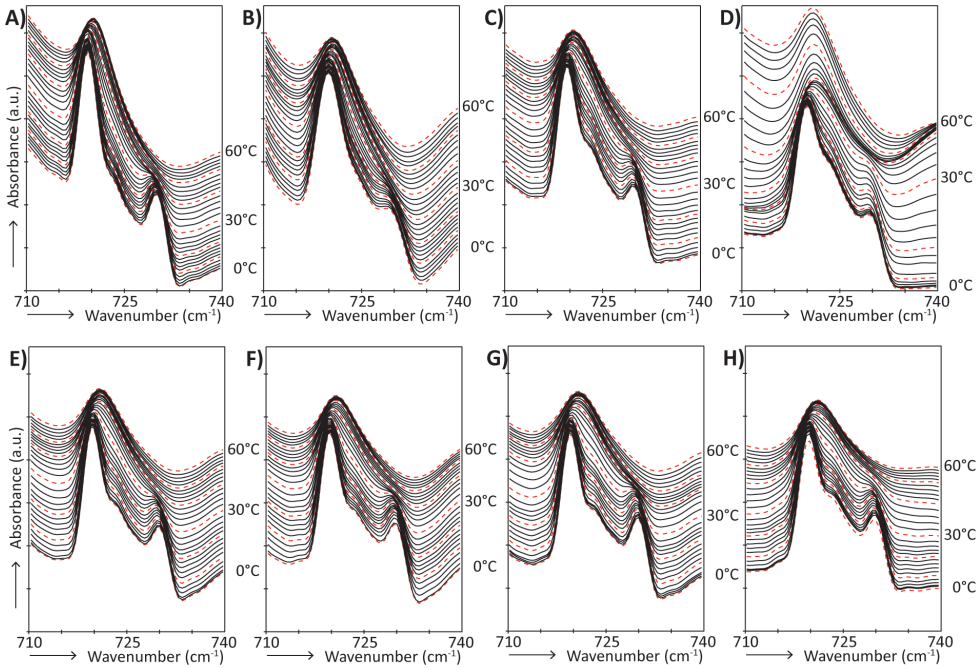

Figure 2. FTIR spectra showing CH_2 rocking vibrations of SC lipids with and without topical application of FA formulation, as a function of temperature (0-60°C). A) regenerated SC, **B)** regenerated SC with topical application of control formulation, **C-H)** regenerated SC with topical application of **C)** $Form^{FA16}$, $Form^{dFA16}$, **E)** $Form^{FA18}$, **F)** $Form^{dFA18}$, **G)** $Form^{FA22}$, and **H)** $Form^{dFA22}$, respectively.

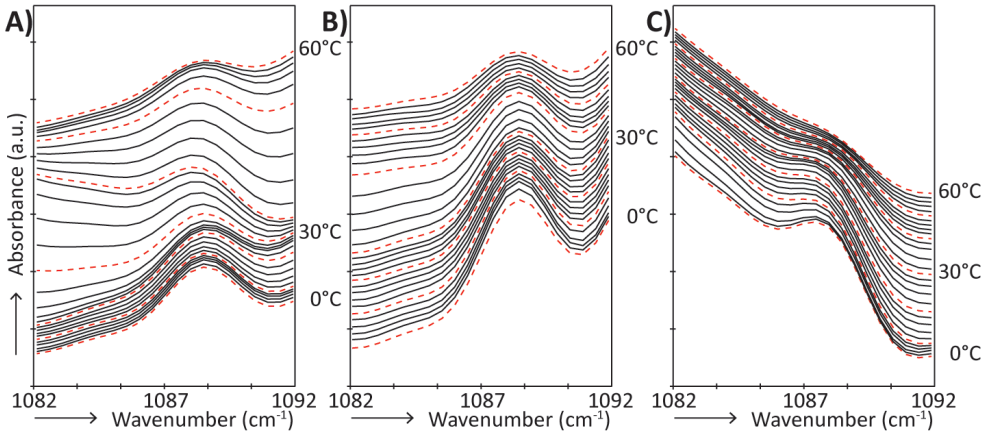

Figure 3. FTIR spectra showing CD_2 scissoring vibrations of SC lipids after application of FA formulation containing dFAs as a function of temperature (0-60°C). A) $Form^{dFA16}$, **B)** $Form^{dFA18}$, **C)** $Form^{dFA22}$.

presence of FAs in the formulation. After application of control formulation the relative intensity of the 730 cm^{-1} band is lower than in regenerated SC (Figure 2B), while the relative intensity of the 730 cm^{-1} band after topical application $Form^{FA22}$ is comparable to that of regenerated SC.
The next question is whether topical FAs are partitioning in the same lattice as SC lipids or that applied FAs form separate orthorhombic domains in the lipid matrix. In order to investigate this, rocking vibrations were also examined after topical application of formulations with dFAs. For all three formulations containing dFAs the relative peak intensity of the band at 730 cm^{-1} is decreased compared to the formulations with the respective protiated FAs (Figure 2D/F/H). However, for $Form^{dFA16}$, the relative intensity of the peak at 730 cm^{-1} is also lower than in regenerated SC.
The reduced intensity of the 730 cm^{-1} band in the spectrum suggests that dFAs from the formulation are not forming separate domains, but are partitioning in one lattice with protiated lipids from the SC.
To confirm the incorporation of dFA in the lipid matrix, CD_2 scissoring vibrations were also examined. A doublet at peak positions of around 1086 and 1090 cm^{-1} indicates phase separated orthorhombic domains, a singlet at around 1088 cm^{-1} denotes that short-range ordering between the deuterated chains does not occur demonstrating partitioning of deuterated lipids in the same lattice as SC lipids. In Figure 3, the singlet scissoring vibration at around 1088 cm^{-1} indicates a mixing between deuterated lipids and protiated skin lipids, as pure FA^{16}, FA^{18} and FA^{22} assemble in an orthorhombic lateral packing.

Topically applied deuterated FAs are elongated in the epidermis

We analyzed topical application of $Form^{dFA16}$, $Form^{dFA18}$, and $Form^{dFA22}$ to examine whether dFAs are used in epidermal lipid biosynthesis. Using LC/MS it was demonstrated that dFA^{16} was present in substantial levels. Interestingly, dFA^{16} with an elongated protiated chain were observed (Figure 4), showing a similar profile as endogenous FAs with the most abundant chain lengths FA^{24D31} and FA^{26D31} (elongated with eight and ten CH_2 groups, respectively).
Topical application of $Form^{dFA18}$ also resulted in elongation of deuterated lipids. However, dFA^{18} has 35 deuterated ions which overlaps with the chloride adduct of the endogenous FA and cannot be fully separated (difference in retention time of 0.06 min). No elongation was observed after addition of $Form^{FA22}$.

Discussion and conclusion

The skin barrier function of for instance AD patients is reduced, as indicated by e.g. transepidermal water loss (TEWL) values that are significantly higher in lesional and non-lesional skin than in healthy skin.[27-30] Several studies report differences in lipid composition in lesional and non-lesional AD skin compared to control skin. This concerns both chain length and levels in subclasses of CERs and FAs.[15,31,32] In more recent papers it was described that an increase in TEWL in lesional and non-lesional skin correlated excellently with a reduction in CER and FA chain length in these

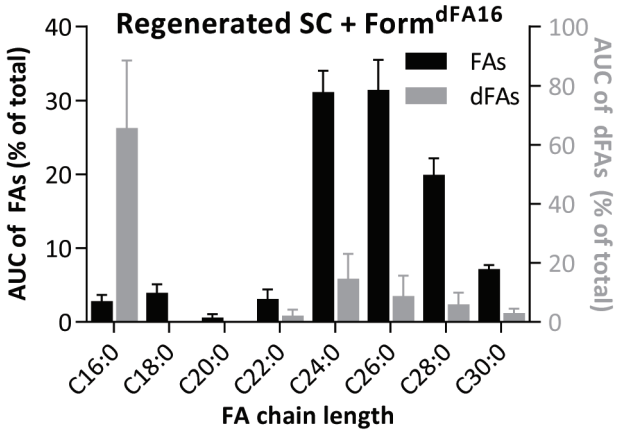

Figure 4. AUC of LC/MS peaks of dFAs after application of Form^{dFA16}. Gray bars represent dFA^{16} and elongated FAs from FA^{22D31} and longer. Black bars represent endogenous FAs present in the SC lipid matrix.

patients, thereby reducing the level of lipids adopting an orthorhombic packing.[16,17,33] These results suggest that normalizing lipid composition and organization in the skin barrier offers a possibility to improve the skin barrier. We selected a FA formulation based on VC, which contains barrier lipids CER, FA and CHOL. In previous studies, it was shown that natural and synthetic VC applied on mouse skin from which the SC was removed enhanced barrier repair as monitored by TEWL.[23,25] In the present study, we examine whether FAs incorporated in the formulation affect lipid organization and composition in human SC after topical application. For this reason, no CERs were included in the present formulation.

Since the number of formulations that can be screened in a clinical setting is limited, alternatives mimicking the *in vivo* situation as closely as possible are required. For drug formulations animal studies are sometimes performed, whereas this is not allowed for cosmetic ingredients and final products in the EU. Furthermore, animal skin is different from human skin regarding morphology and barrier properties.[20] As an alternative, to screen topical formulations on enhancing skin barrier repair, recently we developed the SkinBaR model.[21] This model is based on *ex vivo* human skin from which SC was removed. As previously reported, after 8 days of culture during which SC regenerates, the viable epidermis shows normal expression of early and late differentiation markers. This indicates that this model may serve as an alternative for clinical studies to monitor the effect of formulations on skin barrier repair.

The SkinBaR model has several features that mimic lipid composition and organization of AD skin, namely i) the fraction of lipids in a hexagonal packing is increased at the expense of lipids in an orthorhombic lateral packing[19,34], ii) the levels of CER subclasses NS, EOS and AS are increased compared to native skin.[15,17]

In this study, FTIR was employed using deuterated and protiated FAs in formulations to examine whether FAs are incorporated in the SC lipid matrix and whether FAs partition in the same lattice as SC lipids. To examine this, asymmetric CD_2 and symmetric CH_2 stretching vibrations of lipids in formulations and SC after application of these formulations were used. When formulations were applied on the SkinBaR model, CD_2 asymmetric stretching frequency shift follows the temperature dependence of

CH_2 frequency shift of protiated lipids in SC instead of that of only formulation, the transition of which is located at substantial lower temperatures. This is a first indication that applied dFAs after removal of SC are incorporated in the SC lipid matrix during SC regeneration.

In order to obtain further evidence whether (d)FAs are incorporated in the same lattice as SC lipids, information on rocking frequencies was also required. After topically applying FA formulations with protiated FAs during SC regeneration, the relative intensity of the peak located at 730 cm^{-1} is increased compared to regenerated SC on which control formulation was applied. This increase in intensity is more substantial when topical formulations containing FAs with a longer carbon chain (compare $Form^{FA22}$ with $Form^{FA16}$) is applied. This suggests that after application of FA formulations an increased fraction of lipids form an orthorhombic organization in the SC matrix. However, it is also possible that applied FAs form separate domains within the SC lipid matrix.

Therefore, the next question to answer is whether FAs from formulations are partitioning in one lattice with SC matrix lipids or form separate domains. A first indication is provided by the rocking vibrations after replacement of FAs by dFAs in the formulation: The relative intensity of the peak located at 730 cm^{-1} is decreased after application of dFAs compared to their protiated counterparts, indicating that short-range coupling of CH_2 is disturbed by incorporation of dFA in the same lattice. To obtain more evidence, CD_2 scissoring vibrations were also examined. Here it is very important to notice that pure FA^{16}, FA^{18}, and FA^{22} adopt an orthorhombic lateral packing and thus will have a doublet in the FTIR spectrum.[35] In SC, only a singlet around 1088 cm^{-1} is observed, demonstrating that no phase separated FA domains are formed and that thus the lipids partition in one lattice with the SC lipids.

Until now, no information is available whether topically applied FA that are incorporated in the SC lipid matrix, are also modified by epidermal enzymes. In order to investigate this, LC/MS was employed. Using dFAs in the topical formulation enabled tracking of applied dFA and enzymatically modified products. No elongation of dFA^{22} was observed, suggesting that this FA remains in the regenerated SC and does not reach the viable epidermis. However, very interestingly, addition of dFA_{16} resulted in elongation of dFA with 6 or more carbon atoms up to a chain length of at least 30 carbon atoms. However, elongation products with 18 and 20 carbon atoms were not observed. The most abundant elongation product has 24 carbon atoms, of which 16 are deuterated, which is in accordance with the most abundant FA in SC of healthy skin.[16] These results confirm that lipids from the formulation are not only incorporated in regenerated SC, but are also used in lipid synthesis of the newly formed SC lipid matrix. Furthermore, this indicates that elongation of applied dFA^{16} is performed similarly to that of endogenous FA^{16}. In healthy skin, FA^{16} is produced *de novo* or obtained from the diet and elongated to FA^{18} by the enzyme elongase 6 (ELOVL6). Subsequently, FA^{18} is further elongated by ELOVL1 and ELOVL4, to chain lengths up to C28:0, and >C30:0, respectively.[36,37] Our results suggest that ELOVL1, 6, and possibly ELOVL4, are able to elongate not only endogenous protiated FAs, but also topically applied (partially) deuterated exogenous FAs. Furthermore, the results suggest that elongation of FA^{16} by ELOVL6 is the rate limiting step, since FA^{16} is present but the elongation products with 18 and 20 are not detected. This is in accordance with results showing

that dFAs used as medium supplement during generation of human skin equivalents are incorporated in SC of the generated skin.[38] Both studies indicate that elongation of exogenous FAs is possible. However, this study shows a new approach for barrier repair by topical formulations.
The lamellar lipid organization was studied using small angle X-ray diffraction (results not shown). With this method it is possible to determine the repeat distances of the lamellar phases in SC. Our studies did not show major differences in lamellar repeat distance after application of formulations, indicating that the lamellar lipid organization is not influenced by topical application of this formulation. However, crystallization of the formulation was detected occasionally as indicated by a sharp peak in the profile. As the peak positions at the X-ray diffraction curve matched the peak positions of pure FAs sprayed on a membrane, this indicates that FAs in the formulations sometimes crystallize on the SC surface. This crystallization may be induced by the SC surface, since no crystallization is observed in the formulation itself.
SC lipids of AD patients adopt a less orthorhombic lateral lipid packing compared to healthy skin[19], which correlates with increased TEWL values in these patients.[17] This illustrates the importance of the orthorhombic packing for the skin barrier function. In the present study we used the SkinBaR model, which resembles skin barrier diseases in several aspects.[21] We showed that after topical application of FA formulations containing FAs on the SkinBaR model, an increased fraction of lipids adopt an orthorhombic packing compared to regenerated SC. Therefore, we can hypothesize that this FA formulation has the potential to enhance skin barrier repair *in vivo* in patients with a reduced orthorhombic packing, such as observed in AD patients. To the best of our knowledge, this is the first study reporting that topically applied FAs are incorporated in the SC lipid matrix, that the FAs participate in one lattice with endogenous lipids of newly formed SC, and that the FAs are involved in the epidermal lipid biosynthesis in a similar way as endogenous FAs. We demonstrate two different approaches, depending on FA chain length, that affect the SC lipid barrier using topical formulations: I) a slightly more pronounced presence of the orthorhombic packing induced by FA[16], which is processed and partially elongated to increased chain lengths and II) we do not have evidence that FA[22] become part of the epidermal lipid biosynthesis, however long chain FAs show a significant higher fraction of lipids adopting a orthorhombic lateral lipid packing. This is in line with previously reported results, showing an increase in abundance of FAs with chain length ≥22 carbon atoms is correlated with a reduced TEWL and a more ordered lateral lipid packing in SC of AD patients.[16]
We show that it is possible to improve skin barrier function by topical application of FAs. Therefore, future studies may focus on further optimization of the formulation by using combinations of barrier lipids and testing the formulation in a clinical setting.

Acknowledgements

The authors thank the personnel at DUBBLE beam line (BM26) at the European synchrotron radiation facility (ESRF) in Grenoble, France for assisting with X-ray measurements. This research was financially supported by Dutch Technology Foundation STW (grant no. 12400).

Author contributions

TB, JvS and JB designed the experiments. TB, LvD, and SA performed the research and analyzed the data. TB, JvS, and JB performed the interpretation and wrote the paper.

Author disclosure statement

The authors declare no conflicts of interest.

References

1. Michaels AS, Chandrasekaran SK, Shaw JE. Drug permeation through human skin: Theory and invitro experimental measurement. *AIChE journal* **1975**: 21: 985-996.
2. Bouwstra JA, Gooris GS, Cheng K, et al. Phase behavior of isolated skin lipids. *J Lipid Res* **1996**: 37: 999-1011.
3. Holleran WM, Takagi Y, Uchida Y. Epidermal sphingolipids: metabolism, function, and roles in skin disorders. *FEBS Lett* **2006**: 580: 5456-5466.
4. Man MM, Feingold KR, Thornfeldt CR, et al. Optimization of physiological lipid mixtures for barrier repair. *J Invest Dermatol* **1996**: 106: 1096-1101.
5. Groen D, Gooris GS, Bouwstra JA. New insights into the stratum corneum lipid organization by X-ray diffraction analysis. *Biophys J* **2009**: 97: 2242-2249.
6. Bouwstra J, Pilgram G, Gooris G, et al. New aspects of the skin barrier organization. *Skin Pharmacol Appl Skin Physiol* **2001**: 14 Suppl 1: 52-62.
7. McIntosh TJ, Stewart ME, Downing DT. X-ray diffraction analysis of isolated skin lipids: reconstitution of intercellular lipid domains. *Biochemistry* **1996**: 35: 3649-3653.
8. Pilgram GS, Engelsma-van Pelt AM, Bouwstra JA, et al. Electron diffraction provides new information on human stratum corneum lipid organization studied in relation to depth and temperature. *J Invest Dermatol* **1999**: 113: 403-409.
9. Damien F, Boncheva M. The extent of orthorhombic lipid phases in the stratum corneum determines the barrier efficiency of human skin in vivo. *J Invest Dermatol* **2010**: 130: 611-614.
10. Goldsmith LA, Baden HP. Uniquely oriented epidermal lipid. *Nature* **1970**: 225: 1052-1053.
11. de Jager MW, Gooris GS, Dolbnya IP, et al. The phase behaviour of skin lipid mixtures based on synthetic ceramides. *Chem Phys Lipids* **2003**: 124: 123-134.
12. Bouwstra JA, Gooris GS, Dubbelaar FE, et al. Phase behavior of lipid mixtures based on human ceramides: coexistence of crystalline and liquid phases. *J Lipid Res* **2001**: 42: 1759-1770.
13. van Smeden J, Janssens M, Gooris GS, et al. The important role of stratum corneum lipids for the cutaneous barrier function. *Biochim Biophys Acta* **2014**: 1841: 295-313.
14. Fartasch M. Epidermal barrier in disorders of the skin. *Microsc Res Tech* **1997**: 38: 361-372.
15. Ishikawa J, Narita H, Kondo N, et al. Changes in the ceramide profile of atopic dermatitis patients. *J Invest Dermatol* **2010**: 130: 2511-2514.
16. van Smeden J, Janssens M, Kaye EC, et al. The importance of free fatty acid chain length for the skin barrier function in atopic eczema patients. *Exp Dermatol* **2014**: 23: 45-52.
17. Janssens M, van Smeden J, Gooris GS, et al. Increase in short-chain ceramides correlates with an altered lipid organization and decreased barrier function in atopic eczema patients. *J Lipid Res* **2012**: 53: 2755-2766.
18. Ohno Y, Nakamichi S, Ohkuni A, et al. Essential role of the cytochrome P450 CYP4F22 in the production of acylceramide, the key lipid for skin permeability barrier formation. *Proceedings of the National Academy of Sciences of the United States of America* **2015**: 112: 7707-7712.
19. Janssens M, Mulder AA, van Smeden J, et al. Electron diffraction study of lipids in non-lesional stratum corneum of atopic eczema patients. *Biochim Biophys Acta* **2013**: 1828: 1814-1821.
20. Hirschberg HJ, van RE, Oosterhoff D, et al. Animal models for cutaneous vaccine delivery. *Eur J Pharm Sci* **2015**: 71: 112-122.
21. Danso MO, Berkers T, Mieremet A, et al. An ex vivo human skin model for studying skin barrier repair. *Exp Dermatol* **2015**: 24: 48-54.
22. Boiten W, Absalah S, Vreeken R, et al. Quantitative analysis of ceramides using a novel lipidomics approach with three dimensional response modelling. *Biochimica et biophysica acta* **2016**: 1861: 1652-1661.
23. Oudshoorn MH, Rissmann R, van der Coelen D, et al. Development of a murine model to evaluate the effect of vernix caseosa on skin barrier recovery. *Exp Dermatol* **2009**: 18: 178-184.
24. Rissmann R, Groenink HW, Weerheim AM, et al. New insights into ultrastructure, lipid composition and organization of vernix caseosa. *J Invest Dermatol* **2006**: 126: 1823-1833.
25. Oudshoorn MH, Rissmann R, van der Coelen D, et al. Effect of synthetic vernix biofilms on barrier recovery of damaged mouse skin. *Exp Dermatol* **2009**: 18: 695-703.
26. Boncheva M, Damien F, Normand V. Molecular organization of the lipid matrix in intact Stratum corneum using ATR-FTIR spectroscopy. *Biochim Biophys Acta* **2008**: 1778: 1344-1355.
27. Lebwohl M, Herrmann LG. Impaired skin barrier function in dermatologic disease and repair with moisturization. *Cutis* **2005**: 76: 7-12.
28. Jungersted JM, Scheer H, Mempel M, et al. Stratum corneum lipids, skin barrier function and filaggrin mutations in patients with atopic

eczema. *Allergy* **2010**: 65: 911-918.
29. Rajka G. Transepidermal water loss on the hands in atopic dermatitis. *Arch Dermatol Forsch* **1974**: 251: 111-115.
30. Shahidullah M, Raffle EJ, Rimmer AR, et al. Transepidermal water loss in patients with dermatitis. *Br J Dermatol* **1969**: 81: 722-730.
31. Imokawa G, Abe A, Jin K, et al. Decreased level of ceramides in stratum corneum of atopic dermatitis: an etiologic factor in atopic dry skin? *J Invest Dermatol* **1991**: 96: 523-526.
32. Di Nardo A, Wertz P, Giannetti A, et al. Ceramide and cholesterol composition of the skin of patients with atopic dermatitis. *Acta Derm Venereol* **1998**: 78: 27-30.
33. Ishikawa J, Shimotoyodome Y, Ito S, et al. Variations in the ceramide profile in different seasons and regions of the body contribute to stratum corneum functions. *Arch Dermatol Res* **2013**: 305: 151-162.
34. Pilgram GS, Vissers DC, van der Meulen H, et al. Aberrant lipid organization in stratum corneum of patients with atopic dermatitis and lamellar ichthyosis. *J Invest Dermatol* **2001**: 117: 710-717.
35. Fischmeister I. Infrared absorption spectroscopy of normal and substituted long-chain fatty acids and esters in the solid state. *Prog Chem Fats Other Lipids* **1975**: 14: 91-162.
36. Kihara A. Very long-chain fatty acids: elongation, physiology and related disorders. *J Biochem* **2012**: 152: 387-395.
37. Ohno Y, Suto S, Yamanaka M, et al. ELOVL1 production of C24 acyl-CoAs is linked to C24 sphingolipid synthesis. *Proc Natl Acad Sci U S A* **2010**: 107: 18439-18444.
38. Thakoersing VS, van Smeden J, Boiten WA, et al. Modulation of stratum corneum lipid composition and organization of human skin equivalents by specific medium supplements. *Exp Dermatol* **2015**: 24: 669-674.

Supplementary material

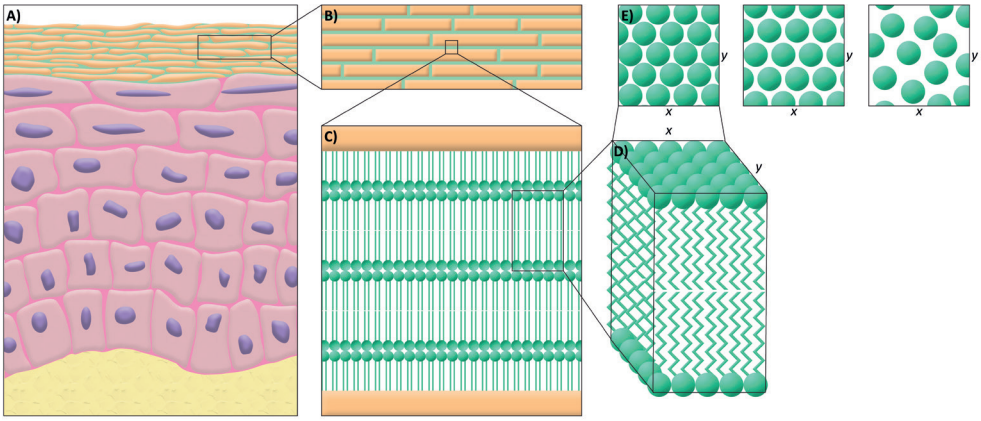

Supplementary Figure 1. Lipid organization in the SC. A) Schematic overview of the skin, **B)** The corneocytes are embedded in the lipid matrix in a brick-and-mortar structure, **C)** The lipids in the matrix are stacked in lamellae in between the corneocytes, **D)** Detail of the lipid lamellae, **E)** Perpendicular to the lamellae, the lipids are organized in a lateral packing. This can be either orthorhombic, hexagonal, or liquid (from left to right).

Materials and methods

Chemicals

Super sterol esters were kindly provided by Croda (Cowick Hall, UK), triglycerides (Miglyol 812) were supplied by Cremer Oleo (Witten, Germany). Perdeuterated palmitic acid was purchased from Sigma, perdeuterated stearic acid, perdeuterated behenic acid, and perdeuterated lignoceric acid were purchased from Cambridge Isotope Laboratories (Tewksbury, MA, USA). Cyanoacrylate (Bison, Goes, the Netherlands) was bought locally. Haematoxylin was obtained from J.T. Baker (Anvator, Center Valley, PA, USA). Xylene was obtained from Biosolve (Dieuze, France), 4% buffered formaldehyde was purchased from Added Pharma (Oss, the Netherlands), paraffin was acquired from Klinipath (Duiven, the Netherlands). DMEM, Ham's F12, and penicillin/streptomycin were purchased from Fisher Scientific (Waltham, Massachusetts, USA). Squalene, cholesterol, eosin, bovine serum albumin, sodium bromide, ethanol, acetone, trypsin, trypsin inhibitor, selenious acid, hydrocortisone, isoproterenol, L-carnitine, L-serine, insulin, α-tocopherol acetate, vitamin C, arachidonic acid, linoleic acid, palmitic acid, stearic acid, behenic acid, myristic acid, arachidic acid, tricosylic acid, lignoceric adic, cerotic acid, montanic acid, melissic acid, oleic acid, linoleic acid, linolenic acid, gondoic acid, erucic acid, and acetic acid were purchased from Sigma-Aldrich (Zwijndrecht, the Netherlands). Myristoleic acid and palmitoleic acid were purchased from Fluka (Buchs, Zwitserland). 2-Hydroxydocosanoic acid, 22-Hydroxydocosanoic acid, 2-Hydroxytricosanoic acid, and 2-Hydroxytetracosanoic acid were bought from Larodan (Solna, Sweden). Pentacosylic acid was purchased from TCI Europe (Zwijndrecht, Belgium). Acetonitrile, methanol, and 2-Propanol were purchased from Biosolve (Valkenswaard, The Netherlands). Heptane was bought from

Actu-All Chemicals (Oss, The Netherlands), Chloroform was obtained from Macron Fine Chemicals (Gliwice, Poland), and Ultra purified water was obtained from Purelab Ultra purification system (Elga Labwater, High Wycombe, UK). All solvents were HPLC grade or higher.

Preparation of formulations

Formulations were prepared as follows: FAs and CHOL were dissolved in chloroform:methanol (2:1), super sterol esters were dissolved in chloroform and squalene was dissolved in acetone; miglyol 812 was used undissolved. All components were pipetted in the required ratio in a small glass vial to achieve the predetermined composition and left to dry under a stream of nitrogen at 40˚C for approximately 3 hours.
For homogeneous distribution of the lipids in the formulation, 100 mg of the lipid mixture was mixed for 5 minutes at 500 rpm by transferring it into a small mixing tube of a modified automatic ointment-mixer Topitec® (WEPA, Germany).[1]

Stripping and culturing of ex vivo skin

The detailed stripping and culturing procedures are described in Danso et al.[2] Briefly, dermatomed skin was punched in circles with a diameter of 26 mm and clamped in a custom made device. A metal cylinder with cyanoacrylate, both preheated to 40˚C, was applied on the skin for 2 minutes with a pressure of 0.7 kg/cm^2. The cylinder was removed in one stroke with attached to it a layer of SC. This stripping was repeated until the skin had a shiny appearance, indicating that most SC has been removed. Subsequently, the skin was placed in a deep 6-well plate on top of a cotton pad and a filter. A metal ring with an inner diameter of 15 mm is placed on top of the skin, in order for formulations to stay in the middle. FA formulations were spread over the back of a small metal vial (diameter 15 mm) and applied on skin by making rotating movements at day 0 of the culturing period. A single dose of about 5 mg/cm^2 was used and left on the skin for the full culturing period of 8 days.
Subsequently, the skin is cultured to regenerate SC for 8 days at 37˚C, 90% relative humidity and 7.2% CO_2. The culture medium is described in Danso et al.[2] and was refreshed twice a week.

Isolation of SC

SC was isolated from cultured skin using trypsin digestion. The skin was incubated overnight in 0.1% trypsin solution in PBS at 4˚C and subsequently at 37˚C for one hour. SC was peeled off and placed in 0.1% trypsin inhibitor solution in PBS. SC sheets were washed twice in Millipore water. SC was stored over silica gel under argon in the dark until use. SC was used for either infrared spectroscopy measurements, LC/MS or X-ray diffraction measurements.

Fourier transform infrared spectroscopy

Hydrated SC samples were placed between two AgBr-windows and measured in transmission mode. SC samples were put under a purge of continuous dry air starting 30 minutes before data acquisition. Spectra were acquired as a co-addition of 256 scans at 1 cm^{-1} resolution during 2 or 4 minutes. The sample temperature was increased from 0 to 90°C (for samples containing only formulations 0 to 60°C) at a heating rate of 0.25 or 0.5°C/min. Resolutions Pro 4.1 (Varian Inc.) software was used to calculate CH_2 and CD_2 rocking, scissoring, and symmetrical and asymmetrical stretching vibrations using deconvolution.[3]

Liquid chromatography mass spectrometry

Two ions per FA were analyzed, namely $[M-H]^-$ and $[M+Cl]^-$. Lipid samples were dissolved in isopropanol. Sample concentrations were set between 1 and 2 mg/ml total lipid. 2 µl of each sample was injected and separated using a reverse phase column (Purospher Star LiChroCART, 55x2 mm i.d., 3 µm particle size, Merck (Darmstadt, Germany)). A gradient solvent system was used from acetonitrile/water/chloroform/acetic acid (90:10:2:0.005) to methanol/heptane/chloroform/acetic acid (90:10:2:0.005) at a flow rate of 500 µl/min using a Waters Acquity UPLC H-class system (Waters, Milford, MA, USA). The UPLC was coupled to a mass spectrometer Waters XEVO TQ-S (Waters, Milford, MA, USA) equipped with an atmospheric pressure chemical ionization source (probe temperature: 425°C), scanning in negative ion mode using selected ion recording acquisition. The discharge current was set to 3 µA.

Results

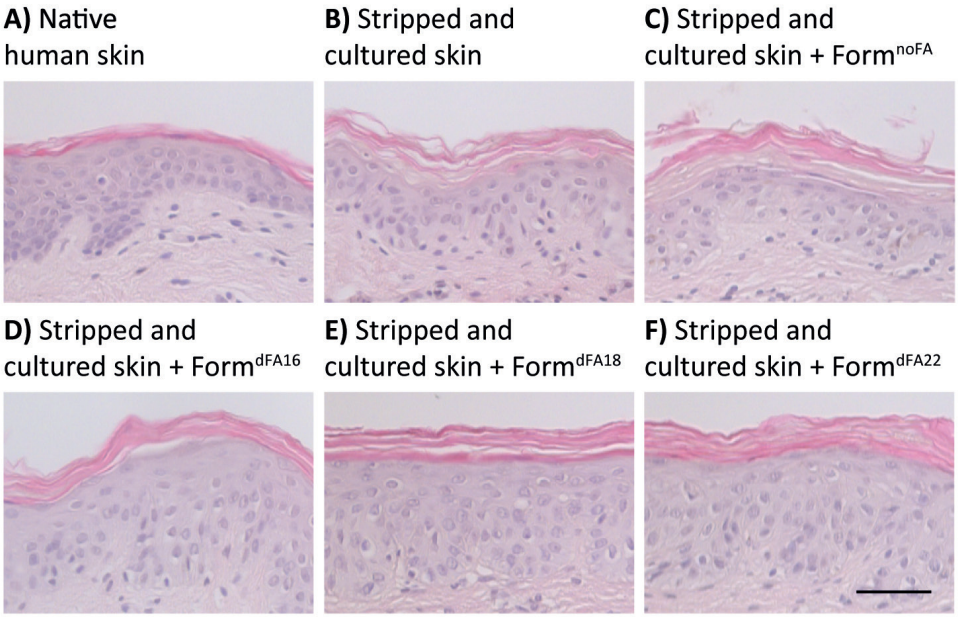

Supplementary Figure 2. Morphology of A) native human skin, **B)** stripped and cultured skin, **C-F)** stripped and cultured skin on which control formulation, Form^{dFA16}, Form^{dFA18}, and Form^{dFA22} were applied, respectively. After culturing the epidermis is slightly thicker compared to native skin and the basal layer is less neatly ordered. However, application of formulations did not influence morphology compared to stripped control demonstrating that the epidermis is viable after 8 days of culture with and without formulation applied. Scale bar: 50 µm

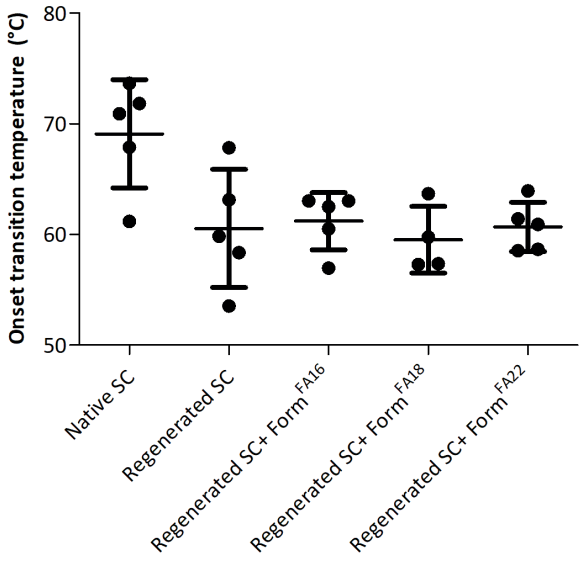

Supplementary Figure 3. Temperature at which the ordered-disordered transition of SC lipids starts. Per condition, calculated from FTIR peak positions of CH_2 symmetric stretching vibrations, for native human and regenerated SC, and regenerated SC on which the Form^{FA16}, Form^{FA18} and Form^{FA22} are applied. Native human skin had a significantly higher transition temperature compared to regenerated SC with or without formulations, which were not significantly different from each other.

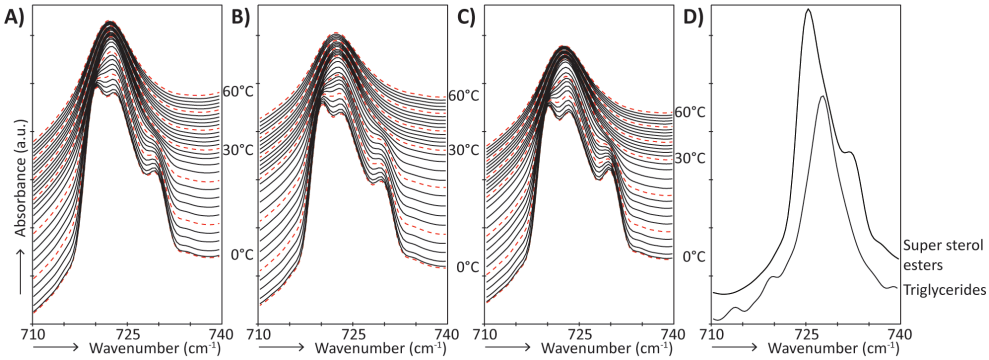

Supplementary Figure 4. FTIR spectra showing CH_2 rocking vibrations of lipids in the formulations as a function of temperature (0-60°C). A) $Form^{FA16}$, **B)** $Form^{FA18}$, **C)** $Form^{FA22}$, **D)** super sterol esters and the triglycerides at 0°C. Spectra of formulations show three peaks at temperatures below 20°C positioned at 720, 723, and 729 cm^{-1}. The peaks at 720 and 729 cm^{-1} indicate that lipids assemble partially in an orthorhombic packing. The contour at 723 cm^{-1} is also observed when triglycerides are examined individually. At elevated temperatures, only one band remains, indicative for a hexagonal or liquid lateral packing. Super sterol esters show a doublet positioned at around 719 and 730 cm^{-1}. Triglycerides show a singlet at a wavenumber of 723 cm^{-1}.

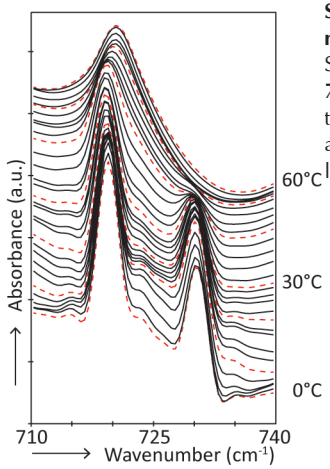

Supplementary Figure 5. FTIR spectra showing CH_2 rocking vibrations of native human skin as a function of temperature. At 0°C, lipids in native SC adopt an orthorhombic packing as indicated by two strong peaks at 719 and 730 cm^{-1} in the spectrum. When increasing the temperature, the 730 cm^{-1} band starts to decrease in intensity at 34°C and disappears around 48°C, indicating the transition from orthorhombic to hexagonal lateral lipid packing.

Supplementary references

1. Rissmann R, Oudshoorn MH, Zwier R, et al. Mimicking vernix caseosa--preparation and characterization of synthetic biofilms. *Int J Pharm* **2009**: 372: 59-65.
2. Danso MO, Berkers T, Mieremet A, et al. An ex vivo human skin model for studying skin barrier repair. *Exp Dermatol* **2015**: 24: 48-54.
3. Damien F, Boncheva M. The extent of orthorhombic lipid phases in the stratum corneum determines the barrier efficiency of human skin in vivo. *J Invest Dermatol* **2010**: 130: 611-614.

Chapter 6

Topically applied ceramides interact with the stratum corneum lipid matrix in compromised ex vivo skin

Tineke Berkers[1], Dani Visscher[1], Gert S. Gooris[1], Joke A. Bouwstra[1]

[1] Department of Drug Delivery Technology, Cluster BioTherapeutics, Leiden Academic Centre for Drug Research, Leiden University, Leiden, 2333 CC, The Netherlands

Pharm Res. 2018 Feb 6;35(3):48

Abbreviations

AD	Atopic dermatitis
CER	Ceramide
Chol	Cholesterol
FA	Fatty acid
ELOVL	Elongation of very long chain fatty acids
ESRF	European synchrotron radiation facility
FA	Fatty acid
$Form^{Basic}$	Basic formulation without CERs
$Form^{COMBI}$	Formulation with CER EOS, CER NS, and FA22
$Form^{EOS}$	Formulation with CER EOS
$Form^{(d)NS}$	Formulation with (deuterated) CER NS
FTIR	Fourier transform infrared spectroscopy
LPP	Long periodicity phase
SAXD	Small angle X-ray diffraction
SC	Stratum corneum
SkinBaR	Skin barrier repair
SPP	Short periodicity phase
TEWL	Transepidermal water loss
VC	Vernix caseosa

Key words

Lipid organization, skin barrier repair, topical formulation, ceramides

Abstract

Purpose: To determine whether formulations containing ceramides (including a ceramide with a long hydroxyl acyl chain linked to a linoleate, CER EOS) and fatty acids are able to repair the skin barrier by normalizing the lipid organization in stratum corneum (SC).
Methods: The formulations were applied on a skin barrier repair model consisting of *ex vivo* human skin from which SC was removed by stripping. The effect of formulations on the lipid organization and conformational ordering in the regenerated SC were analyzed using Fourier transform infrared spectroscopy and small angle X-ray diffraction.
Results: Application of the formulation containing only one ceramide on regenerating SC resulted in a higher fraction of lipids adopting an orthorhombic organization. A similar fraction of lipids forming an orthorhombic organization was observed after application of a formulation containing two ceramides and a fatty acid on regenerating SC. No effects on the lamellar lipid organization were observed.
Conclusions: Application of a formulation containing either a single ceramide or two ceramides and a fatty acid on regenerating SC, resulted in a denser lateral lipid packing of the SC lipids in compromised skin. The strongest effect was observed after application of a formulation containing a single ceramide.

Introduction

One of the major roles of the skin is its protection against penetration of irritants, pathogens, and allergens, and prevention of excessive transepidermal water loss (TEWL) avoiding desiccation of the body. The skin barrier function is located in the uppermost epidermal layer, namely the stratum corneum (SC). SC consists of terminally differentiated corneocytes embedded in a lipid matrix. The main lipid classes present in the matrix are ceramides (CERs), fatty acids (FAs), and cholesterol (CHOL). This lipid matrix is important for a proper skin barrier function.[1] The intercellular lipids are assembled in two lamellar phases, with a repeat distance of either 13 nm or 6 nm, referred to as the long periodicity phase (LPP) and the short periodicity phase (SPP), respectively.[2-6] Within these lamellar sheets, in healthy skin the lipids are mainly packed in an orthorhombic packing, while a small fraction of lipids adopts a hexagonal packing (Figure 1).[7-10] In several inflammatory skin diseases, a higher fraction of the intercellular lipids assembles in a hexagonal packing, such as in atopic dermatitis (AD).[11] This less dense lipid organization is associated with a reduction in lipid chain length in SC of AD patients and a reduced skin barrier function.[11-14] As the lipids play a role in the reduced skin barrier, normalization of the lipid composition and organization may improve the skin barrier function. Normalization of the lipid organization may be achieved by topical application of lipid formulations.

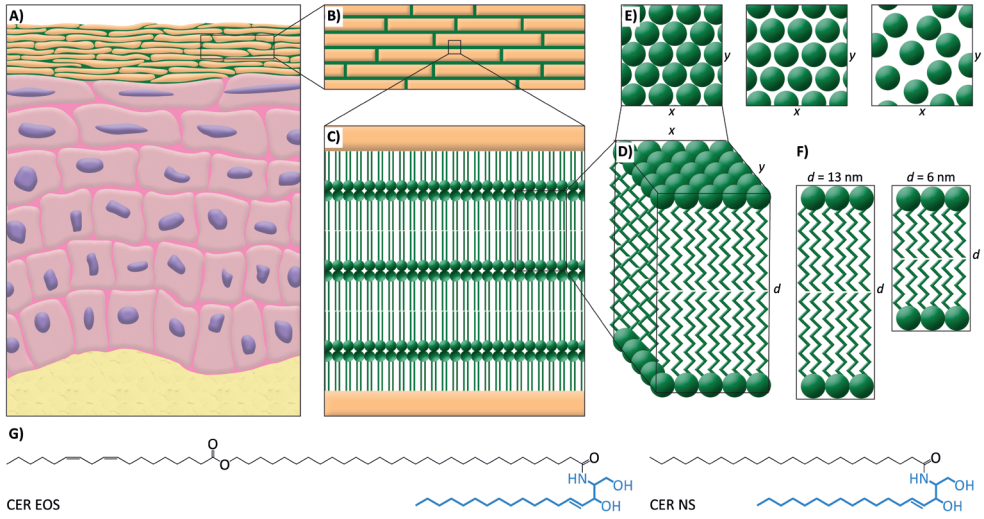

Figure 1. Lipid organization in the SC. A) Schematic overview of the skin morphology, **B)** The corneocytes are embedded in the lipid matrix in a brick-and-mortar structure, **C)** The lipids in the matrix are stacked in lamellae in between the corneocytes, **D)** Detail of the lipid lamellae, **E)** Perpendicular to the lamellae, the lipids are organized in a lateral packing. This can be either orthorhombic, hexagonal, or liquid (from left to right), **F)** The lipid lamellae are stacked on top of each other with a repeat distance (d) of either 13 nm (LPP) or 6 nm (SPP), **G)** Molecular structure and nomenclature of the two CER subclasses used in these studies. The sphingoid base is depicted in blue, and the acyl chain in black.

Previously, topical formulations based on vernix caseosa (VC) were developed. VC is a white cream that is developed on the fetal skin during the last trimester of pregnancy. It serves as a lubricant during delivery and it protects the newborn's skin from dehydration.[15] VC contains barrier lipids CERs, FAs, and CHOL, but also other lipids such as super sterol esters, wax esters, squalene, and triglycerides. VC enhances skin barrier repair in mice.[16,17]

In order to select the most effective formulation for skin barrier repair, studies are required in which the compositions of the formulations need to be altered in a systematic way. When performing these studies *in vivo*, multiple clinical studies and/or animal studies will be needed. This is very challenging as in clinical studies only a limited number of formulations can be investigated. Furthermore, animal skin is very different from human skin.[18] Therefore, we developed an *ex vivo* skin barrier repair (SkinBaR) model.[19] In this model, the SC is removed by stripping and subsequently regenerated during an 8-day culturing period. The regenerated SC of the SkinBaR model shows several features that are also observed in SC of AD patients, e.g. a higher fraction of lipids adopting a hexagonal lateral lipid organization and a CER profile that mimics the altered CER subclass composition in AD skin in several aspects.[19] Using this model, the influence of topical formulations on the lipid organization and composition of the SC can be examined in *in vitro* settings.

In this study, we used the SkinBaR model to examine whether two CERs of a VC based formulation remain on top of the SC, or are incorporated in the lipid matrix of the SC during repair, thereby improving the lipid organization. We used protiated and partially deuterated CERs. One CER subclass had a very long esterified ω-hydroxy acyl chain (Figure 1), referred to as CER EOS. The VC based formulation contains a basic formulation ($Form^{Basic}$) and either a single CER subclass or both CER subclasses in combination with a FA. After regeneration of SC, the organization of the lipids in the matrix was examined. Our results demonstrate that the applied formulations containing a single ceramide are able to enhance the formation of an orthorhombic lateral packing and are, at least partly, incorporated in the SC lipid matrix.

Material and methods

Composition and preparation of formulations

Two subclasses of synthetic CER were used in these studies (Figure 1). One CER subclass was the esterified ω-hydroxy acyl chain with 30 carbon atoms in the acyl chain linked to a sphingosine base (18 carbon atoms), referred to as CER EOS according to the classification of Motta et al.[20] The other CER was composed of a non-hydroxy acyl chain of 24 carbon atoms linked to a sphingosine base (18 carbon atoms), referred to as CER NS. Deuterated CER NS (dCER NS) consists of a perdeuterated acyl chain and a protiated base.

The basic formulation ($Form^{Basic}$) contained a mixture of super sterol esters, triglycerides (Miglyol 812), squalene, and CHOL in a weight ratio of 13.6:10.1:1.8:1. This basic mixture is supplemented with either CER EOS, CER NS, or dCER NS. For the exact compositions of the formulations and the used abbreviations throughout this paper, see

Table 1. The use of dCER NS offers the opportunity to selectively detect the deuterated acyl chain of CER NS as CD_2 vibrations in the infrared spectrum are shifted to lower wavenumbers compared to their protiated counterparts (also see below). In addition to the single CER component in the formulation, a formulation with both CER EOS and CER NS as well as a FA with a chain length of 22 carbon atoms (behenic acid; referred to as FA22) was prepared. Three variations of this formulation were made: i) all lipids were protiated, ii) dCER NS was used instead of CER NS, iii) dFA22 (perdeuterated chain) was used instead of FA22 (see Table 1). Finally, the basic formulation ($Form^{Basic}$) without CER or FA was examined.
The formulations were prepared by dissolving the lipids in either chloroform:methanol (2:1, used for CHOL, CERs, and FA22), chloroform (super sterol esters), or acetone (squalene). Triglycerides were used undissolved. In total 100 mg of the dissolved lipids and triglycerides were mixed in the required ratio in a small glass vial and left to dry under a stream of nitrogen at 40°C for approximately 3 hours. In order to distribute the lipids homogeneously in the formulation, the dried lipid mixture was transferred to a mixing tube modified for small scale purposes and mixed for 5 minutes at 500 rpm using a modified automatic ointment-mixer TopiTec® (WEPA, Germany).[17,21]

Table 1. The names and composition of the various formulations used in this study. Numbers represent the weight percentage of the components.

Name	Basic mixture	CER EOS	CER NS	dCER NS	FA22	dFA22
$Form^{Basic}$	100					
$Form^{EOS}$	98	2				
$Form^{NS}$	98		2			
$Form^{dNS}$	95			5		
$Form^{COMBI}$	94.5	2	2		1.5	
$Form^{COMBI(dNS)}$	94.5	2		2	1.5	
$Form^{COMBI(dFA)}$	94.5	2	2			1.5

Preparation and culturing of ex vivo skin

Human skin was obtained after surgery from a local hospital according to principles of the Declaration of Helsinki, and used within 12 hours after surgery. Stripping and culturing procedures are described in the supplementary material. Formulations were applied in a single dose of about 5 mg/cm^2 in a metal ring placed on top of the skin at day 0 of the culturing period by rotating movements with the back of a small metal vial (ø=15 mm) which was covered with one of the formulations (see Table 1).
Subsequently, the skin was cultured for 8 days in an incubator during which the SC regenerated. The incubator conditions were 37°C, 90% relative humidity, and 7.2% CO_2. The culture medium was refreshed twice a week. The composition of the medium has been described in Danso et al.[19]

Studies were performed at least in triplicate using the following conditions:

i) Stripped and cultured skin
ii) Stripped and cultured skin + Form^{Basic}
iii) Stripped and cultured skin + Form^{EOS}
iv) Stripped and cultured skin + Form^{NS} or Form^{dNS}
v) Stripped and cultured skin + Form^{COMBI}, Form$^{COMBI(dNS)}$ or Form$^{COMBI(dFA)}$

Human skin from the same donor served as control.
After culturing, the skin was harvested and either embedded in paraffin, or SC was isolated (see supplementary material). Isolated SC samples were used to examine the lipid organization or conformational ordering using either Fourier transform infrared spectroscopy (FTIR) or small angle X-ray diffraction (SAXD). Both methods are described in the supplementary material. FTIR provides information about the lateral packing and conformational ordering, while SAXD is used to obtain information about the lamellar organization.

Statistical analysis

T-test and one-way ANOVA with a multiple comparisons post-hoc test were used to analyze the data using GraphPad Prism 7 software (GraphPad software Inc., San Diego, CA, USA).

Results

Formulations do not influence the morphology of cultured skin

As can be observed in Figure 2, after culturing for 8 days, the epidermis of the stripped and cultured skin was slightly thicker than in native skin and the basal layer was less compact. The morphology of the stripped and cultured skin on which Form^{EOS}, Form^{NS}, and Form^{COMBI} were applied was comparable to the stripped and cultured skin without formulation. This indicates a viable epidermis after 8 days of culturing, also in the presence of a formulation.

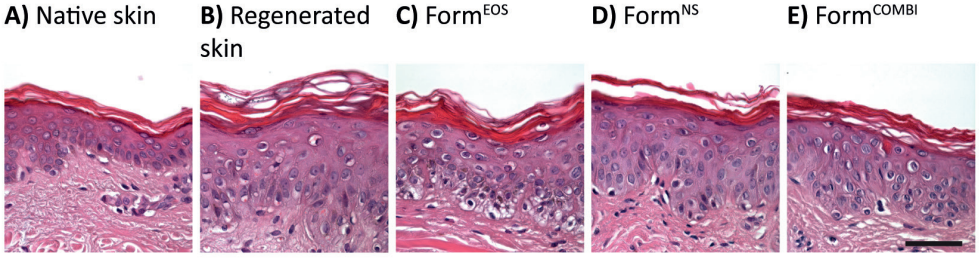

Figure 2. Morphology was examined using HE staining. A) Native human skin, **B)** Skin with stripped and cultured SC, **C)** Stripped and cultured skin on which Form^{EOS} was applied, **D)** Stripped and cultured skin on which Form^{NS} was applied, **E)** Stripped and cultured skin on which Form^{COMBI} was applied. Scale bar: 50 µm.

Ceramides do not influence lateral organization of formulation

CH_2 rocking vibrations in the FTIR spectra were analyzed in order to examine the lateral lipid organization. When lipids are assembled in a hexagonal packing, only one vibration at around 719 cm^{-1} is visible in the FTIR spectrum. When the lipids adopt a more dense orthorhombic lateral packing, short-range coupling occurs due to interactions of adjacent protiated chains which results in a splitting of the contours. In this case, two peaks are visible at around 719 and 730 cm^{-1}. Deuterated chains participating in the same lattice as the protiated lipid chains interfere with the vibrations of the protiated chains, thereby reducing the short-range coupling. This is visible as a reduction in intensity or disappearance of the peak positioned at 730 cm^{-1}. In order to be able to compare the intensity of the peaks, all spectra are displayed with a similar ratio between the lowest point at around 715 cm^{-1} and the top at around 719 cm^{-1}.
First the spectra of the formulations will be reported. CH_2 rocking vibrations of $Form^{EOS}$, $Form^{NS}$, and $Form^{dNS}$ showed a strong peak positioned at 719 and a weak peak at 730 cm^{-1}, indicating that a small fraction of lipids forms an orthorhombic lateral organization. Furthermore, a third peak was observed at a wavenumber of about 723 cm^{-1} (Figure 3A-C). This peak can be attributed to the presence of the triglycerides, which showed a single peak of the CH_2 rocking vibrations at a wavenumber of about 723 cm^{-1} (Figure 3D). No differences were observed between the various formulations below 10°C. The contour at 730 cm^{-1} in all formulations started to decrease at a temperature of around 10°C and disappeared at 28°C in $Form^{EOS}$ and at 22°C in $Form^{NS}$ and $Form^{dNS}$. This transition is indicative for the disappearance of the orthorhombic lateral packing. Above this temperature all formulation showed similar FTIR profiles. When analyzing $Form^{Basic}$ (no barrier lipids present), the FTIR profile was characterized by a doublet of which the peak at a wavenumber of 730 cm^{-1} disappeared between 10°C and 28°C (results not shown).
The profile of pure CER NS was characterized by a single peak located at around 719 cm^{-1}, whereas for pure CER EOS a doublet at around 719 and 730 cm^{-1} was observed which was still weakly present at 60°C (Supplementary Figure 1). However, both CER containing formulations and the control formulation showed a similar profile until 10°C, indicating that the CERs do not influence the lateral packing of the formulation at low temperatures as far as it can be detected by FTIR.

Conformational ordering of the lipids is not affected by ceramides in the formulation

The conformational ordering of the lipids was analyzed in order to examine the ordered-disordered phase transition of the lipids in the formulations. This was determined by assessing the thermotropic behavior of CH_2 symmetric and CD_2 asymmetric stretching vibrations in the FTIR spectrum. When lipids show a high conformational ordering, indicating that the chains are fully extended, CH_2 and CD_2 stretching vibration peaks are positioned below a wavenumber of 2850 and 2195 cm^{-1}, respectively. Peak positions increase to wavenumbers above 2852 and 2196 cm^{-1}, respectively, when the lipids have a high conformational disordering, indicating the presence of a liquid phase. Peak positions of CH_2 symmetric and CD_2 asymmetric stretching vibrations

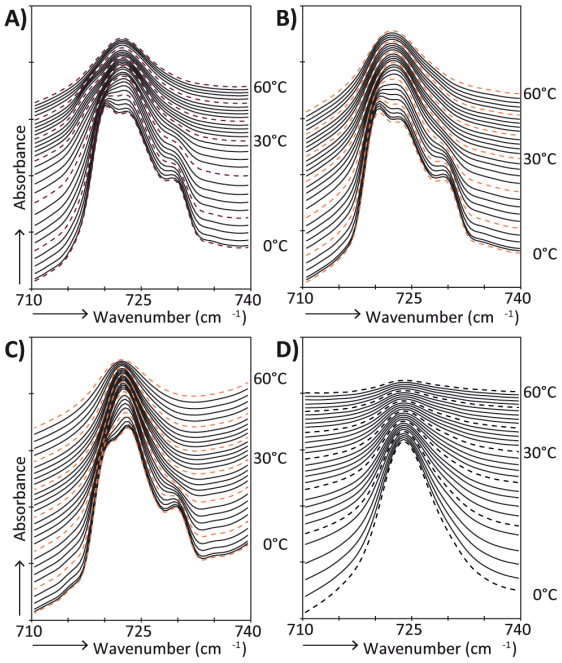

Figure 3. FTIR spectra showing CH_2 rocking vibrations of lipids in formulations as a function of temperature (0-60°C). A) $Form^{EOS}$, **B)** $Form^{NS}$, **C)** $Form^{dNS}$, and **D)** Triglycerides.

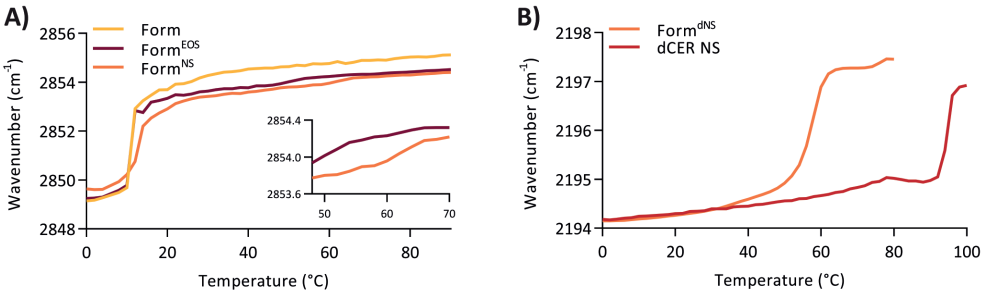

Figure 4. Peak positions of CH_2 symmetric stretching vibrations and CD_2 asymmetric stretching vibrations of FTIR spectra plotted as a function of temperature (0-90°C). A) CH_2 symmetric stretching vibrations of $Form^{Basic}$, $Form^{EOS}$, and $Form^{NS}$. **B)** Asymmetric CD_2 stretching vibrations of the deuterated acyl chain of dCER NS and in $Form^{dNS}$.

of the formulations are plotted against temperature (Figure 4). The onset transition temperature was determined as described in the supplementary methods section. Figure 4A shows the temperature dependence of $Form^{Basic}$, $Form^{EOS}$, and $Form^{NS}$, which are very similar. At 0°C, the peak positions were located at a wavenumber of around 2849 cm^{-1}, indicating an ordered lateral lipid organization. The onset transition temperatures of the ordered-disordered transition of the formulations were approximately 9-10°C. At these temperatures, the CH_2 symmetric stretching vibrations started to shift to a wavenumber of around 2853 cm^{-1} at 20°C. These increases in wavenumber were steep, representing an ordered-disordered transition. During a further rise in temperature, the CH_2 stretching vibrations increased gradually until about 2855 cm^{-1} at 90°C.

Furthermore, a small shift in wavenumber was observed in the profiles of $Form^{EOS}$ and $Form^{NS}$ at around 50-60˚C (see inset). This might be attributed to a change in conformational ordering of CER EOS and CER NS in the formulation (see below).
The temperature dependence of the CD_2 stretching vibrations of the deuterated acyl chain of pure dCER NS and in $Form^{dNS}$ is depicted in Figure 4B. At 0˚C, the CD_2 asymmetric stretching peak positions of both $Form^{dNS}$ and pure dCER NS were located at 2194 cm^{-1}. The onset transition temperatures were 53˚C for $Form^{dNS}$ and 91˚C for pure dCER NS. At these temperatures sharp increases in wavenumbers were observed until a wavenumber of around 2197 cm^{-1} was reached at 64˚C and 100˚C, respectively. The onset transition temperature of pure dCER NS was substantially higher than that of $Form^{dNS}$, indicating that dCER NS interacts with the lipids in the formulation. However, the temperature of transition is not similar to that of the protiated chains indicating that dCER NS is not homogenously mixing with the other protiated components.

Influence of topical formulation on lateral lipid organization of regenerated SC

The CH_2 rocking vibrations in the FTIR spectrum of native SC showed two strong peaks positioned at 719 and 730 cm^{-1} (Supplementary Figure 2), indicative for an orthorhombic lateral packing of the lipids. Figure 5A displays CH_2 rocking vibrations in the FTIR spectra of regenerated SC, which showed a contour with a strong intensity at around 719 cm^{-1} and a peak with a weak intensity at around 730 cm^{-1}. This indicates that a higher fraction of lipids adopted a hexagonal lateral packing compared to native SC.
The formulations were applied on the SkinBaR model in order to examine if the CERs from the formulations are incorporated in the SC lipid matrix and furthermore if they participate in the same lattice as SC lipids. After $Form^{EOS}$ was applied during SC regeneration, the peak at 730 cm^{-1} had a stronger intensity (relative to the intensity of the 719 cm^{-1} peak) than that in the spectrum of regenerated SC, indicating a higher level of lipids adopting an orthorhombic lateral packing. After application of $Form^{NS}$ during regeneration of SC, the relative intensity of the peak at 730 cm^{-1} was slightly lower than after application of $Form^{EOS}$, but higher than in the spectrum of the untreated stripped and regenerated SC. A gradual decrease of the peaks around 730 cm^{-1} occurred between 12˚C and 32˚C (regenerated SC), 20˚C and 36˚C (application of $Form^{EOS}$), and 12˚C and 24˚C (application of $Form^{NS}$). This indicates that the orthorhombic to hexagonal phase transition took place at lower temperatures than in native SC, but that the presence of CER EOS increased the transition temperature slightly.
The next question is whether CERs from the topically applied formulation form separate domains in the lipid matrix or that these CERs are partitioning in the same lattice as SC lipids. In order to examine this, CH_2 rocking vibrations were examined after topical application of $Form^{dNS}$ (Figure 5D). The relative intensity of the peak located at 730 cm^{-1} was similar to the relative intensity of the peak visible after application of its protiated counterpart. This indicates that dCER NS does not partition in the orthorhombic domains. To examine the possibility that CER NS interacts with the hexagonal lateral domains, the temperature dependence of the lateral ordering of the lipids was examined.

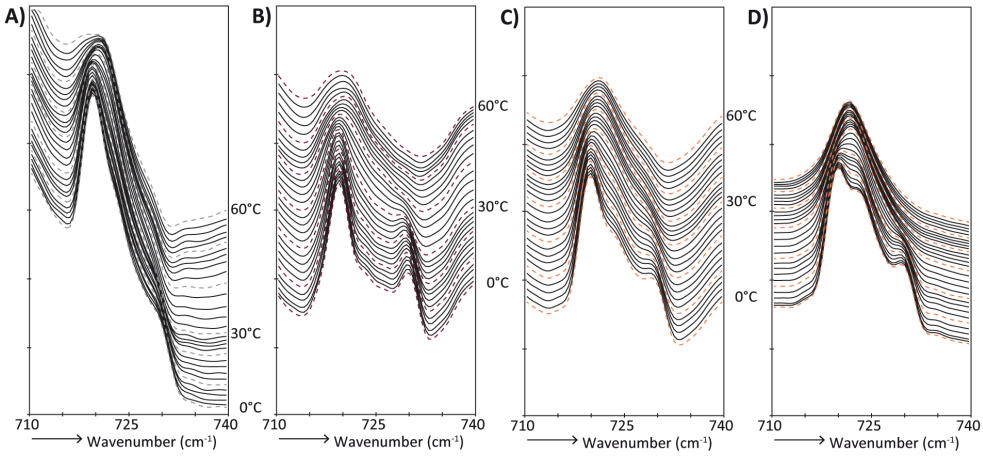

Figure 5. FTIR spectra showing CH_2 rocking vibrations of SC lipids with and without topical application of formulation as a function of temperature (0-60°C). A) regenerated SC, **B)** regenerated SC with topical application of $Form^{EOS}$, **C)** regenerated SC with topical application of $Form^{NS}$, **D)** regenerated SC with topical application of $Form^{dNS}$.

Similar ordering of lipids in regenerated SC in presence or absence of a formulation

When monitoring the CH_2 symmetric stretching vibrations of native, regenerated SC, and regenerated SC after application of formulations, very similar temperature dependence was observed (Figure 6A). A small shift in vibration frequency from 2849 to 2850 cm^{-1} at around 30-40˚C was observed in the spectra of native and regenerated SC, which is attributed to the orthorhombic to hexagonal phase transition. The start of the ordered-disordered phase transitions were observed at temperatures of 69.3˚C ± 4.0 (n=6) for native SC and 64˚C ± 1.5 (n=7) for regenerated SC. The onset transition temperature after application of $Form^{EOS}$ was not affected compared to regenerated SC (62.8˚C ± 2.0 , p=0.99 (n=3)), whereas after application of $Form^{NS}$ the onset transition temperature was significantly lowered to 58.0˚C ± 3.6 (p=0.02 (n=3)).
Figure 6B depicts the temperature dependence of CD_2 asymmetric stretching vibrations of regenerated SC on which $Form^{dNS}$ was applied. A gradual increase in wavenumber was observed between 0˚C and 50˚C. The onset transition temperature was 56˚C and the end of the transition occurred at 71.0˚C ± 1.9. This is a significantly higher temperature than for only $Form^{dNS}$, which was 62.2˚C (Figure 4B, p=0.03). This difference in temperature indicates that there is interaction between dCER NS from the formulation and the SC lipid matrix.

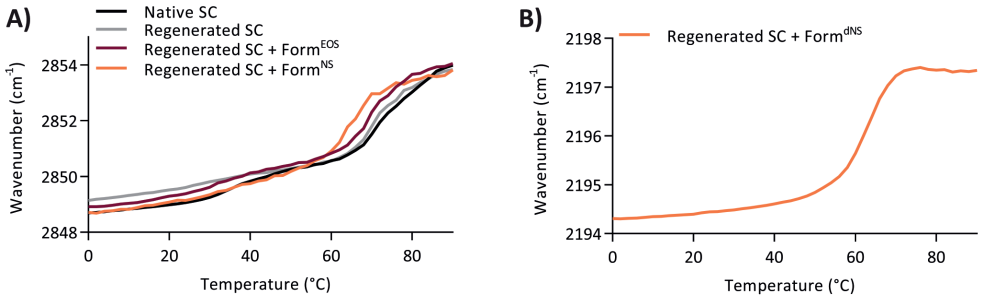

Figure 6. Peak positions of CH_2 symmetric stretching and CD_2 asymmetric stretching vibrations of FTIR spectra plotted as a function of temperature (0-90°C). A) Symmetric stretching vibrations of CH_2 groups in native SC, regenerated SC, and regenerated SC on which $Form^{EOS}$, $Form^{NS}$, or $Form^{dNS}$ was applied **B)** The CD_2 asymmetric stretching vibrations of regenerated SC on which $Form^{dNS}$ was applied.

Combining CER and FA in the formulation

The final studies focused on a formulation in which both CER EOS and CER NS were included, as well as FA22 ($Form^{COMBI}$). First, the formulation was stored for a period of 6 months at room temperature during which the physical stability was examined at regular time intervals. Polarization microscopy and wide and small angle X-ray diffraction (WAXD and SAXD) were used to examine the physical stability. No crystals were observed in the microscopy images during and after 6 months of storage (results not shown). However, some "Maltese cross" were observed using polarization microscopy, which are indicative for lamellar structures. Additionally, diffraction patterns confirmed the presence of lamellar structures and showed that a fraction of lipids in the formulation adopted an orthorhombic lateral packing at room temperature. No additional peaks were observed, indicating that no crystals were present in the formulation (results not shown).

The lateral lipid organization of $Form^{COMBI}$ with only protiated lipids was examined using FTIR (Figure 7A). The contour at 730 cm^{-1} disappeared in the same temperature range as in $Form^{EOS}$ and $Form^{NS}$. However, the relative intensity of the contour at 730 cm^{-1} was higher compared to a formulation with only one CER subclass, indicating that a higher fraction of lipids adopted an orthorhombic lateral packing in $Form^{COMBI}$.

When substituting CER NS by dCER NS (Figure 7B) or FA22 by dFA22 (Figure 7C) in the formulation, the relative intensity of the peak at 730 cm^{-1} was reduced compared to the formulation with only protiated lipids. This suggests that a fraction of the deuterated lipids partitions in the orthorhombic lattice formed by the protiated lipids of the formulation (see above).

The thermotropic behavior of the CH_2 stretching vibration in the spectrum of $Form^{COMBI}$ with only protiated lipids was highly comparable to the formulations with only one CER. However, the onset transition temperature was increased to 16°C (Figure 7D). When replacing FA22 by dFA22 the onset transition temperature of the CD_2 asymmetric stretching vibrations was at 18°C and took place over a large temperature range, indicating an order-disorder transition over a large temperature interval. The onset transition temperature was somewhat higher than the formulation with protiated lipids, but lower than the onset transition temperatures of pure dFA22.[22] When substituting

CER NS by dCER NS, the onset transition temperature was 55°C (Figure 7E), which is also substantially higher than in the protiated formulation in which all lipids contribute to this shift, but a lower temperature than for the same transition in pure dCER NS. This indicates that a fraction of dFA and dCER NS interacts with protiated lipids, but the dCER NS and dFA do no not show a concerted order-disorder transition with most of the protiated lipids. This may demonstrate different structural domains in the formulation, most probably FA-rich and CER-rich domains.

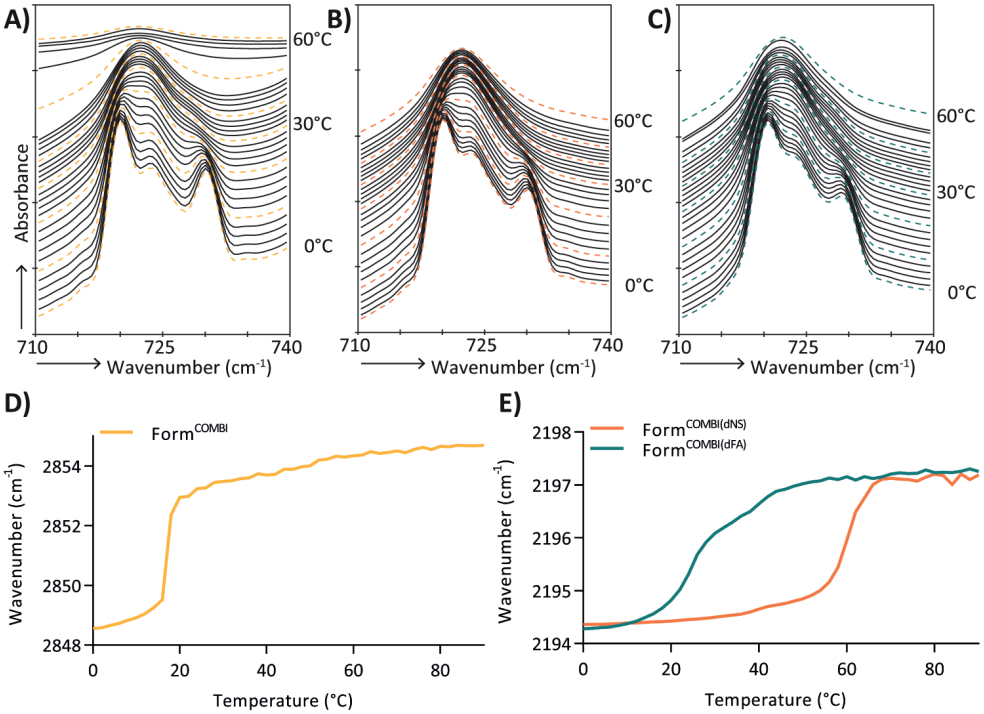

Figure 7. FTIR spectra showing CH_2 rocking vibrations of lipids in formulations as a function of temperature (0-60°C) and peak positions of CH_2 symmetric stretching and CD_2 asymmetric stretching vibrations of FTIR spectra plotted as a function of temperature (0-90°C). A) $Form^{COMBI}$ (only protiated lipids) , **B)** $Form^{COMBI(dNS)}$ (dNS was used) **C)** $Form^{COMBI(dFA)}$ (dFA22 was used), **D)** Symmetric stretching vibrations of CH_2 groups in $Form^{COMBI}$ **E)** The CD_2 asymmetric stretching vibrations of $Form^{COMBI(dNS)}$ and $Form^{COMBI(dFA)}$.

Incorporation of lipids in regenerated SC

After application of $Form^{COMBI}$ on regenerating SC, the CH_2 rocking vibrations in the FTIR spectrum showed two strong peaks at around 719 and 730 cm^{-1}, comparable to regenerated SC on which $Form^{EOS}$ was applied (Figure 8). No major differences were observed after application of a formulation containing dCER NS instead of CER NS. However, after the use of dFA22 instead of FA22, the intensity of the peak at 730 cm^{-1}, relative to the intensity at 719 cm^{-1}, was decreased (Figure 8D). This indicates that the FA22 from the formulation participates at least partly in the orthorhombic packing with the protiated SC lipids.

The temperature dependence of the CH_2 symmetric stretching vibrations after application

of the formulations on regenerating SC was comparable to the temperature dependence of regenerated SC without formulation. When focusing on Form$^{COMBI(dNS)}$, the onset of transition of the CD_2 asymmetric stretching vibrations and CH_2 symmetric stretching vibration after application on SC is very similar, but the transition occurs over a smaller temperature range in the CD_2 asymmetric stretching vibrations (compare Figure 8E and 8F). This temperature range is similar to that of the CD_2 stretching vibrations in the formulation. However, the thermotropic behavior of the CD_2 asymmetric stretching vibrations of Form$^{COMBI(dFA)}$ shows a completely different profile. The ordered-disordered transition starts at around 26°C, as opposed to 16°C for the formulation only, and the transition occurs in a very broad temperature range. This indicates that at least a fraction of the dFA from the formulation interacts with the SC lipids, which show an ordered-disordered phase transition at around 60-70°C. Furthermore, the contours of the CD_2 symmetric stretching vibrations indicate the presence of two vibration modes (see Supplementary Figure 3) with a main peak at a wavenumber of around 2090 cm^{-1} and a shoulder around 2086 cm^{-1}.

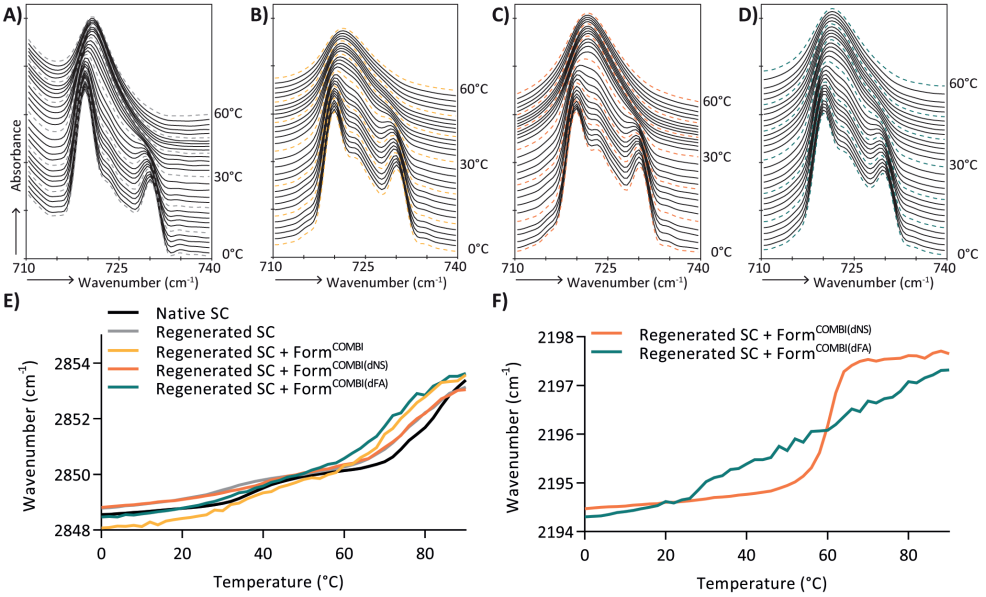

Figure 8. FTIR spectra showing CH_2 rocking vibrations of SC lipids after application of formulations as a function of temperature (0-60°C) and peak positions of CH_2 symmetric stretching and CD_2 asymmetric stretching vibrations of FTIR spectra plotted as a function of temperature (0-90°C). A) Regenerated SC, **B)** Regenerated SC after application of Form^{COMBI} (only protiated lipids), **C)** Regenerated SC after application of Form$^{COMBI(dNS)}$, **D)** Regenerated SC after application of Form$^{COMBI(dFA)}$, **E)** Symmetric stretching vibrations of CH_2 groups in regenerated SC after application of Form^{COMBI} **F)** The CD_2 asymmetric stretching vibrations of regenerated SC after application of Form$^{COMBI(dNS)}$ and Form$^{COMBI(dFA)}$.

Application of CER containing formulation does not influence lamellar lipid organization

The lamellar organization in the lipid matrix was studied using SAXD. The peak positions are indicative for the spacing of the lamellae in the SC. The diffraction patterns of native and regenerated SC with or without formulation are shown in Supplementary Figure 4. All SC samples showed a main peak at a q-position of about 1.0 nm^{-1}, which is attributed to the 1st order SPP peak and the 2nd order LPP peak. In some samples, a small difference in shape of the peak was observed, but the peak position was not changed. Furthermore, sometimes a peak at q=1.9 nm^{-1} was observed, which corresponds to phase separated crystalline CHOL that is present in SC.

Discussion

In the present study, the SkinBaR model that mimics several aspects of the lipid organization in AD skin was used to investigate the effect of topical skin barrier repair formulations. We demonstrate that after application of formulations containing barrier lipids and one CER subclass, a higher fraction of SC lipids adopts an orthorhombic lateral packing in the regenerated SC, mimicking more closely the lipid organization in native human skin. However, when two CER subclasses were combined with a FA, this effect was not observed.

In inflammatory skin diseases, like AD, the skin barrier function is impaired as indicated by an increased TEWL.[23,24] Besides changes in protein levels in the epidermis in these skin diseases, an altered lipid composition and organization compared to healthy skin has also been reported.[13,23-31] Particularly the importance of the lipids for the skin barrier has been indicated by a strong correlation between increased TEWL and reduced chain length of both CER and FA, and a reduced fraction of lipids forming an orthorhombic lateral packing.[11,13,14] These results show that the skin barrier might be improved by normalizing the lipid composition and organization. Previously, several skin barrier repair mixtures containing skin barrier lipids CER, FA, and CHOL were reported.[32-36] However, the precise composition of the formulation is often not described.[34-36] Furthermore, most studies focus on TEWL and/or skin hydration as end point measurements.[32-34,36] None of these studies investigated the effect of the formulations on the lipid composition and/or organization in SC. This demonstrates that little is known about the key interactions of the barrier lipids applied in the formulations and the lipid matrix in the SC, which may be an important underlying mechanism for skin barrier repair. Therefore, additional research is needed to provide detailed insights in these interactions and select the optimal skin barrier repair formulation.

Previously, it has been reported that both natural and synthetic VC applied on tape-stripped mouse skin enhanced skin barrier repair *in vivo*.[16,17] Based on these findings, in the present study we developed formulations containing the barrier lipids CER, FA, and CHOL and examined their effect on the SC lipid organization in an *ex vivo* human skin barrier repair (SkinBaR) model. This model mimics more closely the morphology, the lipid organization, and the lipid composition of AD than that in mice skin: An increased level of short chain CERs and a fraction of unsaturated CERs are present in SC of the SkinBaR model, similarly as in SC of AD skin .[19,37]

In the present study, the CER containing formulation was topically applied on regenerating SC of the SkinBaR model in order to examine whether the lipid organization could be normalized toward that in native human SC and whether barrier lipids in the formulation participate in the SC lipid matrix or mainly remain on the skin surface. In order to examine this, FTIR studies were executed using protiated and (if available) a deuterated CER or FA in the formulations. The use of deuterated lipids in the formulations applied on the SkinBaR model facilitates more detailed analysis of the interactions between the deuterated lipids from the formulations and the SC lipid matrix. First, the effect of only one CER subclass in the formulation was examined. Subsequently, a formulation with a single FA in combination with the two CER subclasses was studied.

Formulations

The physical stability of the formulations was examined during a period of 6 months. During the storage, no crystals were observed. However, when CER NP or CER EOP were introduced in the same formulation, crystals were formed (results not shown). Therefore, all experiments were performed using CER NS and CER EOS.

CERs: Examination of the lateral lipid organization and conformational ordering of the lipids in the formulation indicated that the presence of both the orthorhombic domains and the ordered phase start to disappear at around 10°C. To examine in detail the interaction between CERs and the formulation components, deuterated CER NS was used. Several observations suggest that dCER NS interacts with the other components in the formulation, namely i) the CD_2 stretching frequencies show that the onset transition temperature to a fluid phase is lower for dCER NS in $Form^{dNS}$ than that of pure dCER NS, and ii) no crystals are observed in the formulation during a period of 6 months. However, replacing CER NS by dCER NS did not result in a decrease in the CH_2 rocking vibration contour at 730 cm^{-1}. This suggests that dCER NS does not participate in the orthorhombic lattice in the formulation. As CER NS itself forms a hexagonal lateral packing, it may be that CER NS is located in domains with a hexagonal packing. Supplementation of CER EOS did increase the fraction of lipids forming an orthorhombic packing and increases the stability of the orthorhombic packing slightly. As no deuterated CER EOS is available, it could not be determined whether CER EOS is intercalated in the orthorhombic matrix.

FAs and CERs: In addition to the CERs, FA is another candidate barrier lipid to incorporate in a formulation. In previous studies, FAs with varying chain length were incorporated in the formulation.[21] FA22 showed the most abundant change toward a more orthorhombic lateral packing and was therefore selected for the present studies.

An important question to answer is whether a combination of CER EOS and CER NS with FA22 in the formulation, $Form^{COMBI}$, results in an increased fraction of lipids adopting an orthorhombic packing. The results obtained from CH_2 rocking vibrations in the FTIR spectra indicated an increased fraction of lipids adopting an orthorhombic lateral packing compared to a formulation with only one CER subclass or FA.[21] This is in accordance with previous results showing that both CER EOS and (very) long chain FA are important for the formation of orthorhombic domains.[38-41]

To obtain more detailed information about the interaction of CER and FA in the

formulation, either CER NS or FA22 was replaced by its deuterated counterpart. Participation of at least a fraction of both dCER NS and dFA22 in the orthorhombic lattice in the formulation was demonstrated by the reduced relative intensity of the rocking vibration peak located at 730 cm^{-1} compared to the formulation with only protiated lipids. Interaction of dFA with the other barrier components in the formulation is further demonstrated by an increased onset transition temperature of the CD_2 stretching vibrations in $Form^{COMBI(dFA)}$ compared to that of only dFA in the formulation and decreased compared to that of pure dFA.[21,22] However, a large difference in onset transition temperature of dCER NS ($Form^{COMBI(dNS)}$) with dFA22 ($Form^{COMBI(dFA)}$) was observed. This strongly suggests that at least two different types of domains of barrier lipids are present in the formulation, most probably both containing CERs as well as FAs, but the domains may be either dCER NS rich (high order-disorder transition temperature) or dFA rich domains (lower order-disorder transition temperature).

Interactions between formulations and stratum corneum

After having characterized the formulations, we examined the interactions of the formulations with the regenerating SC. After application of $Form^{EOS}$ or $Form^{NS}$ on regenerating SC, a higher fraction of lipids adopted an orthorhombic lateral packing as indicated by a higher relative intensity of the CH_2 rocking peak at 730 cm^{-1} in the FTIR spectrum. The increase in intensity was more pronounced with CER EOS than CER NS in the formulation, most probably due to the long acyl chain of the former. The increase in the 730 cm^{-1} relative intensity for $Form^{NS}$ is only encountered when the FTIR spectrum in the untreated regenerated SC does not exhibit a 730 cm^{-1} peak, demonstrating the presence of only a hexagonal lateral packing. Based on the similar relative intensity of the rocking vibrations after application of $Form^{NS}$ and $Form^{dNS}$ there is no evidence that CER NS participates in the orthorhombic packing of the SC lipid matrix. Possibly CER NS participates in the hexagonal domains. Therefore, we also examined the lipid ordering of the SC lipid matrix after application of $Form^{NS}$ and $Form^{dNS}$. After application of both formulations on regenerating SC, a comparable onset transition temperature was observed. This onset transition temperature was also comparable to that of $Form^{dNS}$ alone. However, there is a difference in temperature at which the ordered-disordered transition terminates, namely 62.2°C for $Form^{dNS}$ and 71.0°C for regenerated SC treated with $Form^{dNS}$. This indicates that at least a part of the dCER NS interacts with lipids in the SC matrix.

Finally, $Form^{COMBI}$ was applied on regenerating SC and analyzed in the same manner. Application of $Form^{COMBI}$, in which CER EOS, CER NS, and FA22 are combined, did not increase the fraction of lipids adopting an orthorhombic lateral packing compared to untreated regenerated SC. However, the absence of an increase in the formation of the orthorhombic packing is probably due to the high fraction of lipids forming an orthorhombic packing in the untreated regenerated SC, making it a bigger challenge to increase the fraction of lipids forming an orthorhombic packing. The decreased relative intensity of the peak at 730 cm^{-1} after replacing FA22 by dFA22 in $Form^{COMBI}$ indicates that dFA22 participates in the orthorhombic lattice and is most likely intercalated in the SC matrix. Previously, we have reported the application of a formulation containing only one FA.[21] In that paper we show that dFA participate in the orthorhombic lattice

and that it interacts with the SC lipid matrix.[21] It seems that this effect has been slightly reduced when CERs were added to the formulation. Possibly, CER NS and CER EOS interfere with the interaction between FA and the SC lipid matrix probably by stabilizing the FA in the formulation and reducing the partitioning into the orthorhombic lipid matrix in the SC. In contrast, the reduced peak intensity was not observed when CER NS was replaced by dCER NS, suggesting that CER NS is not intercalated in the orthorhombic domains in the SC lipid matrix when FA22 and CER EOS are also present in the formulation. From the stretching vibrations there is also no evidence that CER NS is present in the SC lipid matrix. However, as the ordered-disordered transition of dCER NS in the formulation is in a similar temperature range as that of the SC lipid matrix, some of the CER NS may still intercalate in the hexagonal packing in the lipid matrix, or CER NS may be present in the skin furrows and may still influence barrier repair.
Several other formulations consisting of CERs, FA, and CHOL report enhanced barrier repair for formulations containing CER subclass NP.[42-44] However, mainly TEWL was used as skin barrier repair parameter, and interaction with SC lipid matrix was not examined. In our formulation CER NP crystallizes and therefore CER NP was not suitable to be used in the present study. Other studies report formulations in which CER subclass AdS was used as CER component. Topical application of these formulations resulted in decreased TEWL values and a higher skin hydration after 4 weeks.[45,46] Furthermore, addition of CER AdS to the culture medium of reconstructed human skin resulted in increased CER content, mainly caused by an increase of CER EOS, NS, and NP.[47]

Conclusion

In conclusion, we show that CERs interact with the other components of a lipid formulation, resulting in a higher fraction of lipids adopting an orthorhombic lateral packing compared to a formulation without CERs. These interactions were also observed for FA and CERs when both lipid classes were present in the formulation.
After application of the formulation containing either CER EOS or CER NS on regenerating SC of the SkinBaR model, a denser lipid packing was observed, suggesting that CERs from the formulation interact with the SC lipid matrix. When studying a formulation with the three barrier components FA, CER NS and CER EOS, there is strong evidence that FA is interacting with the orthorhombic domains in the SC lipid domains, while there is no clear indication that CER NS is intercalated within the SC lipid matrix.

Acknowledgements

The authors thank Evonik for supplying the synthetic ceramides, and the personnel at DUBBLE beam line (BM26) at the European synchrotron radiation facility (ESRF) in Grenoble, France for assisting with X-ray measurements. This research was financially supported by Dutch Technology Foundation TTW (grant no. 12400).

References

1. Elias PM. Epidermal lipids, barrier function, and desquamation. *J Invest Dermatol* **1983**: 80: 44s-49s.
2. Bouwstra JA, Gooris GS, van der Spek JA, et al. Structural investigations of human stratum corneum by small-angle X-ray scattering. *J Invest Dermatol* **1991**: 97: 1005-1012.
3. Bouwstra J, Pilgram G, Gooris G, et al. New aspects of the skin barrier organization. *Skin Pharmacol Appl Skin Physiol* **2001**: 14 Suppl 1: 52-62.
4. McIntosh TJ, Stewart ME, Downing DT. X-ray diffraction analysis of isolated skin lipids: reconstitution of intercellular lipid domains. *Biochemistry* **1996**: 35: 3649-3653.
5. Madison KC, Swartzendruber DC, Wertz PW, et al. Presence of intact intercellular lipid lamellae in the upper layers of the stratum corneum. *J Invest Dermatol* **1987**: 88: 714-718.
6. Groen D, Gooris GS, Bouwstra JA. New insights into the stratum corneum lipid organization by X-ray diffraction analysis. *Biophys J* **2009**: 97: 2242-2249.
7. Goldsmith LA, Baden HP. Uniquely oriented epidermal lipid. *Nature* **1970**: 225: 1052-1053.
8. Damien F, Boncheva M. The extent of orthorhombic lipid phases in the stratum corneum determines the barrier efficiency of human skin in vivo. *J Invest Dermatol* **2010**: 130: 611-614.
9. Pilgram GS, Engelsma-van Pelt AM, Bouwstra JA, et al. Electron diffraction provides new information on human stratum corneum lipid organization studied in relation to depth and temperature. *J Invest Dermatol* **1999**: 113: 403-409.
10. de Jager MW, Gooris GS, Dolbnya IP, et al. The phase behaviour of skin lipid mixtures based on synthetic ceramides. *Chem Phys Lipids* **2003**: 124: 123-134.
11. Janssens M, van Smeden J, Gooris GS, et al. Increase in short-chain ceramides correlates with an altered lipid organization and decreased barrier function in atopic eczema patients. *J Lipid Res* **2012**: 53: 2755-2766.
12. Ohno Y, Suto S, Yamanaka M, et al. ELOVL1 production of C24 acyl-CoAs is linked to C24 sphingolipid synthesis. *Proc Natl Acad Sci U S A* **2010**: 107: 18439-18444.
13. Ishikawa J, Narita H, Kondo N, et al. Changes in the ceramide profile of atopic dermatitis patients. *J Invest Dermatol* **2010**: 130: 2511-2514.
14. van Smeden J, Janssens M, Kaye EC, et al. The importance of free fatty acid chain length for the skin barrier function in atopic eczema patients. *Exp Dermatol* **2014**: 23: 45-52.
15. Haubrich KA. Role of Vernix caseosa in the neonate: potential application in the adult population. *AACN Clin Issues* **2003**: 14: 457-464.
16. Oudshoorn MH, Rissmann R, van der Coelen D, et al. Development of a murine model to evaluate the effect of vernix caseosa on skin barrier recovery. *Exp Dermatol* **2009**: 18: 178-184.
17. Rissmann R, Oudshoorn MH, Zwier R, et al. Mimicking vernix caseosa--preparation and characterization of synthetic biofilms. *Int J Pharm* **2009**: 372: 59-65.
18. Hirschberg HJ, van RE, Oosterhoff D, et al. Animal models for cutaneous vaccine delivery. *Eur J Pharm Sci* **2015**: 71: 112-122.
19. Danso MO, Berkers T, Mieremet A, et al. An ex vivo human skin model for studying skin barrier repair. *Exp Dermatol* **2015**: 24: 48-54.
20. Motta S, Monti M, Sesana S, et al. Ceramide composition of the psoriatic scale. *Biochim Biophys Acta* **1993**: 1182: 147-151.
21. Berkers T, van Dijk L, Absalah S, et al. Topically applied fatty acids are elongated before incorporation in the stratum corneum lipid matrix in compromised skin. *Exp Dermatol* **2016**.
22. Inoue T, Hisatsugu Y, Yamamoto R, et al. Solid-liquid phase behavior of binary fatty acid mixtures. 1. Oleic acid/stearic acid and oleic acid/behenic acid mixtures. *Chem Phys Lipids* **2004**: 127: 143-152.
23. Shahidullah M, Raffle EJ, Rimmer AR, et al. Transepidermal water loss in patients with dermatitis. *Br J Dermatol* **1969**: 81: 722-730.
24. Rajka G. Transepidermal water loss on the hands in atopic dermatitis. *Arch Dermatol Forsch* **1974**: 251: 111-115.
25. Lebwohl M, Herrmann LG. Impaired skin barrier function in dermatologic disease and repair with moisturization. *Cutis* **2005**: 76: 7-12.
26. Jungersted JM, Scheer H, Mempel M, et al. Stratum corneum lipids, skin barrier function and filaggrin mutations in patients with atopic eczema. *Allergy* **2010**: 65: 911-918.
27. Imokawa G, Abe A, Jin K, et al. Decreased level of ceramides in stratum corneum of atopic dermatitis: an etiologic factor in atopic dry skin? *J Invest Dermatol* **1991**: 96: 523-526.
28. Di Nardo A, Wertz P, Giannetti A, et al. Ceramide and cholesterol composition of the skin of patients with atopic dermatitis. *Acta Derm Venereol* **1998**: 78: 27-30.
29. Mlitz V, Latreille J, Gardinier S, et al. Impact of filaggrin mutations on Raman spectra and biophysical properties of the stratum corneum in mild to moderate atopic dermatitis. *J Eur Acad Dermatol Venereol* **2012**: 26: 983-990.

30. Angelova-Fischer I, Mannheimer AC, Hinder A, et al. Distinct barrier integrity phenotypes in filaggrin-related atopic eczema following sequential tape stripping and lipid profiling. *Experimental dermatology* **2011**: 20: 351-356.
31. Weidinger S, Novak N. Atopic dermatitis. *Lancet (London, England)* **2016**: 387: 1109-1122.
32. Visscher MO, Barai N, LaRuffa AA, et al. Epidermal barrier treatments based on vernix caseosa. *Skin Pharmacol Physiol* **2011**: 24: 322-329.
33. Man MM, Feingold KR, Thornfeldt CR, et al. Optimization of physiological lipid mixtures for barrier repair. *J Invest Dermatol* **1996**: 106: 1096-1101.
34. Barba C, Parra JL, Coderch L, et al. In vivo and in vitro evaluation of topical formulations containing physiological lipid mixture for replacement of skin barrier function. *G Ital Dermatol Venereol* **2014**: 149: 347-353.
35. Chamlin SL, Kao J, Frieden IJ, et al. Ceramide-dominant barrier repair lipids alleviate childhood atopic dermatitis: changes in barrier function provide a sensitive indicator of disease activity. *J Am Acad Dermatol* **2002**: 47: 198-208.
36. Kircik LH, Del Rosso JQ, Aversa D. Evaluating Clinical Use of a Ceramide-dominant, Physiologic Lipid-based Topical Emulsion for Atopic Dermatitis. *J Clin Aesthet Dermatol* **2011**: 4: 34-40.
37. Boiten W, Absalah S, Vreeken R, et al. Quantitative analysis of ceramides using a novel lipidomics approach with three dimensional response modelling. *Biochim Biophys Acta* **2016**: 1861: 1652-1661.
38. Mojumdar EH, Kariman Z, van Kerckhove L, et al. The role of ceramide chain length distribution on the barrier properties of the skin lipid membranes. *Biochim Biophys Acta* **2014**: 1838: 2473-2483.
39. de Sousa Neto D, Gooris G, Bouwstra J. Effect of the omega-acylceramides on the lipid organization of stratum corneum model membranes evaluated by X-ray diffraction and FTIR studies (Part I). *Chem Phys Lipids* **2011**: 164: 184-195.
40. Groen D, Gooris GS, Bouwstra JA. Model membranes prepared with ceramide EOS, cholesterol and free fatty acids form a unique lamellar phase. *Langmuir* **2010**: 26: 4168-4175.
41. Groen D, Poole DS, Gooris GS, et al. Is an orthorhombic lateral packing and a proper lamellar organization important for the skin barrier function? *Biochim Biophys Acta* **2011**: 1808: 1529-1537.
42. De Paepe K, Roseeuw D, Rogiers V. Repair of acetone- and sodium lauryl sulphate-damaged human skin barrier function using topically applied emulsions containing barrier lipids. *J Eur Acad Dermatol Venereol* **2002**: 16: 587-594.
43. Loden M, Barany E. Skin-identical lipids versus petrolatum in the treatment of tape-stripped and detergent-perturbed human skin. *Acta Derm Venereol* **2000**: 80: 412-415.
44. Yang L, Mao-Qiang M, Taljebini M, et al. Topical stratum corneum lipids accelerate barrier repair after tape stripping, solvent treatment and some but not all types of detergent treatment. *Br J Dermatol* **1995**: 133: 679-685.
45. Simpson E, Trookman NS, Rizer RL, et al. Safety and tolerability of a body wash and moisturizer when applied to infants and toddlers with a history of atopic dermatitis: results from an open-label study. *Pediatr Dermatol* **2012**: 29: 590-597.
46. Simpson E, Bohling A, Bielfeldt S, et al. Improvement of skin barrier function in atopic dermatitis patients with a new moisturizer containing a ceramide precursor. *J Dermatolog Treat* **2013**: 24: 122-125.
47. Castiel-Higounenc I, Chopart M, Ferraris C. Stratum corneum lipids: specificity, role, deficiencies and modulation. *OCL* **2004**: 11: 401-406.

Supplementary material

Materials and methods

Chemicals

Super sterol esters were kindly provided by Croda (Cowick Hall, UK), triglycerides (Miglyol 812) were supplied by Cremer Oleo (Witten, Germany). CER EOS30 and CER NS24 were provided by Evonik (Essen, Germany). Deuterated CER NS24 was kindly supplied by Evonik Industries AG (Essen, Germany), perdeuterated behenic acid was acquired from Cambridge Isotope Laboratories (Tewksbury, MA, USA). Cyanoacrylate (Bison, Goes, the Netherlands) was bought locally. Xylene and methanol were obtained from Biosolve (Valkenswaard, the Netherlands), 4% buffered formaldehyde was purchased from Added Pharma (Oss, the Netherlands), paraffin, haematoxylin, and eosin were acquired from Klinipath (Duiven, the Netherlands). DMEM, Ham's F12, and penicillin/streptomycin were purchased from Fisher Scientific (Waltham, Massachusetts, USA). Squalene, cholesterol, bovine serum albumin, sodium bromide, ethanol, acetone, trypsin, trypsin inhibitor, selenious acid, hydrocortisone, isoproterenol, L-carnitine, L-serine, insulin, α-tocopherol acetate, vitamin C, arachidonic acid, linoleic acid, and palmitic acid were bought from Sigma-Aldrich (Zwijndrecht, the Netherlands). Chloroform was obtained from Macron Fine Chemicals (Gliwice, Poland). All solvents were HPLC grade or higher.

Stripping and culturing of ex vivo skin

Before dermatoming to a thickness of 600 µm (D80 Dermatome, Humeca, Borne, the Netherlands), the subcutaneous fat was removed, and the skin was wiped with 70% EtOH and Millipore water. SC was removed by sequential stripping as described before.[1] Briefly, skin was punched (ø=26 mm) and stretched on a custom made clamping device. SC was removed by preheated (40°C) metal cylinder with preheated cyanoacrylate. During each stripping the metal cylinder was applied on the skin for 2 minutes with a pressure of 0.7 kg/cm^2. This procedure was repeated until the SC was removed which is indicated by a shiny appearance of the skin.
The detailed culturing procedure has been described previously.[1,2] In short, the stripped skin was placed on top of a cotton pad and a transwell filter insert (Corning Life sciences, Amsterdam, Netherlands) in a deep 6-well culturing plate (Organogenesis, Canton, MA, USA). A metal ring (inner diameter 15 mm) was placed on the SC side of the skin.

Isolation of SC

Trypsin was used to isolate SC from cultured skin. The skin was kept at 4°C overnight in 0.1% trypsin solution in PBS, followed by one hour at 37°C. SC was peeled off and washed in 0.1% trypsin inhibitor solution in PBS. SC sheets were cleaned twice in Millipore water and stored over silica gel under argon in the dark until use. SC was used for either infrared spectroscopy measurements or X-ray diffraction measurements.

Fourier transform infrared spectroscopy

The conformational ordering and the lateral packing of the lipids in the SC matrix and

the formulations was examined using Fourier transform infrared spectroscopy (FTIR). SC samples were hydrated over a 27% NaBr solution in D_2O for 24 hours at room temperature. FTIR spectra were recorded using a Varian 670-IR FTIR spectrometer (Agilent Technologies, Santa Clara, USA), equipped with a broadband mercury-cadmium-telluride detector. A hydrated SC sample or a formulation was placed between two AgBr-windows and measured in transmission mode. Samples were put under a continuous purge of dry air starting 30 minutes before the beginning of the measurement. Spectra were obtained as a co-addition of 128 scans at 1 cm^{-1} resolution during 2 minutes, during which the sample temperature was increased from 0 to 90°C at a heating rate of 0.5°C/min. Resolutions Pro 4.1 (Varian Inc.) software was used to analyze the data.[3]

The peak positions of the CH_2 symmetric and CD_2 asymmetric stretching vibrations in the FTIR spectra were used to determine the onset temperature of the ordered-disordered transition. Two regression lines were fitted to the linear parts of the graph obtained after plotting the peak positions against temperature. The intercept of the two regression lines determines the onset transition temperature, as described before.[2] The end of the ordered-disordered phase transition was determined in the same manner as the onset transition temperature.

Small angle X-ray diffraction

The lamellar lipid organization was examined using small angle X-ray diffraction (SAXD). Measurements were performed at the European Synchrotron Radiation Facility (ESRF, Grenoble, France) at station BM26B. The SC samples were hydrated over a 27% NaBr solution during 24 hours prior to the measurements. SC samples were carefully oriented parallel to the X-ray beam in a custom made sample holder. SAXD patterns were detected with a Pilatus 1M detector at room temperature for a period of 5 or 10 min as described earlier.[4] The scattering vector (q) was calculated from the scattering angle (Θ) and the wavelength (λ) by $q=4\pi \sin \Theta/\lambda$. From the position of the peak maxima (q), the spacing of the lamellar phase can be calculated using $2\pi/q$. A peak positioned at a lower q-value corresponds to a larger spacing of the lipid lamellae.

Results

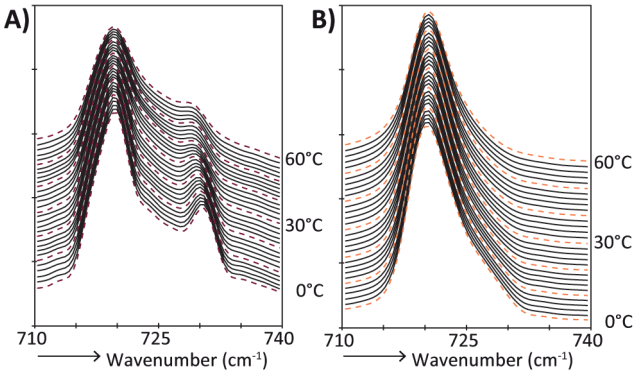

Supplementary Figure 1. FTIR spectra showing CH_2 rocking vibrations of pure CER as a function of temperature (0-60°C). A) CER EOS, characterized by a doublet with vibrations at around 719 and 730 cm^{-1} **B)** CER NS, characterized by a singlet at a wavenumber of around 719 cm^{-1}.

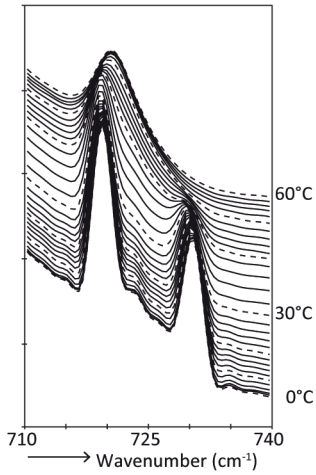

Supplementary Figure 2. FTIR spectrum showing CH_2 rocking vibrations of native SC. Two strong peaks are observed at wavenumbers of around 719 and 730 cm^{-1}. The intensity of the peak at 730 cm^{-1} started to decrease at a temperature of around 30°C and the contour disappeared at 48°C. This change in rocking profile is indicative for the orthorhombic to hexagonal phase transition.

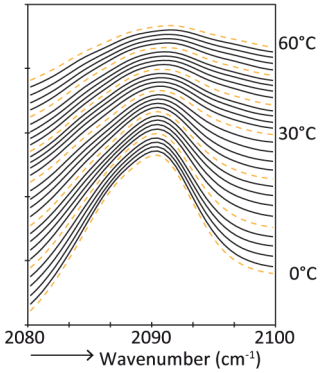

Supplementary Figure 3. FTIR spectrum showing CD_2 symmetric stretching vibrations of Form$^{COMBI(dFA)}$. The shape of the peak indicatest the presence of two types of vibrations, 2090 cm^{-1} and 2086 cm^{-1}.

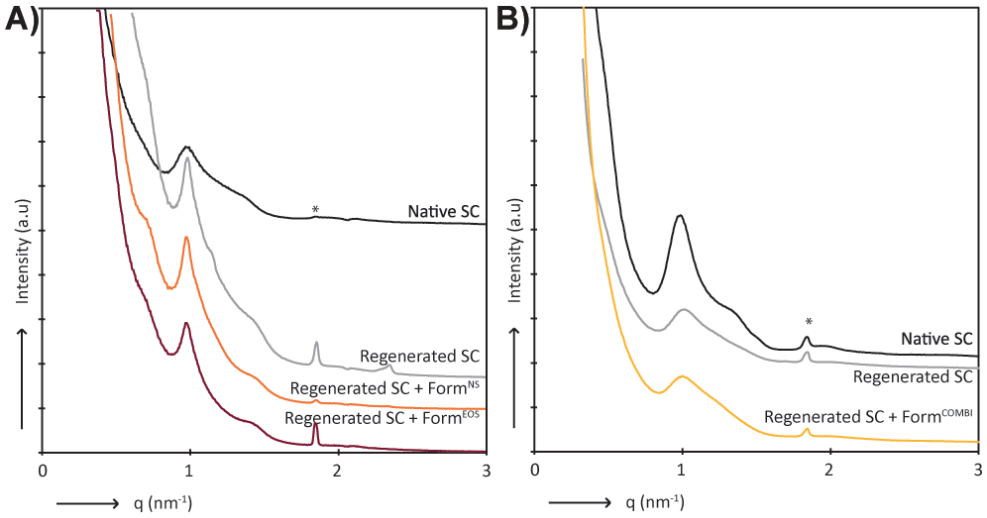

Supplementary Figure 4. X-ray diffraction patterns of native SC and regenerated SC with and without application of formulation. Both SPP and LPP attribute to the peaks at q=1. Phase separated CHOL is observed at q=1.8 and indicated by an asterisk. **A)** SAXD profiles of native SC, regenerated SC, and regenerated SC with application of Form^{EOS} and Form^{NS}, **B)** SAXD profiles of native SC, regenerated SC, and regenerated SC with application of Form^{COMBI}.

Supplementary references

1. Danso MO, Berkers T, Mieremet A, et al. An ex vivo human skin model for studying skin barrier repair. *Exp Dermatol* **2015**: 24: 48-54.
2. Berkers T, van Dijk L, Absalah S, et al. Topically applied fatty acids are elongated before incorporation in the stratum corneum lipid matrix in compromised skin. *Exp Dermatol* **2016**.
3. Damien F, Boncheva M. The extent of orthorhombic lipid phases in the stratum corneum determines the barrier efficiency of human skin in vivo. *J Invest Dermatol* **2010**: 130: 611-614.
4. Groen D, Gooris GS, Bouwstra JA. New insights into the stratum corneum lipid organization by X-ray diffraction analysis. *Biophys J* **2009**: 97: 2242-2249.

Part 3

Chapter 7

Applying a vernix caseosa based formulation accelerates skin barrier repair by modulating lipid biosynthesis

Tineke Berkers[1*], Walter A. Boiten[1*], Samira Absalah[1], Jeroen van Smeden[1], Adriana P.M. Lavrijsen[2], Joke A. Bouwstra[1]

[1] Leiden Academic Centre for Drug Research, Leiden University, Leiden, the Netherlands
[2] Department of dermatology, Leiden University Medical Centre, Leiden, the Netherlands
* Both authors contributed equally

J Lipid Res. 2018 Feb;59(2):250-260

Abbreviations

AD	Atopic dermatitis
ATR-FTIR	Attenuated total reflection Fourier transform infrared spectroscopy
AUC	Area under the barrier recovery curve
C34	Ceramide with 34 carbon atoms
FWHM	Full width at half maximum
LMMs	Linear mixed models
PCA	Principal component analysis
PC	Principal component
SAXD	Small angle X-ray diffraction
SC	Stratum corneum
SQ	SquameScan value
TEWL	Transepidermal water loss
VC	Vernix caseosa

Keywords

Epidermis, clinical study, mass spectrometry, lipidomics, sphingolipids, lipid organization, vernix caseosa, barrier recovery, stratum corneum, treatment

Abstract

Restoring the lipid homeostasis of the stratum corneum (SC) is a common strategy to enhance the skin barrier function. Here, we used a ceramide containing vernix caseosa (VC) based formulation and were able to accelerate barrier recovery in healthy volunteers. The recovery was examined over 16 days by monitoring trans-epidermal water loss (TEWL) after barrier disruption by tape-stripping. Four skin sites were used to examine the effects of both treatment and barrier recovery. After 16 days, samples were harvested at these sites to examine the SC ceramide composition and the lipid organization. Changes in ceramide profiles were identified using principal component analysis (PCA). After barrier recovery, the untreated sites showed increased levels of ceramide subclass AS and ceramides with a 34 total carbon atom chain length, while the mean ceramide chain length was reduced. These changes were diminished by treatment with the studied formulation, which concurrently increased the formulated ceramides. Correlations were observed between SC lipid composition, lipid organization, and TEWL, and changes in the ceramide subclass composition suggesting changes in the ceramide biosynthesis. These results suggest that VC based formulations enhance skin barrier recovery and are attractive candidates to treat skin disorders with impaired barrier properties.

Introduction

Vital functions of the stratum corneum (SC) are preventing excessive water loss from the body and protecting the body from the hostile outside environment by acting as an inside-out and an outside-in barrier, respectively. The SC is generated by a dynamic process in which keratinocytes in the lower layer of the epidermis undergo terminal differentiation and transform into corneocytes.[1] During this differentiation process, lipids are synthesized, stored in lamellar bodies and, at the interface between the viable epidermis and SC, these lamellar bodies are secreted in the intercellular regions.[2] The secreted lipids form an extracellular lipid matrix crucial for a proper skin barrier.[3,4] Three main lipid classes have been identified: cholesterol, fatty acids, and ceramides. The latter constitutes the group of SC lipids that have the most diverse chemical structure. Their building blocks are an array of sphingoid bases and acyl chains chemically linked together by an amide bond, resulting in 16 ceramide subclasses.[5] Both chains (the sphingoid base and acyl chain) can vary substantially in carbon chain length. The composition of the SC ceramide fraction (the ceramide profile) was correlated with and shown to be important for lipid organization and skin barrier function.[6-8] In the present study, the effect of a ceramide containing formulation on skin barrier recovery, the ceramide composition, and lipid organization were studied.

Through the processes of cornification and desquamation, the SC is continuously rejuvenated[9,10] and can thereby quickly recover the barrier function after disruption.[11] An impaired skin barrier function is encountered in several inflammatory skin diseases; one of which is atopic dermatitis (AD). In AD, an inadequate recovery of the impaired skin barrier perpetuates the condition. Normalization of the barrier function in AD is crucial to reduce the penetration of irritants and allergens into the skin. Application of lipophilic formulations that act as an additional barrier is a common treatment.[12-15] Another approach aims at normalization of the ceramide composition.[4] Changes in this composition were correlated to the reduced skin barrier function in AD.[8,16,17] Previously, ceramide containing formulations have been used to study skin barrier repair[18-21] and it was reported that the ratios between the three main SC lipids in a formulation was important for short term recovery.[22] Furthermore, it was suggested that long term application could enhance barrier recovery.[21] Nonetheless, it is disputed whether ceramides in a formulation actually normalize the SC lipid composition or remain on the skin surface.[23] It has been shown that the orally administered essential fatty acids were incorporated in the epidermis.[24]

How these formulations accelerate barrier recovery is not clearly understood. Therefore, the primary aim of this study was to examine how treatment with a formulation during barrier recovery affects the SC lipid composition and subsequently lipid organization. This was done by examining the normal physiological responses in healthy volunteers. In this study, we applied a ceramide containing formulation based on the composition of the vernix caseosa (VC). This is a natural ceramide containing formulation that serves as a protective lipid film covering the fetus in the last trimester of pregnancy and during delivery.[25] Previously, it was shown that VC like formulations were able to significantly accelerate barrier recovery in mice.[26,27] This vernix formulation has the advantage that ceramides can be formulated. The formulation is semi-occlusive.[28] To examine the effect of the formulation on barrier recovery, we used barrier disruption

by tape-stripping, as this is an effective way to remove the barrier and induce barrier recovery in healthy skin.[27,29-32]
Here, it is shown that treatment with the formulation resulted in accelerated barrier recovery of tape-stripped skin compared to the untreated tape-stripped skin. In regenerated untreated SC, an altered ceramide composition was observed. These alterations correlated to a decrease in skin barrier function. When applying the ceramide containing formulation, the ceramide composition was modulated towards a ceramide composition more closely mimicking that of control skin. Combined, these results indicate that barrier disruption induces changes in lipid processing during recovery, related to a decreased barrier function and that these changes in lipid processing can be modulated by application of the VC formulation.

Materials and methods

Chemicals

The following solvents were used for lipid extraction and analysis: Millipore water (18.2 mΩ), HPLC grade methanol and chloroform from Lab-Scan (Gliwice, Poland), UPLC grade isopropanol and ethanol from Biosolve (Valkenswaard, the Netherlands), and HPLC grade heptane from Actu-All (Oss, the Netherlands). The synthetic ceramides listed in Table S1 were used as calibrators for the LC/MS analysis. Trypsin and trypsin inhibitor for SC isolation were purchased from Sigma-Aldrich (Zwijndrecht, the Netherlands).

Clinical study design

The clinical study was approved by the Leiden University Medical Center ethical committee and performed according to the declaration of Helsinki. All volunteers signed an informed consent. 8 female and 7 male Caucasian volunteers, age 18 to 29 years (mean age 23 years) were recruited and checked by a dermatologist. Volunteers were excluded if they had dermatological disorders or a history of dermatological disorders, suffered from chronically inflammatory diseases, used systemic drug therapies, had abundant hair or unnatural abnormalities on the ventral forearms, had a history of drug abuse, or if they were pregnant. All enrolled volunteers completed the clinical study.
Figure 1A depicts the timeline of the study. Before the study commenced, volunteers had a one week washout period in which no soaps or cosmetics were applied on the ventral forearms. At T_0 a site of 3.5 by 2.5 cm of SC was removed at both ventral forearms by consecutive tape-stripping using DSquame tape (Cuderm, Dallas, USA). The tape-stripping continued until the site appeared shiny[33] and a transepidermal water loss (TEWL) of > 60 g/m^2/h was reached (these sites are further referred to as stripped). TEWL was measured using AquaFlux AF200 (BIOX, London, UK). Thereafter, two fingertip units of a VC like formulation (composition is shown in Table S2) were applied twice daily for 14 days on one ventral forearm (referred to as treated), followed by a two day washout period. Treatment allocation to either left or right arm was alternated between volunteers. Figure 1B depicts the 4 sites investigated in this study: control

(no treatment, no tape-stripping), treated (treated with formulation), stripped (tape-stripped at T_0), and stripped+treated (tape-stripped at T_0 and treated with formulation). At the final time point (T_{16}) 21 tape-strips, using polyphenylene sulfide tape (Nichiban, Tokyo, Japan), were harvested at all 4 sites. The amount of SC on each tape-strip was determined by measuring the tape-strips with a SquameScan (Heiland Electronic, Wetzlar, Germany). Tape-strip zero was discarded. After every other tape-strip an infrared spectrum of the tape-stripped skin region was made (see below). After tape-stripping, a 4 mm biopsy of both recovered sites was collected, near the site where Nichiban tape-strips were harvested, to perform small angle X-ray diffraction (SAXD), see below. During the study, TEWL of all sites was monitored at distinct time points, these measurements were performed before formulation application.

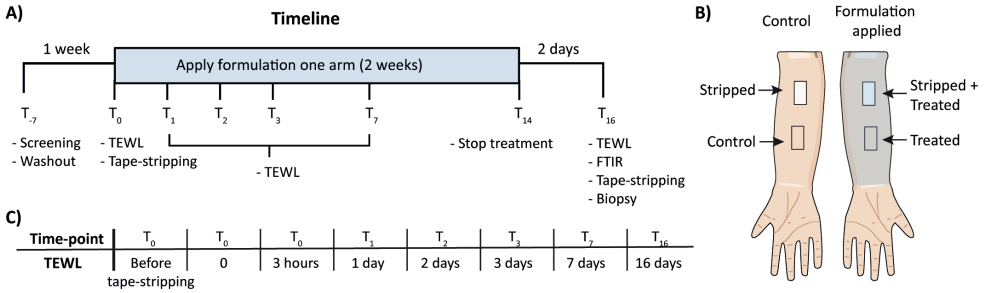

Figure 1. Study design. A) Timeline of the clinical study (Time points are indicated as T with days as subscripts). Volunteers were first screened by a dermatologist (T_{-7}), followed by a one week washout period. At T_0 the SC was removed by tape-stripping. The formulation was applied 2x daily for 2 weeks followed by two days washout. The activities and measurements are indicated at each time point (T_{-7} till T_{16}). At all indicated time-points TEWL was measured, except for T_{-7}. **B)** The studied sites on the ventral forearms. On both arms one site was tape-stripped; on one arm formulation was applied. **C)** The time-points at which TEWL was measured to monitor barrier recovery of the stripped sites.

TEWL measurements to determine barrier recovery

To determine barrier recovery of the stripped sites TEWL was monitored. At each time point depicted in Figure 1C, TEWL was measured at three different sections of each site (Figure S1). The barrier recovery percentage was calculated by defining the average of three TEWL measurements at the non-stripped sites as 100% barrier and TEWL at the stripped sites directly after tape-stripping as 0% barrier. The following equation was used:[26]

Recovery% T_n=(TEWL T_0-TEWL T_n)/(TEWL T_0-Average TEWL non-stripped site T_n)*100

For each volunteer several values were calculated for both the treated and untreated stripped sites: I) the recovery percentage of the site at three sections at each time-point, II) the mean of the three previous values, III) the area under the barrier recovery curve (AUC) of the means over time, using a point-to-point linear fit, IV) using the same fit, the time it took to reach designated recovery percentages between 5-100%, with increment of 5%, V) the difference in time between the stripped and stripped+treated sites at each of the previously mentioned recovery %. Recovery percentages >90% were excluded, as only 5 volunteers reached these values at both stripped sites, biasing these data.

Quantification of ceramides by LC/MS

Tape-stripped SC can be used to examine the lipid content by mass spectrometry.[34-36] Samples for ceramide analysis by LC/MS were prepared from tape-strips 5-8 and 17-20, harvested at the 4 sites on T_{16}. Samples prepared from tape-strips at a depth of 5-8 and 17-20 tapes were analyzed separately to determine if the SC ceramide composition generated in the initial stage of the recovery process (tapes 5-8) was different from that generated in later stages of the recovery process (tapes 17-20). Tape-strips were punched to an area of 2 cm^2, extracted, analyzed and quantified as described in Boiten et al.[34] Shortly, a modified 4 step Bligh and Dyer extraction at 40°C was performed. Extracts were analyzed using an Acquity UPLC H-class (Waters, Milford, MA, USA) connected to an XEVO TQ-S mass spectrometer (Waters, Milford, MA, USA). Separation was performed on a pva-silica column (5 µm particles, 100 × 2.1 mm i.d.)(YMC, Kyoto, Japan). Using the calibrators, a response model was build and used to quantify the ceramides in the analyzed samples. All data were corrected for the cumulative SquameScan value (SQ) of the four tape-strips comprising the corresponding sample. The data resulted in quantitative SC ceramide profiles for each volunteer, at all 4 sites, and at two depths per site. Ceramides are named according to hydrophilic head group (subclass) and chain length (e.g. NS C42, ceramide subclass NS with a total chain length of 42 carbon atoms).[37] For an overview of subclasses and ceramide structures see Figure S2.

Quantitative data were used to calculate several parameters. Ceramides EOS C66 and NS C40 (supplied in the formulation) were excluded from these calculations. The following parameters were calculated:

I) Total amount of the individual subclasses (ng/SQ);
II) Total amount of ceramides with a total chain length 34 carbons (ng/SQ);
III) Mean carbon chain length: (Σ each ceramide (molar amount ceramide x carbon chain length))/total molar amout all ceramides;
IV) Percentage of EO ceramides, as ng EO / total ng ceramides.

Lateral organization and conformational ordering of SC lipids

The lateral organization and conformational ordering of the SC lipids were examined by attenuated total reflection Fourier transform infrared spectroscopy (ATR-FTIR). FTIR spectra were collected using a Varian 670-IR spectrometer (Agilent Technologies, Inc., Santa Clara, CA) equipped with a mercury-cadmium-telluride detector and an external sample compartment containing an ATR accessory (GladiATR, PIKE Technologies, Maddison, WI) with a single reflection diamond. The sample compartment was constantly purged with dry air. Each spectrum was an average of 150 scans, with a spectral resolution of 2 cm^{-1}. Conformational ordering of the lipids was determined using the center of gravity of the peak of the CH_2 symmetric stretching vibrations at 90% of the peak height. The bandwidth from the second derivative of the CH_2 scissoring region was selected as a measure for lateral packing of the lipids and determined as described before.[38,39] CH_2 stretching vibration peak position values <2850 cm^{-1} indicate an ordered phase, whereas values above 2852 cm^{-1} indicate a high degree of disordering being a liquid phase. The second derivative of the CH_2 scissoring region

was baseline-corrected between the endpoints of the scissoring region (~1460-1480 cm^{-1}) and the full width at half maximum (FWHM) was calculated.[39] Values of 5 spectra (tape 2-10 and tape 12-20) per site per volunteer were used for the analyses.

Small angle X-ray diffraction

SC isolated from biopsies harvested at stripped and stripped+treated sites were examined by SAXD. SAXD was used to determine the SC lipids lamellar organization. To isolate SC for SAXD analysis, biopsies were placed overnight in a 0.1% trypsin solution in PBS at 4˚C, followed by one hour incubation at 37˚C. The SC was peeled of and washed in 0.1 % trypsin inhibitor solution in PBS and twice in Millipore water. Dried SC sheets were stored under argon and over silica gel until use. All SAXD measurements were performed at the European Synchrotron Radiation Facility (Grenoble, France) at station BM26B. SAXD patterns were collected on a Pilatus 1M detector at room temperature for 5 minutes. The sample-to-detector distance was 2 m. Prior to data collection, the SC samples were hydrated over a 27% (w/v) NaBr solution for 24 hours at room temperature. The scattering intensity I (arbitrary units) was measured as a function of the scattering vector q (in nm^{-1}), defined as: $q = 4\pi \sin\theta/\lambda$, in which θ is the scattering angle and λ is the wavelength. From the position of the main peak (referred to as peak 2 with position q_2), the spacing (d) of the lipid lamellae was calculated using $d = 2\pi/q_2$. As in SC this peak position is determined by the structure of the two lamellar phases, a change in the spacing indicates a change in these lamellar phases.[8]

Software and statistical analysis

All LC/MS data were processed using MassLynx and TargetLynx software (V4.1 SCN 843 Waters Inc.). FTIR data were processed and analyzed using Resolutions Pro 4.1 (Agilent Technologies, Inc.). Principal component analysis (PCA) is a commonly used analysis of lipidomics data sets.[40,41] It is a mathematical dimensional reduction that can effectively visualize variation and the difference between samples in large data sets by reducing all variables to principal components (PCs). PCA was performed using Multibase add-in for excel (NumericalDynamics.Com). For PCA, the quantitative data obtained from the ceramide analyses were normalized to the total amount of ceramides in the samples. The four individual sites (control, treated, stripped, and stripped+treated) of each volunteer were defined as PCA samples. All quantified ceramides at both depths were defined as variables of that "PCA sample" (total of 584 variables), thereafter the mean of each ceramide/variable in all "PCA samples" was centered at zero (subtracting the mean).
Correlation analysis and point-to-points fits were performed using GraphPad Prism (V6.05, Graphpad). Group-wise comparisons were performed using linear mixed models (LLMs) in SPSS (V24 IBM). All measurements within the same subject were treated as repeated measurement. LMMs were used because these models have the advantage that I) the effect size of individual variables and their interactions can be examined, and II) they can handle missing data.[42] Figure S3 explains how the LMMs were used here. All interactions between fixed variables were included in the first run of a model and when non-significant ($p>0.05$) taken out one by one. Significance levels

are indicated as follows: * ($p<0.05$), ** ($p<0.01$), *** ($p<0.005$) and **** ($p<0.001$).

Results

Barrier recovery in healthy volunteers

To determine the effect of the formulation on barrier recovery, changes in skin barrier over time (measured as TEWL and expressed as recovery %) were examined. Figure 2A shows a typical example of barrier recovery % as function of time for untreated and treated stripped sites of one volunteer. After 16 days, all volunteers had reached a recovery % >85 at both sites. For each volunteer the AUC was calculated of both the untreated and treated stripped sites (Figure 2B). A larger AUC implies less barrier dysfunction during the 16 days. Treatment with the formulation significant increased the AUC, indicating increased recovery.
Yet, the AUC does not take into account the kinetics of the recovery process. To determine if treatment accelerated barrier recovery, differences in time between untreated and treated stripped sites were examined at multiple designated recovery percentages (ΔT in Figure 2A). Figure 2C depicts the median and interquartile range of ΔT at different recovery percentages for all volunteers. A median of zero would indicate no change in recovery time due to treatment. A positive deviation from zero was observed at almost all recovery percentages with a spike at 25%, and a steady increase above 50%. Treatment significantly accelerated barrier recovery ending with a more than two days faster median recovery. As control both the AUC and the ΔT were tested for correlation to the TEWL directly after tape-stripping (Table S3). No correlations were observed, indicating that these parameters were not dependent on the amount of barrier disruption.

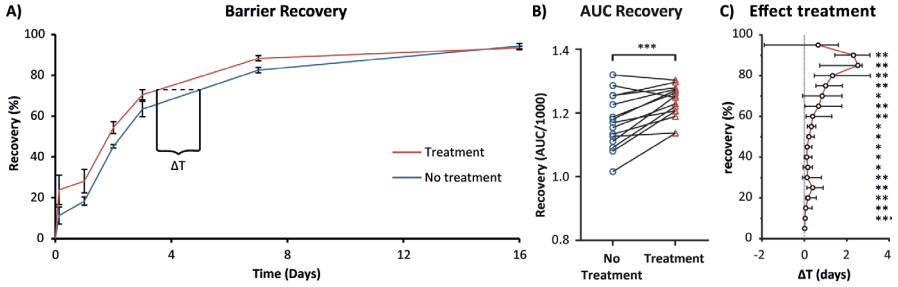

Figure 2. The effect of treatment on barrier recovery. A) The typical elapse of barrier recovery over time for untreated and treated stripped sites, for a single volunteer. Points are means (±SD) of three measurements within one site. Lines are point-to-point connections. The dotted line indicated the difference in time (ΔT) between the untreated and treated curve at a designated recovery %. **B)** The AUCs/1000 for all volunteers. Lines connect data points of the same volunteer. A paired t-test showed significant increase at the treated sites. **C)** The ΔT for all volunteers at recovery percentages between 5 and 90 %. The data were non-normally distributed and are shown as median and interquartile range. Deviations from zero were tested with a Wilcoxon signed-rank test.

Principle component analysis of ceramide profiles

To gain insight into differences between the ceramide profiles of the four different sites PCA was performed on the quantitative ceramide data. Figure 3A depicts the variable loadings, indicating how strongly each variable (ceramides detected in the samples) correlated to PC1 and PC2. If the value is higher (deviates from center of the graph in x or y position) it has contributed more to the variation explained by PC1 or PC2, respectively. The 10 variables with the highest correlation coefficients are indicated in the plot. PC1 and PC2 explained a total inertia (variance) of 66.3%. Figure 3B shows the plot of the "PCA samples", depicting the PC1 and PC2 scores of each "PCA sample". Samples were assigned to clusters corresponding to the 4 sites indicated by different colors. Separation between clusters was observed demonstrating that variation between the ceramide profiles corresponded to variation between samples of different sites. Therefore, changes in ceramide profile due to treatment and tape-stripping can be explained by the variable loadings of the PCs.

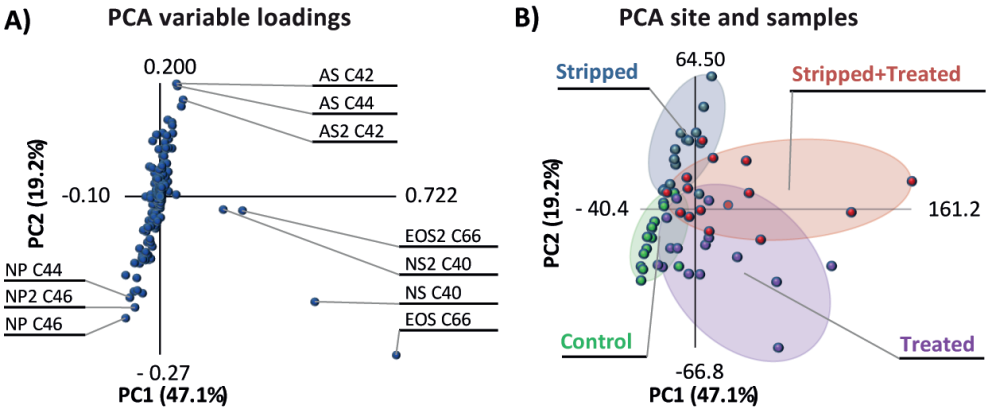

Figure 3. PCA of all SC ceramides and the amount of ceramides NS C40 and EOS C66. A) The PCA loading plot. Inertia per PC is indicted as % variation. Variables are all ceramides quantified in samples obtained from tape-strips 5-8 and samples obtained from tape-strips 17-20, the latter are indicated with a 2 after the subclass name. **B)** A plot of the PCA samples (the 4 sites of all volunteers). The samples were clustered per site.

Clusters of treated sites were separated from untreated sites as depicted in Figure 3B. By examining plot 3A it shows that this was due to 4 variables primarily. These variables corresponded to the two formulated ceramides (NS C40 and EOS C66), detected in samples of both depths. The PCA demonstrated that a large part of the variation in the ceramide profiles was due to the two ceramides in the formulation. The increase, due to formulation application, of these naturally occurring ceramides was examined. Figure S4 shows that the amount at treated sites was increased at both tape-stripping depths. An LMM of the logarithm of these amounts confirmed these observations (Table S4).
Next, separation of clusters corresponding to stripped and non-stripped sites was investigated. Variables correlating strongly to PC2 were primarily responsible for the observed separation. (Figure S5 shows a complete graphic overview of the PC2 loadings). When examining the loadings of PC2, highly positive correlations were

observed for ceramides of subclass AS and, to a lesser extent, ceramides for subclass NS. Highly negative correlations were observed for ceramides from subclass NP. Changes in ceramide profile were observed between the different sites. In the next section, the results of the PCA were used as leads to investigate if these changes correlated to changes in barrier function and the recovery process.

Correlations between ceramide profile and barrier function

To investigate if barrier function correlated to changes in SC ceramide profile, changes in ceramides AS and NS, identified by PCA, were correlated to the TEWL at T_{16} (Figure S6 shows the TEWL at T_{16}). Figure 4A and B depict these correlations for the total amount of subclass AS. At both depths, a significant positive correlation between the amount of subclass AS and TEWL was observed. This illustrates that an increase in subclass AS correlated with a reduced skin barrier function. Next, it was examined whether stripping, treatment, SC depth, or the interaction between these conditions had an effect on the amount of subclass AS using a LMM. The model used stripped, treated, and depth as fixed factors, and subject as random factor. Table 1 depicts the effect sizes obtained with the model. Figure 4C depicts the mean (±SD) of the amount of subclass AS measured at all 4 sites at both depths. Using the model it was determined that subclass AS increased significantly at stripped sites. Treatment or depth alone showed no significant effects compared to the control. However, at the stripped site treatment did have a significant effect. The interaction stripped*treated in Table 1 illustrates this effect. When subjected to stripping and treatment the amount of AS changed by the effect sizes of stripped and treatment, in addition to both effects the interaction term stripped*treated is added. At stripped+treated sites treatment significantly reduced the increase in AS observed due to stripping with 81.2 ng/SQ (treatment + stripped*treated). Similar results were obtained when examining NS C44 (Figure S7 and Table 1). It was decided not to use the total amount of subclass NS, as this value was influenced by ceramide NS C40 of the formulation. NS C44 is most abundantly present of the NS ceramide subclass members and chosen as a proper representative of subclass NS.
Besides subclasses, ceramide chain lengths, especially ceramides with a total carbon chain length of 34 carbons (C34), are known to correlate to barrier dysfunction.[17] Here, a significant positive correlation was observed between the total amount of C34 ceramides (summation of amounts of NdS, NS, NP, NH, AdS, AS, AP, and AH with a total of 34 carbons) and TEWL, at both depths (Figure 4D and E), demonstrating that higher levels of C34 ceramides correlate with reduced barrier function at day 16. A similar LMM as that of subclass AS and NS C44 was built for C34 ceramides (Table 1). The total amount of C34 ceramides at the 4 sites at two depths was plotted as the mean ±SD in Figure 4F. By using the model a significant increase at the stripped sites was observed. Comparable to subclass AS, treatment only significantly affected the stripped+treated sites. Treatment reduced the increase in C34 ceramides with 31.6 ng/SQ compared to stripped sites.
Next, the correlation of each subclass to TEWL was examined (Figure 4G: Pearson r for each subclass). This correlation underlined the observations with PCA, where subclass NS and AS had a positive correlation and subclass NP a negative correlation to PC2. Both subclasses NS and AS have a distinct synthesis route different from

subclasses NP and AP, this suggested a ratio dividing the subclasses as follows: (NdS+NP+NH+AdS+AP+AH)/(NS+AS). This ratio correlated to TEWL (Figure 4G) even for the samples of each site independently. Together, these data showed that I) barrier function correlated to the ratio of ceramide subclasses from different synthesis routes, II) certain ceramide subgroups are increased in stripped SC, III) the amount of these subgroups correlated to TEWL, and IV) treatment is able to reduce the increase of these ceramide subgroups that correlate positively to an increased TEWL (AS, NS C44 and C34 ceramides).

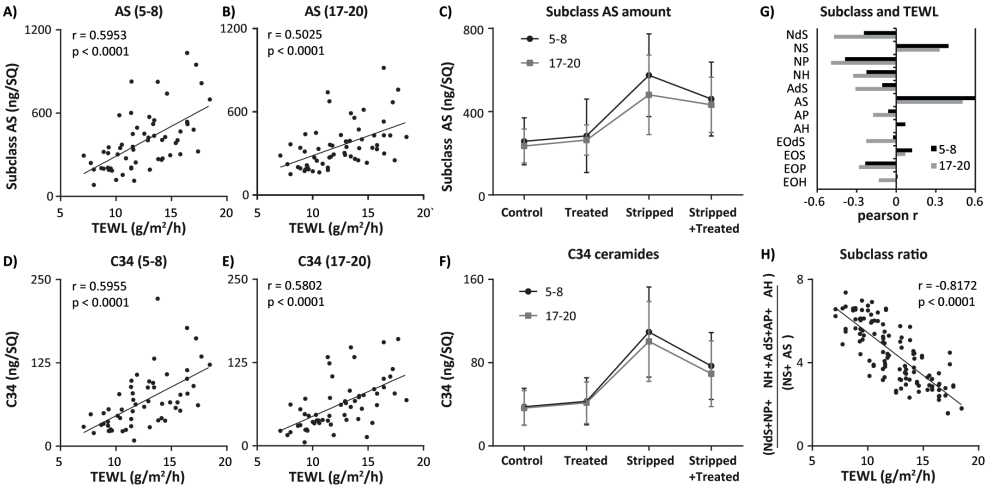

Figure 4. The effect of treatment on ceramide groups correlating to barrier function. A,B) Correlations between TEWL and the amount of subclass AS (ng/SQ). The Pearson r and p-value are indicated (A: Samples of tape-strips 5-8 B: Samples of tape-strips 17-20). **C)** The amount subclass AS (ng/SQ) at all sites at depths of both 5-8 and 17-20 tape-strips (mean ±SD). Effect size was determined with a linear mixed model. **D,E)** Correlations between TEWL and the amount of ceramides with a chain length of 34 carbon atoms (ng/SQ). The Pearson r and p-value are indicated (D: Samples of tape-strips 5-8 E: Samples of tape-strips 17-20). **F)** The amount of ceramides with a chain length of 34 carbon atoms (ng/SQ) at all sites at depths of both 5-8 and 17-20 tape-strips (mean ±SD). Effect size was determined with a linear mixed model. **G)** Pearson r of the correlation between TEWL and the total amount of each subclass at all sites at depths of both 5-8 and 17-20 tape-strips. **H)** The correlation between TEWL and ratio of subclasses (NdS+NP+NH+AdS+AP+AH)/(NS+AS) of both depths, excluding NS C40. Pearson r per site were: control: -0.648 Stripped: -0.808 Treated: -0.729 Stripped+Treated: -0.694. All statistical outputs of the LMM are found in Table 1.

Table 1. The output of the LMMs per ceramide subgroup. The intercept is the estimated amount at the control site at a depth of 5-8 tape-strips. Estimates are in ng/SQ. The effect size is the amount in ng/SQ with which the variable changes the intercept. Significance levels of all effect sizes and interaction are given.

		Subclass AS		Subclass NS C44		C34 ceramides	
		Estimate	p-value	Estimate	p-value	Estimate	p-value
	Intercept (control)	267.1	<0.001	56.6	<0.001	39.4	<0.001
Effect size	Stripped	+281,5	<0.001	+56.4	<0.001	+68.0	<0.001
	Treated	+27.3	0.402	+7.2	0.194	+5.6	0.438
	Depth 17-20	-41.3	0.076	-2.1	0.597	-5.2	0.297
Interactions	Stripped*Treated	-108.5	0.020	-19.5	0.013	-37.2	<0.001

Mean carbon chain length and spacing related to the lamellar phases

Previous studies have shown that the main ceramide chain length is an important parameter of the SC ceramide fraction.[43] For this reason it was decided to study whether a correlation existed between mean chain length and both the EO ceramide fraction and lamellar spacing. Figure 5A shows the mean chain length of the ceramides in samples prepared from tapes 5-8 and 17-20. A similar LMM as for subclass AS was made (Table 2). This showed that stripping decreased the mean chain length significantly. Treatment was able to increase the mean chain length restoring the mean chain length at the stripped+treated sites. The increase in mean chain length of the stripped+treated sites could be due to an increase in the fraction of esterified omega-acyl-ceramide (EO fraction) (Figure S8 shows this correlation per site). Changes in EO fraction due to treatment of the stripped site (stripped - stripped+treated) correlated to changes in the mean chain length due to treatment of the stripped site (Figure 5B). Treatment was able to increase the EO fraction significantly (Figure 5C and Table 2 show the EO fraction and the output of LMM, respectively).
The carbon chain length of the ceramides could influence the spacing of the strong diffraction peak in the diffraction pattern as measured by SAXD. From the position of the strong diffraction peak in the X-ray diffraction curve (peak 2), the corresponding spacing was calculated (referred to as peak 2 in Figure 5D). A significant increase in spacing due to treatment was observed and a positive correlation was observed between the mean chain length and the spacing, (Figure 5E). When comparing the spacing to TEWL, a correlation was observed between an increased TEWL and a decrease in spacing (Figure 5F). Stripping and treatment thus affected the mean chain length, which correlated to EO fraction and the lamellar spacing.

Effects of stripping and treatment on lateral packing

Next to the lamellar spacing, the lateral packing is important for a proper barrier function. For this reason the effect of treatment and stripping on the lateral packing was also examined. All skin sites were studied using ATR-FTIR, where both the CH_2 symmetric stretching vibrations and the CH_2 scissoring vibrations were examined. A LMM was built for the CH_2 symmetric stretching peaks. Stripped, treated, and depth were used as fixed factors and subject as random factor (Table 2). A significant increase in peak position was observed due to barrier disruption and treatment suggesting a slight increase in disordering of the lipids. The effects were stronger deeper in the SC. However, the peak position at all sites is located at wavenumbers between 2848.46 cm^{-1} and 2848.80 cm^{-1}, indicating an ordered lateral lipid organization at all sites. A similar linear mixed model was built for the CH_2 scissoring peak. We determined the FWHM of the scissoring vibrations. Table S5 depicts the result of this model. At the control site the FWHM was significantly decreased at deeper layers (tape-strips 12-20), yet, the FWHM was 11.3 cm^{-1} or higher, indicative for a large fraction of lipids forming an orthorhombic lateral packing. No deviation from an ordered structure by treatment or stripping was observed.

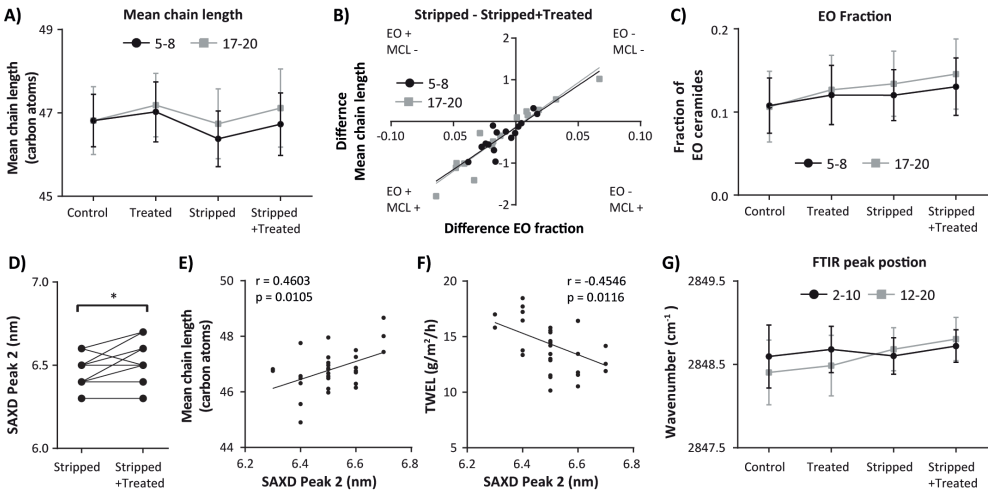

Figure 5. Mean chain length and lamellar spacing. A) The mean total chain length (carbon atoms) for the 4 different sites at two depths excluding the ceramides of the formulation in the calculation. Data were compared using a LMM. **B)** The correlation between changes in fraction EO ceramides and changes in the mean chain lengths (carbon atoms) at the stripped site due to treatment (amount at the stripped site subtracting the stripped+treated). **C)** The EO fraction of the samples at the 4 different sites at two depths. Data were compared using a LMM. **D)** The difference between the SAXD peak 2 position in the stripped and stripped+treated sites. The differences were tested with a Wilcoxon matched pairs signed rank test. **E)** The correlation between the SAXD peak 2 (nm) and TEWL (g/m^2/h) at the end of the study. Pearson r and p-value are provided. **F)** The correlation between the SAXD peak 2 (nm) and the mean chain length (carbon atoms) of all ceramides. Pearson r and p-value are provided. **G)** The wavenumber in cm^{-1} of the stretching peak position. Data were compared using a LMM.

Table 2. The output of the LLMs for mean chain length, EO fraction, and stretching peak position. The mean chain length and EO fraction were calculated excluding ceramides NS C44 and EOS C66. The the wavenumber in cm^{-1} of the stretching peak position was calculated using the center of gravity at 90% peak height. As fixed factors stripped, treated and depth were used. The intercept was the control site at a depth of 5-8 tape-strips or for spectra of tapes 2-10.

		Mean chain length		EO fraction		Wavenumber cm^{-1}	
		Estimate	p-value	Estimate	p-value	Estimate	p-value
	Intercept (control)	46.76	<0.001	0.107	<0.001	2848.60	<0.001
Effect size	Stripped	-0.37	<0.001	+0.011	0.007	+0.02	0.622
	Treated	+0.33	<0.001	+0.014	<0.001	+0.09	0.013
	Depth	+0.08	0.366	0.003	0.537	-0.17	<0.001
Interactions	Stripped*Depth	+0.29	0.021	+0.012	0.043	+0.26	<0.001

Discussion

In this study we showed that a VC based formulation is able to accelerate the barrier recovery of tape-strip disrupted healthy human skin and, for the first time, demonstrate that formulations can act by normalizing the SC lipid composition. Multiple effects of barrier disruption and treatment on barrier recovery, ceramide composition, and lipid organization were examined (Figure 6 provides an overview). Using PCA, samples were clustered into groups of treatment and stripped, based on changes in ceramide profile. Moreover, correlations of ceramide levels to PC2 had great similarities to correlations between ceramide levels and barrier function after barrier recovery. Thus, the loading variables for PC2 were a powerful tool to identify ceramides responsible for profile changes related to barrier disruption. At the stripped sites after recovery, multiple changes in the ceramide profiles were observed. Treatment partially normalized these changes in SC ceramide composition caused by barrier disruption. These ceramide profile changes correlated to the barrier function, indicating a relation of the changes in these lipids and an accelerated barrier recovery process.

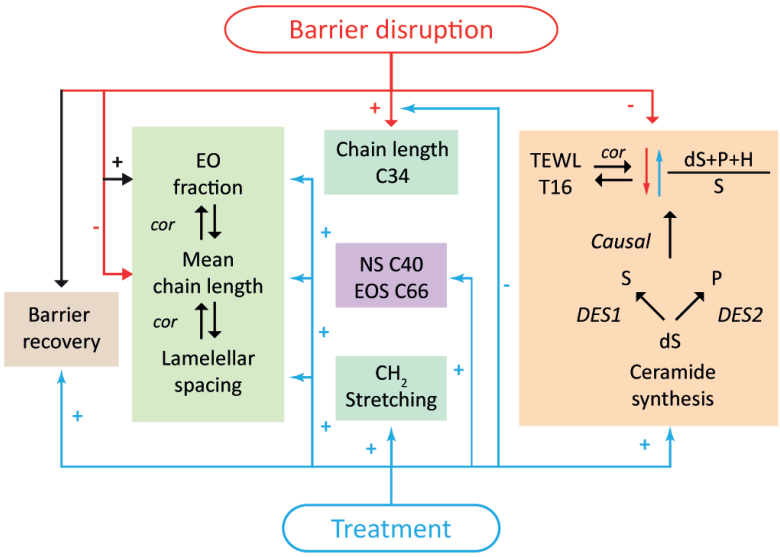

Figure 6. An overview of the effects of barrier disruption and treatment. Negative effects are indicated with an – sign and positive effects with a + sign. Barrier disruption induces barrier recovery and treatment accelerates this process. Changes in the EO fraction, mean chain length, and lamellar spacing showed correlations (*cor*) indicated by the arrows. The changes in lipid composition, organization and subsequent effects are indicated. The ratio (dS+P+H)/S, is mainly determined by the enzymes human-dihydro-Δ4-desaturate (DES1) and human-sphingolipid-C4-hydroxylase (DES2), responsible for the production of sphingosine and phytosphingosine ceramides from dihydrosphingosine ceramides, respectively. The arrows indicate that barrier disruption changed the lipid synthesis decreasing this ratio and treatment had the opposite effect. The correlation of the TEWL at day 16 (T16) to the subclass ratio is indicated, yet, the amount of C34 and the SAXD Peak 2 position correlated to TEWL as well.

When examining barrier recovery, two phases could be distinguished; a first steep increase in barrier recovery % after three hours, followed by second gradually diminishing barrier recovery rate. Treatment increased the level of the first phase, where after three hours a recovery of ~25% was reached compared to ~10% without treatment. However, early effects of formulation on barrier recovery measured by TEWL can be caused by leftover formulation on the skin[27], even though leftover formulation was removed prior to TEWL measurement. The second recovery phase was not affected by residual formulation on the skin surface, because the formulation was applied after TEWL measurement. During the second phase, treatment had a pronounced effect on the barrier recovery rate.

One of the aims of the tested formulation was to replenish SC ceramides. Treatment caused significant increase in the formulated ceramides level; even at deeper SC layers. Although, a 2-day washout period would have removed almost all superficial formulation, it cannot be stated with 100% certainty that the applied ceramides measured with LC/MS were incorporated into the SC. Some formulated ceramides could still be present in folds of the SC. In cultured skin, it was shown that ceramides stay in these folds.[23] Even though the increase of the formulated ceramides was observed at both depths, tape-strips obtained lipid material from various depth of SC[44], and thus, tape-strips at both depths can contain material from these folds. Nevertheless, it has been demonstrated that when treating stripped *ex vivo* SC with deuterated ceramides once, small ceramide amounts were incorporated into the SC lipid matrix after regeneration.[45] Others have shown that dimeric ceramides are able to diffuse into the skin.[46] Together with the relatively large increases of the formulated ceramides, it is likely that a fraction of the applied ceramides did incorporate into the SC lipid matrix and actively enhance barrier recovery.

Multiple studies have used SC lipid containing formulations, either for long or short term treatment[18-21] and it was shown that the SC lipids ratio in formulations is essential for short term barrier recovery.[22,47] Visscher et al. tested the effect of 5 days VC treatment on TEWL and hydration of tape-stripped SC, but they observed no changes in TEWL when comparing with untreated stripped SC.[28] In comparison to our study, the barrier was less extensively disrupted. Therefore, incomplete SC removal may lead to a lower efficacy of the formulation to improve barrier repair. Here, a detailed description of the recovery process is provided and, for the first time, insights are given into changes in the SC ceramide composition due to treatment. Below, a mechanism is suggested on how a VC based formulation affects ceramide synthesis.

At the stripped (non-treated) sites, two prominent changes were observed in the endogenous ceramides: I) the amounts of S subclass were increased, and II) C34 ceramides were increased. The amounts of these ceramide groups correlated to a decrease in barrier function. However, from these data it could not yet be deduced if these increases were causal or contingent with a decreased barrier function. A plausible reasoning is that in a direct response to barrier disruption, the epidermal calcium gradient changed[2] and a subsequent modulation in gene expression occurred.[29] These changes in epidermal homeostasis might have affected the SC ceramide processing in two ways.

First, in the epidermal lipid biosynthesis, ceramides containing a dihydrosphingosine are either converted into sphingosine or phytosphingosine containing ceramide[48,49]

(Figure 6) (biosynthesis of subclass H ceramides has not yet been reported). When defining the ratio between the subclasses as: (dS+P+H)/S, this ratio could only change if either of the two known lipid biosynthesis pathways changed. The present study showed that this ratio was substantially decreased at the stripped sites, indicating barrier disruption influenced the specific synthesis pathways of subclasses S and P. Importantly, the ratio between the subclasses correlated strongly to TEWL after barrier recovery, which suggests that an optimal ratio is important for an optimal skin barrier repair. Furthermore, this correlation was site independent, thus, at stripped sites with a higher TEWL, synthesis of sphingosine ceramides was preferred over phytosphingosine containing ceramides. Treatment was able to favorably change the subclass ratio towards a lipid composition that correlated to a more efficient skin barrier recovery, by reducing the amount of NS and AS subclasses.

The second change in lipid biosynthesis due to barrier disruption was the increased amount of C34 ceramide. These ceramides are produced from the sphingoid and acyl building blocks (a C16 or C18 acyl chain and a C16 or C18 sphingoid chain[50]) and do not require additional elongation steps.[51] Although these C34 ceramides can be produced as a quick first response to mitigate an impaired SC barrier, C34 ceramides are "short" chain ceramides which have been shown to reduce skin barrier function.[6,52] Altogether, the C34 ceramides and the ratio of ceramide subclasses could function as indicators of reduced barrier function and changes in barrier lipid homeostasis. Here, we showed that treatment was able to partly diminish the amount of C34 ceramides and, by diminishing the amount of NS and AS, able to change the subclass ratio and thus the preceding ceramide synthesis. This reduction could be attributed to I) the semi-occlusive effect of the formulation, in which the formulation acted as an additional barrier, II) the presence of excess formulated ceramides reducing the response to replenish the ceramides. As a whole, these data show that the formulation partially normalized the lipid biosynthesis and directed the SC towards a more functional lipid homeostasis. The lipid organization was used to verify if changes in ceramides composition were causal to changes in barrier function.

An important characteristic of the SC ceramide fraction is the mean chain length. The chain length was reduced when the barrier function is impaired e.g.: in stripped sites and AD.[8,17] Here, treatment was able to restore the mean chain length at stripped sites (excluding the added ceramides). The mean chain length correlated strongly to the fraction of EO ceramides and treatment was able to increase the EO fraction. At the treated sites, the spacing was slightly increased indicating an increase in the repeat distances of the lamellar phases. Furthermore, the spacing correlated to the mean chain length and weakly correlated to the EO fraction (data not shown). Taken together, the data suggest that treatment influenced the lamellar lipid organization through increasing the EO fraction thereby increasing the mean change length (Figure 6).

As far as the lateral packing was concerned, our studies showed that a high fraction of lipids formed an orthorhombic packing and this was not affected by stripping. For this reason the fraction of lipids forming an orthorhombic packing could not be increased due to treatment. Changes due to treatment might become more apparent in affected skin of AD patients where the fraction of lipids forming an orthorhombic organization is decreased compared to that in healthy skin.[43]

To summarize the effects of the VC based formulation on barrier recovery in healthy SC, it was observed that treatment: I) accelerated barrier recovery, II) changed the lipid synthesis to a more favorable lipid composition by decreasing the amount of C34 ceramides and changing the subclass ratio (dS+P+H)/S, and increasing the fraction of EO ceramides, III) these changes in lipid composition affected the SC lipid organization and correlated to the SC barrier function. Interestingly, similar increases in S subclass, and increases in the fraction of C34 chain length ceramides were observed in AD.[8,17] An essential application of this formulation could be in a particular group of AD patients, where barrier restoring lipophilic formulations are commonly used.[53] Moreover, the treatment presented here modulated the alterations in lipid composition observed in AD, towards a healthy lipid homeostasis.

Acknowledgments

This research is supported by the Dutch Technology Foundation STW (project number 12400), which is part of the Netherlands Organization for Scientific Research (NWO), and which is partly funded by the Ministry of Economic Affairs. We would like to thank: Evonik industries AG for supplying us with the ceramides, Croda International Plc and Galderma SA for the other ingredients used in the formulation, and special thanks to Galderma SA for producing the formulation.

References

1. Eckhart L, Lippens S, Tschachler E, et al. Cell death by cornification. *Biochimica et biophysica acta* **2013**: 1833: 3471-3480.
2. Feingold KR, Elias PM. Role of lipids in the formation and maintenance of the cutaneous permeability barrier. *Biochimica et biophysica acta* **2014**: 1841: 280-294.
3. van Smeden J, Janssens M, Kaye EC, et al. The importance of free fatty acid chain length for the skin barrier function in atopic eczema patients. *Exp Dermatol* **2014**: 23: 45-52.
4. Sahle FF, Gebre-Mariam T, Dobner B, et al. Skin diseases associated with the depletion of stratum corneum lipids and stratum corneum lipid substitution therapy. *Skin Pharmacol Physiol* **2015**: 28: 42-55.
5. t'Kindt R, Jorge L, Dumont E, et al. Profiling and characterizing skin ceramides using reversed-phase liquid chromatography-quadrupole time-of-flight mass spectrometry. *Analytical chemistry* **2012**: 84: 403-411.
6. Mojumdar EH, Kariman Z, van Kerckhove L, et al. The role of ceramide chain length distribution on the barrier properties of the skin lipid membranes. *Biochim Biophys Acta* **2014**: 1838: 2473-2483.
7. Stahlberg S, Lange S, Dobner B, et al. Probing the Role of Ceramide Headgroup Polarity in Short-Chain Model Skin Barrier Lipid Mixtures by (2)H Solid-State NMR Spectroscopy. *Langmuir* **2016**: 32: 2023-2031.
8. Janssens M, van Smeden J, Gooris GS, et al. Increase in short-chain ceramides correlates with an altered lipid organization and decreased barrier function in atopic eczema patients. *Journal of lipid research* **2012**: 53: 2755-2766.
9. Matsui T, Amagai M. Dissecting the formation, structure and barrier function of the stratum corneum. *Int Immunol* **2015**: 27: 269-280.
10. Rawlings AV. Molecular basis for stratum corneum maturation and moisturization. *Br J Dermatol* **2014**: 171 Suppl 3: 19-28.
11. Tanaka M, Zhen YX, Tagami H. Normal recovery of the stratum corneum barrier function following damage induced by tape stripping in patients with atopic dermatitis. *Br J Dermatol* **1997**: 136: 966-967.
12. Wolf R, Parish LC. Barrier-repair prescription moisturizers: do we really need them? Facts and controversies. *Clin Dermatol* **2013**: 31: 787-791.
13. Hon KL, Leung AK, Barankin B. Barrier repair therapy in atopic dermatitis: an overview. *Am J Clin Dermatol* **2013**: 14: 389-399.
14. Corazza M, Minghetti S, Bianchi A, et al. Barrier creams: facts and controversies. *Dermatitis* **2014**: 25: 327-333.
15. van Zuuren EJ, Fedorowicz Z, Christensen R, et al. Emollients and moisturisers for eczema. *Cochrane Database Syst Rev* **2017**: 2: CD012119.
16. Ito S, Ishikawa J, Naoe A, et al. Ceramide synthase 4 is highly expressed in involved skin of patients with atopic dermatitis. *J Eur Acad Dermatol Venereol* **2016**.
17. Ishikawa J, Narita H, Kondo N, et al. Changes in the ceramide profile of atopic dermatitis patients. *The Journal of investigative dermatology* **2010**: 130: 2511-2514.
18. Meckfessel MH, Brandt S. The structure, function, and importance of ceramides in skin and their use as therapeutic agents in skin-care products. *J Am Acad Dermatol* **2014**: 71: 177-184.
19. Lynde CW, Andriessen A. A cohort study on a ceramide-containing cleanser and moisturizer used for atopic dermatitis. *Cutis* **2014**: 93: 207-213.
20. Oh MJ, Nam JJ, Lee EO, et al. A synthetic C16 omega-hydroxyphytoceramide improves skin barrier functions from diversely perturbed epidermal conditions. *Arch Dermatol Res* **2016**: 308: 563-574.
21. Barba C, Parra JL, Coderch L, et al. In vivo and in vitro evaluation of topical formulations containing physiological lipid mixture for replacement of skin barrier function. *G Ital Dermatol Venereol* **2014**: 149: 347-353.
22. Man MM, Feingold KR, Thornfeldt CR, et al. Optimization of physiological lipid mixtures for barrier repair. *The Journal of investigative dermatology* **1996**: 106: 1096-1101.
23. Zhang Q, Flach CR, Mendelsohn R, et al. Topically applied ceramide accumulates in skin glyphs. *Clin Cosmet Investig Dermatol* **2015**: 8: 329-337.
24. Rhodes LE, O'Farrell S, Jackson MJ, et al. Dietary fish-oil supplementation in humans reduces UVB-erythemal sensitivity but increases epidermal lipid peroxidation. *The Journal of investigative dermatology* **1994**: 103: 151-154.
25. Rissmann R, Oudshoorn MH, Zwier R, et al. Mimicking vernix caseosa--preparation and characterization of synthetic biofilms. *Int J Pharm* **2009**: 372: 59-65.
26. Oudshoorn MH, Rissmann R, van der Coelen D, et al. Effect of synthetic vernix biofilms on barrier recovery of damaged mouse skin. *Exp Dermatol* **2009**: 18: 695-703.
27. Oudshoorn MH, Rissmann R, van der Coelen D, et al. Development of a murine model to evaluate the effect of vernix caseosa on skin barrier recovery. *Exp Dermatol* **2009**: 18: 178-184.
28. Visscher MO, Barai N, LaRuffa AA, et al.

Epidermal barrier treatments based on vernix caseosa. *Skin Pharmacol Physiol* **2011**: 24: 322-329.
29. Sextius P, Marionnet C, Bon FX, et al. Large scale study of epidermal recovery after stratum corneum removal: dynamics of genomic response. *Experimental dermatology* **2010**: 19: 259-268.
30. Bandier J, Carlsen BC, Rasmussen MA, et al. Skin reaction and regeneration after single sodium lauryl sulfate exposure stratified by filaggrin genotype and atopic dermatitis phenotype. *Br J Dermatol* **2015**: 172: 1519-1529.
31. O'Connor RJ, Ogle J, Odio M. Induction of epidermal damage by tape stripping to evaluate skin mildness of cleansing regimens for the premature epidermal barrier. *Int J Dermatol* **2016**: 55 Suppl 1: 21-27.
32. Breternitz M, Flach M, Prassler J, et al. Acute barrier disruption by adhesive tapes is influenced by pressure, time and anatomical location: integrity and cohesion assessed by sequential tape stripping. A randomized, controlled study. *Br J Dermatol* **2007**: 156: 231-240.
33. Pinkus H. Examination of the epidermis by the strip method of removing horny layers. I. Observations on thickness of the horny layer, and on mitotic activity after stripping. *The Journal of investigative dermatology* **1951**: 16: 383-386.
34. Boiten W, Absalah S, Vreeken R, et al. Quantitative analysis of ceramides using a novel lipidomics approach with three dimensional response modelling. *Biochimica et biophysica acta* **2016**: 1861: 1652-1661.
35. Masukawa Y, Narita H, Sato H, et al. Comprehensive quantification of ceramide species in human stratum corneum. *Journal of lipid research* **2009**: 50: 1708-1719.
36. van Smeden J, Boiten WA, Hankemeier T, et al. Combined LC/MS-platform for analysis of all major stratum corneum lipids, and the profiling of skin substitutes. *Biochimica et biophysica acta* **2014**: 1841: 70-79.
37. Motta S, Monti M, Sesana S, et al. Ceramide composition of the psoriatic scale. *Biochimica et biophysica acta* **1993**: 1182: 147-151.
38. Boncheva M, Damien F, Normand V. Molecular organization of the lipid matrix in intact Stratum corneum using ATR-FTIR spectroscopy. *Biochimica et biophysica acta* **2008**: 1778: 1344-1355.
39. Damien F, Boncheva M. The extent of orthorhombic lipid phases in the stratum corneum determines the barrier efficiency of human skin in vivo. *The Journal of investigative dermatology* **2010**: 130: 611-614.
40. Checa A, Bedia C, Jaumot J. Lipidomic data analysis: tutorial, practical guidelines and applications. *Anal Chim Acta* **2015**: 885: 1-16.
41. Vaz FM, Pras-Raves M, Bootsma AH, et al. Principles and practice of lipidomics. *J Inherit Metab Dis* **2015**: 38: 41-52.
42. De Livera AM, Zaloumis S, Simpson JA. Models for the analysis of repeated continuous outcome measures in clinical trials. *Respirology* **2014**: 19: 155-161.
43. van Smeden J, Janssens M, Kaye EC, et al. The importance of free fatty acid chain length for the skin barrier function in atopic eczema patients. *Exp Dermatol* **2014**: 23: 45-52.
44. van der Molen RG, Spies F, van 't Noordende JM, et al. Tape stripping of human stratum corneum yields cell layers that originate from various depths because of furrows in the skin. *Arch Dermatol Res* **1997**: 289: 514-518.
45. Berkers T, Visscher D, Gooris GS, et al. Topically Applied Ceramides Interact with the Stratum Corneum Lipid Matrix in Compromised Ex Vivo Skin. *Pharmaceutical research* **2018**: 35: 48.
46. Neubert RH, Sonnenberger S, Dobner B, et al. Controlled Penetration of a Novel Dimeric Ceramide into and across the Stratum Corneum Using Microemulsions and Various Types of Semisolid Formulations. *Skin Pharmacol Physiol* **2016**: 29: 130-134.
47. Yang L, Mao-Qiang M, Taljebini M, et al. Topical stratum corneum lipids accelerate barrier repair after tape stripping, solvent treatment and some but not all types of detergent treatment. *Br J Dermatol* **1995**: 133: 679-685.
48. Gault CR, Obeid LM, Hannun YA. An overview of sphingolipid metabolism: from synthesis to breakdown. *Advances in experimental medicine and biology* **2010**: 688: 1-23.
49. Uchida Y, Hara M, Nishio H, et al. Epidermal sphingomyelins are precursors for selected stratum corneum ceramides. *Journal of lipid research* **2000**: 41: 2071-2082.
50. Masukawa Y, Narita H, Shimizu E, et al. Characterization of overall ceramide species in human stratum corneum. *Journal of lipid research* **2008**: 49: 1466-1476.
51. Kihara A. Synthesis and degradation pathways, functions, and pathology of ceramides and epidermal acylceramides. *Prog Lipid Res* **2016**: 63: 50-69.
52. Paloncyova M, Vavrova K, Sovova Z, et al. Structural Changes in Ceramide Bilayers Rationalize Increased Permeation through Stratum Corneum Models with Shorter Acyl Tails. *J Phys Chem B* **2015**: 119: 9811-9819.
53. Giam YC, Hebert AA, Dizon MV, et al. A review on the role of moisturizers for atopic dermatitis. *Asia Pac Allergy* **2016**: 6: 120-128.

Supplementary data

Figure S1. Indication of TEWL measurement sites. The TEWL measurements at the sites were performed at three sections of the sites. Here the stripped site is shown which can be identified by the erythroderma. TEWL measurements were performed at the sections indicated with black circles. At every time-point TEWL was measured at the right, middle, and left section.

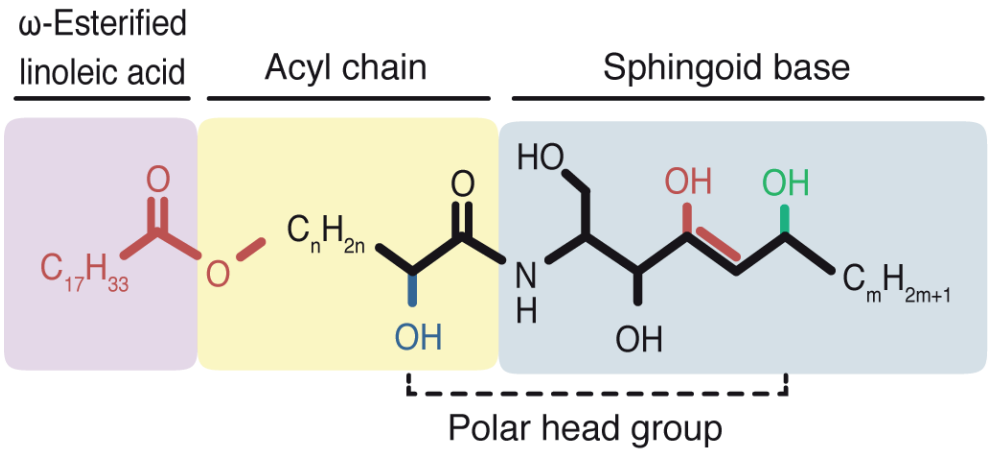

Figure S2. General structure of a ceramide. A ceramide can be composed of three parts which determine the subclass of the ceramide. The polar head group consists of a sphingoid base and an acyl chain. There are 4 different sphingoid bases in human SC: the sphingoid (S), a dihydro-sphingoid (dS), a 4-hydroxy or phyto-sphingoid (P), and a 6-hydroxy-sphinogoid (H). The acyl chain of human SC occurs in 3 different forms. A non-hydroxyl acyl chain (N), an α-hydroxy-acyl, and a ω-hydroxy-acyl chain (O). In SC a specific type of ceramide occurs where the ω-hydroxyl group becomes esterified with a linoleic acid called the EO subclass of ceramides. Together these form 16 different subclasses. Both the acyl and sphingoid chain can vary in carbon chain length.

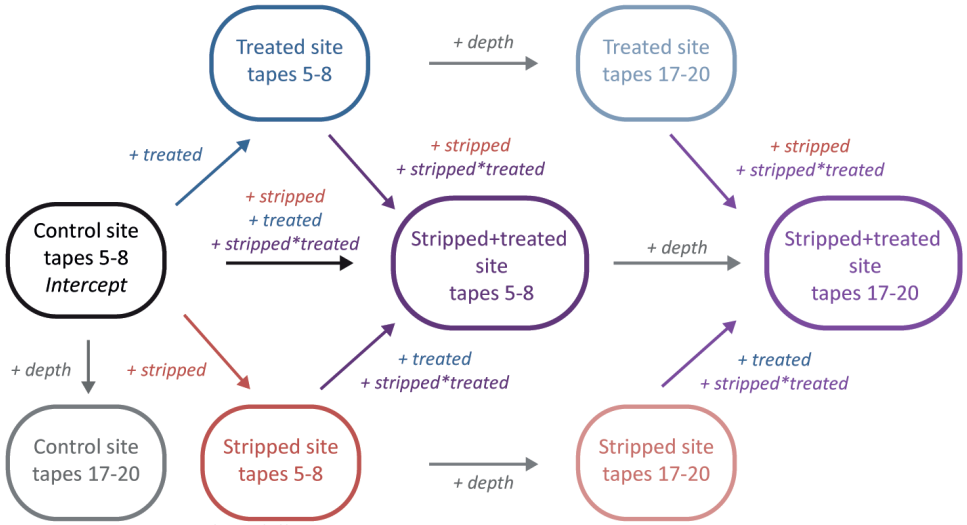

Figure S3. Linear mixed modelling. The LLMs used here compare the effects of treatment, stripping, and depth to the control site of the subject. Using subject as a random factor, gives each subjects control site (starting point) a different value, so it can start at any random point. It then determines the effect size of the fixed factors (treatment, stripping, and depth). 'Fixed' means that the model will say that all these effects have the same size for each subject and for each time this effect occurs, so also the effect at treatment at the stripped site (difference between stripped and stripped+treated). Because a stripped site can respond differently to treatment, an interaction term is added to the model, in this case stripped*treated. In this model the interaction is the effect size of treatment additional to the effects of stripping and treatment (the fixed factors). For most data we were interested in the effect of treatment on the stripped sites. This is the sum of the effect sizes of treatment and stripped*treated (illustrated above as the arrow from stripped site to Stripped+treated site). In the schematic above it is shown which steps are required to calculate the predicted values of the mixed model. The effect sizes are indicated in italics. Here, we were not interested in the mean predicted by the model but in the effect sizes of the different factors, as these calculate how the experimental conditions changed and if these were significant.

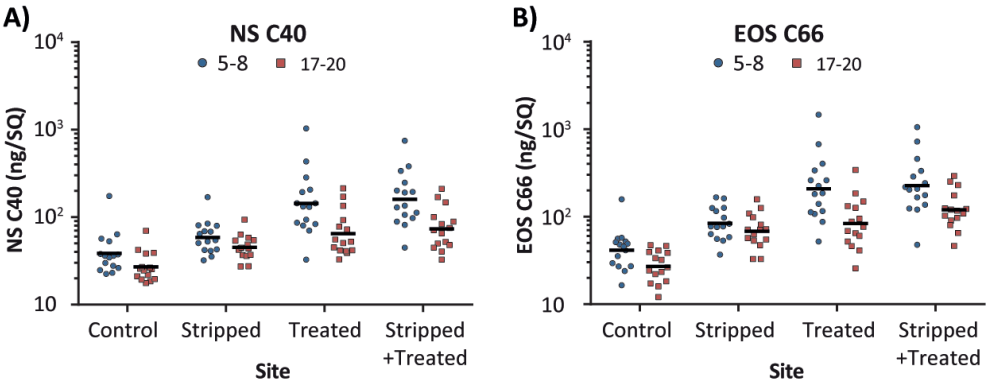

Figure S4. LLM of the formulation ceramides. A,B) Plots of the amounts of NS C40 and EOS C66 (log (ng/SQ)) in all quantified samples. Lines are geometric means. Statistical outputs of the LMMs are reported in supplementary Table S4.

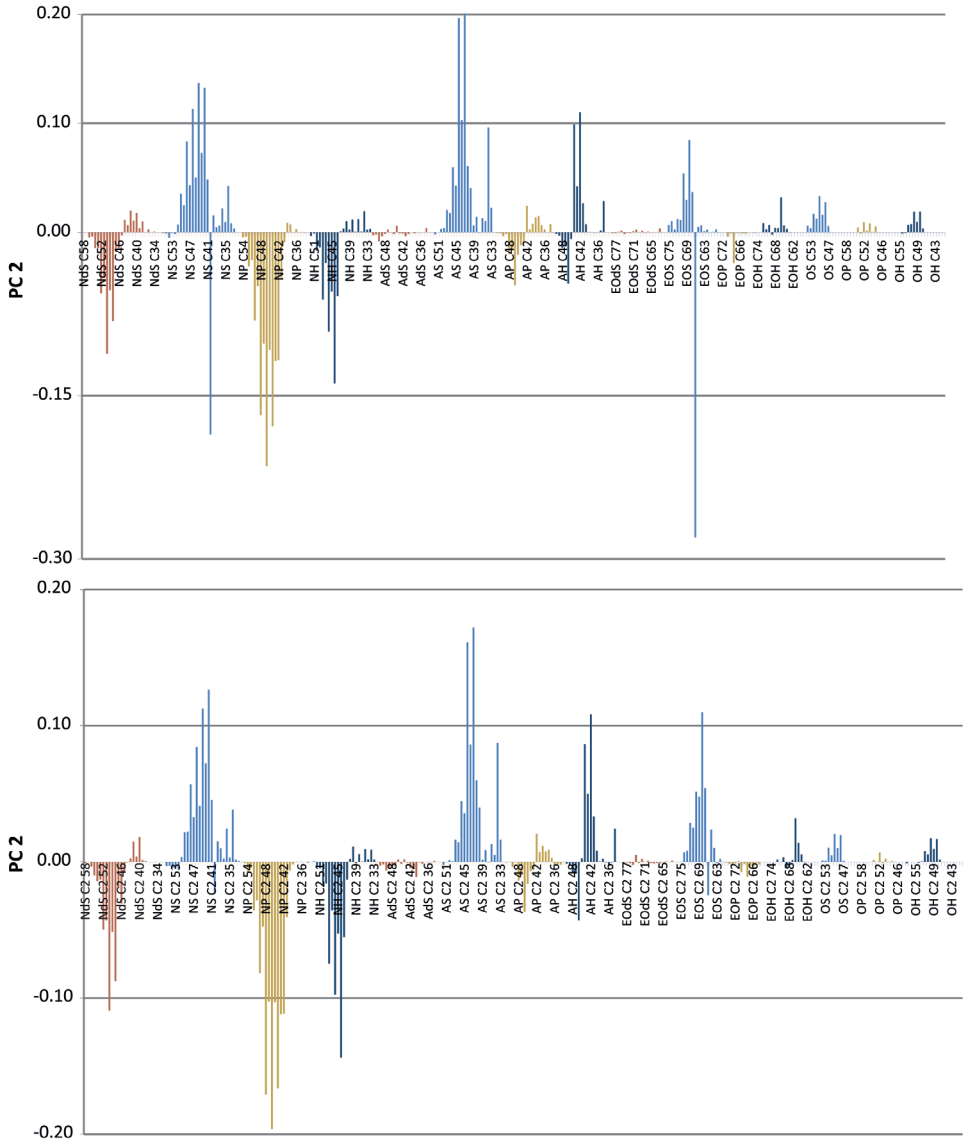

Figure S5. PC2 plot. The two graphs depict the scores/correlation of all ceramides to PC2. The first graph shows all ceramides detected in samples 5-8 and the second graph all ceramides detected in samples 17-20. Subclasses were given different colors. High positive scores indicate a correlation to the stripped sites and a high negative score to the control sites.

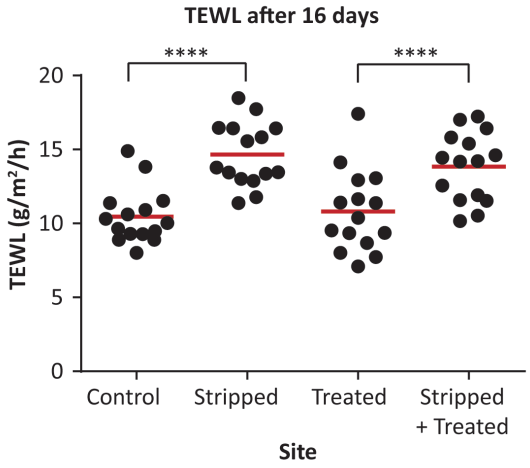

Figure S6. TEWL at day 16. The TEWL (g/m²/h) of all 4 sites after 16 days of treatment and/or barrier recovery. The red line is the mean value and the significance levels that are indicated were tested with a 1-way ANOVA with Bonferroni post-test.

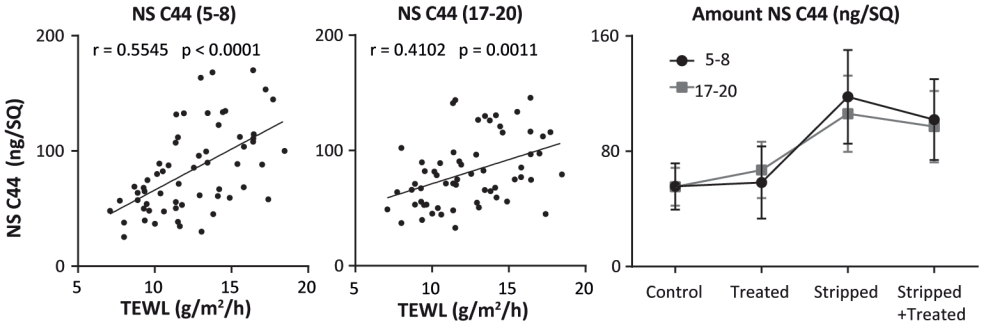

Figure S7. The amount of NS C44 and the correlation to the TEWL. Pearson r and the corresponding p-value are indicated above the data. The amount in ng/SQ of NS C44 at the 4 site and at both depths (5-8 and 17-20 tape-strips).

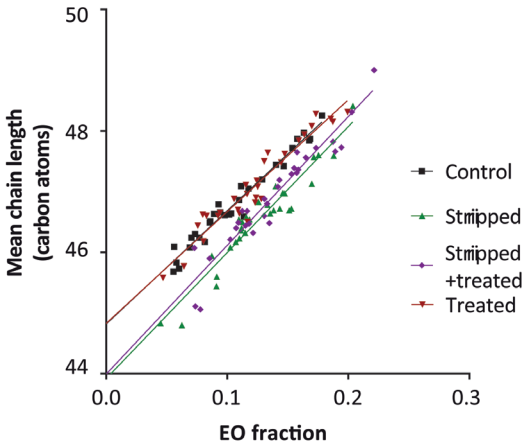

Figure S8. Correlation between mean chain length and EO fraction. The correlations between the mean chain length and the fraction of EO ceramides are depicted per site. Each site showed significant Pearson correlations coefficients: control (0.9817), stripped (0.9565), treated (0.9600), and stripped+treated (0.9568).

Table S1. List of the ceramides standards used with the corresponding supplier.

Ceramide	Supplier	Ceramide	Supplier
N(24)dS(18)	Avanti*	A(24)S(18)	Avanti*
N(18)dS(18)	Avanti*	A(R)(22)S(18)	Avanti*
N(16)dS(18)	Avanti*	A(S)(22)S(18)	Avanti*
N(24)S(18)	Evonik**	A(R)(16)S(18)	Avanti*
N(22)S(18)	Avanti*	A(S)(16)S(18)	Avanti*
N(20)S(18)	Avanti*	A(R)(24)P(18)	Avanti*
N(18)S(18)	Avanti*	E(18:2)O(30)S(18)	Evonik**
N(16)S(18)	Avanti*	E(18:2)O(27)S(18)	Evonik**
N(24)P(18)	Evonik**	E(18:2)O(30)P(S18)	Evonik**
N(22)P(18)	Evonik**	E(18:2)O(27)P(18)	Evonik**
N(16)P(18)	Evonik**	N(24deu)S(18)	Evonik**

* Avanti polar lipids (Alabaster AL, USA), ** Evonik Industries (Essen, Germany)

Table S2. Ingredients of the formulation

Ingredient	Supplier	Proportion
Super sterol esters Crodalan SWL	Croda, UK	49.72% w/w
Crodamol GTCC miglyol	Croda, UK	36.98% w/w
Squalane	Galderma	6.63% w/w
Cholesterol USP/NF	Croda, UK	3.63% w/w
Palmitic acid (FFAC16:0)	Emery	0.83% w/w
Stearic acid (FFA 18:0))	Berg + Schmidt	0.10% w/w
Ceramide NS (C40)	Evonik, Germany	1.18% w/w
Ceramide EOS (C66)	Evonik, Germany	0.83% w/w
Oxynex LM (anti-oxidant; protection of Ceramide EOS) containing:	Merck, Germany	0.10% w/w
DL-γ-Tocopherol (Vitamin E)		0.025% w/w
Lecithin		0.025% w/w
Ascorbyl palmitate		0.020% w/w
Glycerin monostearate		0.020% w/w
Glycerin monooleate		0.0025%w/w
Citric acid		0.0025%w/w

Table S3. Correlations to amount of barrier disruption. The table depict the Pearson r and p-value of the correlation between the TEWL directly after barrier disruption and AUC of the barrier recovery curve. It also contains the correlations between the difference in TEWLs directly after barrier disruption and the ΔT at different recovery %.

	TEWL Start vs. AUC	TEWL Dif. vs. 5%	TEWL Dif. vs. 10%	TEWL Dif. vs. 15%	TEWL Dif. vs. 20%	TEWL Dif. vs. 25%	TEWL Dif. vs. 30%	TEWL Dif. vs. 35%	TEWL Dif. vs. 40%	TEWL Dif. vs. 45%
Pearson r	-0.26	0.05	0.15	0.20	0.17	-0.15	-0.26	-0.27	-0.34	-0.43
p-value	0.17	0.85	0.60	0.47	0.54	0.60	0.35	0.34	0.22	0.11

	TEWL Dif. vs 50%	TEWL Dif. vs. 55%	TEWL Dif. vs. 60%	TEWL Dif. vs. 65%	TEWL Dif. vs. 70%	TEWL Dif. vs. 75%	TEWL Dif. vs. 80%	TEWL Dif. vs. 85%	TEWL Dif. vs. 90%	TEWL Dif. vs. 95%
Pearson r	-0.50	-0.40	-0.34	-0.34	-0.22	-0.09	-0.06	-0.23	-0.11	0.86
p-value	0.06	0.14	0.21	0.22	0.44	0.76	0.82	0.42	0.71	0.06

Table S4. LLM of the formulation ceramides. The table **(A)** shows the output of the LLM of the logarithm of the amount of NS C40 (ng/SQ) and EOS C66 (ng/SQ). The effect sizes are the changes to the intercept (control site tape-strips 5-8), due to the depth, stripping, and treatment. The second part of the table **(B)** shows the amount in ng/SQ. This was calculated by exponentiation of the mean log value outputted by the LLM.

A)

		Log NS C40		Log EOS C66[1]	
		Estimate	p-value	Estimate	p-value
	Intercept	1.575	<0.001	1.50	<0.001
Effect size	Depth	-0.135	0.011	-0.135	0.011
	Stripped	+0.204	<0.001	+0.356	<0.001
	Treated	+0.580	<0.001	+0.697	<0.001
Interactions	Depth*Treated	-0.207	0.006	-0.200	0.006
	Stripped*Treated	-0152	0.040	-0.260	0.040

B)

Calculated amount	NS C40 (ng/SQ)		EOS C66 (ng/SQ)	
	Depth 5-8	Depth 17-20	Depth 5-8	Depth 17-20
Control	37.62	27.57	38.93	28.54
Stripped	60.13	44.09	88.32	64.76
Treated	142.92	65.12	193.64	89.64
Stripped Treated	160.87	73.29	241.68	111.87

Table S5. LLM of the effects on the lateral lipid packing. The output of linear mixed models for the FWHM of the scissoring peak. The intercept is the estimated amount at the control site at a depth of 2-10 tape-strips. Estimates are in cm^{-1}. The effect size is the amount in cm^{-1} with which the variable changes the intercept. Significance levels of all effect sizes and interactions are given.

		FWHM	
		Estimate	p-value
	Intercept	11.86	<0.001
Effect size	Stripped	-0.37	0.19
	Treated	-0.43	0.08
	Depth 12-20	-0.59	0.02
Interactions	Stripped*Treated	0.44	0.23
	Stripped*Depth 12-20	0.67	0.07
	Treated*Depth 12-20	0.47	0.17
	Stripped*Treated*Depth 12-20	-1.32	0.01

Chapter 8

Intra-individual controlled pilot study in moderate to severe atopic dermatitis patients: emollient monotherapy induces stratum corneum lipid changes and complicated clinical outcome.

T. Berkers MSc[1*], W. A. Boiten MSc[1*], S. Absalah MSc[1], Dr. J. van Smeden, Dr. A.P.M. Lavrijsen[2], Prof. Dr. J.A. Bouwstra[1]

[1] Leiden Academic Centre for Drug Research, Leiden University, Leiden, the Netherlands
[2] Department of dermatology, Leiden University Medical Centre, Leiden, the Netherlands
* Both authors contributed equally

Prepared for submission

Abbreviations

AD	Atopic dermatitis
ATR-FTIR	Attenuated total reflection Fourier transform infrared spectroscopy
EASI	Eczema area and severity index
MCL	Mean ceramide carbon chain length
MuCER	Mono-unsaturated ceramide
SC	Stratum corneum
SCORAD	Scoring atopic dermatitis
TEWL	Transepidermal water loss

Keywords

Atopic dermatitis, stratum corneum, emollient, vernix caseosa, monotherapy, clinical study, lipids, lipid composition, lipid organization, ceramide, barrier repair, topical treatment, formulation

Abstract

Background: Skin barrier repair emollients are a commonly used treatment in atopic dermatitis (AD). Yet, their mechanistic effects are poorly understood.
Objective: Determining the mechanistic effects of emollient monotherapy on the skin barrier lipids in AD patients and assessing the clinical outcome.
Methods: An intra-individual controlled pilot study was performed in which moderate to severe AD patients applied a ceramide containing emollient for 2 weeks. The SCORAD, local SCORAD, EASI and TEWL were monitored. The changes in ceramide composition and lipid organization were performed using mass spectrometry and infrared spectroscopy, respectively.
Results: At non-lesional sites improvements in barrier function and lipid parameters were observed. Correlations between lipid parameters and barrier function were determined. Correlating changes during treatment occurring within the same patient showed that changes were equally in size. The AD severity at the start of the study correlated to TEWL at the study its end. Yet, monotherapy with the selected emollient aggravated the clinical outcome
Limitations: Seven patients were studied in an open label study and no non-treated control was included.
Conclusion: Monotherapy with an emollient improved the non-lesional skin barrier, yet, was insufficient treatment for severe AD patients. Lipids parameters could be promising targets for future clinical research.

Capsule summary

- Vernix caseosa based emollient treatment increased barrier recovery in healthy volunteers
- In AD patients a vernix caseosa emollient improved the non-lesional SC lipid barrier, yet, did not prevent lesion formation.
- In moderate to severe AD patients, monotherapy with this emollient was insufficient to counter the progression of AD.

Introduction

Emollients are commonly prescribed for treatment of atopic dermatitis (AD), to counter xerosis, and enhance skin barrier repair.[1,2] A wide variety of emollients are available and have three different supposed mechanisms of action. Firstly, emollients are thought to function as a supplemental barrier decreasing penetration of irritants, allergens, and pathogens and decreasing transepidermal water loss (TEWL). Secondly, they increase stratum corneum (SC) hydration by added humectants. Lastly, emollients could replenish SC barrier lipids.[1,3] These last emollients are a specific group of barrier repair emollients.[4] Of this group the clinical effects on scoring atopic dermatitis (SCORAD), TEWL and skin hydration have been extensively studied.[4-9] However, the mechanism by which these emollients enhance skin barrier repair and affect the SC lipid composition and organization is unknown. This is of particular interest as specific emollient components could normalize lipid composition, thereby enhancing barrier repair.[10,11]

Lipids form an integral part of the SC barrier. This barrier can be represented as a brick-and-mortar structure, with terminally differentiated keratinocytes (corneocytes) as the bricks, and the lipids as mortar.[12] The lipid matrix is the main route of SC penetration[13] and the lipid constitution is important for a proper barrier formation.[14] Three main SC lipid classes are known: sterols, free fatty acids, and ceramides. The latter are the most diverse group of SC lipids, characterized by different hydrophilic head groups defining the subclass, and a large variation in hydrocarbon chain length within these subclasses (Figure S1 shows all subclasses relevant for this paper).

Alterations in composition and organization of SC lipids have been reported in AD[15] and were correlated to a decreased barrier function.[16,17] A recent study showed that barrier disruption induced similar lipid alteration in regenerated SC of healthy volunteers and that a vernix caseosa based emollient treatment ameliorated the lipid composition.[18] The composition of this emollient was based on the composition that was most effective in enhancing barrier repair in mice.[19] It is hypothesized that this emollient could have a similar beneficial effect in AD patients.

Here, a pilot study is presented in which this vernix caseosa based formulation was applied on moderate to severe AD patients as monotherapy. Improvement of lipid organization and barrier function at the non-lesional sites was observed for most patients. Despite that, the local SCORAD of these patients indicated aggravated AD at the treated sites. It was observed that the AD severity at the start of the study impacted the outcome.

Materials and methods

Ethics and inclusion

To determine if the vernix caseosa based formulation, containing ceramides NS and EOS, enhanced the skin barrier by improving the SC lipid composition and organization, a pilot study with 8 AD patients was performed. Institutional approval by the Medical ethical committee of the Leiden University Medical Center was obtained

and all experiments were performed according to the declaration of Helsinki. Before inclusion each patient signed an informed consent. Patients were included when: they suffered from AD for ≥2 years and their base-line TEWL was ≥15 g/m^2/h on non-lesional skin sites. An elevated TEWL was set as selection requirement, as this was associated with an altered lipid organization.[16] This would enable the ability to determine if the emollient could improve the lipid organization. One patient its data was excluded, as another treatment was subscribed during the trail.

Study design

The study commenced at T_{-7}: a photograph was taken and the SCORAD, local SCORAD (ventral forearms), Eczema area and severity index (EASI), and TEWL (AquaFlux AF200, BIOX, London, UK) were determined. For one week patients did not receive any systemic treatment or treatment on their ventral forearms. At T_0, TEWL was measured at non-lesional sites of both ventral forearms and the arm with the highest TEWL was selected. A photograph was taken and 12 tape-strips were obtained for ceramide analysis (according to Boiten et al.[20]). Tape-strips were extracted using a modified Bligh and Dyer and, thereafter, quantified using LC/MS. After every two tape-strips, an infrared spectrum was measured on the stripped site using attenuated total reflected Fourier transfer infrared spectroscopy (ATR-FTIR, Agilent Technologies, Inc., Santa Clara, CA). In the spectrum the CH_2 symmetric stretching peak position of the SC lipids was determined, which is a measure for the SC lipids (conformational) ordering.[21]
Thereafter, patients applied for two weeks 2x daily the vernix caseosa based formulation on both forearms (Table S1: formulation composition). During the entire study patients were allowed to treat the rest of their skin as they normally would. To minimize the burden on the patient, no non-treated control was included. After the treatment period, a two-day washout period commenced. Of the non-lesional and lesional sites at T_{16}, TEWL, lipid composition and lipid organization were determined. The SCORAD, local-SCORAD, EASI, and a photograph were taken as well. Figure S2 gives an overview of the sites investigated and the timeline of the study.

Statistical analysis

Statistical analyses were performed using SPSS (V24 IBM). Group wise comparisons were performed using linear mixed modeling with treatment as fixed factor and lesional as a nested factor within treatment (lesional site were always treated and compared to non-lesional). Subject paring was performed and patients were set as a random variable when comparing sites. Correlations between parameters were examined using GraphPad Prism (version 6.05). To determine if correlations were site/treatment independent, the correlations were determined using a Linear mixed models without subject paring, with site (control, non-lesional, and lesional) as fixed factors and the parameter of interest as covariant (see Table S2 for SPSS scripts used).

Results

Affected lipid parameters in atopic dermatitis

In the present study mechanistic effects of emollient treatment on SC lipid parameters were examined in AD patients. Previously, alterations in AD patients SC lipid composition have been observed.[15] More recently, treatment with an emollient had shown to affect these alterations in lipid parameters in healthy volunteers.[18] Five lipid parameters important for barrier function were examined: 1) CH_2 stretching peak position: higher values indicate more disordering in the SC lipids causing a reduced barrier function;[17] 2) Mean ceramide carbon chain length (MCL), a longer MCL was correlated to increased barrier function;[15] 3) fraction of ceramides with a 34 carbon chain length, which was associated with a decreased barrier function;[15] 4) ceramide subclasses ratio: (dS+P+H)/S excluding (esterified)omega hydroxyl-ceramides (EO, O ceramides). This ratio was shown to decrease with a reduced barrier;[18] 5) fraction of ceramides with a unsaturated carbon chain (MuCER), increased unsaturation was correlated to decreased barrier function.[22]

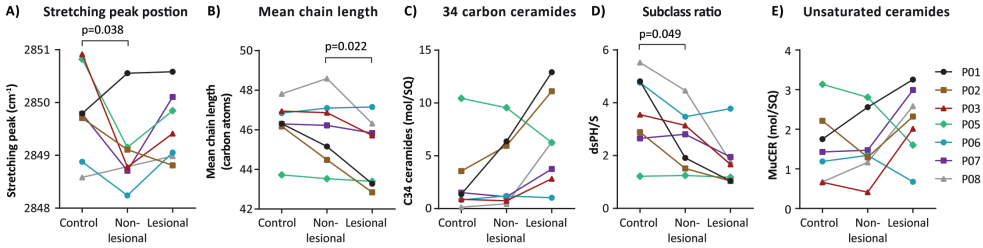

Figure 1. The changes in lipid parameters between the control site (T_0), non-lesional site (T_{16}) and lesional site (T_{16}). The last two were treated sites. **A)** Stretching peak position of the SC lipids in cm^{-1}. **B)** Mean total carbon chain length of the ceramides in carbon atoms. **C)** Amount of ceramides with a carbon chain length of 34 (nmol/sq*10). **D)** Ceramide subclass ratio as: (dS+P+H)/S excluding acyl-ceramides (EO ceramides), **E)** Amount of mono-unsaturated ceramides (nmol/sq*10). Significant changes are indicated by the p-value. The double brackets show the F-test results for treatment, which takes into account treatment effects in both lesional and non-lesional sites.

Figure 1(A-E) depict the 5 parameter as observed in this study. The CH_2 stretching peak position decreased significantly at non-lesional treated site compared to control. No significant changes in MCL, C34, and MuCER amount were observed when skin was treated. The subclass ratio (dS+P+H)/S decreased after treatment. The MCL was shorter in the lesional site compared to the non-lesional. The decreased stretching peak position indicates that the lipid ordering increased which is expected to be beneficial for the skin barrier function. The stretching peak position of the treated lesional skin is expected to increase but it was not significantly higher than at the control or non-lesional site.

Changes in clinical parameters due to treatment

Next to pathophysiological changes in SC lipids, the impact treatment had on the disease progression was examined. Therefore, two scores of AD severity were determined at

the start (T_{-7}) and end (T_{16}) of the study. Figure 2A and B show the SCORAD and EASI, respectively. No significant change in either score was observed. As treatment was only applied on the ventral forearm, the local SCORAD of that area was determined. This parameter increased significantly, also illustrated in Figure 3, in which images of each patients arm at three time points are shown, depicting more lesional sites at T_{16}. During the study the skin barrier function was monitored using TEWL. No significant changes in TEWL occurred between the control (T_{-7}), the control (T_0) and non-lesional treated site (T_{16}). In all patients, TEWL at the lesional sites (T_{16}) was significantly higher than at the non-lesional sites. There was a substantial inter-individual difference in TEWL values: patient one (P01) had a larger increase in TEWL than all other patients; Patient 5 (P05) did not have completely non-lesional sites at the ventral forearm, therefore, had an exceptionally high TEWL value at the control site. Altogether, the emollient treatment effects on barrier function were diverse but beneficial for most patients, i.e. the TEWL decreased for most patients, only the mean difference in TEWL was not significant (Figure S3 depicts TEWL changes).

As the main route of TEWL is through the SC lipids, TEWL was correlated to the lipid parameters. All these parameters were correlated to TEWL or 1/TEWL (Table 1, Table S3 contains correlations between all parameters). Parameters which decrease with an increase in TEWL showed to have inverse (1/x) correlations, therefore, 1/TEWL was used. These correlations to TEWL or 1/TEWL and inter-correlations of the parameters indicate that these lipid parameters and barrier function correspond per patient. Exemplified by P05 where TEWL was high and the lipid parameter C34 and MuCER were high, and MCL and subclass ratio were low. To further investigate the changes during treatment at non-lesional site, the effect size of treatment per patient was studied.

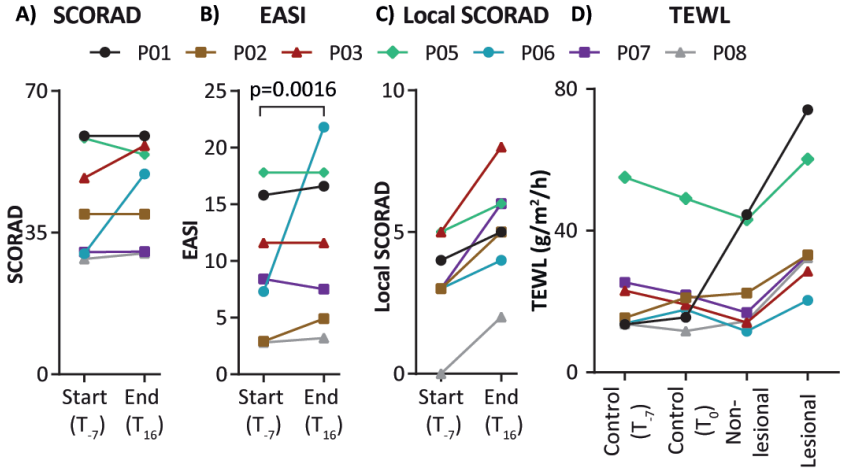

Figure 2. Changes in clinical parameters. A,B,C) SCORAD, EASI and local SCORAD at the start and end of the study for all patients, each patient is indicated by a specific color. **D)** TEWL throughout the study for each patient. Non-lesional and lesional sites were both treated and measured at T_{16}. Lesional sites were significantly different form all other sites (F-test of mixed model p=0.006).

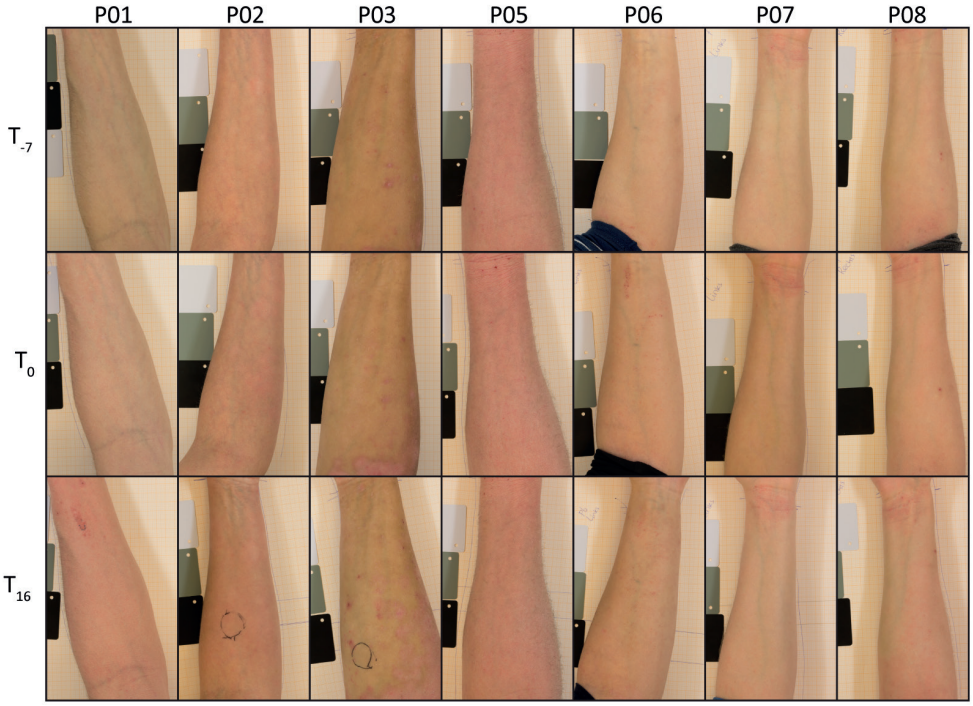

Figure 3. Photographs of the examined ventral forearm of each patient at three time points. Photos were taken one week prior the emollient treatment (T_{-7}), at the start of the treatment (T_0) and 2 days after the treatment period (T_{16}).

Table 1. Correlations of lipid parameters to barrier function. For each parameter the correlation to either TEWL of 1/TEWL is given. The F-test p-values indicated if the correlation (*cor*) was significant, or that this correlation was different per site (Site). The slope and p-value of each site independently is shown below that.

	TEWL (g/m²/h)						1/TEWL (g/m²/h)⁻¹			
	Stretching peak position (cm^{-1})		C34 (nmol/sq*10)		MuCER (nmol/sq*10)		Subclass ratio (dS+P+H/S)		MCL (carbon atoms)	
	Cor.	Site	*Cor.*	Site	*Cor.*	Site	*Cor.*	Site	*Cor.*	Site
F-test p-value	0.001	0.313	<0.001	0.969	0.002	0.821	<0.001	0.447	<0.001	0.146
	Slope	p-value	Slope	p-value	Slope	p-value	Slope	p-value	Slope	p-value
Control	8.84	0.107	3.327	0.009	11.531	0.061	0.0124	0.001	0.0140	0.002
Treated	15.78	0.023	3.468	0.007	15.254	0.023	0.0173	<0.001	0.0115	0.001
Lesional	22.49	0.006	3.114	0.004	10.147	0.097	0.0105	0.032	0.0538	0.067

Patient specific treatment effects

As treatment might affect each patient differently, changes during treatment per patient were examined. The effect sizes, control (T_0) subtracted from the non-lesional site (T_{16}), were compared. For each clinical and lipid parameter, Figure 4A depicts if treatment had a beneficial effect i.e. towards a better skin barrier or less severe AD. Distinctions between patients were observed: P01 had no beneficial effects, whereas treatment had the most beneficial effects for P05, although only lesional sites were examined in this patient. Furthermore, some changes in parameters coincided for multiple patients, in that, if one was beneficial the other was as well: e.g. MCL and EO%, C34 and TEWL, and MuCER and stretching peak position. Effect sizes of these parameters were compared, as shown in Figures 4B to 4E. These correlations in parameters showed that during treatment, parameters were similarly affected, either positively or negatively (Table S4 shows all correlations). Demonstrating that besides correlating in size, parameter changes within a patient correlated as well. Changes in MuCER and Stretching coincided, but were not correlating significantly (Figure S4). Changes during treatment were not dependent on state of the skin at the control time point, exemplified by P05 who showed the most progress with only lesional sites. Altogether, changes were subject dependent, yet, not independent of one another.

However, the AD severity at other body sites could influence the study outcome through a systemically induced flare. To examine if the severity of AD at the beginning of the study had an influence on the barrier function at the end of the study, the SCORAD and EASI scores at T_{-7} were compared with TEWL at T_{16} (Figure 5). Significant correlations for both SCORAD and EASI were observed. Although the limited data points, both correlations indicated that the AD severity had a substantial influence on changes in barrier function. No correlations between AD at T_{-7} and lipid parameters at T_{16} were observed.

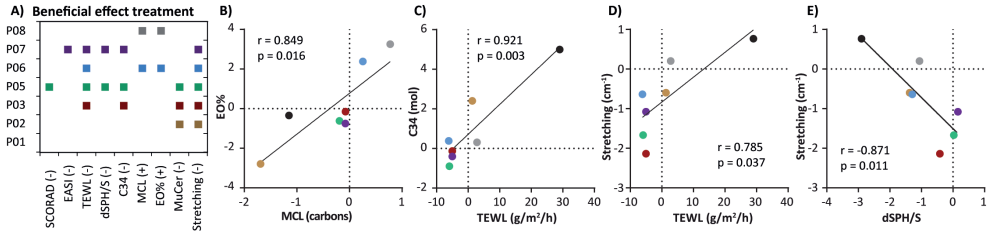

Figure 4. Effects of treatment. A) Plot showing if a change during treatment was beneficial (indicated by a colored square) or non-beneficial (indicated by the absence of a colored square). Each patient has its own color. The – and + signs indicate if beneficial change in parameters were positive or negative values. **B-E)** effects size of the changes and how they compared to one another. If both are negative or positive for the same individual, it indicates if the effects were in a similar direction. The line indicates a linear regression, which is an indication if the effect sizes were comparable.

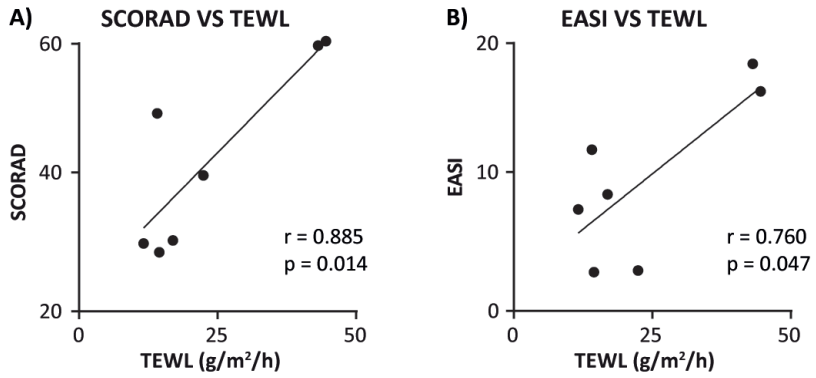

Figure 5. Correlations between clinical parameters and skin barrier function. A, B) Correlation between the SCORAD and EASI at T_{-7} and the TEWL at T_{16}, respectively. The r and p-values are the pearson correlation and the significance level. The line is a linear regression.

Discussion

The goal of this study was to determine how monotherapy with a barrier repair enhancing vernix caseosa based emollient could improve the SC lipid composition and organization. Changes at non-lesional sites showed that for most patients the barrier improved during the study. This was accompanied by significant increases in lipid ordering, indicating that treatment improved the lipid barrier. However, no direct effects of the emollient on ceramide composition parameters were observed. This indicates that effects on lipid organization might be due to a combined effect of different ceramide parameters or other constituents of the emollients like free fatty acids, which were previously shown to incorporate into the SC lipid matrix.[23] At the control and treated site, the SC parameters examined and the correlations between them were comparable to previous studies without treatment.[15,16] Here, it is demonstrated that these correlations were also valid when treatment was included. Moreover, the correlation between changes in parameters during treatment indicated that changes in TEWL correlated to changes in C34 ceramides and changes in the lipid conformational ordering. The latter also correlated to the (dS+P+H)/S subclass ratio, indicating that a change in ceramide subclass could alter the conformational ordering. A trend between changes in MuCERs and changes in conformational ordering was observed.

Previously, we showed that treatment of healthy volunteers with a compromised skin barrier decreased C34 amount and increased MCL.[18] However, these changes induced by barrier disruption and the changes due to treatment (treatment effect sizes, C34: 0.69, MCL: 0.3 carbons), were significantly smaller than changes observed in the present study. In this study, the beneficial effects of the barrier restoring emollient had a small impact compared to the larger changes in SC lipid properties induced by AD. However, these lipid parameters could be used as targets for future research into topical AD treatment to normalize the skin barrier, as changes in these lipids did correspond to changes in TEWL (Figure 4C and D).

Aggravation of the disease state was observed in most patients. During the study no systemic corticosteroids or immunosuppressants were used. Therefore, a systemic

immune response, external factors like weather changes, or formulation sensitization could have had a major impact on the disease state. Other studies have shown that when the AD severity is first reduced by anti-inflammatory treatment, a barrier restoring formulation was beneficial.[24,25] That the AD severity at T_{-7} correlated to the barrier at T_{16} indicates that the disease state influenced the barrier during the study and strengthens the hypothesis that systemic inflammation played a role in the outcome of this study. A specific example was P01, who started with the highest SCORAD of all patients but relative normal barrier function and lipid parameters, both barrier function and lipid parameters changed during treatment to a state comparable to lesional skin. The large variation in lipid parameters between subjects and effects during treatment could, thus, partially be explained by the AD severity. From the result presented here, it can be concluded that in moderate to severe AD patients, monotherapy with this emollient was insufficient to counter the progression of AD.

For several patients treatment did have beneficial effect on the lipid parameters. Because observed effect sizes were small and it might take many cycles of cornification and desquamation before the barrier is properly restored, more than two weeks of formulation application would be desirable to sufficiently restore the lipid composition and organization in SC in AD patients. This should be combined with anti-inflammatory treatment to counter flares during this period. The results in non-lesional AD skin support the assumption that a vernix caseosa emollients can help restore barrier abnormalities in AD as it does in healthy volunteers with artificial induced barrier impairment.

Acknowledgments

This research is supported by Netherlands Organization for Scientific Research (NWO: project number 12400) which is partly funded by the Ministry of Economic Affairs. We thank Evonik industries AG for supplying us with the ceramides, Croda International Plc and for the other ingredients used in the formulation, and Galderma SA for producing the formulation.

References

1. Wolf R, Parish LC. Barrier-repair prescription moisturizers: do we really need them? Facts and controversies. *Clin Dermatol* **2013**: 31: 787-791.
2. Eichenfield LF, Tom WL, Berger TG, et al. Guidelines of care for the management of atopic dermatitis: section 2. Management and treatment of atopic dermatitis with topical therapies. *J Am Acad Dermatol* **2014**: 71: 116-132.
3. Meckfessel MH, Brandt S. The structure, function, and importance of ceramides in skin and their use as therapeutic agents in skin-care products. *J Am Acad Dermatol* **2014**: 71: 177-184.
4. Hon KL, Leung AK, Barankin B. Barrier repair therapy in atopic dermatitis: an overview. *Am J Clin Dermatol* **2013**: 14: 389-399.
5. Lynde CW, Andriessen A. A cohort study on a ceramide-containing cleanser and moisturizer used for atopic dermatitis. *Cutis* **2014**: 93: 207-213.
6. Barba C, Parra JL, Coderch L, et al. In vivo and in vitro evaluation of topical formulations containing physiological lipid mixture for replacement of skin barrier function. *G Ital Dermatol Venereol* **2014**: 149: 347-353.
7. van Zuuren EJ, Fedorowicz Z, Christensen R, et al. Emollients and moisturisers for eczema. *Cochrane Database Syst Rev* **2017**: 2: CD012119.
8. Simpson E, Bohling A, Bielfeldt S, et al. Improvement of skin barrier function in atopic dermatitis patients with a new moisturizer containing a ceramide precursor. *J Dermatolog Treat* **2013**: 24: 122-125.
9. Oh MJ, Nam JJ, Lee EO, et al. A synthetic C16 omega-hydroxyphytoceramide improves skin barrier functions from diversely perturbed epidermal conditions. *Arch Dermatol Res* **2016**: 308: 563-574.
10. Man MM, Feingold KR, Thornfeldt CR, et al. Optimization of physiological lipid mixtures for barrier repair. *The Journal of investigative dermatology* **1996**: 106: 1096-1101.
11. Yang L, Mao-Qiang M, Taljebini M, et al. Topical stratum corneum lipids accelerate barrier repair after tape stripping, solvent treatment and some but not all types of detergent treatment. *Br J Dermatol* **1995**: 133: 679-685.
12. Michaels AS, Chandrasekaran SK, Shaw JE. Drug Permeation through Human Skin - Theory and Invitro Experimental Measurement. *Aiche Journal* **1975**: 21: 985-996.
13. Verdier-Sevrain S, Bonte F. Skin hydration: a review on its molecular mechanisms. *J Cosmet Dermatol* **2007**: 6: 75-82.
14. van Smeden J, Janssens M, Gooris GS, et al. The important role of stratum corneum lipids for the cutaneous barrier function. *Biochimica et biophysica acta* **2014**: 1841: 295-313.
15. Ishikawa J, Narita H, Kondo N, et al. Changes in the ceramide profile of atopic dermatitis patients. *The Journal of investigative dermatology* **2010**: 130: 2511-2514.
16. Janssens M, van Smeden J, Gooris GS, et al. Increase in short-chain ceramides correlates with an altered lipid organization and decreased barrier function in atopic eczema patients. *Journal of lipid research* **2012**: 53: 2755-2766.
17. van Smeden J, Janssens M, Kaye EC, et al. The importance of free fatty acid chain length for the skin barrier function in atopic eczema patients. *Exp Dermatol* **2014**: 23: 45-52.
18. Boiten WA, Berkers T, Absalah S, et al. Applying a vernix caseosa based formulation accelerates skin barrier repair by modulating lipid biosynthesis. *Journal of lipid research* **2017**.
19. Oudshoorn MH, Rissmann R, van der Coelen D, et al. Effect of synthetic vernix biofilms on barrier recovery of damaged mouse skin. *Exp Dermatol* **2009**: 18: 695-703.
20. Boiten W, Absalah S, Vreeken R, et al. Quantitative analysis of ceramides using a novel lipidomics approach with three dimensional response modelling. *Biochimica et biophysica acta* **2016**: 1861: 1652-1661.
21. Boncheva M, Damien F, Normand V. Molecular organization of the lipid matrix in intact Stratum corneum using ATR-FTIR spectroscopy. *Biochimica et biophysica acta* **2008**: 1778: 1344-1355.
22. Mojumdar EH, Helder RW, Gooris GS, et al. Monounsaturated fatty acids reduce the barrier of stratum corneum lipid membranes by enhancing the formation of a hexagonal lateral packing. *Langmuir* **2014**: 30: 6534-6543.
23. Berkers T, Visscher D, Gooris GS, et al. Topically Applied Ceramides Interact with the Stratum Corneum Lipid Matrix in Compromised Ex Vivo Skin. *Pharmaceutical research* **2018**: 35: 48.
24. Koppes SA, Charles F, Lammers L, et al. Efficacy of a Cream Containing Ceramides and Magnesium in the Treatment of Mild to Moderate Atopic Dermatitis: A Randomized, Double-blind, Emollient- and Hydrocortisone-controlled Trial. *Acta Derm Venereol* **2016**: 96: 948-953.
25. Angelova-Fischer I, Neufang G, Jung K, et al. A randomized, investigator-blinded efficacy assessment study of stand-alone emollient use in mild to moderately severe atopic dermatitis flares. *J Eur Acad Dermatol Venereol* **2014**: 28 Suppl 3: 9-15.

Supplement

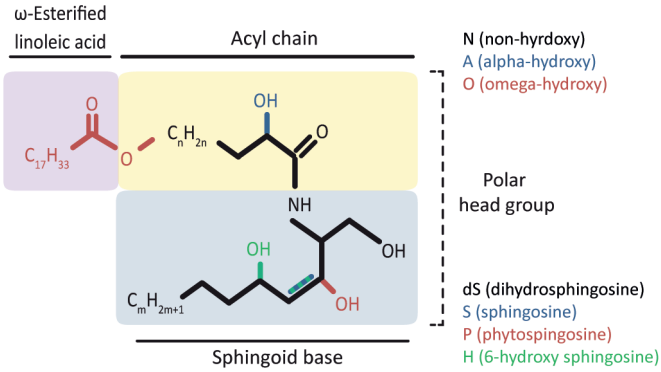

Figure S1. Ceramide structure. The ceramide consists of an acyl chain bound to a sphingoid base. The subclass is defined by these two parts of the ceramide. There are 3 different acyl chains indicated by the letters N, A, and O and one where there is an linoleic acid esterified to the omega hydroxyl (EO). There are 4 different sphingoid bases dS, S, P, and H. The color in the text corresponds to the structural moiety with the same color. The name of the ceramide subclass is a combination of the letters that define the acyl chain and the sphingoid base e.g. EOS is an Esterified-Omega-hydroxy acyl-Sphingosine.

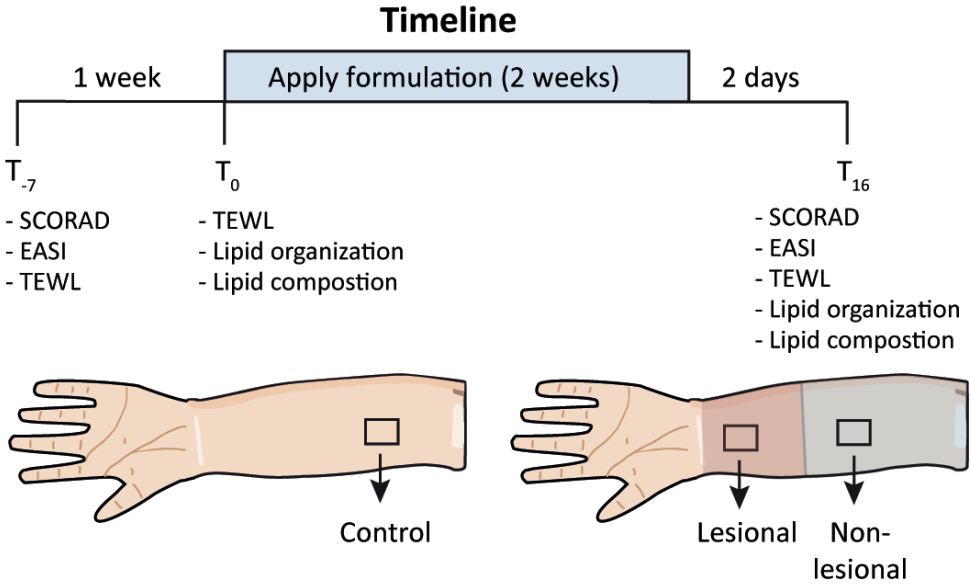

Figure S2. Study design. Showing the timeline of the study and sites examined. At each time point the tests that were performed are indicated. Below the test the sites of the arm that were examined are shown.

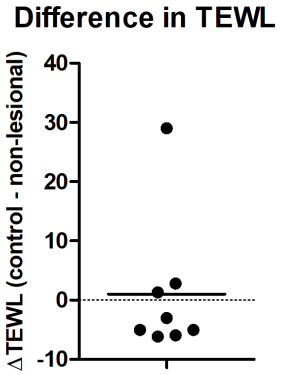

Figure S3. Difference in TEWL. Difference between T_0 and T_{16} of non-lesional sites.

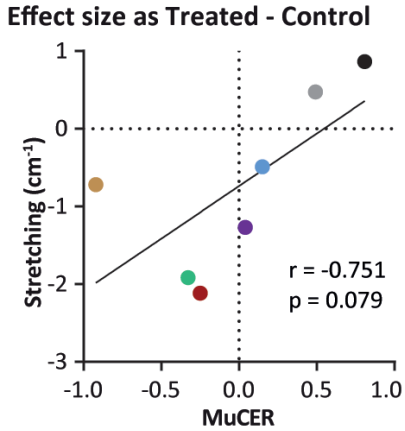

Figure S4. Correlation between changes in MuCER and CH_2 Stretching peak of the FTIR.

Table S1. Composition vernix caseosa formulation.

Ingredient	Supplier	Proportion
Super sterol esters Crodalan SWL	Croda, UK	49.72% w/w
Crodamol GTCC miglyol	Croda, UK	36.98% w/w
Squalane	Galderma	6.63% w/w
Cholesterol USP/NF	Croda, UK	3.63% w/w
Palmitic acid (FFAC16:0)	Emery	0.83% w/w
Stearic acid (FFA 18:0))	Berg + Schmidt	0.10% w/w
Ceramide NS (C40)	Evonik, Germany	1.18% w/w
Ceramide EOS (C66)	Evonik, Germany	0.83% w/w
Oxynex LM (anti-oxidant; protection of Ceramide EOS) containing:	Merck, Germany	0.10% w/w
DL-γ-Tocopherol (Vitamin E)		0.025% w/w
Lecithin		0.025% w/w
Ascorbyl palmitate		0.020% w/w
Glycerin monostearate		0.020% w/w
Glycerin monooleate		0.0025%w/w
Citric acid		0.0025%w/w

Table S2. SPSS scripts

Code used to compare groups	*MIXED stretch BY Treated Lesional* */CRITERIA =CIN(95) MXITER(100) MXSTEP(10) SCORING(1) SINGULAR(0.000000000001) HCONVERGE(0, ABSOLUTE) LCONVERGE(0, ABSOLUTE) PCONVERGE(0.000001, ABSOLUTE)* */FIXE D= Treated Lesional(Treated)| SSTYPE(3)* */METHOD=REML* */PRINT =SOLUTION TESTCOV* */RANDOM = INTERCEPT | SUBJECT(Volunteer) COVTYPE(VC).*	* Treated and lesional are the fixed factors and lesional is nested within Treated * Volunteer is the pairing per subject.
Code used to plot correlations	*MIXED MCL BY Site WITH C34* */CRITERIA=CIN(95) MXITER(100) MXSTEP(10) SCORING(1) SINGULAR(0.000000000001) HCONVERGE(0, ABSOLUTE) LCONVERGE(0, ABSOLUTE) PCONVERGE(0.000001, ABSOLUTE)* */FIXED=Site C34 Site*C34 | SSTYPE(3)* */METHOD=REML* */PRINT=SOLUTION TESTCOV.*	* Site 1 to 3 are control, non-lesional, and lesional and is a fixed factor * MCL and C34 are the dependent variable and covariate. These were changed dependent on the correlation that was examined.

Table S3. Correlations between lipid and barrier parameters

	TEWL		1/TEWL		MCL		MuCER	
	pearson r	p-value	pearson r	p-value	pearson r	p-value	pearson r	p-value
TEWL			-8.78	<0.001	-0.806	<0.001	0.725	<0.001
1/TEWL	-0.877	<0.001			0.813	<0.001	-0.765	<0.001
MCL	-0.806	<0.001	0.813	<0.001			-0.670	<0.001
MuCER	0.725	<0.001	-0.765	<0.001	-0.670	<0.001		
EO%	-0.475	0.030	0.537	0.012	0.695	<0.001	-0.323	0.153
C34	0.845	<0.001	-0.810	<0.001	-0.906	<0.001	0.796	<0.001
Ratio	-0.753	<0.001	0.850	<0.001	0.852	<0.001	-0.696	<0.001
Stretching	0.586	0.005	-0.616	0.003	-0.384	0.086	0.466	0.033

	EO%		C34		Ratio		Stretching	
	pearson r	p-value	pearson r	p-value	pearson r	p-value	pearson r	p-value
TEWL	-0.475	0.030	0.845	<0.001	-0.753	<0.001	0.586	0.005
1/TEWL	0.537	0.012	-0.810	<0.001	0.850	<0.001	-0.616	0.003
MCL	0.695	<0.001	-0.906	<0.001	0.852	<0.001	-0.384	0.086
MuCER	-0.323	0.1534	-.796	<0.001	-0.696	<0.001	0.466	0.033
EO%			-0.483	0.0266	0.406	0.0676	-0.403	0.070
C34	-0.483	0.027			-0.819	<0.001	0.387	0.083
Ratio	0.406	0.068	-0.819	<0.001			-0.365	0.104
Stretching	-0.403	0.070	0.387	0.083	-0.365	0.1037		

Table S4. Correlations between the changes in parameters during treatment

	TEWL		MCL		EO%		MuCER	
	pearson r	p-value	pearson r	p-value	pearson r	p-value	pearson r	p-value
TEWL			-0.467	0.291	0.081	0.863	0.597	0.157
MCL	-0.467	0.291			0.849	0.016	0.392	0.384
EO%	-0.081	0.863	0.849	0.016			0.642	0.121
MuCER	0.597	0.157	0.392	0.384	0.641	0.121		
C34	0.921	0.003	-0.692	0.085	-0.259	0.575	0.334	0.464
Ratio	-0.871	0.011	0.457	0.302	-0.063	0.893	-0.477	0.279
Stretching	0.785	0.037	-0.177	0.705	0.277	0.547	0.640	0.121
SCORAD	0.288	0.531	-0.349	0.443	-0.505	0.248	-0.110	0.814
EASI	0.205	0.660	-0.181	0.698	-0.427	0.339	-0.063	0.893
local SCORAD	0.373	0.410	-0.138	0.768	0.197	0.671	0.274	0.552

	C34		Ratio		Stretching		SCORAD	
	pearson r	p-value	pearson r	p-value	pearson r	p-value	pearson r	p-value
TEWL	0.921	0.003	-0.871	0.011	-0.785	0.037	0.288	0.531
MCL	-0.692	0.085	0.457	0.302	-0.177	0.705	-0.349	0.433
EO%	-0.259	0.575	-0.063	0.893	0.277	0.547	-0.505	0.248
MuCER	0.334	0.464	-0.477	0.279	0.640	0.121	-0.110	0.814
C34			-0.934	0.002	0.744	0.055	0.137	0.770
Ratio	-0.934	0.002			-0.815	0.026	0.114	0.808
Stretching	0.744	0.055	-0.815	0.036			0.088	0.851
SCORAD	0.137	0.770	0.114	0.808	0.088	0.851		
EASI	0.017	0.971	0.233	0.615	-0.110	0.815	0.874	0.010
local SCORAD	0.365	0.421	-0.518	0.234	0.442	0.321	-0.093	0.842

	EASI		Local SCORAD	
	pearson r	p-value	pearson r	p-value
TEWL	0.205	0.660	0.373	0.410
MCL	-0.181	0.698	-0.138	0.768
EO%	-0.427	0.339	0.197	0.671
MuCER	-0.063	0.893	0.274	0.552
C34	0.017	0.971	0.365	0.421
Ratio	0.233	0.615	-0.518	0.234
Stretching	-0.110	0.815	0.442	0.321
SCORAD	-0.874	0.010	-0.093	0.842
EASI			-0.473	0.284
local SCORAD	-0.473	0.284		

Chapter 9

Summary and Perspectives

Summary

Introduction

The skin consists of three layers, the hypodermis, dermis, and epidermis, and protects the body from the external environment by reducing transepidermal water loss and penetration of pathogens, allergens, and irritants. The epidermis is subdivided in 4 strata, of which the stratum corneum (SC) is the outermost layer. The SC consists of terminally differentiated corneocytes embedded in a lipid matrix. The corneocytes and lipid matrix are assembled in a brick-and-mortar structure, in which the bricks represent the corneocytes and the mortar represents the lipid matrix.[1] The lipid matrix is a major penetration pathway. The lipids in the lipid matrix are excreted at the interface between the viable epidermis and the SC, after *de novo* synthesis in the keratinocytes or uptake from the systemic circulation (e.g. essential fatty acids).

Three main lipid classes in the SC are free fatty acids (FAs), ceramides (CERs), and cholesterol. A wide chain length distribution is observed for both FAs and CERs, as well as unsaturation of the carbon chain.[2-5] At least 18 subclasses of CERs are identified, based on the chemical structure of the sphingoid base and acyl chain, see Figure 1.[6-14] The SC lipids in the extracellular matrix are highly ordered in lamellae stacked on top of each other, with repeat distances of 6 nm (short periodicity phase, SPP) and 13 nm (long periodicity phase, LPP).[15-19] Within the lamellae, the lipids adopt either an orthorhombic, hexagonal, or liquid organization (Figure 2). The relative fraction of lipids adopting an orthorhombic lateral packing, the relative fraction of lipid lamellae with a repeat distance of 13 nm, and the CER composition affect the skin barrier function.[15,20-22]

In several inflammatory skin diseases, the skin barrier function is impaired. Although the underlying cause of these inflammatory diseases is different, the impaired skin barrier partly based on changes in lipid composition are very similar. These changes are e.g. increased level of CER subclass NS, decreased levels of CER NP and CER EOS, an increased fraction of unsaturated lipids, and a reduced average carbon chain length of CERs and FAs. These changes in lipid composition may contribute to a less dense lateral ordering, and a reduced lamellar repeat distance.[4,5,17,23-31] The skin barrier function is most extensively studied in atopic dermatitis (AD), and many studies focused on possible treatment strategies. However, to date treatment of AD is far from optimal: corticosteroids are used to reduce the inflammatory response, but they are associated with side effects, such as skin atrophy.[32] To reduce the absorption of pathogens, allergens, and irritants, topical application of endogenous skin barrier lipids to repair the skin barrier may be an attractive approach.[33]

Vernix caseosa (VC) is a white, cheesy substance covering and protecting a fetus in the last trimester of pregnancy and during delivery.[34-36] It consists of the barrier lipids CERs, FAs, cholesterol, as well as squalene, wax esters, sterol esters, triglycerides, and phospholipids.[36,37] Skin barrier repair in mice is enhanced after application of VC, but also after application of synthetic formulations mimicking VC.[38,39] However, the skin barrier repair response in animal skin is different from that in human skin.[40] Currently cultured human skin models (e.g. human skin equivalents) are often labor intensive and time consuming to generate. Therefore, less time consuming skin models mimicking

the *in vivo* human skin barrier response are attractive to study topical treatment, especially when focusing barrier repair of AD skin or other inflammatory skin diseases.

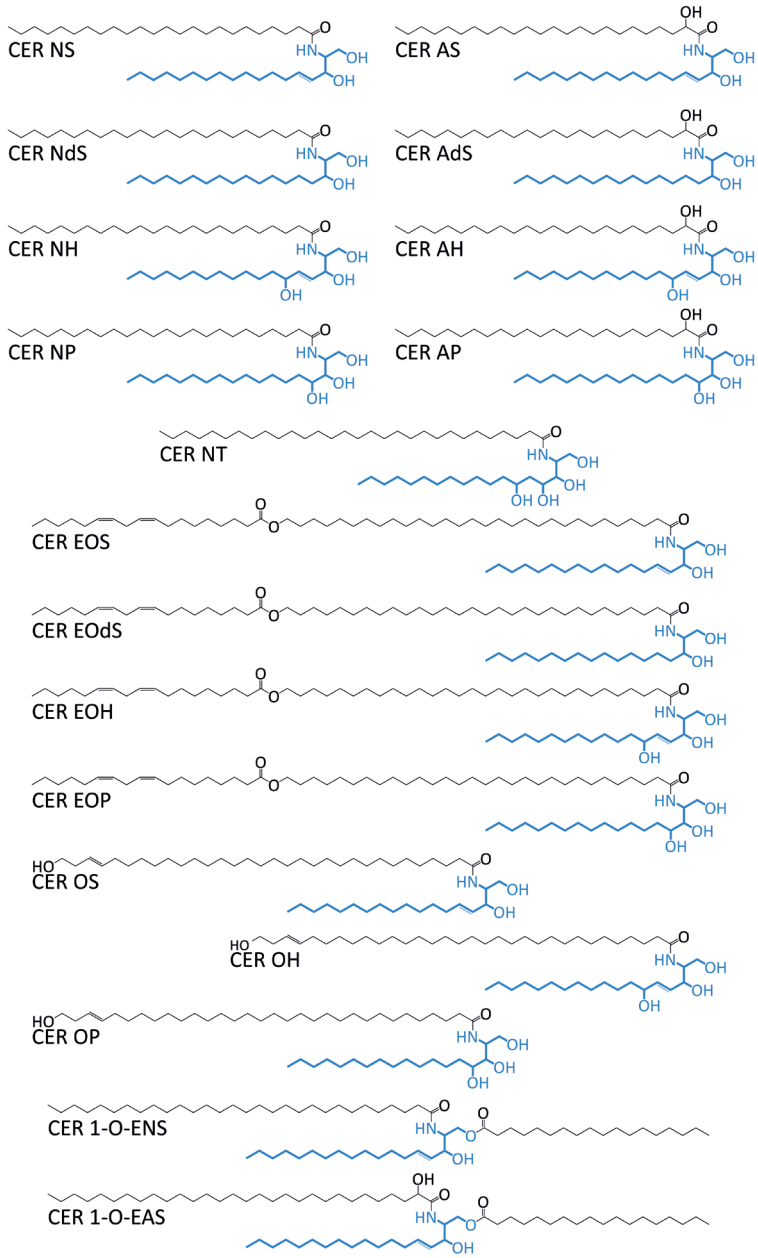

Figure 1. Ceramides subclasses in the stratum corneum lipid matrix. CERs consist of a sphingoid base coupled to a FA, which can both vary in molecular structure. CERs are named according to their molecular structure. The acyl chain can either be non-hydroxylated (N), α-hydroxylated (A), ω-hydroxylated (O), or esterified ω-hydroxylated (EO), whereas the sphingoid base is either a sphingosine (S), dihydrosphingosine (dS), phytosphingosine (P), 6-hydroxysphingosine (H), or dihydroxy dihydrosphingosine (T).

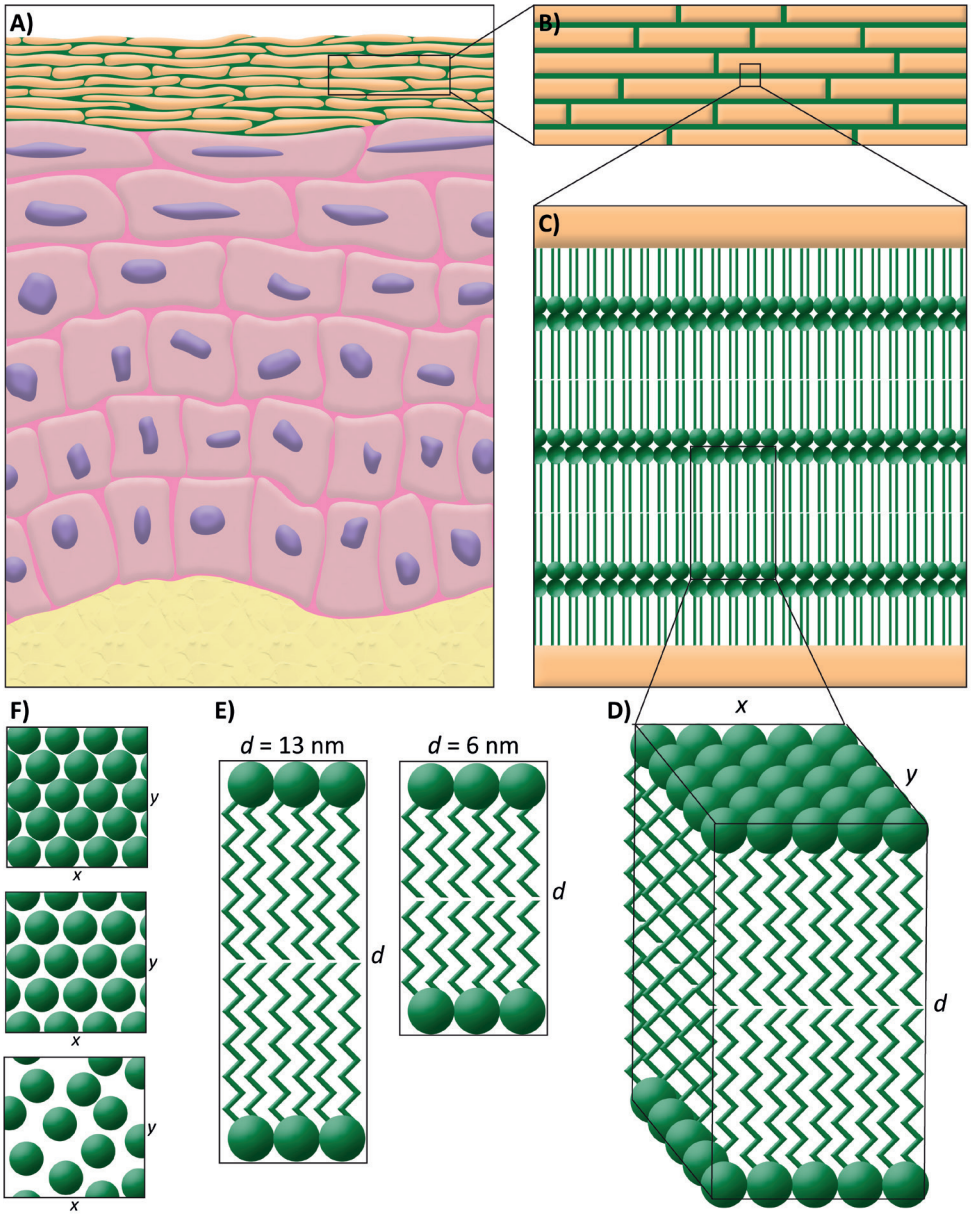

Figure 2. Organization of the lipids within the stratum corneum lipid matrix. A) Schematic overview of the epidermal morphology. **B)** The corneocytes are embedded in the lipid matrix in a brick-and-mortar structure. **C)** The lipids in the matrix are stacked in lamellae in between the corneocytes. **D)** More details of the lipid lamellae. **E)** Two lamellar phases are identified with a repeat distance (d) of either 13 nm (LPP) or 6 nm (SPP). **F)** Within the lamellae, the lipids are organized in either an orthorhombic, hexagonal, or liquid packing (from top to bottom).

Aim of the study

The aim of this thesis was to determine whether a novel VC based formulation effectively enhances skin barrier repair in AD patients and normalizes the SC lipid composition and organization. In order to achieve this goal, the following studies were performed:

1. An *ex vivo* human skin barrier repair (SkinBaR) model was developed for studying the interactions between topical applied compounds and the skin barrier. The SC lipid properties during and after skin barrier repair process were examined. The lipid composition and organization in the regenerated SC of this SkinBaR model were compared to the lipid composition and organization in regenerated SC in healthy human skin *in vivo*.
2. The effects of a selected number of barrier FAs and/or CER subclasses applied in a VC based formulation on the SkinBaR model during skin barrier repair were examined. Especially the interactions between the VC components and the SC lipid matrix were studied.
3. The effect of the VC based formulation on skin barrier repair in compromised healthy skin, and in AD skin was assessed.

Development of a skin barrier repair model

In order to study skin barrier repair *in vitro*, no suitable skin models are available. Generation of human skin equivalents is very labor intensive and therefore less attractive. In Chapter 2 a novel *ex vivo* human skin barrier repair (SkinBaR) model was developed. Cyanoacrylate was used to remove SC from the skin thereby reducing the barrier function. Epidermal morphology, differentiation, SC lipid composition and organization were examined after culturing the skin for 8 days at 37˚C and 32˚C. The results showed that the skin was actively proliferating and differentiating, which resulted in regeneration of SC. The lipids in the regenerated SC mainly adopted a hexagonal lateral lipid organization at the expense of lipids forming an orthorhombic lateral organization as observed in healthy native human SC. The altered skin barrier properties showed similarities with AD skin. Consequently, the SkinBaR model has the potential to study the skin barrier repair process and how this process may be influenced by application of topical formulations and/or by changing the environmental factors.

In Chapter 3, the reproducibility of the stripping of the SkinBaR model was examined in more detail. The influence of initial degree of barrier disruption on the lipid organization of the regenerated SC was assessed. The results showed that when 25%, 50%, and 75% of the SC was removed the SC is able to regenerate fully in a period of 8 days to a comparable number of corneocyte layers as in native SC. Major morphological differences (e.g. parakeratosis) and a change in lamellar structure were only observed when initially 75% of the SC was removed. As far as the lateral lipid organization was concerned, a gradual increase in degree of barrier disruption (percentage of SC removed) resulted in a gradually less dense packing, but the lipid ordering was only affected if at least 50% of the SC was removed. These results led to the conclusion that the degree of barrier disruption in the SkinBaR model can be controlled and that the SkinBaR model can be adjusted to match the desired lateral or

lamellar lipid organization. Therefore, the SkinBaR model offers the possibility to study the interaction of skin barrier repair formulations with the lipid matrix, in which the degree of deviation in lipid organization to that in healthy human skin can be adjusted on demand.

It is unknown how well the SkinBaR model reflects in detail the lipid properties in the regenerated SC in human skin *in vivo*. Hence, the lipid properties of the SkinBaR model were compared to those of *in vivo* skin after tape stripping. The studies are described in Chapter 4. The comparison focused on the CER composition (i.e. CER subclass, CER chain length, and degree of unsaturation), and lipid conformational ordering. Compared to control skin, in both models, levels of S subclass CERs (e.g. CER NS and CER AS, see Figure 1) were increased, whereas levels of P subclass CERs (e.g. CER NP, CER AP, and CER EOP, see Figure 1) were decreased. Furthermore, the mean ceramide chain length was decreased, and higher levels of CERs with i) a total chain length of 34 carbon atoms and/or ii) mono-unsaturation were observed. The lipid chains were less ordered in regenerated SC of the SkinBaR model, however, this was not statistically significant. Overall, changes in CER composition in the SkinBaR regenerated SC were more pronounced than changes in CER composition in the *in vivo* regenerated SC. The only pronounced difference between the models was the level of EO ceramides, which was decreased in the SkinBaR model and increased in the *in vivo* regenerated skin. Nevertheless, the lipid properties in both models mimicked quite closely the ceramide composition in AD, but also showed similarities with other inflammatory skin diseases. Therefore, the SkinBaR model and *in vivo* tape stripped healthy skin can serve as a first model to study skin barrier repair of compromised inflamed skin.

Application of VC based formulations on the skin barrier repair model

Since a VC based lipid formulation was shown to enhance skin barrier repair in mice models, this formulation was applied on the regenerating SC of the SkinBaR model. In Chapter 5 we focused on the interaction of the FA component incorporated in the VC based formulation and studied its interaction with the SC lipid matrix. FAs with a chain length of either 16, 18, or 22 carbon atoms were used in the formulation. The lipid organization and composition of the regenerated SC on which a formulation was applied immediately after stripping with cyanoacrylate were examined after regeneration. The applied formulations, especially when incorporating FA C18 and C22 resulted in an increase in the fraction of lipids adopting an orthorhombic packing. Deuterated FAs were used in order to i) distinguish between the FAs in the formulation from the endogenous FAs and ii) to examine whether FAs were partitioning in the same lattice as the SC lipids. The thermotropic behavior of the formulated deuterated FAs applied on the SC matched that of native SC, indicating that the deuterated FAs are incorporated in the SC lipid matrix. When focusing on the lateral lipid organization, the studies demonstrated that i) application of FAs with a longer chain length resulted in a higher fraction of lipids adopting an orthorhombic lateral packing, and ii) the applied deuterated FAs partitioned in one lattice with the SC lipids. Analyzing the FA composition with LC/MS showed that a fraction of the deuterated FAs with a chain length of 16 carbon atoms were elongated to mainly a chain length of 24 carbon

atoms. The studies described in this chapter demonstrate that the VC based formulation is able to improve the SC lipid properties of the *ex vivo* SkinBaR model.

Another important class of SC barrier lipids are CERs. In Chapter 6, studies are described in which CERs were used in the VC based formulation and applied on the SkinBaR model. CER subclasses NS and EOS were formulated, as well as a combination of both subclasses and FA with 16 carbon atoms. Compared to non-stripped and stripped control skin, application of the formulation with a single CER did not change the morphology of the cultured skin. A higher fraction of lipids adopted a dense orthorhombic lateral lipid packing when the formulation was applied, and CER EOS was more effective than CER NS. As CER NS was available with a deuterated acyl chain, interactions of deuterated CER NS with the SC lipid matrix were also studied, but no strong evidence could be obtained indicating that CER NS is incorporated in the lipid matrix. With regards to a formulation in which CER NS, CER EOS, and the FA were combined, interactions of these components with other lipids in the VC based formulation were examined. Interactions of CER NS with the other lipids of the formulation were observed as well as interactions of FA with the other formulation lipids. However, these studies revealed separate FA rich and CER NS rich domains. Applying the combined VC based formulation on regenerating SC resulted in participation of FA in the SC lipid matrix. When participation of CER NS from the combined formulation with the SC lipid matrix was examined, the thermotropic behavior of the formulation alone and the SC on which the formulation was applied were very similar. Therefore, changes in thermotropic behavior induced by application of CER NS (i.e. participation in the lipid matrix) could not be used to examine whether CER NS participated in the lipid matrix. As no deuterated CER EOS was available, it was not possible to determine participation of CER EOS in the SC lipid matrix. The lamellar organization of the SC lipids was not affected by application of either the formulations with a single CER or the formulation in which CER NS, CER EOS, and FA were combined. These results indicate that CERs enhance the fraction of lipids adopting a dense orthorhombic lateral packing and that the barrier lipids of the VC based formulation are, at least partly, incorporated in the SC lipid matrix. The VC based formulations might have the potential to restore a compromised skin barrier function as observed in inflammatory skin diseases.

Application of VC based formulations on human skin

As described above, tape-stripping and regeneration of healthy human skin *in vivo* resulted in i) increased levels of S subclass CERs, especially CER NS and CER AS, ii) decreased levels of P subclass CERs, especially CER NP, iii) a reduced mean chain length, iv) a higher level of CERs with a total chain length of 34 carbon atoms, and v) a higher fraction of mono-unsaturated CERs. In Chapter 7 studies are described in which a VC based formulation was applied on tape-stripped human skin *in vivo* during a regeneration period of 14 days. The formulation contained CER NS, CER EOS, and two FAs with chain lengths of 16 and 18 carbon atoms. The skin barrier repair was monitored over time for a tape-stripped treated and a tape-stripped non-treated site. For both sites and two control sites (treated and non-treated), the ceramide composition, lateral lipid ordering, and the lamellar lipid organization were examined. Accelerated

barrier repair was observed after application of the VC based formulation. Application of the VC based formulation resulted in a CER composition that was shifting toward the CER composition of the control sites. The shift was most pronounced for CERs with a chain length of C34 carbon atoms, the subclass CER AS (both reduced in relative amounts), and the average chain length (increase in chain length). Furthermore, a ratio dividing the CERs based on their synthesis route (e.g. (dS + P + H)/S) correlated with skin barrier function, with a higher ratio indicating a better barrier function. As the changes induced by tape-stripping of the skin were partially normalized by treatment with the VC based formulation indicating a positive effect of the formulation on the skin barrier, it is of interest to study its effect on the skin barrier in AD patients.

The promising results obtained after application of the VC based formulation on disrupted healthy skin justified application on naturally compromised skin of AD patients. A pilot study in which 8 moderate to severe AD patients were included is described in Chapter 8. The patients applied the formulation for 2 weeks, twice a day. The changes in disease activity, skin barrier function, ceramide composition, and lipid ordering were analyzed. After 2 weeks of treatment, the lipid ordering improved compared to control before treatment, indicating an improved skin barrier. For most patients, the transepidermal water loss decreased after applying the VC based formulation. Treatment did not affect the mean carbon chain length of the CERs, the level of CERs with 34 carbon atoms, and the level of mono-unsaturated CERs. The ratio between several CER subclasses ((dS + P + H)/S) showed a slight decrease. Overall, the lipid parameters highly correlated with transepidermal water loss and with each other. Some changes in parameters coincided for multiple patients, in that, if one was beneficial the other was as well: e.g. mean carbon chain length and level of EO CERs, CERs with 34 carbon atoms and transepidermal water loss, and level of mono-unsaturated CERs and lipid ordering. The clinical outcome, however, was negatively affected, and the severity of the AD at the start of the study was of influence on the skin barrier repair. Furthermore, the treatment affected each patient differently. Emollients could be helpful to treat AD, however, monotherapy with only a VC based formulation might not be sufficient in patients with moderate to severe AD.

Conclusions

The studies in this thesis describe the development of an *ex vivo* SkinBaR model and a novel VC based formulation to treat the skin of AD patients. We showed that the SkinBaR model is highly reproducible and the model can be used to mimic multiple degrees of skin barrier disruption. The SkinBaR model shows many parallels in lipid composition and organization with *in vivo* disrupted and regenerated skin and with that in AD skin. Application of a VC based formulation containing CERs and FAs resulted in a denser lipid organization in the SC of the SkinBaR model. Furthermore, in *in vivo* regenerated healthy human skin the VC based formulation enhanced skin barrier repair and reduced modulation in lipid composition induced by tape-stripping and SC regeneration. However, when applied as monotherapy on moderate to severe AD skin, the lipid ordering is positively affected, but limited changes in lipid composition were

observed. The overall disease activity was not influenced and the local disease severity was increased. The optimal treatment aiming to repair the skin barrier for moderate to severe AD skin needs further research.

Perspectives

Enhancement of the SkinBaR model

The SkinBaR model has been successfully developed to study the human skin barrier repair response. It is an easy to use model mimicking closely the lipid properties of AD skin. The SkinBaR model can be used to study the skin barrier repair response in *ex vivo* conditions, with a focus on the barrier lipid composition and organization. Furthermore, the effect of topical formulations on the intercellular lipid matrix can be studied. As discussed in Chapter 4, the *ex vivo* SkinBaR model shows many parallels with *in vivo* compromised skin.

Currently, the SkinBaR model reflects several aspects of AD skin. However, the ultimate goal is to have a SkinBaR model which reflects the lipid composition in healthy compromised human skin in clinical studies. However, there are several differences in the SkinBaR model compared to the compromised model *in vivo*. This is demonstrated by a substantially accelerated skin barrier repair response in the SkinBaR model compared to the *in vivo* compromised skin. This is demonstrated by a hyperproliferation indicated by a higher expression of Ki67, and more pronounced changes in the CER composition compared to *in vivo* compromised skin, especially the increase in ceramide subclass AS and NS, the level of CER with total chain length of 34 carbon atoms, and a reduction in subclass NP demonstrates an activation of the keratinocytes. In order to bring the SkinBaR model closer to the *in vivo* situation, changing the culturing conditions and environmental factors offer a suitable starting point. These are:

i) It is widely known that enzyme activity and expression are temperature dependent. In the skin, a temperature gradient exists from the core body temperature of 37˚C to the skin surface temperature of around 32˚C. This gradient might be essential for proper functioning of epidermal differentiating proteins and enzymes involved in lipid biosynthesis. A temperature gradient in the skin during culture might be obtained by maintaining the culture medium at 37˚C and reducing the environmental temperature to 32˚C, the skin surface temperature.

ii) Other factors that might influence the skin barrier repair process of the *ex vivo* cultured skin are relative humidity, UV light exposure, and physical stress. In the *in vivo* situation, the relative humidity to which the skin is exposed is much lower than in culturing conditions. Additionally, skin is exposed to a certain dose of UV light and physical stress (e.g. movement, washing, clothes) in real-life conditions. Implementing these factors during generation of the SC in the SkinBaR model might lead to a SC of the SkinBaR model mimicking the *in vivo* SC generation much closer.

iii) In the SkinBaR model common inflammatory responses that slow down the skin barrier repair in healthy compromised skin is partly lacking.[41] The inflammatory response can be established by supplementing cytokines to the medium of the SkinBaR model. For example, cytokines IL-1α and IL-6 attract immune cells to the injured site.
iv) During the culturing period, the medium composition changes because the skin uses the nutrients from the medium and releases the waste products into the medium. This may be improved by a flow through system of the medium mimicking more closely the *in vivo* situation.

Having a SkinBaR model which reflects healthy compromised human skin *in vivo*, offers a starting point to expand the use of the SkinBaR model to study detailed aspects of the skin barrier and the repair process:

i) The SkinBaR model could be used to study multiple other inflammatory skin diseases. Each inflammatory skin disease is characterized by a unique subset of changes compared to healthy human skin. These changes involve the lipid properties as well as protein expression and immunological aspects, e.g. upregulation of inflammatory cytokines.[42,43] Being able to mimic several aspects of inflammatory skin diseases in addition to the altered lipid properties induced by inflammation, may be achieved by adding pro-inflammatory cytokines to the culture medium. This may affect the morphology, enzyme expression, and lipid properties.[44] Mimicking these unique changes of each inflammatory skin disease offers the opportunity to develop disease-specific treatments tackling specific problems of the skin barrier repair response, such a disease-specific lipid composition and lipid ordering, reducing the inflammatory response, or influencing the expression and activity of specific proteins. These disease-specific treatments might involve topical formulations, but also medium supplements could be used to represent systemic treatment.
ii) Systemically circulating substances could potentially be of influence on regeneration of the SC. Therefore, adding those substances to the culture medium of the SkinBaR model allows us to examine the influence of the uptake of systemically circulating substances on the regenerated SC.

Improvement of the skin barrier repair formulation

The studies described in Chapter 5 and 6 of this thesis showed that the VC based formulation improves the lipid packing and that the applied FA with a chain length of 16 carbon atoms are elongated in the epidermis and therefore are part of the epidermal biosynthesis. Application on compromised healthy skin *in vivo* resulted in enhanced skin barrier repair. However, further improvement of the VC based formulation might be possible by changing the composition:

i) In AD skin, the level of CER subclass NS is increased and the levels of CER EOS and NP is decreased.[5,27,29,30,45,46] As described in Chapter 7, an increased CER subclass ratio ((dS+P+H)/S) correlated with an improved barrier function, indicating that increasing the relative level of CER NP in the SC might improve the skin barrier function. This novel information suggests that CER NP might

even be a better candidate to incorporate in the VC based formulation. However, due to its very stable crystal formation, CER NP is difficult to formulate. Natural VC consists of a combination of a large number of CER subclasses that are also present in human SC, including CERs NS, EOS, and NP and variations in CER chain length.[37] Perhaps changing the CER fraction of the VC based formulation by using various CER subclasses with a variation in chain length might improve the barrier repair potential of the formulation, but is not an easy task.

ii) FAs are another main lipid class in the SC lipid matrix. In healthy SC, FAs with a chain length of 24 and 26 carbon atoms are most abundant.[2-4] Unfortunately, these FAs were not available for clinical studies. Furthermore, FAs with a chain length of only 16 carbon atoms are most abundant in VC.[37] As the FA with 16 carbon atoms was elongated in the studies described in Chapter 5, this FA was used in the VC based formulation in the clinical settings. In AD skin, the average chain length of the lipids is reduced, and a higher abundance of FAs with 16 and 18 carbon atoms has been reported.[4] This might indicate that elongation of the FAs in AD skin is impaired.[47] Therefore, using FAs with longer chain lengths in the VC based formulation might be more beneficial in treating AD skin.

In the studies described in Chapter 8, the VC based formulation was applied on the skin of patients with moderate to severe AD and resulted in improvements in the lipid composition in some patients and improved lipid conformational ordering in most patients when applied on non-lesional skin. Unfortunately, the local disease severity did not improve, but this might be expected as the local disease severity is influenced by the overall disease severity and thus the degree of systemic inflammation. This might suggest that monotherapy with a VC based formulation is not sufficient. Therefore, in future it might be of interest to use this formulation in the treatment of patients with only mild AD skin or even dry skin. Another option is to investigate the use of this formulation to prevent the development of AD in those humans that have a high risk factor to develop AD.

References

1. Elias PM. Epidermal lipids, barrier function, and desquamation. *J Invest Dermatol* **1983**: 80: 44s-49s.
2. Norlen L, Nicander I, Lundsjo A, et al. A new HPLC-based method for the quantitative analysis of inner stratum corneum lipids with special reference to the free fatty acid fraction. *Arch Dermatol Res* **1998**: 290: 508-516.
3. Ansari MN, Nicolaides N, Fu HC. Fatty acid composition of the living layer and stratum corneum lipids of human sole skin epidermis. *Lipids* **1970**: 5: 838-845.
4. van Smeden J, Janssens M, Kaye EC, et al. The importance of free fatty acid chain length for the skin barrier function in atopic eczema patients. *Exp Dermatol* **2014**: 23: 45-52.
5. Janssens M, van Smeden J, Gooris GS, et al. Increase in short-chain ceramides correlates with an altered lipid organization and decreased barrier function in atopic eczema patients. *J Lipid Res* **2012**: 53: 2755-2766.
6. Wertz PW, Miethke MC, Long SA, et al. The composition of the ceramides from human stratum corneum and from comedones. *J Invest Dermatol* **1985**: 84: 410-412.
7. Ponec M, Weerheim A, Lankhorst P, et al. New acylceramide in native and reconstructed epidermis. *J Invest Dermatol* **2003**: 120: 581-588.
8. Masukawa Y, Narita H, Shimizu E, et al. Characterization of overall ceramide species in human stratum corneum. *J Lipid Res* **2008**: 49: 1466-1476.
9. Stewart ME, Downing DT. A new 6-hydroxy-4-sphingenine-containing ceramide in human skin. *J Lipid Res* **1999**: 40: 1434-1439.
10. Robson KJ, Stewart ME, Michelsen S, et al. 6-Hydroxy-4-sphingenine in human epidermal ceramides. *J Lipid Res* **1994**: 35: 2060-2068.
11. Farwanah H, Wohlrab J, Neubert RH, et al. Profiling of human stratum corneum ceramides by means of normal phase LC/APCI-MS. *Anal Bioanal Chem* **2005**: 383: 632-637.
12. van Smeden J, Hoppel L, van der Heijden R, et al. LC/MS analysis of stratum corneum lipids: ceramide profiling and discovery. *J Lipid Res* **2011**: 52: 1211-1221.
13. Rabionet M, Gorgas K, Sandhoff R. Ceramide synthesis in the epidermis. *Biochim Biophys Acta* **2014**: 1841: 422-434.
14. t'Kindt R, Jorge L, Dumont E, et al. Profiling and characterizing skin ceramides using reversed-phase liquid chromatography-quadrupole time-of-flight mass spectrometry. *Anal Chem* **2012**: 84: 403-411.
15. Groen D, Poole DS, Gooris GS, et al. Is an orthorhombic lateral packing and a proper lamellar organization important for the skin barrier function? *Biochim Biophys Acta* **2011**: 1808: 1529-1537.
16. McIntosh TJ, Stewart ME, Downing DT. X-ray diffraction analysis of isolated skin lipids: reconstitution of intercellular lipid domains. *Biochemistry* **1996**: 35: 3649-3653.
17. Janssens M, van Smeden J, Gooris GS, et al. Lamellar lipid organization and ceramide composition in the stratum corneum of patients with atopic eczema. *J Invest Dermatol* **2011**: 131: 2136-2138.
18. Hatta I, Ohta N, Inoue K, et al. Coexistence of two domains in intercellular lipid matrix of stratum corneum. *Biochim Biophys Acta* **2006**: 1758: 1830-1836.
19. Bouwstra JA, Gooris GS, van der Spek JA, et al. Structural investigations of human stratum corneum by small-angle X-ray scattering. *J Invest Dermatol* **1991**: 97: 1005-1012.
20. Damien F, Boncheva M. The extent of orthorhombic lipid phases in the stratum corneum determines the barrier efficiency of human skin in vivo. *J Invest Dermatol* **2010**: 130: 611-614.
21. de Jager M, Groenink W, Guivernau R, et al. A novel in vitro percutaneous penetration model: evaluation of barrier properties with p-aminobenzoic acid and two of its derivatives. *Pharm Res* **2006**: 23: 951-960.
22. Grubauer G, Feingold KR, Harris RM, et al. Lipid content and lipid type as determinants of the epidermal permeability barrier. *J Lipid Res* **1989**: 30: 89-96.
23. van Smeden J, Janssens M, Boiten WA, et al. Intercellular skin barrier lipid composition and organization in Netherton syndrome patients. *J Invest Dermatol* **2014**: 134: 1238-1245.
24. Motta S, Monti M, Sesana S, et al. Ceramide composition of the psoriatic scale. *Biochim Biophys Acta* **1993**: 1182: 147-151.
25. Motta S, Sesana S, Ghidoni R, et al. Content of the different lipid classes in psoriatic scale. *Arch Dermatol Res* **1995**: 287: 691-694.
26. van Smeden J, Janssens M, Gooris GS, et al. The important role of stratum corneum lipids for the cutaneous barrier function. *Biochim Biophys Acta* **2014**: 1841: 295-313.
27. Imokawa G, Abe A, Jin K, et al. Decreased level of ceramides in stratum corneum of atopic dermatitis: an etiologic factor in atopic dry skin? *J Invest Dermatol* **1991**: 96: 523-526.
28. Ishikawa J, Narita H, Kondo N, et al. Changes in the ceramide profile of atopic dermatitis patients. *J Invest Dermatol* **2010**: 130: 2511-2514.
29. Yamamoto A, Serizawa S, Ito M, et al. Stratum corneum lipid abnormalities in atopic dermatitis. *Arch Dermatol Res* **1991**: 283: 219-

223.
30. Bleck O, Abeck D, Ring J, et al. Two ceramide subfractions detectable in Cer(AS) position by HPTLC in skin surface lipids of non-lesional skin of atopic eczema. *J Invest Dermatol* **1999**: 113: 894-900.
31. Pilgram GS, Vissers DC, van der Meulen H, et al. Aberrant lipid organization in stratum corneum of patients with atopic dermatitis and lamellar ichthyosis. *J Invest Dermatol* **2001**: 117: 710-717.
32. Chong M, Fonacier L. Treatment of Eczema: Corticosteroids and Beyond. *Clin Rev Allergy Immunol* **2016**: 51: 249-262.
33. Coderch L, Lopez O, de la Maza A, et al. Ceramides and skin function. *Am J Clin Dermatol* **2003**: 4: 107-129.
34. Chiou YB, Blume-Peytavi U. Stratum corneum maturation. A review of neonatal skin function. *Skin Pharmacol Physiol* **2004**: 17: 57-66.
35. Haubrich KA. Role of Vernix caseosa in the neonate: potential application in the adult population. *AACN Clin Issues* **2003**: 14: 457-464.
36. Hoath SB, Pickens WL, Visscher MO. The biology of vernix caseosa. *Int J Cosmet Sci* **2006**: 28: 319-333.
37. Rissmann R, Groenink HW, Weerheim AM, et al. New insights into ultrastructure, lipid composition and organization of vernix caseosa. *J Invest Dermatol* **2006**: 126: 1823-1833.
38. Oudshoorn MH, Rissmann R, van der Coelen D, et al. Effect of synthetic vernix biofilms on barrier recovery of damaged mouse skin. *Exp Dermatol* **2009**: 18: 695-703.
39. Oudshoorn MH, Rissmann R, van der Coelen D, et al. Development of a murine model to evaluate the effect of vernix caseosa on skin barrier recovery. *Exp Dermatol* **2009**: 18: 178-184.
40. Visscher MO, Barai N, LaRuffa AA, et al. Epidermal barrier treatments based on vernix caseosa. *Skin Pharmacol Physiol* **2011**: 24: 322-329.
41. Lin TK, Zhong L, Santiago JL. Anti-Inflammatory and Skin Barrier Repair Effects of Topical Application of Some Plant Oils. *International journal of molecular sciences* **2017**: 19.
42. Bieber T, Novak N. Pathogenesis of atopic dermatitis: new developments. *Current allergy and asthma reports* **2009**: 9: 291-294.
43. Kim BE, Leung DYM. Significance of Skin Barrier Dysfunction in Atopic Dermatitis. *Allergy, asthma & immunology research* **2018**: 10: 207-215.
44. Danso MO, van Drongelen V, Mulder A, et al. TNF-alpha and Th2 cytokines induce atopic dermatitis-like features on epidermal differentiation proteins and stratum corneum lipids in human skin equivalents. *The Journal of investigative dermatology* **2014**: 134: 1941-1950.
45. Di Nardo A, Wertz P, Giannetti A, et al. Ceramide and cholesterol composition of the skin of patients with atopic dermatitis. *Acta Derm Venereol* **1998**: 78: 27-30.
46. Jungersted JM, Scheer H, Mempel M, et al. Stratum corneum lipids, skin barrier function and filaggrin mutations in patients with atopic eczema. *Allergy* **2010**: 65: 911-918.
47. Danso M, Boiten W, van Drongelen V, et al. Altered expression of epidermal lipid biosynthesis enzymes in atopic dermatitis skin is accompanied by changes in stratum corneum lipid composition. *Journal of dermatological science* **2017**: 88: 57-66.
48. Orton DI, Wilkinson JD. Cosmetic allergy: incidence, diagnosis, and management. *American journal of clinical dermatology* **2004**: 5: 327-337.

Appendices

Nederlandstalige samenvatting

Introductie

De huid is ontworpen om het lichaam te beschermen tegen invloeden van buitenaf. Hierdoor wordt het binnendringen van ziekteverwekkers, allergenen en irriterende stoffen beperkt. De huid bestaat uit drie lagen: het onderhuidse vetweefsel (ook wel hypodermis genoemd), de lederhuid (de dermis) en de opperhuid (de epidermis) met huidcellen die keratinocyten genoemd worden. Dit wordt schematisch weergegeven in Figuur 1A. De epidermis is onderverdeeld in 4 lagen, waarvan de hoornlaag de buitenste laag is. De hoornlaag wordt ook wel het stratum corneum (SC) genoemd. Het SC bestaat voornamelijk uit dode huidcellen (corneocyten) die worden omsloten door een lipidenmatrix (vetten). De structuur van het SC lijkt op een gemetselde muur waarin de corneocyten de stenen zijn en de lipidenmatrix het cement (Figuur 1B).[1] Deze intercellulaire lipiden vormen een belangrijke penetratieroute door het SC. In de levende epidermis worden de lipiden opgeslagen in keratinocyten en aan het grensvlak van de levende epidermis en het SC worden ze uitgescheiden.

De drie hoofdklassen van de lipiden in het SC zijn vetzuren, ceramiden en cholesterol. Vetzuren en ceramiden hebben beide een grote variatie in lengte van de koolstofketens. Naast verzadigde koolstofketens, zijn ook ceramiden en vetzuren met een onverzadigde koolstofketen aanwezig.[2-5] Ten minste 18 ceramide subklassen zijn inmiddels geïdentificeerd. De indeling in subklassen is gebaseerd op hun chemische structuur.[6-14] Een ceramide bestaat uit een sfingosine en een vetzuurketen (ook wel acylketen genoemd), zoals weergegeven in Figuur 2. Een bijzondere groep ceramiden zijn die van de subklassen EO en O. Deze EO en O ceramiden hebben een extra vetzuur, waardoor deze ceramiden een zeer lange koolstofketen hebben. De lipiden in de matrix van het SC zijn georganiseerd in gestapelde lipidenlagen, ook wel de lamellaire lipidenstructuur genoemd. De lagen in de lamellaire structuur herhalen zich over een afstand van 6 of 13 nanometer, die respectievelijk de SPP (short periodicity phase) en de LPP (long periodicity phase) genoemd worden (Figuur 1E).[15-19] Binnen deze lipidenlagen zijn de lipiden geordend met een bepaalde dichtheid: de laterale lipidenorganisatie. Het overgrote deel van de lipiden is zeer compact geordend, dit wordt een orthorombische organisatie genoemd. Een kleinere fractie is geordend in een minder compacte structuur, dit wordt een hexagonale organisatie genoemd. Wanneer de lipiden nog minder geordend zijn, bevinden ze zich in een vloeibare structuur (Figuur 1F). Zowel de aanwezigheid van een orthorombische structuur als de aanwezigheid van de long periodicity phase zijn belangrijk voor de barrièrefunctie van de huid. De samenstelling van de ceramiden en vetzuren heeft hier een grote invloed op.[15,20-22]

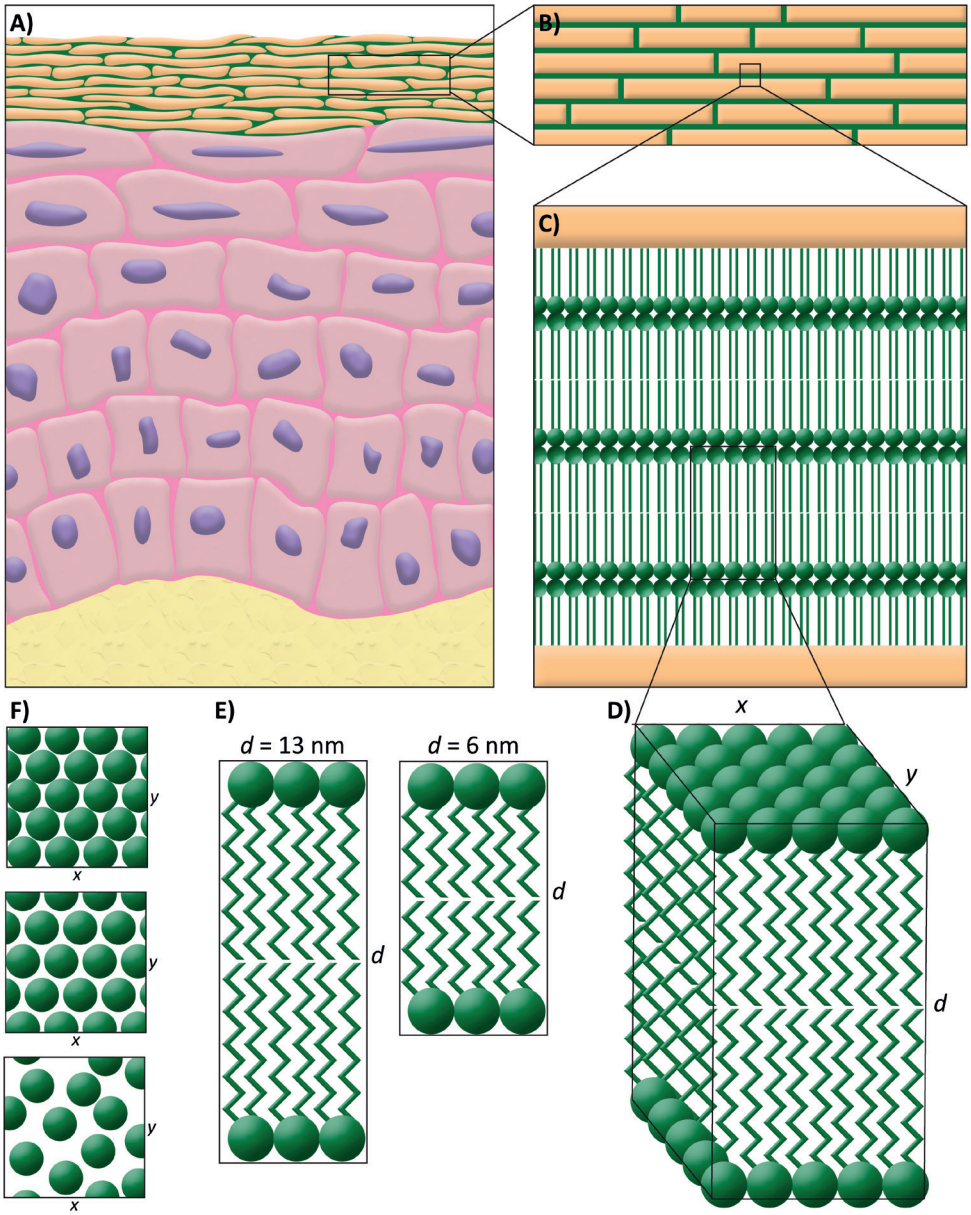

Figuur 1. Organisatie van de lipiden in de SC lipidenmatrix. A) Schematisch overzicht van de structuur van de opperhuid. **B)** De structuur van het SC lijkt op een gemetselde muur waarin de corneocyten de stenen zijn en de lipidenmatrix het cement. **C)** De lipiden in de matrix zijn op elkaar gestapeld en deze lagen worden lamellen genoemd. **D)** De lipidenlamellen in meer detail. **E)** De lengte (d) waarover zich de structuur herhaald wordt de repetitieafstand genoemd. In SC zijn de lange periodiciteitsfase (13 nm) en de korte periodiciteitsfase (6 nm) aanwezig . **F)** Binnen deze lamellaire structuur zijn de lipiden geordend in een laterale organisatie. De laterale organisatie kan een hoge dichtheid hebben (orthorombisch), een iets lagere dichtheid (hexagonaal) of een nog lagere dichtheid hebben (vloeibare fase). Deze zijn van boven naar beneden weergeven.

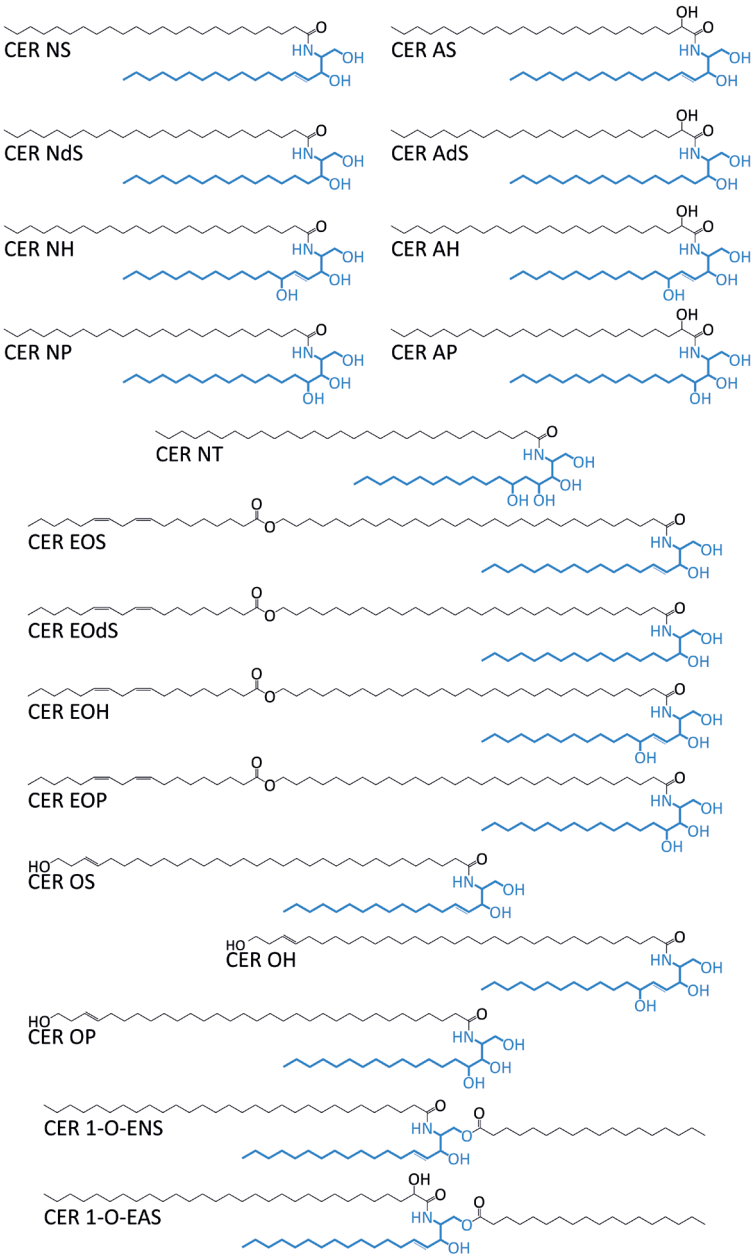

Figuur 2. Ceramide subklassen in de SC lipidenmatrix. Ceramiden bestaan uit een sfingosine (weergegeven in blauwe kleur) gekoppeld aan een vetzuur (weergegeven in zwart), die beide in moleculaire structuur kunnen variëren. De moleculaire structuur van de ceramiden bepaalt de naam. De vetzuurketen kan ofwel niet-gehydroxyleerd (N), α-gehydroxyleerd (A), ω-gehydroxyleerd (O), of veresterd ω-gehydroxyleerd (EO) zijn, terwijl de sfingosinketen ofwel een sfingosine (S), dihydrosfingosine (dS), fytosfingosine (P), 6-hydroxysfingosine (H) of dihydroxy dihydrosfingosine (T) is.

Bij huidziekten waarbij de huid ontstoken is, is de barrièrefunctie van de huid vaak verminderd. Deze huidziekten worden ook wel inflammatoire huidziekten genoemd. Alhoewel de onderliggende factor(en) van deze inflammatoire huidziekten per ziekte verschilt, zijn de veranderingen in de lipidensamenstelling erg vergelijkbaar. Deze veranderingen zijn bijvoorbeeld een verhoogde aanwezigheid van ceramide subklasse NS, verlaagde aanwezigheid van ceramide subklassen NP en EOS, een verhoogde fractie lipiden met onverzadigde koolstofketens, en een kortere gemiddelde ketenlengte van de ceramiden en vetzuren. Deze veranderingen in lipidensamenstelling kunnen leiden tot een minder geordende laterale lipidenorganisatie en een verandering in de lamellaire structuur.[4,5,17,23-31] De barrièrefunctie van de huid is het meest uitgebreid onderzocht in patiënten met constitutioneel eczeem (ook wel atopisch eczeem of atopische dermatitis (AD) genoemd). Veel studies richtten zich op het effect van mogelijke behandelmethoden. Ondanks deze inzet is de behandeling van AD nog steeds niet optimaal: corticosteroïden worden gebruikt om de ontstekingsreactie te remmen, maar ze hebben ook bijwerkingen zoals een dunner wordende huid.[32] Om de opname in de huid van allerlei ongewenste stoffen te verminderen en daarbij de kans op ontsteking te verkleinen, is lokale behandeling van de huid met huideigen barrièrelipiden een aantrekkelijke aanpak.[33]

Vernix caseosa (VC) is een witte, water bevattende, vettige substantie die op de huid van baby's aanwezig is. VC beschermt de baby zowel in het laatste trimester van de zwangerschap als ook tijdens de geboorte.[34-36] VC bestaat uit de barrièrelipiden ceramiden, vetzuren en cholesterol in ongeveer dezelfde samenstelling als aanwezig is in het SC, maar ook andere lipiden zoals squaleen, waxesters, sterolesters, triglyceriden en fosfolipiden zijn aanwezig.[36,37] Uit studies met muizen blijkt dat het barrièreherstel van de huid gestimuleerd wordt na behandeling met VC in vergelijking met onbehandelde huid. In het lab werd een formulering ontwikkeld die veel aspecten van de natuurlijke VC nabootst. Ook na behandeling met deze formulering werd het barrièreherstel van de muizenhuid gestimuleerd.[38,39] Alhoewel, het herstel van de huidbarrière in dierenhuid anders is dan het herstel in menselijke huid, was dit een belangrijke waarneming.[40]
Het kweken van *in vitro* huidmodellen (bijv. humane huid equivalenten) is arbeidsintensief en tijdrovend. Minder tijdrovende huidmodellen die het herstel van de huidbarrière in de menselijke huid *in vivo* ('in het lichaam') nauwkeurig nabootsen zijn daarom erg aantrekkelijk. Vooral als het gaat om huidmodellen die de barrièreeigenschappen van AD of andere inflammatoire huidziekten nabootsen.

Doel

Het doel van het onderzoek beschreven in dit proefschrift was tweeledig. Ten eerste, bepalen of een formulering gebaseerd op VC effectief het barrièreherstel van huid van AD patiënten kan bevorderen. Ten tweede, bepalen of deze formulering de lipidensamenstelling en –organisatie in het SC kan normaliseren. Om deze doelen te bereiken zijn de volgende studies uitgevoerd:

1. Een *ex vivo* ('buiten het lichaam') huidmodel werd ontwikkeld specifiek om het barrièreherstel te onderzoeken (SkinBaR model). Hiertoe werd SC van de huid verwijderd, waarna SC door de huid werd geregenereerd onder gecontroleerde kweekcondities. Om de gelijkenis van het model te testen werd de lipidensamenstelling en –organisatie in hersteld (geregenereerd) SC van het SkinBaR model vergeleken met die in geregenereerd SC *in vivo* menselijke huid, waarvan het SC ook was verwijderd.
2. Het SkinBaR model werd vervolgens gebruikt om het effect van de formulering gebaseerd op VC op het barrièreherstel te onderzoeken. Hierbij werd vooral de interacties tussen een aantal geselecteerde vetzuren en/of ceramiden subklassen van de VC formulering en de SC lipidenmatrix onderzocht.
3. Het effect van de formulering gebaseerd op VC op huidbarrièreherstel in gezonde huid waarvan het SC verwijderd was werd onderzocht. Tenslotte werd het effect van de formulering op het barrièreherstel in huid van AD patiënten onderzocht.

Ontwikkeling van een huidbarrièreherstel model

Momenteel zijn er geen geschikte *in vitro* modellen beschikbaar om het huidbarrièreherstel te onderzoeken. Het genereren van humane huid equivalenten is erg arbeidsintensief en daarom minder aantrekkelijk. In het onderzoek beschreven in Hoofdstuk 2 werd daarom een nieuw model ontwikkeld om huidbarrièreherstel te meten (het SkinBaR model). In dit model werd SC van de huid verwijderd door middel van 'strippen' met cyanoacrylaat (secondelijm). Uit resultaten bleek dat de huid zich actief ontwikkelde en differentieerde, wat resulteerde in het herstel van het SC. Tevens werd de lipidensamenstelling en –organisatie in het SC onderzocht De samenstelling van de lipiden in het geregenereerde SC was veranderd en de lipiden waren voornamelijk hexagonaal geordend. Dit in tegenstelling tot de oorspronkelijk gezonde huid waarin de lipiden voornamelijk een orthorombische structuur vormden. De veranderingen in de samenstelling en organisatie van de lipiden leken veel op de lipidenorganisatie en samenstelling in SC van AD patiënten. Dit betekent dat het SkinBaR model een eerste indicatie kan geven of formuleringen het huidbarrièreherstelproces kunnen beïnvloeden en of de formuleringen geschikt zouden kunnen zijn voor het barrièreherstel van de huid van AD patiënten.

In Hoofdstuk 3 werd onderzocht of de hoeveelheid verwijderd SC invloed heeft op het barrièreherstel van het SkinBaR model. Uit de resultaten bleek dat verwijdering van 25%, 50% of 75% van het SC, het totale aantal cellagen in het SC na 8 dagen kweken

niet beïnvloedde. Grote verschillen in de structuur van de epidermis, zoals celkernen in de dode cellen (parakeratosis) en een verandering in de lamellaire structuur, werden alleen waargenomen wanneer 75% van het SC was verwijderd. Met betrekking tot de laterale lipidenstructuur bleek, dat wanneer er geleidelijk meer SC verwijderd was, de lipidenorganisatie geleidelijk minder dicht georganiseerd was in het geregenereerde SC. De ordening van de lipiden was alleen veranderd nadat minstens 50% van het SC was verwijderd. Hieruit blijkt dat de mate van verstoring van de lipidenorganisatie in de huidbarrière van het SkinBaR model gecontroleerd veranderd kan worden en dat het SkinBaR model aangepast kan worden aan de gewenste laterale of lamellaire lipidenstructuur om formuleringen te testen. Het SkinBaR model biedt dus de mogelijkheid om de wisselwerking van huidbarrièreherstelformuleringen met de lipidenmatrix te onderzoeken, waarin de mate van afwijking in lipidenorganisatie ten opzichte van gezonde huid naar wens kan worden aangepast.

Het is onbekend in welke mate het SC van het SkinBaR model het geregenereerde SC nabootst van *in vivo* menselijke huid waarvan het SC verwijderd was. Dit is interessant om te onderzoeken omdat de barrièrefunctie van gestripte en herstelde *in vivo* huid wel als model gebruikt wordt voor inflammatoire huidziekten. Om dit te onderzoeken zijn de SC lipideneigenschappen van het SkinBaR model vergeleken met die van *in vivo* huid na het strippen en regeneratie van het SC. Deze studies zijn beschreven in Hoofdstuk 4. Vooral de lipiden in het SC werden onderzocht, zoals de ceramide subklasse samenstelling, ceramide ketenlengte, mate van onverzadiging van de ceramiden en de lipidenordering. In beide modellen waren de S subklasse ceramiden (bijv. ceramide NS en ceramide AS, zie Figuur 2) verhoogd t.o.v. de controles (niet gestripte huid). Tevens bleek dat de P subklasse ceramiden (bijv. ceramide NP, ceramide AP en ceramide EOP, zie Figuur 2) juist verlaagd waren. Daarnaast was de gemiddelde ketenlengte van de ceramiden korter. Hiervoor was vooral een grotere aanwezigheid van ceramiden met een totale ketenlengte van 34 koolstofatomen verantwoordelijk. Ten slotte was de fractie enkelvoudig onverzadigde ceramiden verhoogd. Het bleek dat in het geregenereerde SC *in vitro* de lipidenketens minder goed geordend waren dan in geregenereerd SC *in vivo,* alhoewel dit niet statistisch significant was. In het algemeen waren de veranderingen in de ceramidensamenstelling van het geregenereerde SC van het SkinBaR model meer uitgesproken dan de veranderingen in de ceramidensamenstelling van het geregenereerde SC *in vivo,* maar wel vergelijkbaar. De enige opvallende tegenstelling tussen beide modellen was de fractie EO ceramiden. Deze fractie was verlaagd in het SkinBaR model en verhoogd in het geregenereerde SC *in vivo*. Desalniettemin bootsten beide modellen de ceramidesamenstelling in SC van AD na, maar ook overeenkomsten in lipidensamenstelling met andere inflammatoire huidziekten werden gevonden. Daarom kunnen zowel het SkinBaR model als *in vivo* strippen met tape dienen als een eerste model om te voorspellen of formuleringen geschikt zouden kunnen zijn voor barrièreherstel van aangedane en ontstoken huid.

De interactie van formuleringen gebaseerd op VC met het SkinBaR model

Omdat de formulering gebaseerd op VC een sneller herstel van de huidbarrière in muizen tot gevolg had, is deze formulering aangebracht op het SkinBaR model direct na strippen. In Hoofdstuk 5 zijn studies beschreven waarin de interactie van vetzuren in de formulering met de SC lipidenmatrix werd onderzocht. De vetzuren die gebruikt werden, hadden een ketenlengte van 16, 18 of 22 koolstofatomen. De lipidenorganisatie en –samenstelling van het gegenereerde SC werden gemeten. De aangebrachte formuleringen, voornamelijk die waarin vetzuren met 18 of 22 koolstofatomen verwerkt waren, verhoogden de fractie lipiden die zich in de orthorombische fase bevinden. Dezelfde studies zijn ook uitgevoerd met gedeutereerde vetzuren, d.w.z. vetzuren waarbij de waterstofatomen in de koolstofketen vervangen zijn door deuterium. Gedeutereerde vetzuren zijn gebruikt i) om onderscheid te kunnen maken tussen vetzuren uit de formulering en huideigen vetzuren, en ii) om te kunnen onderzoeken of de vetzuren uit de formulering opgenomen worden in de structuur gevormd door de SC lipiden. Het temperatuurafhankelijke gedrag van de op de huid opgebrachte gedeutereerde vetzuren kwam overeen met het temperatuurafhankelijke gedrag van de lipiden in het controle SC (niet gestript, niet gekweekt) zonder formulering. Dit was een eerste aanwijzing dat de gedeutereerde vetzuren opgenomen worden in de lipidenmatrix van het geregenereerde SC. Betreffende de laterale lipidenorganisatie, bleek uit de studies dat i) het aanbrengen van vetzuren met een langere koolstofketen resulteerde in een grotere fractie lipiden die een orthorombische fase vormen en ii) de aangebrachte gedeutereerde vetzuren opgenomen worden in de SC lipidenmatrix. Uit de analyse van de vetzuren met massaspectrometrie (techniek gebruikt om de lipidensamenstelling te meten) bleek dat een gedeelte van de gedeutereerde vetzuren met een ketenlengte van 16 koolstofatomen werd verlengd tot een ketenlengte van voornamelijk 24 koolstofatomen. Uit de studies blijkt dat de formulering gebaseerd op VC de SC lipideneigenschappen van het *ex vivo* SkinBaR model verbeterde.

Een andere belangrijke klasse barrièrelipiden zijn de ceramiden. In Hoofdstuk 6 worden studies beschreven waarin ceramiden gebruikt zijn in de formulering gebaseerd op VC. Ceramide subklassen NS en EOS werden in de formulering gebruikt, maar ook een combinatie van beide subklassen en het vetzuur met 16 koolstofatomen. Door vergelijken van niet gestripte huid en gestripte controlehuid (geen formulering gebruikt) bleek de structuur van de huid niet te veranderen na het aanbrengen van de formulering met een enkele ceramide subklasse tijdens het herstel. De fractie lipiden in de orthorombische fase in het SC was hoger na het aanbrengen van de formulering, en ceramide subklasse EOS was effectiever in het verhogen van de fractie lipiden die een orthorombische fase vormen dan subklasse NS. Omdat ceramide subklasse NS ook beschikbaar is met een gedeutereerde vetzuurketen konden de interacties tussen gedeutereerd ceramide NS en de SC lipidenmatrix in meer detail worden onderzocht. Uit de resultaten konden we echter niet de conclusie trekken dat NS werd opgenomen in de lipidenmatrix. Vervolgens werd de formulering onderzocht waarin zowel ceramide subklassen NS en EOS en het vetzuur aanwezig waren. Zowel ceramide NS als het vetzuur gingen interacties aan met de andere lipiden in de formulering. Deze studies lieten ook zien dat er vetzuurrijke en ceramiderijke domeinen in de

formulering aanwezig waren. Deze gecombineerde formulering werd ook op de gestripte huid aangebracht. Het bleek dat de vetzuren van deze formulering in de SC lipidenmatrix werden opgenomen. Er kon echter niet onderzocht worden of de opname van ceramide subklasse NS plaats vond, omdat het temperatuursafhankelijke gedrag van de geregenereerde huid en de VC formulering te veel op elkaar leken. De lamellaire organisatie in de SC lipiden matrix werd niet beïnvloed door het aanbrengen van een formulering. Uit deze resultaten blijkt dat de ceramiden in de formulering de vorming van de orthorombische fase bevorderen en dat de lipiden in de formulering (ten minste gedeeltelijk) worden opgenomen in de SC lipidenmatrix. Dit geeft aan dat de formulering gebaseerd op VC een interessante kandidaat is om de aangedane huidbarrièrefunctie, zoals in inflammatoire huidziekten, te herstellen.

Het testen van de formuleringen op menselijke huid in vivo

Zoals hierboven beschreven is in hoofdstuk 4, resulteerde het strippen van menselijke huid *in vivo* met tape in i) een grotere fractie van S subklasse ceramiden, voornamelijk ceramiden NS, AS en EOS, ii) een kleinere fractie van P subklasse ceramiden, voornamelijk ceramide NP, iii) een kortere gemiddelde ketenlengte, iv) een grotere fractie van ceramiden met een totale ketenlengte van 34 koolstofatomen en v) een grotere fractie van onverzadigde ceramiden. In Hoofdstuk 7 zijn studies beschreven waarin de formulering gebaseerd op VC aangebracht werd op *in vivo* gestripte gezonde menselijke huid tijdens een herstelperiode van 14 dagen. De formulering bevatte ceramiden subklassen NS en EOS en twee vetzuren met ketenlengtes van 16 en 18 koolstofatomen. Het huidbarrièreherstel van een gestripte behandelde plek en een gestripte niet-behandelde plek werd in de tijd gevolgd. Voor beide plekken en twee controle plekken (behandeld en niet-behandeld) werd de ceramidensamenstelling, de laterale lipidenorganisatie en de lamellaire lipidenorganisatie onderzocht. Het aanbrengen van de formulering resulteerde in een versneld herstel van de huidbarrière. Daarnaast was de ceramidensamenstelling van de herstelde huid na het aanbrengen van de formulering veranderd en gedeeltelijk genormaliseerd t.o.v. de gestripte en geregenereerde huid zonder formulering. Deze verschuiving was het meest zichtbaar bij de ceramiden met een totale ketenlengte van 34 koolstofatomen, de ceramide subklasse AS (beide afgenomen in relatieve hoeveelheden) en de gemiddelde ketenlengte (toename in ketenlengte). Daarnaast was de verhouding die ceramiden subklassen verdeeld op basis van hun synthese route ((dS + P + H)/S) hoger. De formulering had een positief effect op het huidbarrièreherstel. Daarom is het zeer interessant om het effect van de formulering op de huid van AD patiënten te onderzoeken.

De veelbelovende resultaten die verkregen werden na het aanbrengen van de formulering gebaseerd op VC op gezonde huid met een verminderde barrièrefunctie rechtvaardigde het testen van de formulering op de huid van AD patiënten met een verminderde barrièrefunctie. Een verkenningsstudie waarin patiënten met matig tot ernstig AD mee deden is beschreven in Hoofdstuk 8. De patiënten smeerden de formulering 2 weken lang, twee keer per dag. De veranderingen in de huidbarrièrefunctie, ceramidensamenstelling, lipidenordening en ziekteactiviteit werden geanalyseerd. Na

een behandeling van 2 weken was de lipidenorganisatie verbeterd vergeleken met de huid voor de behandeling. Voor de meeste patiënten was het waterverlies door de huid verlaagd na behandeling met de formulering gebaseerd op VC. De gemiddelde ketenlengte van de ceramiden, de fractie ceramiden met een ketenlengte van 34 koolstofatomen en de fractie onverzadigde ceramiden waren niet beïnvloed door de behandeling. De verhouding tussen de ceramiden subklassen ((dS + P + H)/S) was licht verlaagd. Over het algemeen waren er verbanden tussen lipidenvariabelen en het waterverlies door de huid. Sommige veranderingen gaven hetzelfde verband voor meerdere patiënten. Als de ene parameter verbeterd werd, was ook de andere verbeterd, bijvoorbeeld: de gemiddelde ketenlengte en de fractie EO ceramiden, ceramiden met een ketenlengte van 34 koolstofatomen was gerelateerd aan het waterverlies door de huid, en de fractie onverzadigde ceramiden en de laterale lipidenorganisatie. De klinische uitkomst werd echter negatief beïnvloed door het aanbrengen van de formulering. De mate waarin AD zich manifesteerde aan het begin van de studie had invloed op het huidbarrièreherstel. Dit laatste is een indicatie dat systemische ontsteking ook een rol speelt in het barrièreherstel. Daarnaast werd elke patiënt anders beïnvloed door de behandeling. De formulering gebaseerd op VC zou bevorderlijk kunnen zijn voor de behandeling van AD, maar het gebruik van enkel de formulering is niet voldoende als therapie voor patiënten met matig tot ernstig AD.

Referenties

1. Elias PM. Epidermal lipids, barrier function, and desquamation. *J Invest Dermatol* **1983**: 80: 44s-49s.
2. Norlen L, Nicander I, Lundsjo A, et al. A new HPLC-based method for the quantitative analysis of inner stratum corneum lipids with special reference to the free fatty acid fraction. *Arch Dermatol Res* **1998**: 290: 508-516.
3. Ansari MN, Nicolaides N, Fu HC. Fatty acid composition of the living layer and stratum corneum lipids of human sole skin epidermis. *Lipids* **1970**: 5: 838-845.
4. van Smeden J, Janssens M, Kaye EC, et al. The importance of free fatty acid chain length for the skin barrier function in atopic eczema patients. *Exp Dermatol* **2014**: 23: 45-52.
5. Janssens M, van Smeden J, Gooris GS, et al. Increase in short-chain ceramides correlates with an altered lipid organization and decreased barrier function in atopic eczema patients. *J Lipid Res* **2012**: 53: 2755-2766.
6. Wertz PW, Miethke MC, Long SA, et al. The composition of the ceramides from human stratum corneum and from comedones. *J Invest Dermatol* **1985**: 84: 410-412.
7. Ponec M, Weerheim A, Lankhorst P, et al. New acylceramide in native and reconstructed epidermis. *J Invest Dermatol* **2003**: 120: 581-588.
8. Masukawa Y, Narita H, Shimizu E, et al. Characterization of overall ceramide species in human stratum corneum. *J Lipid Res* **2008**: 49: 1466-1476.
9. Stewart ME, Downing DT. A new 6-hydroxy-4-sphingenine-containing ceramide in human skin. *J Lipid Res* **1999**: 40: 1434-1439.
10. Robson KJ, Stewart ME, Michelsen S, et al. 6-Hydroxy-4-sphingenine in human epidermal ceramides. *J Lipid Res* **1994**: 35: 2060-2068.
11. Farwanah H, Wohlrab J, Neubert RH, et al. Profiling of human stratum corneum ceramides by means of normal phase LC/APCI-MS. *Anal Bioanal Chem* **2005**: 383: 632-637.
12. van Smeden J, Hoppel L, van der Heijden R, et al. LC/MS analysis of stratum corneum lipids: ceramide profiling and discovery. *J Lipid Res* **2011**: 52: 1211-1221.
13. Rabionet M, Gorgas K, Sandhoff R. Ceramide synthesis in the epidermis. *Biochim Biophys Acta* **2014**: 1841: 422-434.
14. t'Kindt R, Jorge L, Dumont E, et al. Profiling and characterizing skin ceramides using reversed-phase liquid chromatography-quadrupole time-of-flight mass spectrometry. *Anal Chem* **2012**: 84: 403-411.
15. Groen D, Poole DS, Gooris GS, et al. Is an orthorhombic lateral packing and a proper lamellar organization important for the skin barrier function? *Biochim Biophys Acta* **2011**: 1808: 1529-1537.
16. McIntosh TJ, Stewart ME, Downing DT. X-ray diffraction analysis of isolated skin lipids: reconstitution of intercellular lipid domains. *Biochemistry* **1996**: 35: 3649-3653.
17. Janssens M, van Smeden J, Gooris GS, et al. Lamellar lipid organization and ceramide composition in the stratum corneum of patients with atopic eczema. *J Invest Dermatol* **2011**: 131: 2136-2138.
18. Hatta I, Ohta N, Inoue K, et al. Coexistence of two domains in intercellular lipid matrix of stratum corneum. *Biochim Biophys Acta* **2006**: 1758: 1830-1836.
19. Bouwstra JA, Gooris GS, van der Spek JA, et al. Structural investigations of human stratum corneum by small-angle X-ray scattering. *J Invest Dermatol* **1991**: 97: 1005-1012.
20. Damien F, Boncheva M. The extent of orthorhombic lipid phases in the stratum corneum determines the barrier efficiency of human skin in vivo. *J Invest Dermatol* **2010**: 130: 611-614.
21. de Jager M, Groenink W, Guivernau R, et al. A novel in vitro percutaneous penetration model: evaluation of barrier properties with p-aminobenzoic acid and two of its derivatives. *Pharm Res* **2006**: 23: 951-960.
22. Grubauer G, Feingold KR, Harris RM, et al. Lipid content and lipid type as determinants of the epidermal permeability barrier. *J Lipid Res* **1989**: 30: 89-96.
23. van Smeden J, Janssens M, Boiten WA, et al. Intercellular skin barrier lipid composition and organization in Netherton syndrome patients. *J Invest Dermatol* **2014**: 134: 1238-1245.
24. Motta S, Monti M, Sesana S, et al. Ceramide composition of the psoriatic scale. *Biochim Biophys Acta* **1993**: 1182: 147-151.
25. Motta S, Sesana S, Ghidoni R, et al. Content of the different lipid classes in psoriatic scale. *Arch Dermatol Res* **1995**: 287: 691-694.
26. van Smeden J, Janssens M, Gooris GS, et al. The important role of stratum corneum lipids for the cutaneous barrier function. *Biochim Biophys Acta* **2014**: 1841: 295-313.
27. Imokawa G, Abe A, Jin K, et al. Decreased level of ceramides in stratum corneum of atopic dermatitis: an etiologic factor in atopic dry skin? *J Invest Dermatol* **1991**: 96: 523-526.
28. Ishikawa J, Narita H, Kondo N, et al. Changes in the ceramide profile of atopic dermatitis patients. *J Invest Dermatol* **2010**: 130: 2511-2514.
29. Yamamoto A, Serizawa S, Ito M, et al. Stratum corneum lipid abnormalities in atopic dermatitis. *Arch Dermatol Res* **1991**: 283: 219-

223.
30. Bleck O, Abeck D, Ring J, et al. Two ceramide subfractions detectable in Cer(AS) position by HPTLC in skin surface lipids of non-lesional skin of atopic eczema. *J Invest Dermatol* **1999**: 113: 894-900.
31. Pilgram GS, Vissers DC, van der Meulen H, et al. Aberrant lipid organization in stratum corneum of patients with atopic dermatitis and lamellar ichthyosis. *J Invest Dermatol* **2001**: 117: 710-717.
32. Chong M, Fonacier L. Treatment of Eczema: Corticosteroids and Beyond. *Clin Rev Allergy Immunol* **2016**: 51: 249-262.
33. Coderch L, Lopez O, de la Maza A, et al. Ceramides and skin function. *Am J Clin Dermatol* **2003**: 4: 107-129.
34. Chiou YB, Blume-Peytavi U. Stratum corneum maturation. A review of neonatal skin function. *Skin Pharmacol Physiol* **2004**: 17: 57-66.
35. Haubrich KA. Role of Vernix caseosa in the neonate: potential application in the adult population. *AACN Clin Issues* **2003**: 14: 457-464.
36. Hoath SB, Pickens WL, Visscher MO. The biology of vernix caseosa. *Int J Cosmet Sci* **2006**: 28: 319-333.
37. Rissmann R, Groenink HW, Weerheim AM, et al. New insights into ultrastructure, lipid composition and organization of vernix caseosa. *J Invest Dermatol* **2006**: 126: 1823-1833.
38. Oudshoorn MH, Rissmann R, van der Coelen D, et al. Effect of synthetic vernix biofilms on barrier recovery of damaged mouse skin. *Exp Dermatol* **2009**: 18: 695-703.
39. Oudshoorn MH, Rissmann R, van der Coelen D, et al. Development of a murine model to evaluate the effect of vernix caseosa on skin barrier recovery. *Exp Dermatol* **2009**: 18: 178-184.
40. Visscher MO, Barai N, LaRuffa AA, et al. Epidermal barrier treatments based on vernix caseosa. *Skin Pharmacol Physiol* **2011**: 24: 322-329.

Curriculum Vitae

Tineke Berkers was born on the 23th of March 1989 in Helmond. After graduating from Peelland College in Deurne in 2007, she started her study Biomedical Sciences at the Radboud University in Nijmegen, which she completed in 2013 with the distinction 'Bene Meritum'. During her study she did two major internships. The first one she performed at Sanquin Blood Supply entitled "The value of red cell indices and zinc protoporphyrin in donor deferral for low haemoglobin: a case-control study". She performed the second internship at DSM Biomedical which was called "Evaluation of an anti-fouling coating for continuous glucose monitoring".
In 2013 she started her PhD project under the supervision of Prof. Dr. J.A. Bouwstra and Dr. A.P.M. Lavrijsen at the division of Drug Delivery Technology at the Leiden Academic Center for Drug Research. The results of this PhD project are described in this thesis.
She is currently working as Clinical Research Associate at Medpace in Capelle aan den IJssel, a contract research organization.

List of publications

Berkers T, Boiten WA, Absalah S, van Smeden J, Lavrijsen APM, Bouwstra JA. *Compromising human skin in vivo and ex vivo to study skin barrier repair.* (prepared for submission)

Berkers T, Boiten WA, Abasalah S, van Smeden J, Lavrijsen APM, Bouwstra JA. *An Intra-individual controlled pilot study with emollient monotherapy in moderate to severe atopic dermatitis patients, induced stratum corneum lipid properties changes, but did not improve the disease severity.* (prepared for submission)

Berkers T, Visscher D, Gooris GS, Bouwstra JA. *Degree of skin barrier disruption affects lipid organization in regenerated stratum corneum.* Acta Derm Venereol. **2018** Apr 16;98(4):421-427.

Berkers T, Visscher D, Gooris GS, Bouwstra JA. *Topically applied ceramides interact with the stratum corneum lipid matrix in compromised ex vivo skin.* Pharm Res. **2018** Feb 6;35(3):48.

Berkers T, Boiten WA, Absalah S, van Smeden J, Lavrijsen APM, Bouwstra JA. *Applying a vernix caseosa based formulation accelerates skin barrier repair by modulating lipid biosynthesis.* J Lipid Res. **2018** Feb;59(2):250-260.

Berkers T, van Dijk L, Absalah S, van Smeden J, Bouwstra JA. *Topically applied fatty acids are elongated before incorporation in the stratum corneum lipid matrix in compromised skin.* Exp Dermatol. **2017** Jan;26(1):36-43.

Danso MO, Berkers T, Mieremet A, Hausil F, Bouwstra JA. *An ex vivo human skin model for studying skin barrier repair.* Exp Dermatol. **2015** Jan;24(1):48-54.

Dura P, Berkers T, van Veen EM, Salomon J, te Morsche RH, Roelofs HM, Kristinsson JO, Wobbes T, Witteman BJ, Tan AC, Drenth JP, Peters WH. *Polymorphisms in alcohol-metabolizing enzymes and esophageal carcinoma susceptibility: a Dutch Caucasian case-control study.* J Hum Genet. **2013** Nov;58(11):742-8.